Development of Novel Positron Emission Tomography Pharmacodynamic Markers for Response Assessment in Cancer

Laura Kenny

A thesis presented to University of London for the degree of Doctor of Philosophy

MRC Cyclotron Unit
Hammersmith Hospital
Imperial College London

August 2008

Declaration

This thesis has been performed personally, except where due acknowledgement is made.

Laura Kenny

August 2008

Dedicated to Paul, Claudia,

my parents, Raymond,

and the patients who participated in the research.

Acknowledgements

The research reported in this thesis was performed in the Medical Research Council Cyclotron Unit at Hammersmith hospital, in collaboration with the Department of Oncology, Charing Cross hospital London.

I would like to thank my supervisors, Professor Charles Coombes and Professor Eric Aboagye, whose support and encouragement were invaluable throughout this project. My colleagues Dr Nishi Gupta and Dr Kaiyumars Contractor provided good camaraderie during my time as a research fellow, and assisted me in the initial and final stages of the projects in this thesis. I am also indebted to Ms Sian Thomas whose role as a research nurse was vital for recruiting patients.

This project would not have been possible but for the willingness of the patients to participate. Their ability to demonstrate altruism in times which were very difficult for them was truly inspirational.

The scans were funded by the Medical Research Council, and assisted by the staff of Hammersmith Imanet ®.

Whilst it may be impossible to thank everyone a number of people deserve a special mention:

The radiographers: Mr A Blyth, Mrs A Williams, Mrs H McDevitt, and Mr J Anscombe, treated my patients with great care and ensured the smooth running of the scans made my time in research very enjoyable.

The radiochemists, Dr S Creasy, Mr R Khan, Mr N Steel, Mr S Hill for the synthesis of [18F]FLT, [11C]Choline, and Dr D Turton for the development of [18F]-AH111585.

Miss S Osman for her expertise in acquiring blood data and providing quality control of the radiotracers.

The Westminster Medical School Oncology Research Trust for funding me for one year of the project, and Cancer Research UK for providing me with four months funding.

The data analysis software for the project was written originally by Dr Vin Cunningham, and updated by Dr R Hinz. I am also grateful to Dr F Turkheimer and Dr L Rosso who helped with the modelling software modifications for the capecitabine and [18F]-AH111585 studies.

Finally, I wish to thank my husband Paul and my family, who have never feigned in their support of me and my work.

Abstract

There is an urgent need to develop sensitive and specific biomarkers of response to treatment in oncology. This thesis explores the utility of three novel positron emission tomography (PET) radiotracers: [18F]-3'deoxy-3'fluorothymidine (FLT), [11C]choline and [18F]-AH111585. All patients in the PET studies had breast cancer.

Aims: 1) To quantify the uptake and retention of [18F]FLT, [11C]choline and [18F]-AH111585 in breast cancer, and evaluate the role of mathematical modelling compared to standard techniques for quantifying tracer uptake. 2) To correlate [18F]FLT and [11C]choline PET data with immunohistochemical markers of proliferation. 3) To establish if [18F]FLT and [11C]choline PET are reproducible in breast cancer. 4) To determine the effect of anti-cancer treatment on [18F]FLT and [11C]choline PET. 5) To evaluate the diagnostic utility of [18F]-AH111585, a novel αvβ3 imaging agent, in breast cancer.

Methods: 15 patients with primary and metastatic breast cancer were studied with [18F] FLT-PET at baseline, 2-7 days later, and then 7 days post-chemotherapy. [11C]Choline-PET was evaluated in 21 separate breast cancer patients, 13 for repeatability and 8 for response to trastuzumab. Finally, in 7 further patients [18F]-AH111585-PET was used to monitor angiogenesis in metastatic breast cancer.

Findings: All tumour lesions had positive uptake of FLT, which correlated with cell proliferation, FLT uptake was found to have good repeatability,, and patients who clinically responded to chemotherapy also demonstrated significant early changes in FLT uptake.

In the choline studies, all tumour lesions demonstrated significant uptake compared to normal tissue, and patients who clinically responded to trastuzumab also had a decrease in choline retention parameters.

In seven patients studied with [18F]-AH111585-PET all but one lesion had significant retention of the tracer, suggesting that this agent may be promising for imaging angiogenesis.

Abbreviations

ATP	Adenosine triphosphate
ARSAC	Administration of Radioactive Substances Advisory Committee
ASCO	American Society of Clinical Oncology
AUC	Area under the curve
AUC_{perf}	Area under the time activity curve corrected for perfusion
BF	Blood flow
BGO	Bismuth germanate, $Bi_4GE_3O_{12}$
Bq	Bequerel (unit of radioactivity)
BUdR	Bromodeoxyuridine
C_a	Continuous arterial input function
CI	Confidence Interval
C_{max}	Maximum tissue concentration
C_T	PET tissue TAC data, utilised in perfusion measurement (Kety-Schmidt model)
CR	Complete response
CT	Computed tomography
2D	Two dimensional
3D	Three dimensional
DCIS	Ductal carcinoma in situ
DNA	Deoxyribonucleic acid
dTMP	Deoxythymidine monophosphate
dTTP	Deoxythymidine triphosphate
dUMP	Deoxyuridine monophosphate
EGF	Epidermal growth factor
EGFR	Epidermal growth factor receptor
FMAU	2'-fluoro-2-deoxyuridylate

FIAU	1-(2'-deoxy-2'-fluoro-beta-D-arabinofuranosyl)-5-iodouracil
FLT	3'-deoxy-3'-fluorothymidine
FOV	Field of view
FRT	Fractional retention of tracer
5-FU	5-Fluorouracil
Fur	Fluorodeoxyuridine
FWHM	Full width half-maximum
GBq	Gigabequerel
GLUT	Glucose transporter
HPLC	High performance liquid chromatography
Kg	Kilogram
IUdR	Iododeoxyuridine
IRF	Impulse response function
LI	Labelling index
MAPK	Mitogen activated protein kinase
MBq	Megabequerel
MDR	Multidrug resistance
MEK	Mitogen activated protein kinase kinase
MIB1	Molecular Immunology Borstel
MRC	Medical Research Council
MR_{glu}	Metabolic rate of glucose
MRI	Magnetic resonance imaging
MRNA	Messenger ribonucleic acid
MRT	Mean residence time
MTD	Maximum tolerated dose
MVD	Microvessel density
NCI	National Cancer Institute
PCNA	Proliferating cell nuclear antigen

PD	Pharmacodynamic
PET	Positron emission tomography
PK	Pharmacokinetic
PR	Partial Response
RECIST	Response Evaluation Criteria in Solid Tumours
RGD	Arginine-Glycine-Aspartate
RNA	Ribonucleic acid
ROI	Region of interest
RT-PCR	Reverse transcription polymerase chain reaction
RTK	Receptor tyrosine kinase
SD	Standard deviation
SPECT	Single photon emission computed tomography
SPF	S phase fraction
SUV	Standardised uptake value
TAC	Time activity curve
TAF	Tumour angiogenic factor
TK	Thymidine kinase
TP	Thymidine phosphorylase
T_{pot}	Potential doubling time
TS	Thymidylate synthase
TTP	Thymidine triphosphate
UMP	Uridine monophosphate
UDP	Uridine diphosphate
UK	United Kingdom
USS	Ultrasound scan
VD	Volume of distribution

α	Alpha particle
β	Beta particle
γ	Gamma particle
μ	Attenuation coefficient, cm^{-1}

Contents

List of Tables 17

List of Figures 19

List of Figures 19

CHAPTER 1: Background 22

1.0 Introduction 22

1.1 Cancer 22

1.2 Breast cancer 24

1.3 Tumour Proliferation 27

1.3.1 Cell Proliferation and Cyclins 28

1.4 Growth factors 29

1.4.1 Ras-MAPK pathway 33

1.4.2 Ras 34

1.4.3 PI3 kinase/AKT pathway 35

1.4.4 mTOR 37

1.5 Angiogenesis 38

1.5.1 Integrins 42

1.6 Current methods for studying cell proliferation and angiogenesis 46

1.6.1 Proliferation 46

1.6.2 Angiogenesis 48

1.7 Clinical response assessment to cancer therapy 51

1.7.1 Tumour tissue 54

1.7.2 In Vitro and Preclinical systems for evaluating tumour response 55

1.8 PET As A Tumour Biomarker 58

1.9 Physical Imaging in Cancer 60

1.9.1 Ultrasound 61

1.9.2 X-ray 62

1.9.3 Magnetic Resonance Imaging (MRI) 63
1.10 Nuclear Imaging 64
1.10.1 The Gamma Camera 64
1.10.2 Planar Imaging 65
1.10.3 SPECT 65
1.11 Basic Principles of PET 66
1.11.1 Coincidence detection 69
1.11.2 Scatter and Attenuation 70
1.11.3 Dead Time 72
1.11.4 Random Events 73
1.11.5 Detector efficiency 73
1.11.6 Attenuation 74
1.11.7 Data reconstruction 76
1.11.8 Partial volume effect 76
1.11.9 Noise 77
1.11.10 Resolution 78
1.11.11 Two dimensional (2D) and three dimensional (3D)PET 79
1.11.12 Calibration 80
1.11.13 PET/CT 81
1.11.14 Arterial Blood Sampling 81
1.11.15 Mathematical models 82
1.11.13 Semi-quantitative methods 86
1.12 FDG 88
1.13 PET radiotracers for studying proliferation 91
1.13.1 Thymidine 91
1.13.2 [18F]Fluorothymidine (FLT) 98
1.13.3 FMAU 101
1.13.4 Bromodeoxyuridine 102

1.14 Choline 103

1.15 [18F]-AH111585 107

CHAPTER 2: [18F]Fluorothymidine ([18F]FLT) 111

2.0 Outline of [18F]FLT Projects 111

2.1 [18F]FLT-PET Correlation with Proliferation in Breast Cancer 112

2.1.1 HYPOTHESIS 112

2.1.2 AIMS 112

2.1.3 INTRODUCTION 113

2.1.4 METHODOLOGY 115

2.1.4.1 Eligibility criteria and recruitment 115

2.1.4.2 Scanning procedure and [18F]FLT synthesis 117

SUV and AUC 120

Plasma Input Functions 121

2.1.5 RESULTS 125

2.1.5.1 Patients 125

2.1.5.2 Metabolism of [18F]FLT and effect of β-glucuronidase 125

2.1.5.3 [18F]FLT uptake in tumour and normal lesions 130

2.1.5.4 Correlation between [18F]FLT uptake and Ki-67 LI 139

2.1.5.5 Results of cardiac blood pool analysis 144

2.1.6 CONCLUSIONS 149

2.2 Repeatability of [18F]FLT Pharmacokinetic Parameters 150

2.2.1 HYPOTHESIS 150

2.2.2 AIMS 150

2.2.3 Introduction 151

2.2.4 Methods 152

2.2.5 Results 154

2.2.6 Discussion 160

2.2.7 Conclusion 161

2.3 [18F]FLT-PET Prediction of Early Response to Treatment in Breast Cancer 162
2.3.1 Hypothesis 162
2.3.2 Aims 162
2.3.3 Introduction 163
2.3.4 Methods 165
2.3.5 Results 166
2.3.7 Conclusion 177
2.4.1 Hypothesis 178
2.4.2 Aims 178
2.4.3 Introduction 179
2.4.4 Methods 184
2.4.4.1 Radiotracer Synthesis and Scanning Procedure 187
2.4.5 Results 190
2.4.6 Discussion 199
CHAPTER 3: CHOLINE 203
3.1 Hypothesis 203
3.2 Aims 203
3.3 Introduction 204
3.4 Methods 207
3.4.1 Patients 207
3.4.2. Radiotracer synthesis and scanning 208
3.4.3 Blood sampling and [11C]Choline metabolite analysis 209
3.4.4. Image and Data Analysis 211
3.4.5 Immunohistochemistry 211
3.4.6 Statistical analysis 213
3.5 Results 215
3.5.1. Patient Characteristics 215
3.5.2 [11C]Choline Analysis in Arterial Plasma 216

3.5.3. Comparison of tumour and normal tissue uptake of [11C]Choline 219

3.5.4 Repeatability of [11C]Choline PET 225

3.5.5 Correlation of [11C]Choline–PET parameters with immunohistochemistry of breast tumour lesions 229

3.5.6 Measurement of response to trastuzumab with [11C]Choline 233

3.6 Discussion 238

CHAPTER 4: Study of [18F]-AH111585-PET Pharmacokinetics, Efficacy, and Sensitivity in Patients with Metastatic Breast Cancer. 241

4.1 Hypothesis 241

4.2 Aims 241

4.3 Introduction 242

4.4 Methods 242

4.4.1 Ethical Approval 243

4.4.2 Procedure for radioactivity counting in blood and urine 244

4.4.3 Biodistribution and Radiation Dosimetry in Healthy Volunteers 245

4.4.4 Breast Cancer Patient study 245

4.4.5 Scan procedure- Patients 246

4.4.6 PET Imaging of Patients 248

4.4.7 Patient Characteristics 250

4.4.8 Activity injected for the Patient Study 251

4.4.9 Region of Interest Analysis 251

4.5 Results 254

4.5.1 Advanced Breast Cancer Study Patients and Regions of Interest 258

4.5.2 Metabolism of [18F]-AH111585 262

4.5.3 Mathematical analysis results 264

4.5.4 Summary of Statistical Analysis 272

4.6 DISCUSSION 278

CHAPTER 5: CONCLUSION **284**

PUBLICATIONS, PRESENTATIONS, AND PRIZES ASSOCIATED WITH THIS THESIS **286**

REFERENCES **291**

List of Tables

Table 1.1: Risk factors for developing breast cancer 25

Table 1.2: Human angiogenic growth factors and inhibitors 42

Table 1.3: Integrins and their ligands 45

Table 1.4: The RECIST Criteria 51

Table 1.5. PET radioisotopes: Characteristics and Production. 69

Table 2.1: Dimensions of the ECAT 962 HR+ Tomograph 118

Table 2.2: Semiquantitative parameters of [18]FLT uptake 128

Table 2.3: Modelled pharmacokinetic parameters of [18]FLT uptake 129

Table 2.4: [18F]FLT-PET correlation with Ki-67 LI 142

Table 2.5 Results obtained using the cardiac blood pool ROI and dynamic radial artery sampling 145

Table 2.6 Correlation between cardiac AUC and radial artery total blood AUC 146

Table 2.7 Repeatability of semi-quantitative and modelled parameters in tumour lesions 156

Table 2.8: Spontaneous fluctuation range for each [18F]FLT pharmacokinetic parameter 157

Table 2.9 Clinical response to FEC chemotherapy 170

Table 2.10 Patients in the [18F]FLT Pharmacodynamic study 186

Table 2.11: Dynamic water scans 187

Table 2.12: Dynamic [18F]FLT Imaging 187

Table 2.13: Comparison of tumour Vd, K1, and PS product pre- and post-capecitabine. 197

Table 3.1 Reconstruction of [11C]choline time frames (version 1) 209

Table 3.2 Reconstruction of [11C]choline time frames (version 2) 209

Table 3.3 Blood sampling protocol for [11C]Choline-PET study 210

Table 3.4: Grading of c-erbB2 staining intensity in tissue 213

Table 3.5 [11C]Choline Repeatability Study Patients 215
Table 3.6 [11C]Choline Response to Treatment Study Patients 216
Table 3.7 Tumour and normal tissue uptake of [11C]Choline 220
Table 3.8 Repeatability of semi-quantitative and modelled parameters in tumour lesions 225
Table 3.9: Spontaneous fluctuation range for each [11C]Choline pharmacokinetic parameter 227
Table 3.10. Immunohistochemistry analysis of tumour samples 229
Table 3.11 Pearson's Correlation between pharmacokinetic parameters and tumour 231
Table 3.12 Assessment of differences in McCarty score by [11C]Choline-PET parameters 232
Table 3.13 Comparison of Changes in Pharmacokinetic Parameters and Clinical 234
Table 4.1 Discrete Blood Sampling Protocol for the Patient Study 247
Table 4.2 Frame acquisition for the Patient Study 248
Table 4.3.Study Schedule of Events for Subjects with Late Stage Breast Cancer 249
Table 4.4 Patient Characteristics 250
Table 4.5 Activity of [18F]-AH111585 Administered to Patients with Advanced Breast Cancer 251
Table 4.6. Regions of Interest for the Patient Study 252
Table 4.7 Results of SUV and AUC Analysis in Tumour and Non-Tumour Tissue 265
Table 4.8 Results of Patlak Analysis in Tumour and Non-Tumour Tissue 266
Table 4.9 Results of Spectral Analysis in Tumour and Non-Tumour Tissue 267
Table 4.10 Difference between tumour and normal tissue uptake for all parameters 274

List of Figures

Figure 1.1 : The Cell Cycle 29

Figure 1.2 EGF signalling pathways for proliferation and apoptosis 31

Figure 1.3: EGF signalling 32

Figure 1.4. MAPK signalling cascades 34

Figure 1.5: PIP3/Akt Signalling pathway 37

Figure 1.6: Folkman model of tumour angiogenesis 39

Figure 1.7 Positron decay 68

Figure 1.8: Annihilation detection 69

Figure 1.10 Attenuation in PET 75

Figure 1.11 The Sokoloff compartmental model for FDG uptake 83

Figure 1.12. Compartmental model for radiolabelled metabolites 84

Figure 1.13: Cellular uptake and metabolism of FDG. 89

Figure 1.15: Tissue compartmental model for thymidine 97

Figure 1.16 Structure of choline 103

Figure 1.17. Michaelis-Menten equation for enzyme catalysis 104

Figure 1.18: Biosynthesis and hydrolysis of PtC 105

Figure 2.1: Two Tissue Compartment Model for [18F]FLT 122

Figure 2.2: HPLC Chromatograms from arterial plasma showing [18F]FLT and metabolite 126

Figure 2.3 Sagittal view of [18F]FLT-PET image showing high uptake in a primary breast tumour, normal liver, and vertebrae. 130

Figure 2.4: [18F]FLT-SUV in tumour and normal tissues 131

Figure 2.5: Heterogeneous uptake of [18F]FLT in a patient with a large primary tumour. 132

Figure 2.6: Metabolism of [18F]FLT 134

Figure 2.7 Tumour TAC curve and arterial parent plasma input function 135

Figure 2.8 Comparison of tumour and normal breast [18F]FLT retention using modified Patlak analysis 135
Figure 2.9 Comparison of the IRF for breast tumour and normal tissue 136
Figure 2.10 Spectrum of kinetic components in breast tumour 137
Figure 2.11 Difference between tumour and normal tissue [18F]FLT pharmacokinetic parameters 138
Figure 2.12: [18F]FLT PET images and corresponding Ki-67 immunohistochemistry sections 140
Figure 2.13 Correlation between Ki-67 LI and pharmacokinetic parameters 141
Figure 2.14 Relationship between cardiac ROI and total blood arterial input function 146
Figure 2.15 Correlation between two forms of input function 147
Figure 2.16 Correlation of Baseline and Repeatability Scan Parameters for [18F]FLT uptake in breast tumour lesions 158
Figure 2.16 Correlation of Baseline and Repeatability Scan Parameters for [18F]FLT uptake in breast tumour lesions 159
Figure 2.17 Comparison of [18]FLT-PET response and non-response 168
Figure 2.18 [18]FLT-PET response for all tumour lesions 169
Figure 2.19 Relationship between clinical response and changes in [18F]FLT-PET parameters 173
Figure 2.20 Mechanism of action of Capecitabine 179
Figure 2.21 Structures of Capecitabine and 5-FU 181
Figure 2.22 [18F]FLT-PET Images Pre and Post Capecitabine 192
Figure 2.23 Changes in [18F]FLT Pharmacokinetic Parameters Post-Capecitabine 193
Figure 2.24 Significance of [18F]FLT response to capecitabine for all lesions 195
Figure 3.1: Plasma concentration of [11C]Choline and metabolite post-injection 217
Figure 3.2. HPLC Chromatograms of Arterial Plasma Post-Injection with [11C]Choline 218

Figure 3.3 Comparison of tumour and normal tissue [11C]choline uptake 221
Figure 3.4. Time Activity Curves for [11C]choline in different tissues 222
Figure 3.5 Patlak and Spectral models of choline uptake 224
Figure 3.6 Repeatability of choline PET parameters in tumour lesions 228
Figure 3.8 [11C]Choline-PET Images of response and non-response to trastuzumab 236
Figure 3.9 Significance Plots for [11C]Choline-PET Pharmacokinetic Response 237
Figure 4.1. Structure of AH111585 as described by Indervoll et al. 243
Figure 4.2. [18F]-AH111585 PET Images over time in a Healthy Volunteer 256
Figure 4.3. Corresponding transverse [18F]-AH111585-PET and MRI images of a healthy volunteer. 257
Figure 4.4 Transverse [18F]-AH111585 PET Images and CT Images in Patients 260
Figure 4.5. [18F]-AH111585 PET in a Primary Breast Tumour with Bone Metastases 261
Figure 4.6 Summary of [18F]-AH111585 metabolism data for patients 262
Figure 4.7 HPLC Analysis of [18F]-AH111585 and Metabolites in Arterial Plasma... 263
Figure 4.8 Typical Time versus Radioactivity Curves from Tumour Regions and Corresponding Normal Tissue 268
Figure 4.9 Heterogeneity of uptake within a single tumour lesion 269
Figure 4.10. [18F]-AH111585 uptake in a liver metastasis and normal liver 269
Figure 4.11 [18F]-Radioactivity in Arterial Blood and Plasma 270
Figure 4.12 Modified Patlak analysis of a tumour lesion compared to normal tissue 271
Figure 4.13 Classical Patlak analysis in a tumour lesion 271
Figure 4.14 Comparison of Heart ROI and Total Blood Input Function 276

CHAPTER 1: Background

1.0 Introduction

This thesis will focus on the development of new molecular markers for positron emission tomography (PET) and their ability to determine response to treatment in cancer. A brief overview on cancer will now be presented, followed by a section on breast cancer which will be used as a model system in this thesis. The molecular mechanisms leading to tumour proliferation, signal transduction pathways of interest, and tumour angiogenesis then follow. Finally, current methods for assessing tumour response, the science behind PET and rationale for using: [18F]fluorothymidine ([18F]FLT), [11C]choline, and [18F]-AH111585 as radiotracers in this thesis will be presented.

1.1 Cancer

Cancer is a genetic disease. Tumour development is thought to arise by a complex process known as transformation which consists of initiation leading to changes in the genetic material of the cell, followed by promotion of the initiation cell and finally by metastasis. During transformation the physiological properties of cells become altered; conferring a survival advantage (comparable to Darwinian evolution) from the normal to malignant phenotype. This has been particularly well characterised in the Fearon-Vogelstein model of colorectal carcinoma where a genetic basis for the histological pathway from normal tissue to hyperplasia, dysplasia, carcinoma *in situ*, and invasive carcinoma was presented (Fearon et al. 1990). The hallmarks of cancer cells include: self-sufficiency in growth signals, insensitivity to anti-growth signals, evasion of apoptosis (programmed cell death), limitless capacity to replicate, sustained angiogenesis, and tissue invasion and metastasis (Hanahan et al. 2000).

Most cancers have mutations in oncogenes, tumour suppressor genes or DNA repair genes. Oncogenes are mutant versions of normal genes which drive cell growth. The difference between an oncogene and a normal gene can be as little as one single amino acid, which can have a dramatic effect on protein function. The most commonly mutated oncogene is called *ras*, with a frequency of 20-30% in human tumours. When the *ras* oncogene is transfected into appropriate models the cells can acquire a metastatic and invasive phenotype (Thorgeirsson et al. 1985). This is also true for other oncogenes such as *mos, raf, src, fes*, and *fms*.

Tumour suppressor genes work normally to suppress the development of malignancy. The two best known examples are p53 and retinoblastoma (Rb). Many tumours result from loss or malfunction of the proteins that these genes encode. The Rb protein, in its active form, slows DNA replication. Up to 40% of cancers have inactivated Rb which causes cell proliferation to continue unchecked (Knudsen et al. 2006). The p53 oncogene has been referred to as the guardian of the genome, as its role is to prevent damaged DNA from replicating and to promote apoptosis (programmed cell death) in cells with abnormal DNA. Faulty p53 protein allows abnormal DNA to replicate; the cells pass on their faulty DNA to their progeny which can then acquire additional mutations permitting tumorigenesis. The p53 gene appears to be defective in most human cancers (Lane 1992; Gomez-Lazaro et al. 2004).

The third group of genes which are involved in cancer development are the DNA repair genes. Processes which damage DNA include ultraviolet radiation, ionising radiation, and endogenous free radicals. The integrity of DNA is often damaged during replication, and this is checked and fixed by DNA repair genes. Genes which are important in DNA repair in colon cancer include MLH1, MSH2, PMS1 and PMS2. A second category of genes which act indirectly in DNA repair encode checkpoint proteins, which prevent progression through the cell cycle if faults have occurred. This includes ATM and p53. If the DNA repair mechanisms are not effective then damaged DNA will be passed onto the progeny. The activity of most anticancer drugs is

dependent on overwhelming the tumour cell's natural ability to repair drug induced damage to its DNA.

New cancer therapies are being developed using gene therapy to replace defective genes, or inactivate defective gene products. Whilst most gene therapies are still in the early phases of development, molecular targeted agents are gaining increasing importance in the medical treatment of cancer. One of the earliest examples of such agents is tamoxifen, a selective oestrogen receptor modulator, which has been used for over 30 years in the treatment of breast tumours which have over-expression of the oestrogen receptor.

1.2 Breast cancer

Breast cancer is a leading cause of cancer death in women from the industrialised world; 1 in 8 women will develop breast cancer at some stage in their lifetime. Approximately 30% of patients who present with locoregional disease will develop metastatic disease, which despite recent advances in treatment, is incurable for the vast majority of patients. In Europe in 2004, it is estimated that the incidence of new breast cancer cases was 371000, and that there were 129000 deaths due to the disease(Boyle et al. 2005). Since 1990 there has been a decreased mortality in the western world from breast cancer. This has been attributed to screening with mammography, more precise diagnosis, and better treatments including the extensive use of tamoxifen in appropriate patients. Although genetic causes due to inherited mutations in the BRCA 1 and 2 genes are responsible for some cases, the vast majority (8 out of 9 cases) have no history of the disease in a first degree relative. Most cases occur in women aged over 50. The current accepted risk factors for development of breast cancer are shown in Table 1.1 (Veronesi et al. 2005).

Table 1.1: Risk factors for developing breast cancer

	Relative Risk	*Group Affected*
Age	>10	Elderly
Location	5	Western world
Breast density	>5	High density detected on mammogram
Age at menarche	3	Age < 11yrs
Age at menopause	2	Age > 54 yrs
Age at first pregnancy	3	Age > 40 yrs
Family history	≥2	1st degree relative
Previous benign breast disease	4-5	Atypical ductal hyperplasia
Contralateral breast cancer	>4	Previous breast cancer
Socioeconomic group	2	1, 2
Premenopausal body mass index, BMI	0.7	High BMI
Postmenopausal BMI	2	High BMI
Alcohol	1.07	7% increase with every daily drink
Ionising radiation exposure	3	Girls after age 10 yrs
Breastfeeding and parity	Decreased by 4.3% for every 12 months breastfeeding and 7% for every birth	Women who don't breastfeed
Oral contraceptive pill	1.2	Current users
Hormone replacement therapy	1.66	Current users
Diethylstilbestrol	2	Use during pregnancy

(data taken from Veronesi and Boyle 2005).

In contrast to carcinoma of the colon, the intervening stages of the spectrum spanning from benign tissue to malignant breast cancer have not been determined. This is underlined by the fact that dysplastic changes are often evident in non-malignant breast proliferative diseases such as papillomas. The condition atypical

ductal hyperplasia was previously viewed as the link between healthy duct hyperplasia and ductal carcinoma *in situ* (DCIS). However cytogenetic analysis is unable to separate DCIS from atypical ductal hyperplasia, with the result that this is now not seen as a precancerous lesion.

The techniques used to diagnose breast cancer in conjunction with biopsy include physical examination, mammography, ultrasound, magnetic resonance imaging (MRI), and PET. The first three investigations remain the most commonly used, with MRI and PET being reserved for difficult cases such as lobular carcinoma, and staging of distant metastases, respectively.

Adjuvant treatment for early stage breast cancer involves surgery followed by radiotherapy. Patients at high risk of recurrence are treated with anthracycline based cytotoxic chemotherapy, which is designed to eradicate any micrometastases. In cases where it is thought down staging of the tumour prior to surgery may result in a breast conserving operation instead of mastectomy, the chemotherapy is given first and is referred to as neoadjuvant treatment. This has the advantage of determining the chemosensitivity of the tumour *in vivo*, without affecting survival (Kaufmann et al. 2006).

Approximately 75% of patients with breast cancer will have positive immunostaining for the oestrogen and/or progesterone receptor. Endocrine manipulation in terms of drugs such as tamoxifen, aromatase inhibitors (used in post-menopausal women to prevent production of oestradiol in peripheral tissues), and ovarian ablation is important in patients with positive oestrogen receptor status. These treatments have been shown to improve risks of local recurrence, contralateral breast cancer, and overall survival (EBCTCG 1992; Group 1992). Endocrine treatment is typically given following primary adjuvant therapy for approximately 5 years, though recent trials suggest that prolonged treatment may be of benefit in high-risk individuals (Goss et al. 2005). The practice of using tamoxifen for 2½ years and then switching to an aromatase inhibitor has also shown to be beneficial (Coombes et al. 2003;

Coombes et al. 2004). The role of endocrine therapy with regard to progesterone receptor status is currently being evaluated; it may be of benefit as there is evidence of cross-talk between the two receptors and their signal transduction pathways (Cui et al. 2005; Winer et al. 2005). For patients with advanced disease, treatment options include endocrine therapy for those patients with positive hormonal receptors, systemic chemotherapy, and radiotherapy for palliation of bone and brain metastases.

The treatments in this thesis include cytotoxic chemotherapy and trastuzumab. Trastuzumab is a humanised monoclonal antibody targeted to the human epidermal growth factor receptor 2 (HER2)-neu (also known as c-erbB2) receptor which is over expressed in approximately 20-30% of breast tumours, and has been shown to improve survival and decrease local recurrence in both the adjuvant and metastatic setting (Hortobagyi 2005; Slamon et al. 2006).

Over-expression of the HER-2/neu receptor is associated with the pathogenesis and prognosis of breast cancer (Slamon et al. 1987; Slamon et al. 1989). One of the proposed mechanisms of action of trastuzumab is that it prevents HER-2/neu receptor dimerisation and internalisation leading to inhibition of downstream signalling (Nahta et al. 2003). The rationale for using [11C]choline-PET as a readout of inhibition of this pathway will be explained later in this chapter.

1.3 Tumour Proliferation

Cell proliferation is essential for tumour growth. Normally the cell cycle is tightly regulated so that there is a balance between proliferating and non-proliferating cells appropriate for the tissue concerned. Loss of regulation for instance at the restriction point at the end of G_1 is thought to be critical in the development of cancer and may

occur due to altered signal transduction pathways (Malumbres et al. 2001), (Malumbres et al. 2001)(see fig 1.0). Once past the G1 restriction point, cells become independent of mitogenic signals and growth factors. In this section the cell cycle, growth factors, current classical methods for measuring cell proliferation, and PET imaging applications will be described.

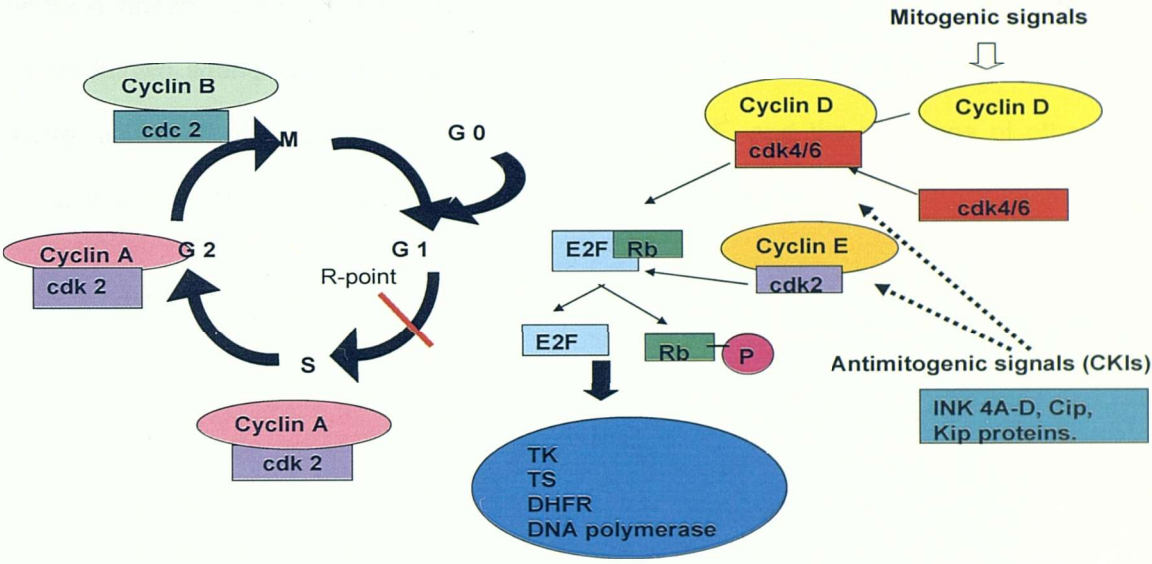
1.3.1 Cell Proliferation and Cyclins

All eukaryotic cells have a cell cycle divided into 4 phases through which they progress in order to divide: G_1, S, G_2, and M. In addition, there is a fifth phase, G_0 that should be considered as a resting phase(Lajtha 1963). Cells in this phase of the cycle can re-enter the cycle after mitogenic induction. Phosphorylation of the tumour suppressor protein Rb is one of the key mechanisms that controls progression through the G_1/S phase of the cell cycle (Dyson 1998). Hypophosphorylated Rb is bound to and inhibits E2F (Flemington et al. 1993). Upon phosphorylation of Rb, E2F is released and activates transcription factors such as dihydrofolate reductase (DHFR), tyrosine kinase (TK), thymidylate synthase (TS), DNA polymerase, E2F itself, and cyclin E (Harbour et al. 2000). Repression of E2F is mediated by histone deacetylase (HDAC) recruitment to Rb and inhibition of E2F promoters which renders cells independent of extracellular mitogenic signals (Soghomonyan et al. 2005).

Most oncogenic processes exert their greatest effect by targeting the regulation of the G_1 phase (Sherr 1996). Cyclin-cyclin dependent kinases (cdks) complexes drive cells in G_1, to initiate S phase and in G_2 to initiate mitosis (Molinari 2000). Cdks are expressed at a constant level during the cell cycle. The level of cyclin expression however, varies with cell cycle stage as they are subject to ubiquitin-proteosome degradation(Coqueret 2002). In G_1, genes encoding D type cyclins (D1-3) become activated and bind to either cdk 4 or 6. Only D type cyclins are mitogen dependent. Factors such as STAT proteins, NF-κB, CREB, and nuclear receptors have been found to transactivate the cyclin D promoter. Transcription of the cyclin D1 gene, synthesis,

and association with cdk4 has been found to be strongly dependent on receptor mediated *ras* and PI3 kinase signalling(Marshall 1999). Upon the binding of cyclin D to its dependent kinase, the protein-substrate binding site becomes exposed and ATP phosphates become correctly positioned to allow the transfer of phosphate from ATP to the target protein (Nabel 2002).

Figure 1.1 : The Cell Cycle



1.4 Growth factors

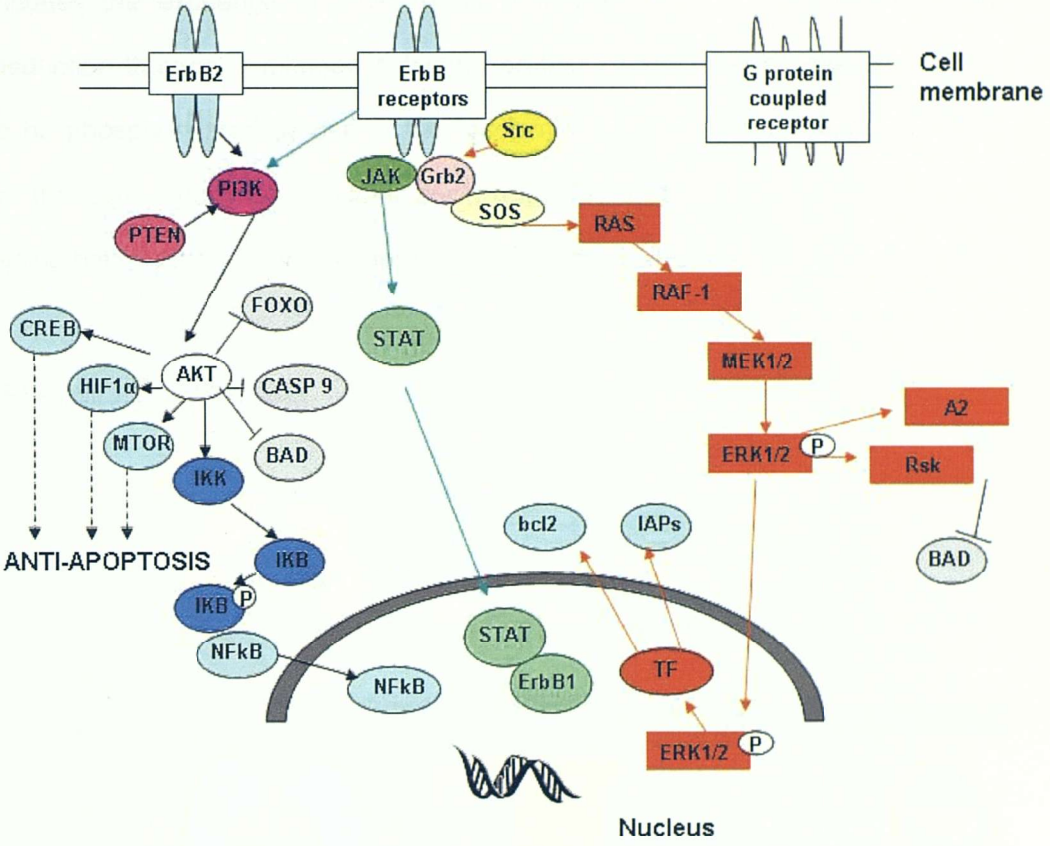
Under normal physiology, there is a balance between cell survival and programmed cell death by apoptosis. This is controlled by the response of the cell to cell survival and cell death signals in the extracellular environment. This process ensures that healthy cells survive and that unhealthy cells are destroyed.

One of the most important cell survival proteins is the epidermal growth factor (EGF). A summary of the role of EGF in anti-apoptotic signalling is shown in Figure 1.2. EGF elicits cellular responses by binding to specific transmembrane receptor

tyrosine kinases (RTK) which set off a chain of signalling events within the cell by activating serine-threonine kinases that phosphorylate serine or threonine residues on other protein kinases and/or transcription factors.

In the EGF receptor family (otherwise known as ErbB family) there are four closely related transmembrane RTKs: ErbB1 (EGFR), ErbB2 (HER2/neu), ErbB3 (her3), and ErbB4 (her4), which bind to a wide range of ligands. All the members of this family are broadly composed of the same structure: an extracellular ligand binding domain, a transmembrane spanning region, and an intracellular region containing tyrosine kinase. EGF binds exclusively to EGFR; ErbB2 is thought to be a co-receptor as no known ligand binds to it directly. Signalling through EGF is regulated by the expression level of ErbB receptors, the amount of EGF, and the presence of other positive and negative signalling regulators(Henson et al. 2006).

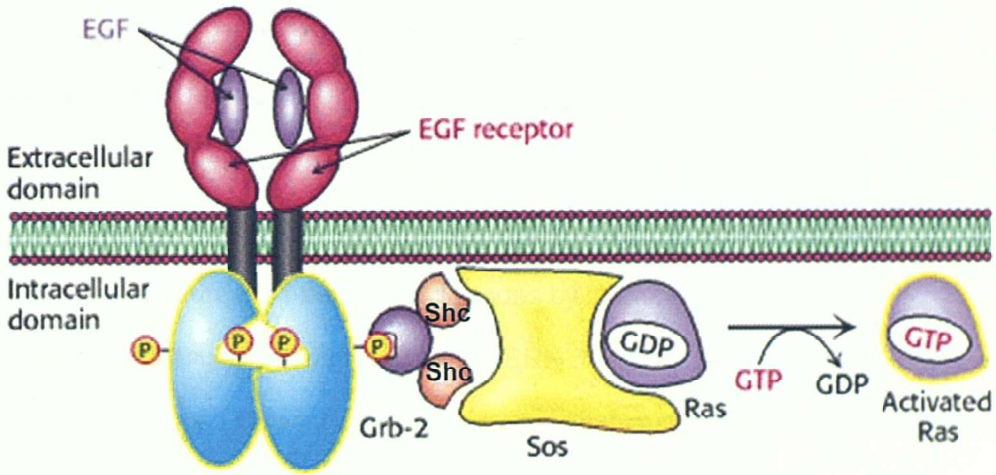
Figure 1.2 EGF signalling pathways for proliferation and apoptosis



Adapted from Henson and Gibson 2006

When EGF binds to ErbB1, the receptor homo- or hetero-dimerises with the other three receptors, and then activates RTKs by phosphorylation(Citri et al. 2006). The phosphorylated RTK then binds to the adaptor protein Shc, which then complexes with Grb-2. Grb-2 in turn activates the guanine-nucleotide exchange factor Sos. Sos stimulates the exchange of GDP for GTP in ras. Activated ras stimulates signal transduction through a mitogen activated protein kinase (MAPK) cascade. Shc may also be phosphorylated by one of the src family kinases or other kinases. After this point the EGF receptors are either down regulated and degraded via endocytosis or recycled back to the plasma membrane (Henson et al. 2006).

Figure 1.3: EGF signalling



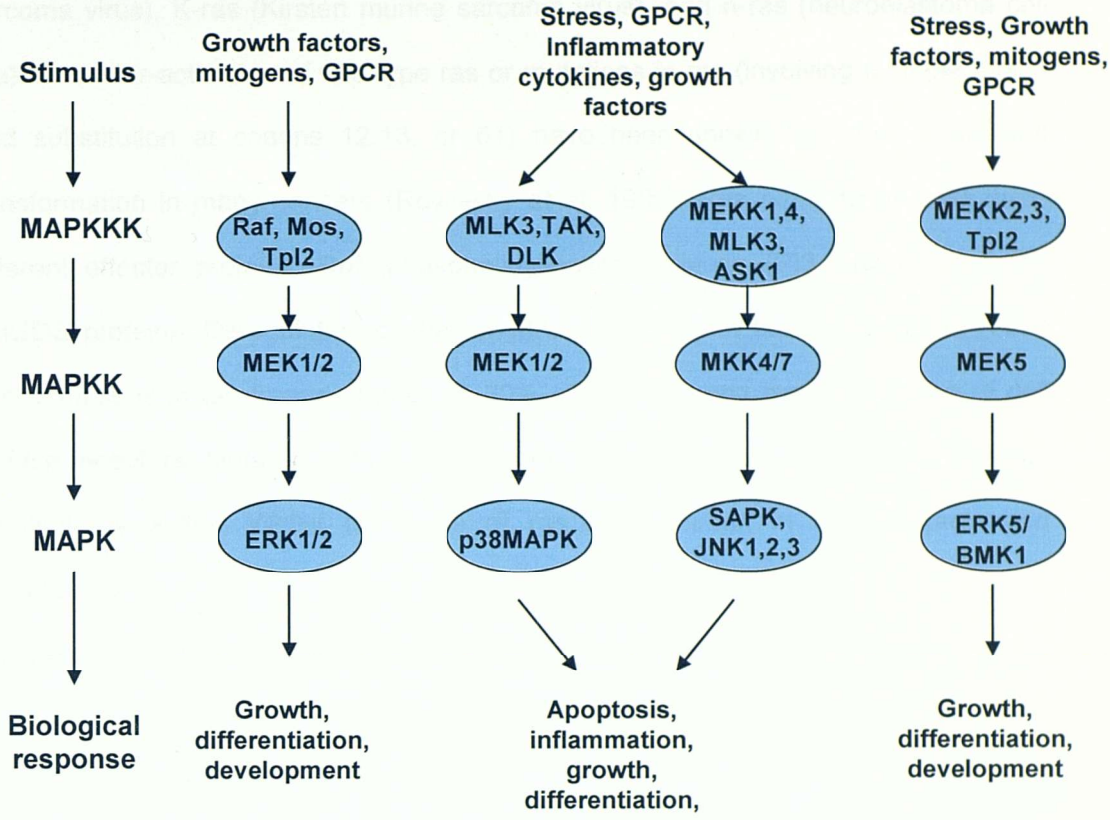
1.4.1 Ras-MAPK pathway

The MAPK signalling cascades are responsible for relaying extracellular signals responsible for cell proliferation and differentiation into the cell and cell nucleus. Such signals include growth factors, cytokines, and stresses such as UV irradiation. The stimulation of this pathway culminates in gene transcription (including immediate-early genes) and chromatin remodelling (see Figure 1.4).

MAPKs are a super family of protein serine-threonine kinases, which can be activated by a diverse array of stimuli including EGF. A highly specific ligand-receptor interaction initiates activation of the MAPK cascade which is followed by amplification of the signal due to larger amounts of substrate in each subsequent step resulting in a signal of high intensity. Usually the kinase cascade consists of MAP kinase kinase kinase (MAPKKK) followed by MAP kinase kinase (MAPKK) followed by MAPK. Each of these kinases is activated by phosphorylation (two serine residues in the case of MAPKK, and one threonine and one tyrosine residue in the case of MAPK). Low level noise in the system is eliminated by the biological demand for two phosphorylations; a single phosphorylation will not result in signal transduction. Measurement of activated MAPK can be measured in fresh or fixed tissues by immunohistochemistry.

The extracellular regulated kinases, ERK 1 and 2 are types of MAPK which play an important role in breast cancer. This signalling cascade relays signals from cell surface receptors to transcription factors, thus regulating gene expression. ERK 1 and 2 are activated by phosphorylations on residues T183 and Y185, which result in dimerisation of ERK with other ERK proteins including nuclear translocation and activation of a variety of nuclear targets. ERK1 and 2 are mainly regulated by peptide growth factors; the other major regulators of ERK-1 and -2 apart from EGF are insulin-like growth factor-1, prolactin, heregulin and its family members: insulin, TGF-α and TGF-β. Other pathways which can activate ERK-1 and -2 involve G-protein receptor mediated processes or calcium related receptors (Pearson et al. 2001).

Figure 1.4. MAPK signalling cascades



(where GPCR= G protein coupled receptors, SAPK= stress activated protein kinase, all others represent tyrosine kinases involved in the MAPK signalling cascade).

Oestrogen can activate the Ras/Raf/MAPK signalling cascade by direct interactions through the oestrogen receptor and c-src (Migliaccio et al. 1996). Progesterone activation of the pathway can occur by cross-talk between the progesterone receptor and the oestrogen receptor (Migliaccio et al. 1998).

.

1.4.2 Ras

Ras GTPase proteins activate multiple signalling pathways. Ras genes were first discovered in the1960s as homologues to the viral oncogenes of transforming

retroviruses. Three mammalian isoforms have been identified: H-ras (Harvey murine sarcoma virus), K-ras (Kirsten murine sarcoma virus), and n-ras (neuroblastoma cell line). The over-activation of wild-type ras or mutations in ras (involving a single amino acid substitution at codons 12,13, or 61) have been shown to induce malignant transformation in many cancers (Rowinsky et al. 1999). Ras binds to at least three different effector proteins: Raf, phosphatidylinositol-3-kinase (PI3 kinase), and the RalGDS proteins. Deregulation of the ras-MAPK pathway in tumour cells can result from mutations in ras (reported in up to 30% of cancers) and over-expression of cell surface receptors. Mutations of ras lock it in the GTP-bound state such that it remains constitutively active. Whilst mutations of ras are common in cancer, prolonged activation of ras can occur via other mechanisms involving loss of the tumour suppressor gene, NF1. Activation of ras by phosphorylation of GDP, leads to the activation of raf-1. Raf-1 kinase then phosphorylates MEK1/2, which then phosphorylates and activates ERK1/2. ERK1/2 translocates to the cell nucleus where it phosphorylates a variety of substrates including transcription factors (such as myc, ELK-1, c-Fos, and cyclin d), and leads to the inhibition of apoptosis via down-regulation of p53, inactivation of caspase and the pro-apoptotic protein, BAD.(Shaw et al. 2006).

1.4.3 PI3 kinase/AKT pathway

To date only one of the three classes of PI3 kinases – class 1A has been implicated in cancer. This is a heterodimer of a regulatory p85 subunit and a catalytic p110 subunit. PI3 kinase is activated by both RTKs and ras, and in turn phosphorylates phosphatidylinositol-4,5-bisphosphate(PIP2) forming phosphatidylinositol-3,4,5-triphosphate (PIP3). PIP3 acts as an anchor for AKT (a serine threonine kinase, also known as protein kinase B PKB)(Burgering et al. 1995). Mutations in the p110 subunit of PI3 kinase, have been reported in breast cancers with a frequency of 25%(Samuels et al. 2004). In breast epithelial cell lines expression of

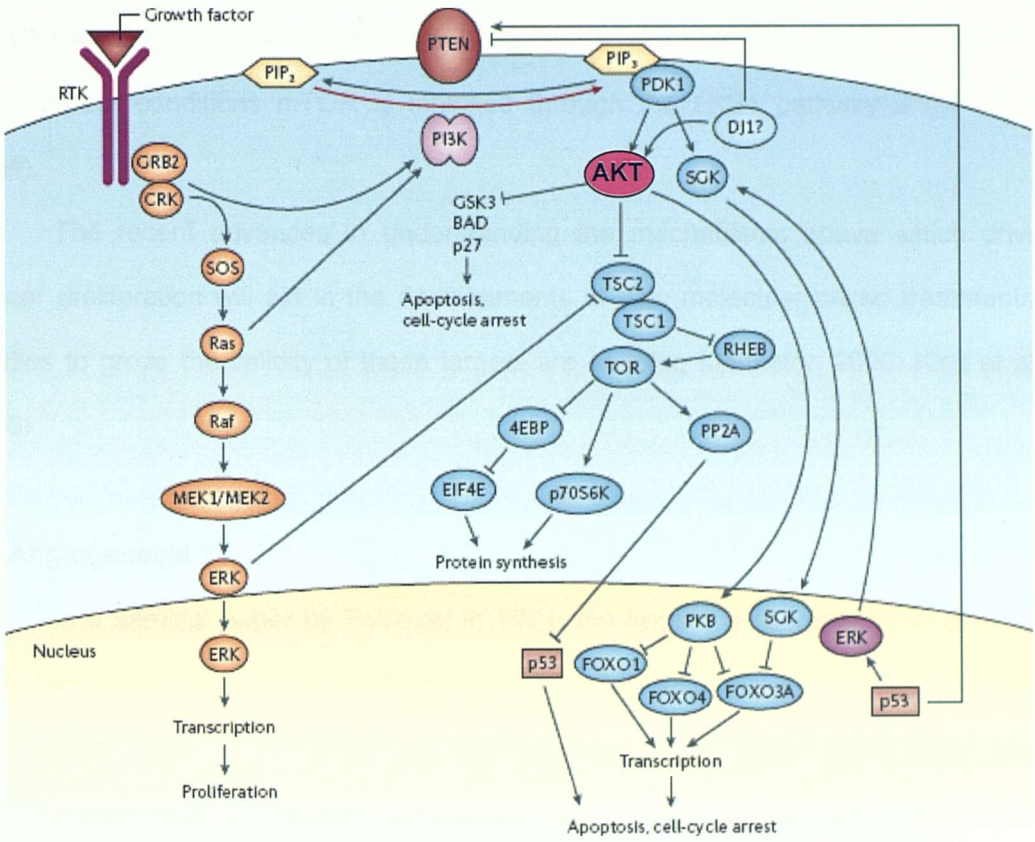
the specific mutant isoforms (E545K and H1047R) of p110 is associated with anchorage independent proliferation, growth-factor independent proliferation, resistance to anoikis and the chemotherapy drug, paclitaxel(Isakoff et al. 2005).

The most common method for PI3 kinase activation appears to be loss of the tumour suppressor enzyme phosphatase with tensin homology (PTEN) which is responsible for catalysing the dephosphorylation of PI3 (i.e. the reverse of the reaction catalyzed by PI3 kinase)(Maehama et al. 1998). Although immunohistochemical analysis of breast tumour samples has found hyperactive Akt in 50% of cases, mutations of PTEN have only been found in 3%, leading some authors to speculate that the alternative mechanisms for Akt activation include mutations in ras or inactivation of p53(Cully et al. 2006). The recent discovery of the Parkinson's disease associated gene (PARK7 also known as DJ1) over expression which is inversely correlated with PTEN expression was found to be associated with increased cell survival in breast cancer is a third method by which Akt could be come hyper-activated (Kim et al. 2005).

Activated Akt transduces signals that regulate multiple biological processes including apoptosis, cell metabolism, gene expression and cell proliferation (see Figure 5). Akt inhibits glycogen synthetase kinase 3 (GSK-3) through serine phosphorylation, which in turn controls crucial cell-cycle regulators e.g. cyclin D1, therefore leading to transcription to proceed unchecked(Cross et al. 1995). Cell growth and ATP production are stimulated by directly activating glycolysis and fatty acid synthesis via phosphofructo-2-kinase and ATP citrate lyase respectively (Garber 2006). Akt also regulates cellular uptake of glucose (see section on FDG later in this chapter). The pro-apoptotic proteins BAD, caspase 9, and FOXO are also inhibited by Akt. The activity of the anti-apoptotic proteins: malignant target of rapamycin (MTOR), HIF-1α, and c-AMP response element binding protein (CREB) are stimulated by Akt. In breast cancer, tumours which were positive for activated-Akt have been shown to be more

resistant to endocrine treatment than those which were negative(Tokunaga et al. 2006).

Figure 1.5: PIP3/Akt Signalling pathway



(taken from (Cully et al. 2006)).

1.4.4 mTOR

Recent studies suggest that the ras and PI3 kinase pathways form an intersecting biochemical network which converges on the serine/threonine kinase mTOR to stimulate cell growth(Shaw et al. 2006). Translation by the mTOR complex,

mTORC1, is responsible for controlling the cell-growth regulator HIF-1α, which in turn drives cell growth, glycolysis, and angiogenesis. Rapamycin treatment of a breast cancer mouse model with an activated PI3 kinase pathway resulted in decreased proliferation, angiogenesis, and increased apoptosis in premalignant and malignant lesions(Namba et al. 2006). ErbB2 increases angiogenesis and the metastatic potential of breast cancer cells via production of vascular endothelial growth factor (VEGF) which is mediated by ERK/AKT/PI3 kinase and mTOR (Klos et al. 2006). In nutrient-poor conditions mTOR is inhibited through the LKB1 pathway(Shaw et al. 2004).

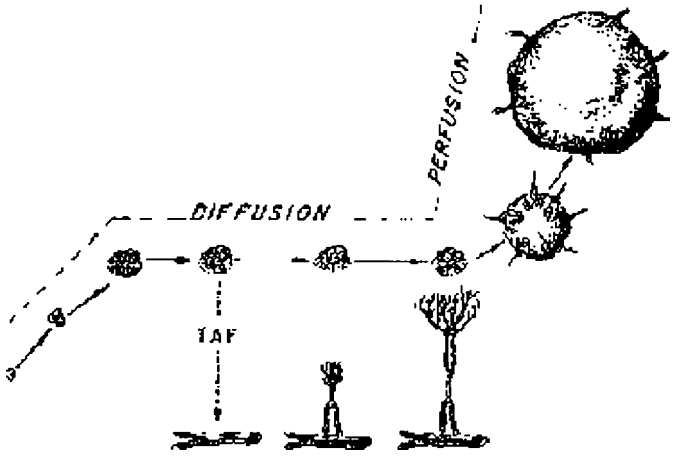
The recent advances in understanding the mechanisms above which drive cancer proliferation will aid in the developments of new molecular based treatments. Studies to prove the validity of these targets are ongoing (Johnston 2006; Klos et al. 2006).

1.5 Angiogenesis

In a seminal paper by Folkman in 1971, the necessity for tumours to develop their own blood supply was postulated. He believed that growing tumours need to develop new blood vessels. To do so they secrete an angiogenic factor (at that time named tumour angiogenic factor, TAF), and that by inhibiting angiogenesis tumour growth would be limited, see Figure 5 (Folkman 1971). Purification of the angiogenic factor, a cationic polypeptide, was finally achieved in 1984(Shing et al. 1984). Tumour enlargement greater than 2mm is dependent on what is now referred to as an angiogenic switch whereby proangiogenic factors outweigh angiogenic inhibitors resulting in neovascularisation. Currently 17 proangiogenic factors have been isolated (see Table 1.2). Physiological angiogenesis only occurs in endometrial endothelium, wound healing and inflammation. In other tissues angiogenesis is inhibited by angiogenic inhibitors such as thrombospondin-1. In the absence of angiogenesis tumours enter a dormant state characterised by a balance between proliferation and

apoptosis with a volume of a few mm^3 (i.e. 10^5 -10^6 cells). Tumour angiogenesis also encourages metastatic spread by providing a route for cells to escape through the systemic circulation (Folkman 2002; Carmeliet 2005) to distant sites.

Figure 1.6: Folkman model of tumour angiogenesis



Tumour angiogenesis has recently become a key target in therapeutics. Most agents are directed towards vascular endothelial growth factor (VEGF) Although the early clinical trials of some angiogenesis inhibitors was complicated by adverse reactions, bevacizumab, a humanised monoclonal antibody targeted towards VEGF is now licensed in combination with 5-fluorouracil for the treatment of metastatic colorectal cancer. Bevacizumab acts by binding the VEGF ligand and preventing receptor binding and signal transduction.

The main anti-angiogenic agents which have been developed are designed to target the VEGF ligand or inhibit matrix metalloproteinases(Cooney et al. 2006). Integrins have been explored as a therapeutic target. Inhibition of endothelium derived nitric oxide synthase (an angiogenesis promoter) has been shown to inhibit expression of the $\alpha v\beta_3$ integrin(Murohara et al. 1999). A humanised monoclonal antibody to the $\alpha v\beta_3$ integrin, Vitaxin, has been developed and reached phase 1 clinical trials in

patients with metastatic cancer. Although only a small group of patients were treated, disease stabilisation lasting 22 months occurred in 1 patient (Gutheil et al. 2000; Posey et al. 2001). Cilengitide is an RGD peptide which has shown promising results when given in combination with radioimmunotherapy in a preclinical breast cancer model(Burke et al. 2002). Increased apoptosis of tumour and endothelial cells was noticed in mice treated with cilengitide and radioimmunotherapy compared to radioimmunotherapy alone(Burke et al. 2002). This agent has now entered phase 1/2 clinical trials in metastatic cancer patients (Eskens et al. 2003).

In breast cancer, angiogenesis is associated with a more aggressive phenotype. A study of 197 patients with node-positive and node-negative breast cancer found that expression of $\alpha v\beta_3$ integrin was the most important predictor of relapse-free survival (Gasparini et al. 1998). The $\alpha v\beta_3$ integrin is expressed on endothelial cells, osteoclasts, and melanoma cells. $\alpha v\beta_3$ supports adhesion and migration of breast, melanoma, and prostate tumour cells on bone matrix proteins(Sung et al. 1998; Byzova et al. 2000; Cooper et al. 2002; Nemeth et al. 2003), The effect of growth factors such as EGF, insulin, and PDGF on mitosis is potentiated by $\alpha v\beta_3$ integrin, integrin mediated cell attachment can even result in transactivation of growth factor receptors in the absence of their cognate ligands.

The Chalkley count determines the vessel content in immunostained cryosections as the relative area of the immunostained vessels expressed as an index. Breast tumour angiogenesis was measured using the Chalkley count in 836 patients by Hansen et al, and found to correlate strongly with the presence of lymph node metastases, tumour grade, and large tumour size(Hansen et al. 2000). The authors found that estimation of tumour angiogenesis using this method was an independent prognostic factor, i.e. there was an inverse correlation between Chalkley count with recurrence free and overall survival. VEGF expression also correlates with risk and

outcomes in breast cancer, and is associated with tumour resistance to tamoxifen and chemotherapy(Foekens et al. 2001).

Many commonly prescribed treatments for breast cancer also have an anti-angiogenic mode of action. The anti-angiogenic activity of tamoxifen is due to direct inhibition of VEGF and basic fibroblastic growth factor (bFGF), which is independent of oestradiol (Gagliardi et al. 1993; Gagliardi et al. 1996).The anti-angiogenic action is thought to be enhanced by metronomic scheduling of treatment, whereby low doses of drugs are given for prolonged periods(Hanahan et al. 2000). This is in contrast to the typical scenario for cytotoxic agents where maximum tolerated doses (MTD) are given to promote cell kill. In a preclinical pancreatic islet cell tumour model, using upfront MTD chemotherapy with cyclophosphamide followed by metronomic therapy with the same drug combined with inhibition of VEGF and platelet derived growth factor, resulted in complete responses compared to MTD alone which led to initial tumour regression followed by rapid regrowth (Pietras et al. 2005).

Table 1.2: Human angiogenic growth factors and inhibitors

Pro-angiogenic factors	*Angiogenesis Inhibitors*
Angiogenin	Angioarrestin
Angiopoietin-1	Angiostatin (plasminogen fragment)
Del-1	Antiangiogenic antithrombin III
Fibroblast growth factors: acidic (aFGF) and basic (bFGF)	Cartilage-derived inhibitor (CDI)
Follistatin	CD59 complement fragment
Granulocyte colony-stimulating factor (G-CSF)	Endostatin (collagen XVIII fragment)
Hepatocyte growth factor (HGF) /scatter factor (SF)	Fibronectin fragment
Interleukin-8 (IL-8)	Gro-beta
Leptin	Heparinases
Midkine	Heparin hexasaccharide fragment
Placental growth factor	Human chorionic gonadotropin (hCG)
Platelet-derived endothelial cell growth factor (PD-ECGF)	Interferon alpha/beta/gamma
Platelet-derived growth factor-BB (PDGF-BB)	Interferon inducible protein (IP-10)
Pleiotrophin (PTN)	Interleukin-12
Progranulin	Kringle 5 (plasminogen fragment)
Proliferin	Metalloproteinase inhibitors (TIMPs)
Transforming growth factor-alpha (TGF-alpha)	2-Methoxyestradiol
Transforming growth factor-beta (TGF-beta)	Placental ribonuclease inhibitor
Tumor necrosis factor-alpha (TNF-alpha)	Plasminogen activator inhibitor
Vascular endothelial growth factor (VEGF)	Platelet factor-4 (PF4)
	Prolactin 16kD fragment
	Proliferin-related protein (PRP)
	Retinoids
	Tetrahydrocortisol-S
	Thrombospondin-1 (TSP-1)
	Transforming growth factor-beta (TGF-b)
	Vasculostatin
	Vasostatin (calreticulin fragment)

1.5.1 Integrins

One of the projects in this thesis will focus on an [18F]-labelled peptide which is proposed as a novel PET radiotracer for angiogenesis by binding to the $\alpha v\beta_3$ integrin. The integrins are a family of heterodimeric transmembrane proteins which act as an

integral membrane complexes involved in the transmembrane association between the extracellular matrix and the cytoskeleton (Tamkun et al. 1986). Integrins are formed by the noncovalent association of two subunits (α and β). To date 18α and 8β genes, which are capable of forming 24 different α-β combinations at the protein level, have been identified. Some subunits are present only in a single heterodimer, however 12 contain the β1 subunit and five contain the αV subunit.

Integrins function as receptors for spatially restricted extracellular ligands including components of the extracellular matrix and several matrix associated growth-factors and proteases. The ligand specificity is mainly determined by the composition of the heterodimer. The structure of the heterodimer is composed of a large extracellular domain (1000 amino acids for α and 750 amino acids for β), a single transmembrane domain (22-24 amino acids), and a short cytoplasmic tail (15 to 58 amino acids, apart from the β_4 subunit which contains 1000 residues). On the extracellular surface integrins engage extracellular matrix macromolecules or co-receptors on adjacent cell surfaces. Integrins in the cytoplasm co-ordinate signalling complexes and cytoskeletal polymers.

Therefore, integrins are seen to have a crucial role in the tissue microenvironment, cell movement, and differentiation(Bokel et al. 2002). In non-ligated integrins (i.e. resting), the β domain interacts with the α domain, maintaining the receptor as inactive. When the cytoplasmic protein talin binds to the cytoplasmic β domain the integrin becomes activated and capable of binding extracellular ligands, which initiate cytoskeletal rearrangement and cell signalling (Calderwood et al. 2002).

Integrins themselves lack enzymatic activity; therefore they need to recruit cytoplasmic structural (e.g. talin) and signalling proteins (e.g. Src kinases) to initiate signal transduction. The activation of signalling pathways by growth factors is enhanced by concomitant activation of integrins (Alghisi et al. 2006).Integrins are capable of binding to multiple ligands, and many ligands are capable of binding to multiple integrin receptors. The most important of the ligand-integrin reactions are

summarised in Table 1.3. Integrin-ligand interactions can be divided into four main groups based on the molecular structure of the interaction, namely: arginine-glycine-aspartate (RGD) binding, an acidic motif (LDV) functionally related to RGD, A-domain β1 integrins which are involved in collagen and laminin binding, and non-αA-domain-containing laminin binding integrins(Humphries et al. 2006).

The role of integrins in stimulating angiogenesis is accomplished via four main signalling pathways: Ras-MAPK, PI3K/Akt, Rho-family GTPases, and NF-κB (Giancotti et al. 1999; Del Pozo et al. 2002; Stupack et al. 2002).

Table 1.3: Integrins and their ligands

Ligand	*Integrin*
Vitronectin	αIIbβ3, α8β1, aVβ3, αVβ5
Von Willebrands Factor	αVβ3, αIIbβ3
PECAM-1 (platelet endothelial cell adhesion molecule 1)	αVβ3
Tenascin	α9β1, α8β1
LAP-TGF-β (latency assoc. peptide transforming growth factor β)	αVβ3, αVβ6, αVβ8, αVβ1
Fibrillin	αVβ3
Fibrinogen	αVβ3, αMβ2, αXβ2, αIIbβ3
Factor X	αMβ2
iC3b (Inactivated complement component 3b)	αMβ2, αXβ2
E-cadherin	αEβ7
Collagen	α10β1, α2β1, α1β1, α11β1
Laminin	α10β1, α2β1, α1β1, α7β1, α6β4, α6β1, α3β1
Thrombospondin	α3β1, α2β1, α4β1, αvβ3, αIIbβ3
ICAM (intercellular cell adhesion molecule)	αXβ2, αMβ2, αLβ2, αDβ2
MAdCAM-1 (mucosal addressin cell adhesion molecule 1)	α4β7, α4β1
VCAM-1 (vascular cell adhesion molecule 1)	αDβ2, α9β1, α4β7, α4β1
Fibronectin	α4β1, α4β7, α8β1, α5β1, αVβ1, αVβ6, αVβ3, αIIbβ3
Osteopontin	α4β1, α4β7, α8β1, α5β1, α9β1, αVβ1, αVβ6, αVβ3, αVβ5
MFG-E8, Del-1 (milk fat globule EGF factor 8)	αVβ3, αVβ5
BSP (bone sialoprotein)	αVβ3, αVβ5

The role of the $\alpha v\beta_3$ integrin in angiogenesis was first established by studying the effects of a cyclic peptide and monoclonal antibody antagonist to $\alpha v\beta_3$ on tumours implanted onto chick chorioallantioic membrane(Brooks et al. 1994). Treatment with antagonists led to tumour regression and apoptosis of the proliferative angiogenic

cells. Using the same model, it was found that the peptide inhibited neovascularisation induced by basic fibroblastic growth factor (bFGF), tumour necrosis factor α (TNFα), and human melanoma fragments; but no effect was found on pre-existing vessels(Brooks et al. 1994). The explanation of inhibition of angiogenesis being dependent on a single integrin is countered by the fact that proliferative endothelial cells express multiple integrins. However sustained MAPK activity in chick chorioallantoic membranes is dependent on the $\alpha v\beta_3$ integrin (Eliceiri et al. 1998). Expression of non-ligated β_3 and β_5 integrins activate a caspase 8 cell death pathway, on the other hand β_3 and β_5 integrin ligation prevents this pathway from causing cell death and increases cell survival(Stupack et al. 2001).

1.6 Current methods for studying cell proliferation and angiogenesis

1.6.1 Proliferation

For several years proliferation has been assessed by microscopic analysis of mitoses (Kempson 1976). The mitotic count is defined as the number of mitoses per high power field. Although commonly used in clinical practice it is subject to limitations, including inter-observer variation, different methods of analysis, no account of cell size, and the results may be affected by the time delay between surgery and fixation (Quinn et al. 1990; Thunnissen et al. 2001). The mitotic index is the number of mitoses expressed as a percentage of the number of interphase nuclei counted, usually 1000. Although this is more standardised than the mitotic count, it is also more laborious to measure.

Alternatively, immunohistochemistry can be performed to analyse cell cycle proteins, Ki67 and proliferation cell nuclear antigen (PCNA). Ki67 is a 395kDa protein, which undergoes phosphorylation and dephosphorylation during mitosis(MacCallum et al. 1999). It is subject to proteolytic degradation, and its localisation within the nucleus changes during the cell cycle(Schluter et al. 1993). Expression of Ki67 rises in late G_1 to peak at M phase, and is low in newly divided cells (MacCallum et al. 1999; Shaw et

al. 2004). Whilst the function of Ki67 remains unclear, it appears to be vital for cell proliferation as its removal using antisense oligonucleotides prevents cell proliferation(Schluter et al. 1993).

Ki67 can be assayed using a monoclonal antibody to Ki67, or MIB1 antibody, which is directed towards an epitope of the Ki67 antigen. The advantage of MIB1 is that it can be used in formalin fixed tissue, whereas the monoclonal antibody to Ki67 can only be used in fresh frozen tissue(Brown et al. 2002). Ki67 immunohistochemical staining has been shown to be of prognostic value in breast cancer (Jacquemier et al. 1998; Haubner et al. 2005), and in subtypes of lymphoma where it may correlate with both survival and relapse-free survival (d'Argy et al. 1988; Abele et al. 1997; Mochen et al. 1997; Korkolopoulou et al. 2001; Ramirez de Molina et al. 2002). In colorectal cancer most studies suggest no correlation between Ki67 and overall survival in the primary tumour, although one study has shown correlation between Ki67 expression and metastatic disease (Kyzer et al. 1997; Brown et al. 2002). The less clear agreement between Ki67 and survival has also been shown in cervical cancer (Coleman 1991; Tsang et al. 1999; Follen et al. 2001; Graflund et al. 2002; Perumal et al. 2006). Ki67 immunohistochemistry has found a role in diagnosis by differentiating benign from malignant disease, such as follicular hyperplasia from lymphoma (Brown et al. 2002).

PCNA is involved in both DNA repair and synthesis and functions as an auxiliary protein for DNA polymerase-δ(Bravo et al. 1987). Expression of PCNA is higher in late G1-phase, S-phase, and early G_2 phase, than in quiescent cells(McCormick et al. 1992). It is tightly bound in the nucleus during DNA replication. PC10, 19A2, and 19F4 are amongst the monoclonal antibodies available for the detection of PCNA(Hall et al. 1990). Although PCNA can be detected in formalin fixed tissue, levels of expression change depending on the length and mode of fixation(Rowlands et al. 1991). PCNA is a useful prognostic marker in gastric cancer (Schipper et al. 1998).

The proportion of cells in S-phase is also a useful index of proliferation. Flow cytometry can be used to measure the percentage of cells in S phase (the S phase fraction). Results from such studies have been shown to be of prognostic importance in primary and metastatic breast cancer (Chassevent et al. 2001; Chang et al. 2003) and non-Hodgkins lymphoma(Pauwels et al. 2000). The results may be affected by technical difficulties in creating a suspension of single cells, and some conflict remains as to whether formalin fixed tissue is as beneficial as fresh tissue for analysis (Hall P.A 1991).

[3H]-thymidine is the gold standard for measuring the percentage of cells in the S phase *in vitro* (known as the labelling index, LI). This tracer has been used for many years for autoradiography and flow cytometry. Cell cultures are treated or animals injected with [^{3}H]-thymidine and cells analysed or animals sacrificed and tumours analysed one hour later. Thymidine metabolites are washed away during processing and mitotic cells counted using auto radiographic techniques. The procedure is slow, involves manual counting, and takes several weeks for the auto radiographic film to be developed. Replacement of the methyl group of thymidine with iodine or bromine yields iodo- or bromo-deoxyuridine (IUdR, BrdU), which can be used *in vitro* or *in vivo* and are incorporated into cells that are synthesizing DNA. Monoclonal antibodies or fluorescent dyes in combination with a laser cytometer detect the BrdU- or IUdR-labelled cells obtained from biopsies(Rew et al. 2000).

1.6.2 Angiogenesis

In relation to studying the rate of tumour angiogenesis, the ideal would be to study the number of new vessels developed in a region or change in vascular surface area per day. Whilst this is an attractive concept, it is limited to normal tissues with stable populations of cells as proliferation of the tumour cells in addition to vascular endothelium makes such assessments and determination of end-points difficult. Scientists have relied upon microvessel density (MVD) counted in samples from

tumour biopsies as an alternative measure. The limitations of this technique are the invasiveness of the biopsy procedure, and the heterogeneity of tumour angiogenesis as MVD is rarely uniform(Eberhard et al. 2000). As the tumour becomes larger in size, central areas may become necrotic whilst still having active angiogenesis at the periphery. Unless the biopsy includes the active area (also known as the "hot spot") then incorrect conclusions may be drawn, rendering quantification of response to treatment difficult.

The Chalkley point grid overlay morphometric technique provides an objective estimate of MVD rather than exact MVD and is calculated by counting the number of grid points which hit stained microvessels(Fox et al. 1995). High Chalkley counts were predictive of overall survival in a study of patients node negative and node positive breast cancer(Hansen et al. 2000) .As MVD is a ratio of tumour cells to vessels, changes in either component will affect the overall MVD. The fraction of apoptotic endothelial cells also needs to be considered in addition to the MVD, and can be measured using immunohistochemical measurement of single stranded DNA(Chalmers et al. 2006), or the terminal deoxynucleotidyl transferase-mediated nick-end labelling (TUNEL) assay which labels 3' free hydroxyl ends of fragmented DNA with flourescein-dUTP catalyzed by terminal deoxynucleotidyl transferase(Matsunaga et al. 2004). Anti-angiogenic therapy may be successful in reducing the number of endothelial cells and, as a consequence, the number of viable tumour cells may also decrease without a change in overall MVD. Tumour angiogenic factors also increase vascular permeability which is not a component of MVD. The same is also true for capillary size, which is abnormal in tumours and distorts the relationship between vessel number and blood volume (Miller et al. 2005).

A consensus has been reached for the determination of angiogenesis in tumour specimens(Vermeulen et al. 2002). Endothelial cell fraction is determined by double immunostaining biopsies with separate antibodies for the tumour (such as Ki-67) and the endothelium. A ratio of tumour cell proliferation to endothelial cell proliferation can

thus be obtained. Pericyte recruitment to the tumour microvasculature is thought to be indicative of vessel maturation. The pericyte coverage index uses immunostaining for CD34, CD31, and actin in tumour and adjacent normal tissue. The principle for this method came from observations in the post-natal retina that blood vessel remodelling is only possible in the absence of a pericyte covering(Benjamin et al. 1998).

Imaging of tumour vasculature can be used to study vascular parameters including blood flow, blood volume, semiquantitative and quantitative kinetic haemodynamic parameters. Sensitive techniques to measure such parameters include dynamic contrast enhanced computed tomography (CT) or magnetic resonance imaging (MRI), PET and ultrasound using microbubble technology. [15O]H_2O-PET is the most accurate method for determining tissue blood flow(Miller et al. 2005). The short half-life of 2 minutes precludes using the tracer outside centres with an on-site cyclotron. An alternative strategy is to image molecular markers of angiogenesis; the targets for such tracers include VEGF-receptor 2, $\alpha v\beta 3$ integrin, endoglin, and endosialin. With the exception of radiolabelled water PET studies, the imaging methods mentioned above are still in development.

1.7 Clinical response assessment to cancer therapy

Despite recent advances in the development of novel targeted therapeutics, the options of methods for response assessment to anti-cancer treatment rely largely upon physical changes in tumour volume. As a surrogate to tumour volume, criteria have been developed to define clinical response in solid tumours by using changes in the maximum target lesion(s) diameter, known as the Response Evaluation Criteria in Solid Tumours (RECIST)(Therasse et al. 2000), see table 1.4.

Table 1.4: The RECIST Criteria

Complete response	Complete resolution of all target lesions
Partial response	Decrease of ≥ 30% of longest diameter
Stable disease	Neither partial response or progressive disease
Progressive disease	More than 20% increase in size

The lesion diameter changes can be assessed in several ways: clinical examination, ultrasound, computed tomography (CT), or magnetic resonance imaging (MRI). The tests mentioned above for detecting physical changes in tumour volume have limitations, for each method there will be inherent variable sensitivity and specificity dependent on the type of scanner, operator, and tumour (size, location, and histological type). A recent study, which evaluated clinical examination, ultrasound, mammography, and MRI in patients who received neoadjuvant treatment for breast cancer found that the accuracy for predicting complete pathological response was 75,

89, 82, and 89% respectively, and recommended that patients continue to have histological confirmation of response(Schott et al. 2005).

Recently, the logic for using RECIST for new treatments has been questioned, as it is unlikely to be appropriate for treatments which result in cytostasis (Michaelis et al. 2006). Indeed any treatment which results in necrosis, apoptosis, or development of inflammation may not produce a decrease in physical tumour size and therefore be wrongly categorised as ineffective due to a lack of response by RECIST. The identification of progressive disease may be delayed when using the RECIST criteria compared to using the previous standard World Health Organsiation (WHO) criteria, which were based on the product of the maximum bidimensional tumour diameter(Therasse et al. 2006). The lack of a physical response on standard anatomical imaging may cause the failure of new compounds to progress beyond phase II clinical trials as size reductions of 15-20% are often expected from previous experience with cytotoxic agents(Ratain et al. 1993). PET has been found to be more accurate than CT for predicting early response of gastrointestinal stromal tumours to imatinib(Antoch et al. 2004).

One alternative has been to use time to progression (TTP) or progression free survival (PFS) as surrogate endpoints for the assessment of cytostatic agents in phase II trials. PFS does directly relate to patient benefit, which is not always the case with physical tumour size reduction. However the use of TTP is biased as it depends on how frequently evaluation is performed. The use of a control group (treated with an alternative agent) who are evaluated at the same time intervals could reduce this bias, but also requires larger numbers of patients entered into the study and results in increased expenditure(Michaelis et al. 2006).

An index of tumour viability before and after treatment is clearly required. The measurement of tumour antigens, which are detectable in serum (such as prostate specific antigen (PSA), carcinoembryonic antigen (CEA) and Ca-125) has been utilised for some years; however the sensitivity of such tests remains problematic. Serological

tumour markers for monitoring response should reflect tumour burden; an inherent principle in their use is the assumption that there is homogeneity of production of the marker by the entire tumour population which may not actually be the case.

A biomarker has recently been defined by the FDA in the United States as "a characteristic that is objectively measured and evaluated as an indicator of biologic processes, pathological processes, or pharmacologic responses to therapeutic intervention". Surrogate markers are seen as those which measure the drug effect without directly measuring the drug target. The ideal biomarker should be sensitive and specific, easily accessible for collection, simple and adaptable for clinical use. Simply because a tumour expresses a specific biomarker doesn't guarantee 100% therapeutic success for target-specific agents. In this regard, the pharmacokinetics of the drug are important, i.e. absorption of the drug, delivery of the drug to the target in sufficient quantities, metabolism (which can be affected by polymorphisms in cytochrome p450s), and excretion (which can decrease in patients with renal and hepatic impairment).

Tumour cells may possess additional molecular abnormalities allowing indirect down-stream activation of signalling cascades and bypassing the initial target. Heterotypia in the receptor phenotype is a real phenomenon, as demonstrated recently by lack of response in lung cancer patients to the EGFR inhibitor gefitinib. A point mutation in tumour DNA which resulted in a threonine-methionine amino acid switch at position 790 in the EGFR receptor was found to be responsible (Kobayashi et al. 2005). Alternative strategies involving biomarkers to predict response to treatment are currently being explored; these include the rapidly expanding fields of proteomics and gene expression profiling. These latter methods may, in the future, permit individualisation of treatment but require further wide scale validation before they can be incorporated into routine clinical care.

Response assessment needs be optomised and become more specific to the treatment target(s). Increased accuracy in determining response will enable patient

outcomes to improve, minimise prolonged courses of ineffective treatments together with their associated potential toxicities. The outlook for patients with advanced cancer remains bleak. If drug resistance could be predicted early then treatment could be tailored to an alternative agent with a superior anti-cancer effect. In this regard, a unique opportunity exists for molecular imaging of biological processes and of the signal transduction pathways which drive them as a predictive clinical tool.

1.7.1 Tumour tissue

Sampling of tumour tissue can be obtained at surgery during excision, or as a core or fine needle aspirate. Imaging technologies such as ultrasound or computed axial tomography (CT) may be necessary to guide the procedure. The tissue can then be snap frozen in liquid nitrogen and used later for Western blotting and polymerase chain reaction (PCR). Other samples are stored in paraffin prior to haematoxylin and eosin (H+E) or stained for specific molecular markers using immunohistochemistry and analysed by a pathologist. Tumour heterogeneity is a significant challenge, and biomarkers may additionally label connective tissue and stroma as well as tumour cells. To address these issues multiple biopsies are often performed, and techniques such as laser capture microdissection have been developed to obtain pure cell populations for isolation of DNA, RNA, and protein. High-throughput analysis of these samples can be achieved by using cDNA expression microarrays.

The other challenges in using tumour tissue from patients for biomarker assays include the invasiveness and safety of the biopsy procedure limiting the ability to perform serial measurements, sampling errors, and the finite amount of available tissue. The anatomical location of the tumour or tumour metastasis may in fact preclude biopsy. Obtaining biopsies to assess drug pharmacodynamics is usually performed as a research procedure, and may be difficult to justify ethically or obtain patient consent where there is no expected therapeutic gain to the individual patient.

1.7.2 In Vitro and Preclinical systems for evaluating tumour response

When choosing a surrogate tissue, i.e. a tissue other than the actual tumour, the ability to detect marker expression is crucial, for example skin biopsies are suitable for detecting EGFR but not phosphorylated ERK. One of the main disadvantages for using surrogate tissue instead of tumour is that it may not accurately reflect tumour biological events. To date few studies have been published which correlate the pharmacodynamic effects in surrogate tissue with that of tumour.

Peripheral blood mononuclear cells (PBM) are the most commonly used surrogate, primarily because of the ease of access – samples can be obtained by any health care worker trained in phlebotomy. Typically a 10ml sample of peripheral blood is taken and centrifuged at room temperature for 15 min at 2500 rpm. The mononuclear cell layer is then diluted with PBS to 50 ml and sedimented at 1200rpm for 10 min(Di Paolo et al. 2007). The cells are then re-suspended and counted. Finally the lysates are dialyzed and lypohilized, subjected to electrophoresis on SDS-polyacrylamide gels, transferred to nitrocellulose, and probed with the relevant primary and secondary antibodies.

Skin sampling is also relatively non-invasive and can be performed as an outpatient procedure. Multiple biopsies can be taken with minimal morbidity. The development of gefitinib (an epidermal growth factor receptor, EGFR, inhibitor) is an example of where skin biopsies provided an important role in assessing drug pharmacodynamics. Typically 0.5cm^2 of tissue is taken and then either studied immediately, frozen or embedded in paraffin for analysis later. This technique is useful for immunohistochemistry and analyses which depend upon the PCR, but unfortunately the amount of tissue is insufficient for Western blotting.

Buccal mucosa cells are the easiest surrogate tissue to obtain, their procurement is painless and can be achieved by any healthcare worker. Due to their high turnover rate, they are useful in the study of anti-proliferative agents (Adjei et al. 2003). Like skin however, the size of the samples limits their utility to

immunohistochemistry and PCR. The technique involves patients fasting, as digestive enzymes in the mouth may reduce the number of cells available and interfere with the results. Immediately prior to sampling patients rinse their mouths with 100 ml of saline twice, and then a wooden tongue depressor is used to scrape the inside of the mouth. The samples (usually four in total) are then spread onto separate microscope slides and then dried and fixed in acetone prior to storage(Bartelink et al. 2000).

The use of such systems depends upon the same pathways and same dose response relationship being present in the tumour as in the surrogate tissue. Drug resistance mechanisms present in the surrogate tissue are also important. The use of surrogate tissues still requires further validation leaving the gold standard as tumour biopsies.

In the preclinical setting (in vivo and in vitro), tumours can be selectively modified to optimise the assay with gene transfections and knockouts, experiments can be performed multiple times with the same cell population, and homogeneity exists in the cell lines and animal models used for hypothesis testing. Pre-clinical evaluation of tumour chemosensitivity is essential for drug development. Tumour xenografts represent one of the most common mechanisms for this approach, and provide an excellent method of target validation. In vitro studies of biopsy tissue and cell cultures have the ability to detect changes in molecular biology which lead to tumour growth and sensitivity. Several factors such as the host environment, tumour genotype, and immune system are challenges of this methodology. Translation into clinical practice is not always straightforward, for example striking responses seen in mouse tumours treated with the anti-angiogenic agent endostatin were not translated into human response(O'Reilly et al. 1997; Herbst et al. 2002).

In vitro assays can be used to test chemosensitivity or chemoresistance of tumour cells(Krasna et al. 2003). The assays comprise of 4 basic steps: isolation of cells, incubation of cells with drugs, measurement of cell survival, and interpretation of the result. Although chemoresistance assays have a high predictive value for excluding

ineffective drugs, no prospective trial using either chemosensitivity or chemoresistance assays has been shown to improve patient survival. For example, such an in vitro assay was used to evaluate cytotoxic chemotherapy in 77 patients with breast and ovarian tumours and compared to clinical response. The overall positive predictive value for chemosensitivity was only 50%, however the negative predictive value (i.e. for chemoresistance was 100%)(Agiostratidou et al. 2001).Whilst chemosensitivity assays remain an exciting concept in drug development, their use is currently not recommended outside a clinical trial setting(Schrag et al. 2004).

Human xenografts, transgenic, and orthoptic models.

The models described below are commonly used in drug development today. Fundamentally what is required is a model which is accurately predictive of clinical response in humans. Murine models were initially developed 50 years ago. The use of human xenografts in immunodeficient mice has played a vital role in assessing anti-tumour activity of new drugs(Sausville et al. 2006). Typically the mice are divided into a treatment and control group, and response is defined by size reduction of the transplanted tumour. Limitations of the technique include the rapidity of tumour growth compared to humans, absence of metastases, expense, and lack of characterisation of response at the molecular target. Implantation of human tumours in mice may affect tumour biological features such as their metastatic potential which can be much lower in the mice compared to patients, though the correlation with human tumours is thought to be better for orthoptically transplanted tumours compared to tumours which are transplanted into subcutaneous or intramuscular sites. Despite the massive efforts in research using xenografts, only a limited number of drugs which are clinically active at well tolerated doses have been developed(Troiani et al. 2008).

Orthoptic models (where the tumour is implanted into their natural sites) offer an alternative to xenografts, as do transgenic models where spontaneous development of specific tumours occurs due to oncogene transfections(Hoffman 1999).

Examples of such models include spontaneous orthoptic bone metastasis models of breast, prostate, and lung cancer.

Over the past two decades preclinical evaluation systems have evolved from testing non-specific cytotoxic agents in general tumour types to target specific systems. By using PET in a preclinical setting, valuable information about precise mechanisms of drug resistance can be obtained and correlated with specific biomarkers from ex-vivo tumour specimens. MicroPET systems are essential for the development of new PET radiotracers, and are now being recognised as a method which can expedite drug development. This technology allows correlation of in vivo PET data with events happening at the molecular level enabling technologies such as gene therapy and hypoxia probes to be developed (Groot-Wassink et al. 2002; Barthel et al. 2004).

1.8 PET As A Tumour Biomarker

One technique which has already gained wide acceptance as an imaging biomarker is positron emission tomography (PET) using 2-[18F]fluorodeoxyglucose (FDG) (Larson et al. 2006). PET is the most sensitive method for imaging molecular processes in vivo. By imaging regions in their entirety it can provide a quantitative measure of regional variation in metabolic processes. Compared to other methods for studying molecular processes that typically involve biopsies, PET is non-invasive which enables serial studies to be performed. Criteria and recommendations for using FDG-PET to stage and measuring tumour response to treatment have been established(Young et al. 1999).

In America FDG-PET scans are reimbursable for the following tumours/lesions: solitary pulmonary nodule, non-small cell lung cancer, oesophageal cancer, colorectal cancer, melanoma, lymphoma, head and neck (excluding central nervous system), breast, and cervical cancer(Czernin et al. 2002). The majority of indications in

oncology are for diagnosis and staging; apart from breast cancer where there is an allowance for monitoring response of locally advanced and metastatic disease when a change in therapy is anticipated(Czernin et al. 2002).

FDG is the most commonly used tracer for PET studies, however changes in FDG uptake may occur due to other biological processes which affect glucose metabolism such as inflammation. More specific radiotracers are currently being developed. Probes for PET are developed by identifying a target process and then synthesizing a positron-labelled molecule which can be used as a surrogate biological assay. Generally, the PET imaging probe traces between one and four steps of a biochemical process. This enables kinetic analysis to estimate the concentration of the reactants over time and measure the rate of the process.

In drug development, pharmacokinetic studies of tracer doses of radiolabelled drugs can be given as a pre-Phase 1 clinical trial, or as part of phase 1 and 2 studies (Aboagye et al. 2003). PET can provide information about the distribution, excretion, and metabolism of drug in tumours and normal tissue. Examples of drugs which have been directly labelled with radioisotopes and used as PET probes include: a methylating agent used in the treatment of glioma [11C]temozoloamide (Brown et al. 2002), the alkylating agent [11C]-1,3,bis(2-choloroethyl)-1-nitrosurea(BCNU) (Tyler et al. 1986), a topoisomerase inhibitor [11C]-N-[2-9dimethylamino)ethyl]acridine-4-carboxamide (DACA)(Brady et al. 1997), [13N]cisplatin (Ginos et al. 1987), the anti-pyrimidine [18F]-5-fluoruracil (Dimitrakopoulou-Strauss et al. 1998), and [18F]tamoxifen(Inoue et al. 1996).

PET-based pharmacodynamic studies can utilise selective or generic biological endpoints. Typical examples of generic endpoints include changes in glucose utilisation (FDG), proliferation ([11C]thymidine or [18F]fluorothymidine), amino acid metabolism ([11C]methionine or methyl-fluorodopa), and tricarboxylic acid cycle activity (using [11C]acetate). Specific biological endpoints using selective tracers include: thymidylate synthase inhibition using [11C]thymidine (Wells et al. 2003),

hypoxia using [18F] labelled nitroimidazoles(Valk et al. 1992; Rasey et al. 2000), and detection of oestrogen receptor status and Erbb2 status with 16-α-[18F]-17-β-oestradiol(Mortimer et al. 1996) and [68Ga] labelled trastuzumab(Smith-Jones et al. 2006), respectively. With the exception of FDG, validation studies are being performed to assess the clinical utility of these probes.

The anatomical resolution of PET images is low, however combination of PET with CT or MRI should optomise lesion detection and monitoring(Delbeke et al. 2006). The metabolism of the PET tracer is also an important consideration as PET cannot distinguish between the injected compound (referred to as the parent) and its metabolites. Therefore PET probes should ideally be metabolised slowly, otherwise a method for calculating the concentration of metabolites is required to determine their contribution to the PET signal from a region of interest(Shields et al. 1992). The concentration of metabolites can be measured in arterial blood during dynamic studies calculated by sampling blood from the radial artery together with various correction methods.

This thesis will focus on pharmacokinetic analyses of new radiotracers in clinical PET. Before discussing the specific PET radiotracers, a general overview of cancer imaging is presented below.

1.9 Physical Imaging in Cancer

Successful diagnosis and treatment response monitoring in cancer is dependent upon adequate imaging techniques. This section will focus on physical imaging, and will be followed by a more detailed explanation of molecular imaging technologies, with a focus on PET which is the subject of this thesis.

1.9.1 Ultrasound

Ultrasound relies on sonar technology to form pictures of the region of the body being scanned. A transducer is held over the region and emits a high frequency sound wave which is then reflected back by the tissues at different rates (depending on their density) and detected by the transducer. Cystic structures do not return the signal such as the bladder will appear dark, and on the reverse solid structures such as stones appear white.

The advantages of the technique are that it is painless, does not involve ionising radiation, the images reflect real-time, it can be used to assist other procedures e.g. needle biopsy of a breast mass, and compared to other technologies it is relatively straightforward to use and inexpensive. The disadvantages are that it has limited repeatability as it is highly operator dependent, obese patients may have suboptimal images due to body habitus interfering with sonar transduction, and finally it is not good for imaging bony and air-filled structures (such as the lungs). In oncology ultrasound is used mainly for the detection of metastases in the liver, breast imaging to determine the size and location of lesions, for detection of gynaecological cancers, and as said above, as a targeting aid for tumour biopsies.

For studying breast cancer, ultrasound is optimal for detecting small lesions in pre-menopausal women with dense breasts and for differentiating solid from cystic lesions(Benson et al. 2004). In a study of 67 patients, breast ultrasound was found to underestimate the size of the tumour by 40% when compared to pathological findings (Van Goethem et al. 2004), and another study found a correlation of only 0.45 between ultrasound measurements and pathological size(Davis et al. 1996). Recent developments in ultrasound technology include the use of microbubbles as contrast agents e.g. for the detection of liver metastases(Blomley et al. 2002; Cosgrove et al. 2004). The microbubbles are gas particles covered in lipid or lipoprotein shells which reflect sound leading to increased brightness on the ultrasound image.

1.9.2 X-ray

X-ray is the most commonly used imaging modality in modern medicine today. The principle on which it is based involves directing a beam of photons through the patient onto a film, and the resulting image represents a map of tissue opaqueness to the photon beam. Different strengths of photons can also affect the image so that lower energies are used for mammograms (typically 40 kilovolts) compared to x-rays of more solid structures such as bone.

Mammography is used for diagnosis of breast cancer both as a screening tool and in the assessment of symptomatic patients. It remains the test of choice in women with non-dense breasts. Typically suspicious areas are seen as abnormal microcalcifications. The limitations of mammography include its inability to separate tissues of different densities, and difficulties in detecting lobular carcinoma, Paget's disease of the nipple, inflammatory breast carcinoma, and small peripheral tumours.

Computed tomography (CT) is a form of X-ray where the beam and detectors are physically rotated around the patient. The data are acquired in 2D and can be reconstructed to form 3D images, with excellent anatomical resolution. CT is commonly used for the staging of tumours and for monitoring response. In breast cancer, the main utility is for visceral metastases as its use is limited for detecting primary lesions. The dose of radiation in CT scans is viewed as moderate to high, for example the effective dose of a chest CT examination is 5.8mSv compared to 0.01mSv for a standard chest X-ray.

1.9.3 Magnetic Resonance Imaging (MRI)

MRI is used widely to determine tumour morphology, define tumour location, and extent of tumour size and depth of invasion into local and distant tissues. The use of gadolinium based contrast agents can provide additional information by enhancing visibility of lesions particularly in brain studies, where abnormal uptake can be seen in tumours due to abnormal blood vessel growth and/or breakdown of the blood-brain barrier. Dynamic contrast enhanced MRI (DCE-MRI) is used to obtain information of contrast uptake overtime so that kinetic parameters such as the permeability-surface area product and rate of uptake of the agent (Ktrans) from the vascular space can be defined(Padhani et al. 2004).

Recently DCE-MRI was used to measure changes in tumour angiogenesis in inflammatory breast cancer treated with the anti-VEGF agent, bevacizumab (Wedam et al. 2006). Diffusion weighted MRI is used to measure parameters associated with the rate of diffusion of water molecules without the need for contrast. Functional MRI (fMRI) is relies upon venous oxygenation (i.e. deoxyhaemoglobin) to act as an endogenous contrast agent, so that local changes in deoxyhaemoglobin levels lead to altered signal intensity. To date the main utility of fMRI has been in neurological studies.

The advantages of the aforementioned magnetic resonance techniques are the lack of radiation used and high spatial resolution of the produced images which allows in-depth studies of anatomy (which is higher for standard MRI compared to DCE-MRI and fMRI). The disadvantages include suboptimal imagining of bony structures, cost, and the inability to study patients with implanted objects such as cardiac pacemakers. In breast cancer, MRI is mainly used for tumours which are difficult to image by other techniques e.g. lobular carcinoma which has a diffuse growth pattern, and for diagnosing metastases to the central nervous system.

Magnetic resonance spectroscopy (MRS) can distinguish and measure the concentration of different chemical compounds non-invasively. MRS provides distinct

chemical spectra instead of anatomical images. Biological processes such as proliferation and apoptosis can result in changes in the phospomonoester and fructose-1,6-biphosphate peaks. The radioisotopes used for MRS include: [1H], [13C],[19F] and [31P]. MRS studies can be combined with MRI as a useful tool for drug development, although the sensitivity of MRS needs to be improved for pharmacokinetic studies as currently only drugs given in quantities of $\geq 0.5 g/m^2$ can be detected (Workman et al. 2006).

1.10 Nuclear Imaging

Nuclear imaging employs a gamma camera to detect gamma rays emitted by compounds labelled with radioisotopes to study human anatomy and physiology. The radionuclide can be administered to patients via inhalation, injection, or ingestion.

1.10.1 The Gamma Camera

The gamma camera was invented by H. Anger in 1952, and further modified in 1957 by the addition of photomultiplier tubes. Since then, it has changed little since its original design and is widely used in clinical medicine today. One of the commonest isotopes used for radiolabelling compounds under study is Technetium 99m, which has a half-life of 6 hours.

After emission from the body, the gamma particles pass through a collimator and are projected onto a detector crystal made of thallium-activated sodium iodide. The rays then react with the iodide ions of the crystal by the photoelectric effect or Compton scattering to cause the release of electrons, which in turn react with the lattice of the crystal to produce light by a process known as scintillation. The light is detected by photomultiplier tubes which lie behind the crystal and converts the energy into electrons. As only a small amount of light is emitted by the scintillation detector, the electron signal is multiplied many times by the photomultiplier tubes into a large cluster of electrons which are converted into an electrical pulse by an anode at the

base of the photomultiplier tube. A typical gamma camera contains 37-91 geometrically arranged tubes. Position logic circuits follow the array of the tubes, and receive the impulses in a summing matrix circuit. Finally the data are reconstructed into a 2-dimensional (2D) image by a computer.

1.10.2 Planar Imaging

For this application the camera remains stationary over the patient and acquires data from only one angle. In oncology this is commonly used to diagnose bone metastases. Dynamic planar imaging refers to the situation where a series of images is acquired over time, thereby allowing the motion of the radiotracer through the body to be detected; this technique is used to measure the glomerular filtration rate in the kidneys(Delpassand et al. 2000).

1.10.3 SPECT

In single photon emission computed tomography (SPECT) the gamma camera is rotated around the body on a gantry, so that a variety of different angles can be observed and then reconstructed into a 3-dimensional (3D) image. In oncology it is used for the detection of bone metastases and neuroendocrine tumours. Compared to planar imaging, the images are susceptible to artifacts, attenuation, and poor resolution (Kjaer 2006). Mathematical algorithms are used to compensate for attenuation.

PET and SPECT can detect picomolar concentrations of radiotracers, however PET is more sensitive. SPECT is less expensive and does not require the presence of an on-site cyclotron. The tracers used in SPECT have longer half-lives than those used in PET. Typical SPECT radionuclides include ^{99m}Tc (6 h), ^{111}In (2.8 days), ^{123}I (13.2 h) and ^{125}I (59.5 days). Recently, preclinical studies of apoptosis have utilised [^{99m}Tc]-annexin-V SPECT to monitor response to radiotherapy in patients with

lymphoma (Haas et al. 2004). Other uses for this technique include the diagnosis of cerebrovascular disease, Alzheimer's disease, and determining the origin of infection.

1.11 Basic Principles of PET

Positron emission tomography (PET) differs from SPECT in that two gamma rays 180^0 apart are detected simultaneously. The first PET camera for human studies was built for by Hoffman, Ter-Pogossian, and Phelps in 1973 at Washington University, USA. The original tracers at that time were used to image regional blood flow in the lungs.

The radiotracers used in PET are isotopes of carbon, nitrogen, oxygen, and fluorine (also used as a substitute for hydrogen), which have a closer resemblance to naturally occurring compounds within the body than those used for SPECT (e.g. Xenon-133, Technetium-99, Iodine-123), therefore they are less likely to alter the biochemical properties of the compound which has been labelled. Positron emitting compounds do not normally exist in nature, and are produced by a cyclotron which uses powerful electric and magnetic fields to accelerate charged particles to high energies. These then bombard stable atoms in a target to produce proton-rich radioactive isotopes. Generators can also be used to produce positron emitting isotopes, such as [68Ga]. As the half-lives of the radionuclides used in PET are shorter than SPECT, production of radioactive isotopes such as [11C] generally requires the presence of an on-site cyclotron; however these properties of PET radiotracers do allow patients and normal volunteers to be studied with acceptable low doses of radiation. The reactions used to produce the radioisotopes in this thesis are shown in Table 1. Another advantage of PET over SPECT is that the collimation is electronic in PET (compared to SPECT where physical collimation is used) resulting in increased sensitivity and uniformity of the point source response function.

The basic principle of gamma decay is the same in PET as for SPECT; however in PET gamma decay is preceded by beta decay as the radionuclides used are positron (positive electron) emitters. After administration, a positron is emitted by the radionuclide to reduce the excess positive charge of the nucleus and render it more stable.

After travelling a short distance the positron collides with an electron in tissue to form a positronium that annihilates into two gamma rays of equal energy shown in Figure 1.7 (511 keV), along a line 180° apart known as the line of response (LOR), which are detected and used to quantify and localise the position of the positron emitter. This final process is known as simultaneous coincidence detection, and allows the annihilation event to be placed in the centre of a line between the two detectors on opposite sides of the object (Figure 1.8).

Figure 1.7 Positron decay

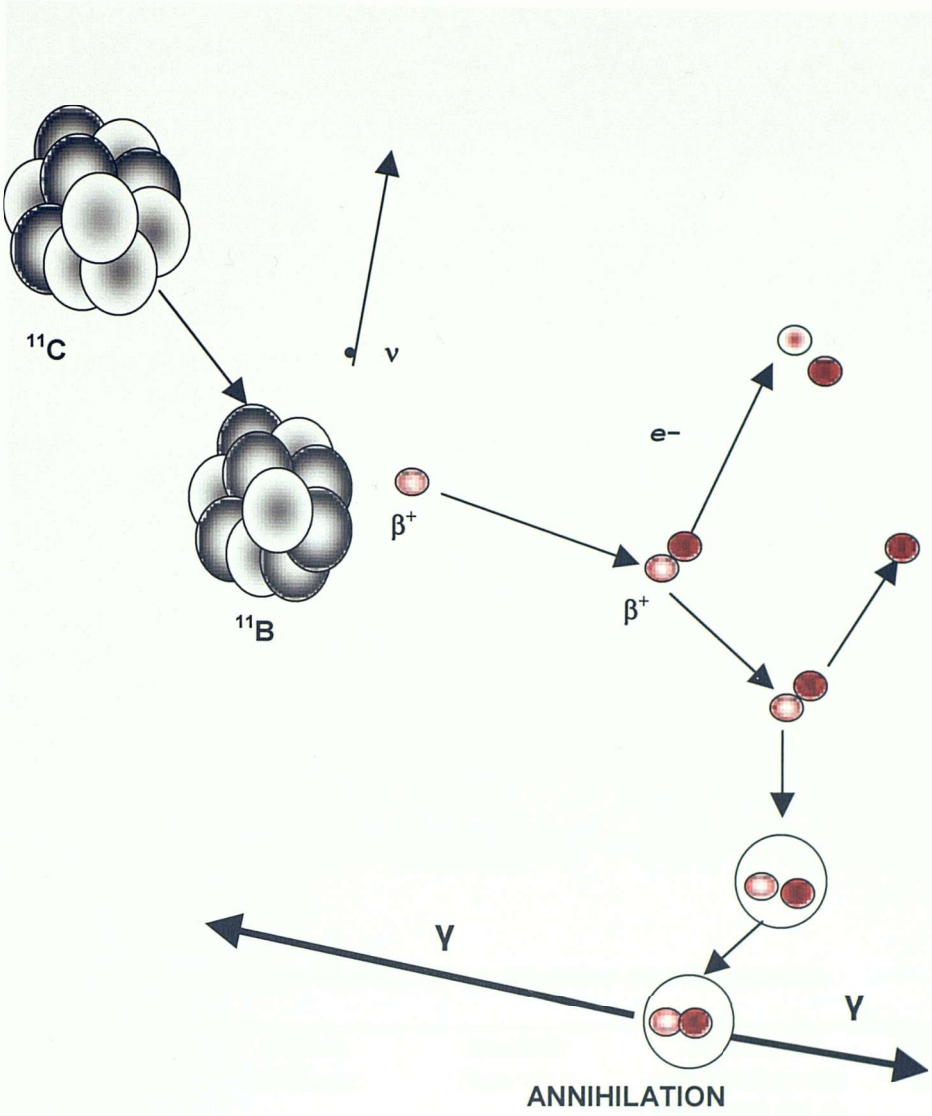
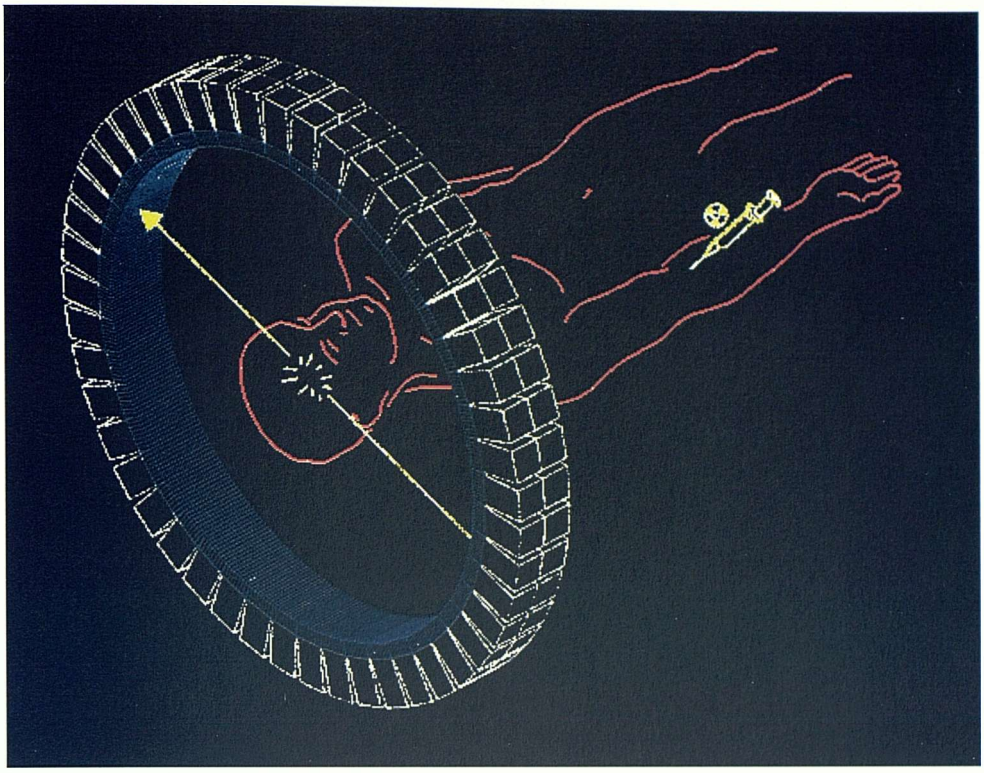


Figure 1.8: Annihilation detection



The characteristics of the radioisotopes used in this thesis are shown in Table 1.5 below.

Table 1.5. PET radioisotopes: Characteristics and Production.

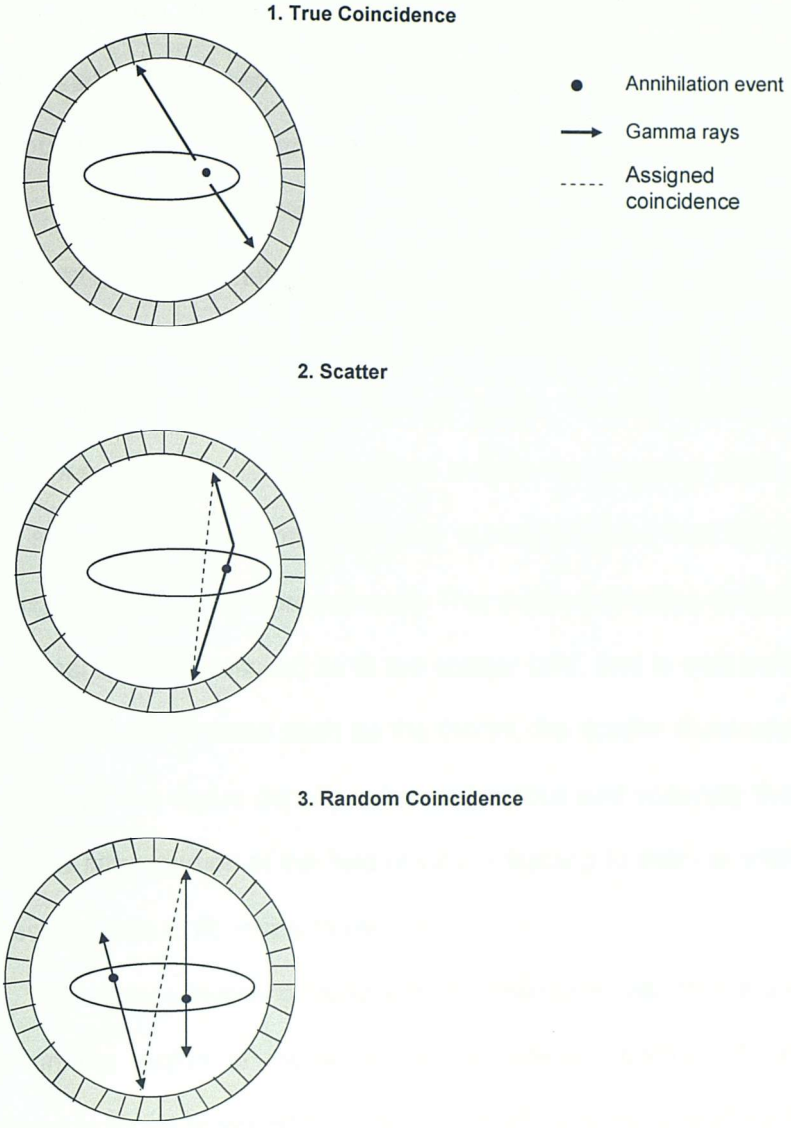
Positron Emitter	*Stable Element*	*Nuclear Reaction*	*Number of protons(p) and neutrons (n) in product nucleus*	*Half-life ($t_{½}$ of product) in min*
^{11}C	Nitrogen (^{14}N)	^{14}N (p,α)^{11}C	6p,5n	20.4
^{18}F	Oxygen (^{18}O)	^{18}O(p,n) ^{18}F	9p,9n	109.8
^{15}O	Nitrogen (^{14}N)	^{14}N(d,n) ^{15}O	8p,7n	2.03

1.11.1 Coincidence detection

PET is significantly more (approximately 100 x) efficient and provides better spatial resolution than SPECT, as two gamma rays are detected simultaneously compared to SPECT where only one ray is detected at a time. Modern PET detectors consist of thousands of coincidence detectors. If annihilation occurs outside the

volume between the detectors, only one gamma ray will be recorded and since this is not a coincidence event the event will be rejected.

Figure 1.9. Coincidence and Scatter Detection



1.11.2 Scatter and Attenuation

Scatter occurs when the gamma rays change direction without (coherent) or with (incoherent) energy loss. The incoherent form of scattering is known as Compton

scattering. This is predominant at 511keV in the body and is thus totally responsible for the removal of a gamma ray/photon from a line of response (the line along which two coincident photons travel), and is referred to as attenuation. Correction for attenuation is used to obtain an accurate measurement of the regional distribution of radioisotope within the field of view of the scanner. The inclusion of scatter within reconstructed data lessens the contrast between different regions and can cause inaccuracies in measurement of activity concentration.

Four alternative scatter correction techniques have been proposed for PET: i) empiric approaches, ii) methods based on two or more energy windows, iii) convolution (or equivalently, deconvolution), and iv) methods which model the scatter distribution on an initial estimate of the scatter-free image. Empiric approaches are based on observations that coincidences recorded outside the boundary of an object are entirely due to scatter (with randoms previously subtracted) and that the scatter distribution contains mainly low spatial frequencies. This method employs an analytic function (e.g. a one-dimensional Gaussian) to fit the scatter tails, and is well suited to neurological studies. However, in areas such as the thorax, the scatter distribution may not always be smooth as the tissue density is heterogeneous and secondly the object of interest occupies a large portion of the field of view – leading to over- or under-subtraction and small scatter tails to fit, respectively.

Techniques involving multiple energy windows rely on i) a greater proportion of scatter in the region of the single photon energy spectrum below the photopeak, compared to those recorded near the photopeak (i.e. the characteristic energy emitted by a radionuclide), and ii) there is an energy threshold above which only unscattered photons are recorded. Therefore data recorded in energy windows below or above the photopeak can be used to estimate the amount of scatter within the photopeak window.

In contrast to energy-based methods, the convolution methods for scatter correction employ an integral transformation of the projections recorded in the

photopeak window. Originally developed for 2D scanners, this method consisted of convolving the measured projection data line by line with an experimentally determined scatter function and then subtracting the resulting scatter estimate from the measured projections, and has since been modified for crosslane scattering for large area PET scanners and multi-ring scanners with the septa retracted. The advantage of these techniques is their low noise scatter estimates. As with the previous method, this is reliable for neurological studies, but is less robust for the thorax. Another limitation of this method is that it fails to account for scatter arising from activity outside the scanner's field of view(Bailey 1998).

The final method involves modelling photon interactions in matter and estimate the scatter contribution to projections given an accurate map of attenuation coefficients in the scattering medium and initial estimate of the scatter-free radioactivity distribution. Whilst this method is potentially more accurate than the others above as they use well understood physical principles to produce precise scatter estimates, it is complex to implement, computationally demanding, and requires assumptions to model scatter arising from activity outside the axial field of view.

1.11.3 Dead Time

During the time that the detector electronics connected to the photomultiplier tubes take to process each event they are unable to record any other events within that period, meaning that some may be missed – this is known as dead time. Data must be corrected for dead time to obtain accurate quantification. The fundamental determinant of dead time is the rate of single events that are striking the detectors. Tomographs continuously record this rate and use it as a basis of the calculation of dead time correction factors. For *in vivo* studies dead time correction is thought to be accurate to within 5% of the range of counting rates, however the magnitude of the correction factor should not be too large, and scanning should not be carried out near to or beyond the peak of the trues curve.

1.11.4 Random Events

A true or real event is a detection of two photons (within the coincidence timing window) originating from one annihilation. A random event is a detection of two photons within the coincidence timing window which did not originate from one single annihilation event. Prompts are all detected coincidences. By having a delayed circuit where one detector is delayed by e.g. 100ns relative to the other it is possible to calculate the number of randoms, as any coincidence events recorded in the delay circuit cannot be true. Then by assuming that the number of delayed events is equal to the number of randoms in the primary circuit, the number of true events can therefore be determined by subtracting the calculated number of randoms from prompts in the primary circuit.

1.11.5 Detector efficiency

The detector efficiency is defined as the probability of a detector registering an event when a gamma ray intersects with it. In the scanner used in this study the scintillator detector is made from bismuth germinate oxide (BGO) crystal. The typical efficiency of BGO arranged in blocks is 64% for 511KeV gamma rays(Townsend et al. 1993). For each detector this is liable to change over time. To monitor detector efficiency, weekly tests using uniform phantoms are performed in the PET scanner. The results are then applied as a correction factor to the reconstructed PET data. Another correction factor, termed "z-scaling" allows for non-uniformity of detector efficiency along the longitudinal axis (z axis) in the field of view, this is also applied post-reconstruction. The process by which data is corrected for efficiency is known as normalisation.

1.11.6 Attenuation

This describes the loss of detection of true coincidences due to their attenuation within body tissues. Without attenuation correction, significant artifacts which may occur on PET include: (1) prominent activity at body surface edges due to relative lack of attenuation at the surfaces compared to deeper structures, (2) distorted appearance of areas of intense activity (e.g. urinary bladder) due to variable degrees of attenuation in different directions of activity originating from these areas, and (3) diffuse, relatively increased activity in tissues of relatively low attenuation (e.g. lungs). To correct for attenuation a transmission scan is performed with the patient in the scanner prior to injection of the radiotracer. In this study, rotating ^{68}Ge rods ($t_{½}$ of 270.82 days) were used as the positron emitting source for the transmission scan which lasted 20 minutes. The count rate is measured for all possible lines of response (LOR), the line along which the coincidence event occurred. A blank scan is performed on a daily basis prior to any patient scans, and the ratio of blank counts to the transmission counts yields a correction factor which can be applied to each line of response.

Figure 1.10 below, represents one of the unique features of PET, i.e. that for a given coincidence line, the probability of attenuation is the same for any source, independent of its location along the line, even if the source is external to the object. Therefore by using a transmission source which is external, attenuation correction is straightforward. If we consider a point source located x cm inside a cylinder of diameter D, with a linear attenuation coefficient of the cylinder material μ, then the proportion of emitted photons that reach the nearest detector is $e^{-\mu x}$ and the proportion of photons that reach the farthest detector is $e^{-\mu(D-x)}$. For a certain initial count rate (N_0) the number of detected coincidences (N) is determined by combining these tow probability terms:

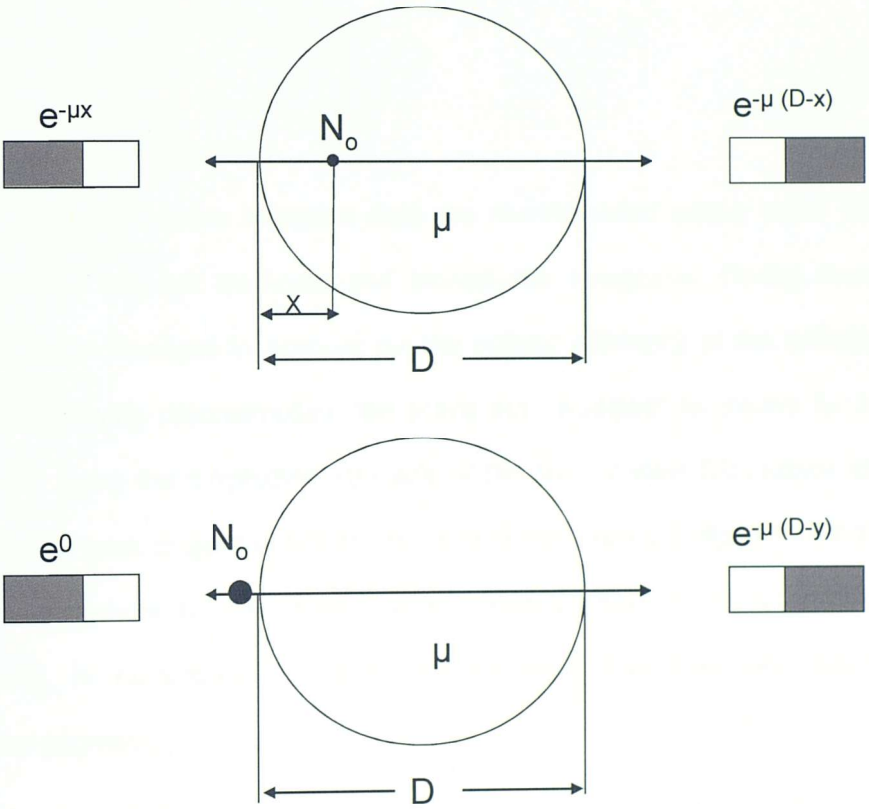
$$N = N_0 (e^{-\mu x} e^{-\mu(D-x)}) = N_0 e^{-\mu D}$$

Thus, the probability of coincidence detection is independent of source depth, x. This is true even if the source is positioned outside the body. In this case the probability terms are e^0 and $e^{-\mu D}$ for the nearest and farthest detectors respectively and the number of detected coincidences is:

$$N = N_0(e^D e^{-\mu D}) = N_0 e^{-\mu D}$$

which is the same as that obtained for the internal source. Therefore the probability of attenuation for all sources can be determined by comparing the count rate from a transmission source, with the unattenuated count rate from the same source when the patient is not in the tomograph; this is referred to as a blank scan.

Figure 1.10 Attenuation in PET



A transmission scan lasts 20 minutes on average to acquire, and is normally performed prior to administration of the radiotracer, although it can be performed afterwards. The transmission count rate is measured for all possible lines of response using one or more rod or point sources that rotate around the patient, or alternatively, using a stationary ring source. Typically the transmission source contains a positron emitter with a long half-life, e.g. ^{68}Ge ($t_{½}$ 275 days), which is retracted behind lead shielding when not in use. An alternative, more efficient option, is to employ a high-energy single photon emitter such as ^{137}Cs ($E\gamma$ = 667 keV) and acquire the data in "singles" mode. This latter approach is more suited to septaless 3D scanners where dead-time is a challenge for coincidence-based transmission scanning. Attenuation correction factors can also be derived from spatially co-registered X-ray CT data in combined PET/CT systems.

1.11.7 Data reconstruction

After annihilation detection data are reconstructed (using either filtered back projection or iterative methods) and binned into sinograms. During reconstruction, images are normalised to account for the current efficiency of the different detector blocks. Following reconstruction, the scans are "z-scaled" to correct for the varying efficiency along the longitudinal (z-) axis of the field of view (Grootoonk et al. 1996). The filtered back projection (FBP) algorithm is the standard algorithm of tomography and is equivalent to the direct Fourier reconstruction in the limit of continuous sampling. In comparison, iterative reconstruction algorithms are independent of detector geometry.

1.11.8 Partial volume effect

Partial volume effects encompass: i) poor spatial resolution due the constraints of the imaging system leading to spillover from surrounding structures, and ii) image sampling, resulting in altered intensity values for a particular region of interest(Soret et

al. 2007). The sensitive volume has dimensions approximately equal to twice the FWHM resolution of the reconstructed image. The partial volume effect results in small objects (i.e. those smaller than twice the system resolution) having an apparent reduction in isotope concentration and overestimation in the size of the object. A number of methods have been proposed for partial volume correction. Resolution recovery techniques can be applied to the data prior to reconstruction, or by using an iterative reconstruction framework. However if the size of the object approaches the resolution of the imaging system then the measured dimensions are unreliable unless there are co-registered images from CT, MRI. Finally, spill-over and partial volume effects can be built into the kinetic model and their magnitude estimated along with the physiological parameters of interest. This technique does not require anatomical co-registration but may reduce the accuracy of the modelled parameters, especially for noisy dynamic data.

1.11.9 Noise

Statistical noise in PET images results from the limited number of counts in each pixel, and the randomness of radioactive decay. Image noise (random variations in pixel intensity) is decreased with more counts, which in turn are obtained by scanning longer, injecting more radiotracer, or improving the efficiency of the scanner for detecting emitted radiation. The injected dose of radioactivity is limited by safety constraints including the potential for short-term and long-term damage to DNA, however generally the highest dose possible within the safety range should be administered. In some cases, the amount of tracer cannot be increased because of dead time and random event rate limits in the camera.

The efficiency of the camera also limits the sensitivity of coincidence detection which is only 0.5% in 2-D mode, with a scintillation crystal efficiency of only 50-80%, depending on detector material and size. In 3D septa-less mode the PET scanner can

only detect 1-3% of the annihilation events; even when there are no photon attenuation effects (Bailey et al. 1991).

Noise is also influenced by the reconstruction process, corrections for random and scatter coincidences, attenuation, detector non-uniformities, and the size and location of the region of interest (Carson et al. 1993). The duration of the scan is dependent on the physical and biological half-lives of the radiotracer, and is influenced by patient comfort, as longer scan times lead to potentially more errors due to motion.

The design of the scan protocol has therefore to be optomised to allow a balance between the permissible dose of radiation to the patient, tracer characteristics, camera sensitivity, and the type of study required.

1.11.10 Resolution

Resolution in PET is defined by the minimum distance between two point sources to be interpreted as separate, and is known as the full width at half maximum (FWHM). The FWHM is variable for different types of scanners, but at present varies between 4 - 8mm for clinical scanners. The type of acquisition i.e. two-dimensional, 2D, or three-dimensional, 3D, can also affect resolution. The resolution of a PET scan can be affected by several factors including the physical dimensions of the detector elements, the distance the positron travels in tissue before annihilation and the deviation from strict co-linearity between emitted annihilation photons. The in plane spatial resolution is characterised by the spread of a point or line source in the reconstructed image along a line from the centre of the gantry to the source position (radial) and perpendicular to that line (tangential); producing the line spread function (LSF). The LSF is the commonest measurement of spatial accuracy in PET and also defines the limit of spatial resolution for the PET image. The shape of the LSF is dependent on the width of the detectors, the type of reconstruction method, and the precision with which the tomograph has been reconstructed. The FWHM is equal to the LSF at its widest value divided in two. The most constant region for LSF

measurements is the central third of the region between coincidence detectors, and therefore that region constitutes the most useful field of view for accurate measurements in PET.

The accuracy of localisation by PET is physically dependent on the energy of positron emission, which is related to the individual isotope. The point of interest is the position of the positron emitting nuclide; however the inaccuracy of localisation increases with increasing kinetic energies which is reflected by an increase in FWHM.

The accuracy of annihilation coincidence detection is limited by the intrinsic motion of the electrons and positrons at the time of capture, as they are not completely at rest there is deviation of the annihilation photons from the normal 180° angle to each other. The angular distribution of this non-colinearity has been described as +/- 0.3° (Hoffman 1986). However, in a tomograph with 6mm resolution (FWHM), the above two effects contribute less than 1mm with the commonly used positron emitters.

Loss of resolution can also occur due to patient motion during the scan. To prevent this happening patient comfort is made a priority and scan times are minimised as much as possible. In the case of brain studies, a head holder can be used. Patients are constantly observed during the scanning period, and if any movement occurs the time is recorded. Diaphragmatic motion during respiration is particularly relevant in scans of the thorax, and if the scan is not long enough to allow time averaging over enough breaths the data will be inconsistent and subject to artefacts. A technique known as gating has been developed for use in respiratory and cardiac imaging which freezes the motion of the lungs or heart relative to the respiratory and cardiac cycles respectively(Saab et al. 2003; Livieratos et al. 2006).

1.11.11 Two dimensional (2D) and three dimensional (3D)PET

The images acquired during a PET scan provide information about the 3D distribution of radioactivity within the subject. 2D PET and 3D PET relate to the physics

of acquisition, i.e. in 2D PET septae made from lead or tungsten are present between the detector rings, whereas in 3D PET acquisition is without septa. The purpose of the septa is to reduce the registration of random and scattered events. 2D PET acquires data in a number of contiguous planes or slices, with each plane consisting of data from coincidences either within an individual ring or in closely adjacent rings. The disadvantage of using septa is that it also reduces the efficiency of the scanner by reducing the number of counted true coincidence events, therefore increasing noise (see above). 3D PET allows all possible lines of response (LORS) to be recorded and results in a 10-fold increase in efficiency of the PET scanner. 3D PET is now used routinely in all brain scans. However 3D PET results in increased scatter detection, and estimates of 45% of all measured coincidences due to scatter compare unfavorably with that of 15% in 2D PET(Bailey et al. 1998).

1.11.12 Calibration

For most clinical applications of PET, the above corrections can be applied to produce images that are free from artefacts and reflect regional concentration of radiotracer in the body. However, for most kinetic study protocols as discussed in this thesis, the PET images need to be calibrated in terms of absolute units of tracer concentration. Calibration is the process by which the relationship between the measured count rate per unit volume and true activity concentration is established(Geworski et al. 2002). Accurate calibration between the well counter (which measures tracer concentrations in blood samples withdrawn from patients) and the scanner is performed by scanning a phantom source with uniform radioactivity concentration and then counting an aliquot removed from the phantom in a well counter. Images obtained from the phantom are then reconstructed using the same corrections as for the research studies, and the voxel values are directly compared with the counted aliquot to determine the calibration factor.

1.11.13 PET/CT

Combined PET/CT systems are now widely available, and are particularly useful in oncology, where they can be used to co-register data from both scans thereby providing precise tumour location. This can enhance radiotherapy treatment planning by providing a more precise tumour volume (known as the planned target volume). A PET/CT consists of a full ring PET gantry abutted to a single- or multi-slice CT gantry with a common patient couch and aperture and integrated computer system. One of the main advantages is shorter scanning time, as a whole-body CT scan can be acquired in 2 minutes compared to a conventional PET transmission scan, which lasts 20 minutes. At present the main role for PET/CT is in staging and restaging of disease; though the technology may also be of benefit in drug development by combining the superior spatial resolution of CT with the sensitivity of PET in measuring drug pharmacokinetics(Boss et al. 2008).

1.11.14 Arterial Blood Sampling

To perform the tracer kinetic models in this thesis, measurements of the tracer concentration in tissue (provided by the PET scanner) and arterial plasma were required. The localisation of the radiotracer in the region of interest (in this case tumour) is affected by its biochemical properties such as plasma protein binding, lipophilic and hydrophilic attributes and polarity. The concentration of the radiotracer in blood, partitioning between plasma and blood cells, and metabolism are also important. PET is unable to distinguish between radioactivity from the parent radiotracer and that due to a radiolabelled metabolite present in the same region of

interest. For that reason the total amount of radioactivity in arterial blood is sampled continuously for a defined interval at the start of the scan, and discrete aliquots are taken at pre-defined time points to measure the relative proportions of the parent radiotracer and its respective metabolite(s). By subtracting the fraction of radioactivity concentration due to the metabolite in arterial plasma, the true concentration due to the parent compound is derived throughout the dynamic imaging period; this is the gold standard for kinetic modelling of PET data (Wells et al. 2005).

The alternatives to arterial blood sampling include arterialised venous blood sampling (Eberl et al. 1997) and image-based methods i.e. using a visible arterial blood area (left ventricle, or large artery) to provide an input function(Iida et al. 1992). The first method involves heating the hand to approximately 45°C using a water bath or electric blanket, causing arterial blood to be shunted into the venous circulation. Arterialised venous blood samples are then withdrawn (usually from a vein in the antecubital fossa). The second method is used where a pool of arterial blood is within the field of view of the scanner, e.g. the left ventricular chamber of the heart which is used in cardiac studies.

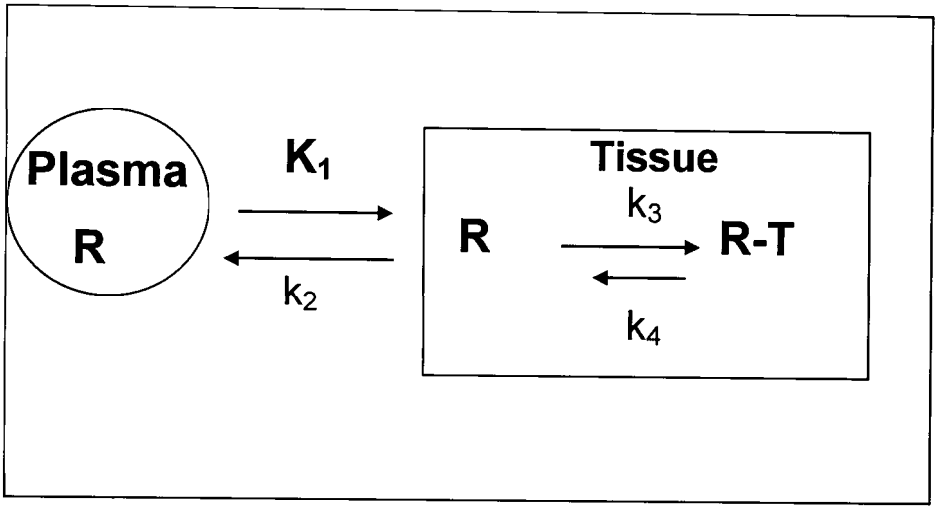
1.11.15 Mathematical models

To analyse the data, hypothesis-led mathematical models which explain tracer kinetic behaviour are employed. Hence the relative rate of biological processes can be determined. Examples of the possible measurements include tracer delivery, washout, and retention. Mathematical models used in this thesis include: compartmental, spectral, and Patlak.

The models used can have fixed assumptions about tracer behaviour based on previously obtained biological information e.g. the Sokoloff model for FDG, a two-compartmental model assumes one reversible compartment, and a second inner

irreversible compartment (Sokoloff L 1977).. K1 is the unidirectional clearance of the tracer from arterial plasma to tissue, k_2 is the clearance in the opposite direction, k_3 is the rate of association of the radiotracer in the irreversible compartment, k_4 is the dissociation rate constant of the radiotracer in the fixed compartment (see Figure 1.11 below).

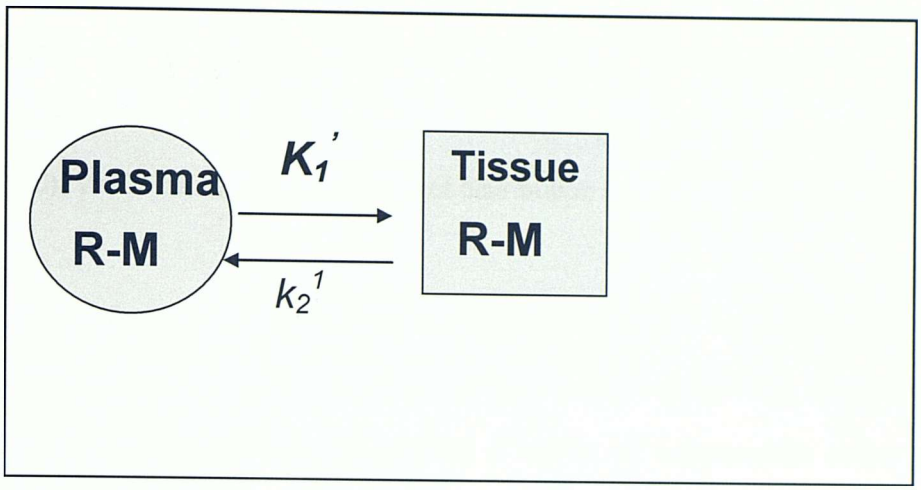
Figure 1.11 The Sokoloff compartmental model for FDG uptake



(where R= radiotracer, K1 is the unidirectional clearance of the tracer from arterial plasma to tissue, k_2 is the clearance in the opposite direction, k_3 is the rate of association of the radiotracer in the irreversible compartment, k_4 is the dissociation rate constant of the radiotracer in the fixed compartment).

For a tracer with metabolites, there may also be transfer of the radiolabelled metabolite from the plasma into the tissue, as shown below in Figure 1.12. The rate constants describing this are labelled K1' and k_2', the degree of binding affinity depends upon the chemical properties of the metabolite; i.e. some possess strong affinity within tissue, but for others such as [18F]FLT and [11C]choline the metabolites are assumed to be free and non-specifically bound within the tissue compartment.

Figure 1.12. Compartmental model for radiolabelled metabolites



(where R-M= radiolabelled metabolite, K_1' = transport into tissue, k_2' = transport back into plasma).

The Patlak-Rutland method assumes irreversible binding of the tracer within the region of interest(Patlak et al. 1985).

$$R(t) = K \int c(t)dt + V_0 c(t)$$

(where R(t) is the amount of tracer in the region of interest, c(t) is the concentration of the tracer in arterial blood, K is the constant describing the rate of entry into the peripheral compartment, V_0 is the distribution volume of the tracer in the central compartment)..The model assumes a single source for the radiotracer, the plasma, and rapid first-order exchange between compartments.

A modified version of the Patlak plot (shown below) which takes account of the presence of tracer metabolites in the tissue of interest was initially developed by Mankoff et al for [11C]thymidine-PET studies was used in this thesis and applied to the

tissue data. The results were compared to the classical Patlak model described above(Mankoff et al. 1996)

$$\frac{A}{C_{Tot}} = \mathrm{K}_x \frac{\int \mathrm{C}_x \delta\tau}{\mathrm{C}_{Tot}} + V \qquad V = V_{ox}\frac{C_x}{C_{Tot}} + \sum V_{om}\frac{C_m}{C_{Tot}} + V_b$$

(where A = Total tissue radioactivity (parent tracer and metabolites), C_{TOT} = total blood radioactivity, C_x= Radioactivity of parent tracer by metabolite analysis of blood data (HPLC), V= Combination of volumes of distribution for parent tracer and metabolites).

On the other hand, spectral analysis is a data-led approach and makes no a priori assumptions about tracer behaviour(Cunningham et al. 1993; Meikle et al. 1998). Spectral analysis operates by creating a series of exponentials which relate the measured concentration of the radiotracer in tissue from the PET data and relate them to arterial plasma data, using the equations below:

$$C_{tiss}(t) = \frac{1}{t_{i+1}-t_i}\int_{t_i}^{t_{i+1}}(\sum_{j=1}^{N} C_a(t) \otimes \alpha_j \exp(-\beta_j t)dt \qquad \begin{matrix} \alpha_j \geq 0 \\ \lambda \leq \beta_j \leq 1 \end{matrix}$$

where *Ctiss* = concentration of the radiotracer in tissue, *t* is time, ⊗ denotes the convolution operator , λ = decay constant for the radioisotope, N = number of basis functions in the model, β values are chosen to describe the entire spectrum of expected kinetic behaviour from the slowest possible clearance λ, to the fastest measurable dynamic, α is the intensity of the component at β).

The impulse response function (IRF) is calculated for the entire scan duration shown below:

$$h(t) = \sum_{j=1}^{N} \alpha_j \exp(-(\beta_j - \lambda)t)$$

($h(t)$ = IRF). The fractional retention of tracer at various intervals (FRT ratios) can be calculated by dividing the IRF values for e.g. 60 minutes, and 90 minutes by the IRF for 1 minute, to obtain the FRT at 60min and FRT at 90 min respectively.

The IRF can then be used to calculate the following parameters:

I) The rate constant for the transport from plasma to tissue for the radiotracer, K_1 (sec^{-1}), (equivalent to regional flow x extraction)

$$K_1 = h(0) = \sum_{j=1}^{N} \alpha_j$$

II) The apparent volume of distribution, *VD, i.e.* the partitioning between blood and tissue (i.e. the steady-state ratio of tracer concentrations in tissue and plasma).

$$VD = \int_0^{\infty} h(t)dt = \sum_{j=1}^{N} \frac{\alpha j}{\beta j - \lambda}$$

An explanation of how radiotracer uptake is routinely measured in the clinical setting now presented.

1.11.13 Semi-quantitative methods

Standardised uptake value

The standardised uptake value (SUV) is the most commonly used parameter in clinical PET practice. It provides a measure of uptake within a defined region of interest at a specified mid-frame time which is corrected for the dose of injected radioactivity and either weight or body surface area (BSA).

i)

$$SUV = \frac{Weight(Kg)}{Q_{inj}} xQ$$

or

ii)
$$SUV = \frac{BSA}{Q_{inj}} xQ$$

The correction of SUV for body weight is the most common version used in clinical studies. However, this value can be subject to increases as high as two-fold in normal tissues when heavier-weight patients are studied in comparison to lighter ones, hence the use of SUV corrected for lean body mass has been suggested as an alternative method in FDG-PET scans(Zasadny et al. 1993). As yet, no information has been published regarding weight-dependence and the tracers that will be presented in this thesis, therefore it was elected to employ the SUV corrected for BSA method, as a previous FDG-PET study of breast cancer has shown that this method is does not correlate with body weight (Sugawara et al. 1999).

The time when tracer uptake is measured post-injection is an important determinant of reliability of SUV values, which is of particular relevance to tumours with slow metabolism (Keyes 1995). In oncology, recent studies have suggested that measuring SUVs at later time-points post-injection in FDG-PET scans can help differentiate tumour from inflammatory lesions (Nishiyama et al. 2005). The advantages of using SUV are that its calculation is relatively straightforward to perform, and does not require blood sampling.

Area under the curve

The area under the curve (AUC) provides an integral measure of the summated activity over time also corrected for dose and body surface area. As activity is nominally measured at mid-frame time, then it follows that AUC is calculated by the

sum of the product of corrected activity at time (t) (i.e. SUV) by the duration of the frames.

AUC= Σ Frame duration(s) x Corrected activity (t) [m^2/ml]

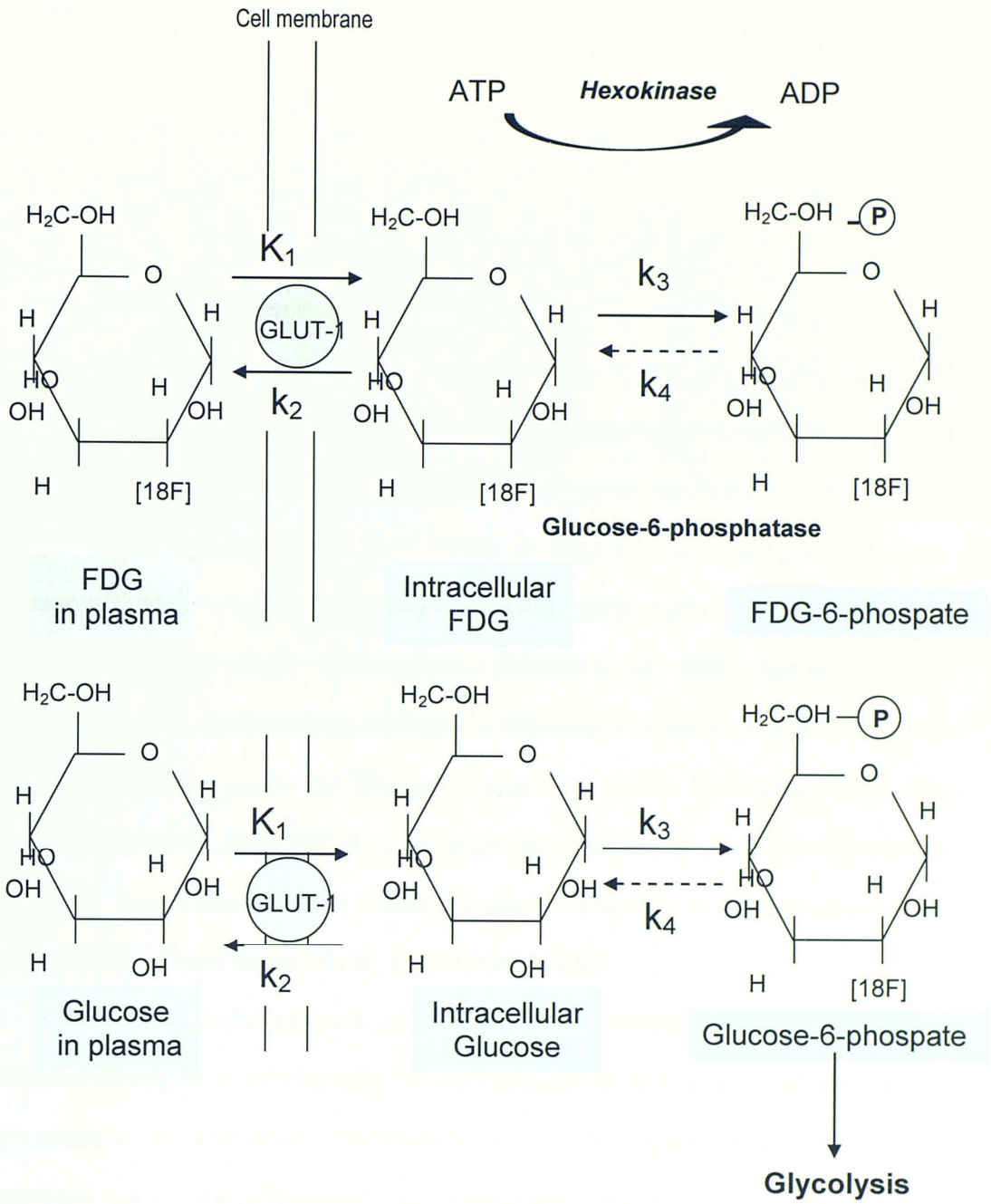
For AUC to be accurate, it follows that more than one frame needs to be acquired, as the total area under the curve is obviously dependent on the slopes either side of the peak activity.

The tracers used in oncology and this thesis will now be discussed.

1.12 FDG

2-[18F]fluorodeoxyglucose, FDG is the most commonly used PET tracer in oncology. It was originally labelled with [18F] in Brookhaven in the 1970's and used for preclinical imaging of regional myocardial glucose metabolism (Gallagher et al. 1977). The use of FDG in oncology is dependent on Warburg's observations in the 1920's that cancer cells display an increased rate of glycolysis compared to normal cells(Warburg O 1924). Typically normal cells rely on oxidative phosphorylation for energy production rather than glycolysis which is energy inefficient.

Figure 1.13: Cellular uptake and metabolism of FDG.



The transmembrane transporters Glut 1-5 are responsible for the transport of glucose intracellularly. Various cancers (breast, lung, colon, oesophagus) have shown

over expression of the Glut 1 transporter (Smith 1998). Other changes associated with the transformed phenotype are increased expression of the enzyme hexokinase which catalyses the formation of glucose 6-phosphate from glucose, redistribution of hexokinase to the outer mitochondrial surface, alteration of the glycolytic enzymes aldolase and enolase (although the latter will have no effect on FDG uptake)(Pauwels et al. 2000). Weber et al have shown that hepatic glucose-6-phosphatase activity is reduced during carcinogenesis, in adenocarcinoma bearing mice compared to normal controls, and absent in hepatomas in a preclinical study (Weber et al. 1955).

Transfection with the oncogenes src, ras and c-myc and stimulation by growth factors such as EGF results in upregulation of the genes which encode hexokinase and glucose transporters(Scimeca et al. 1989). In response to certain growth factors, PI3 kinase activates the serine/threonine kinase Akt which leads to overexpression of Glut 1 and increased activity of hexokinase (Barthel et al. 1999; Plas et al. 2001; Elstrom et al. 2004). Drug-induced inhibition of PI3 kinase in glioblastoma cells blocks the activation of glycolysis by Akt (Elstrom, Bauer et al. 2004). Downstream from Akt, regulation of glycolysis is mediated by, amongst other factors, hypoxia inducible facor-1α (HIF 1α). In a recent study in breast carcinoma, absence of Akt phosphorylation was associated with low levels of HIF 1α (Gort et al. 2006).

Originally deoxyglucose was developed as a chemotherapeutic agent to block accelerated glycolysis in cancer cells, but was abandoned due to neurological toxicity. 2-deoxyglucose is transported intracellularly in a similar fashion to glucose by Glut transporters, and phosphorylated by hexokinase. Further progression of 2-deoxyglucose-6-phosphate down the glycolytic pathway does not occur as the compound lacks an oxygen atom at the C2 position. 2-deoxyglucose-6-phosphate is trapped intracellularly as it cannot diffuse back out of the cells, and the dephosphorylation reaction catalysed by glucose-6-phosphatase occurs slowly(Sokoloff L 1977).

Some of the limitations of using FDG as an imaging tracer include its lack of specificity (i.e. any tissue which has a high rate of glycolysis will show increased uptake), therefore discrimination between tumour tissue and inflammation may become difficult. Most clinical scans utilise static imaging rather than dynamic studies. Differences in uptake kinetics between tumour and inflammation have been observed using dynamic imaging in a study of thoracic lesions. Tumour uptake of FDG increases to a plateau over time compared to inflammatory lesions where after an initial rise the uptake tapers off (Zhuang et al. 2001). Serum glucose levels are known to have an effect on FDG uptake (Wahl et al. 1992). It has also been reported that elevated serum glucose results in increased uptake of FDG in inflammatory lesions, compared to tumours where a negative effect is seen (Zhuang et al. 2001).

1.13 PET radiotracers for studying proliferation

Investigators have recently sought alternatives to FDG which are more specific for studying selected molecular processes such as proliferation. Glycolysis is not limited to tumour tissues and may occur in areas of inflammation, leading to increased uptake of FDG in benign processes. Most of the proliferation markers being developed are thymidine analogues, their structures are shown in Figure 1.14.

1.13.1 Thymidine

The basis for using thymidine as a PET radiotracer for studying proliferation originated from the use of tritiated thymidine in autoradiography and flow cytometry. Thymidine is the only base which is incorporated into DNA and not RNA (where it is replaced by uracil), making it appropriate for studying DNA metabolism. It is transported intracellularly using a facilitated non-energy dependent transporter which

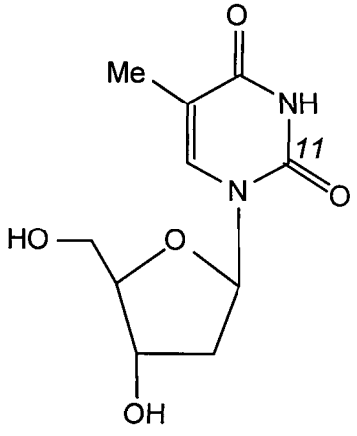
produces equilibration in seconds (Wohlhueter et al. 1979). Thymidine nucleotides are unsuitable for growth measurements as they are unable to cross the cell membrane. The rate of proliferation is dependent on the rate of DNA synthesis of the tissue of interest, provided that there is no shortage of DNA nucleosides(Cleaver 1967). Therefore, as 50% of base pairs contain thymidine the synthetic rate of DNA (SR_{DNA}) has been defined as:

$$SR_{DNA} = 2 \times \frac{1}{f_{ext}} \times fluxTdR$$

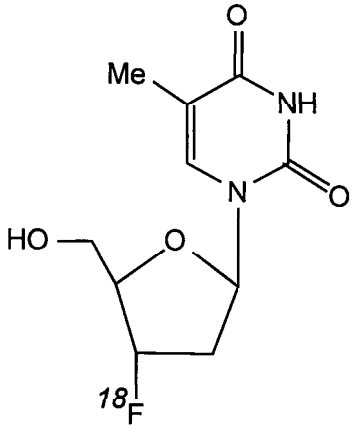
where f_{ext} is the flux of thymidine via the exogenous pathway and fluxTdR is the flux of thymidine nucleotides from the precursor pool into DNA (μmol/min/g)(Mankoff et al. 1999).

Thymidine labelled with carbon-11 in the methyl position was first produced by Christman (Christman et al. 1972). Labelling in this position produced a complex set of metabolites, making modelling difficult(Shields et al. 1987). Investigators then tried labelling in the ring-2 position (Vander Borght et al. 1991), which led to rapid degradation into carbon dioxide and metabolites(Shields et al. 1992).

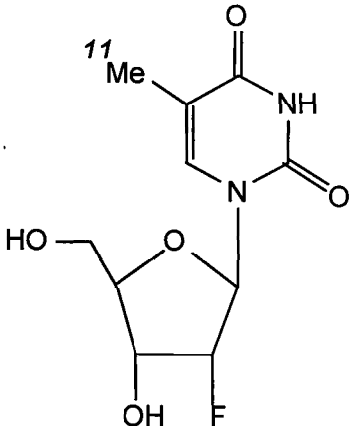
Figure 1.14: Pyrimidine Nucleosides in Development as PET radiotracers



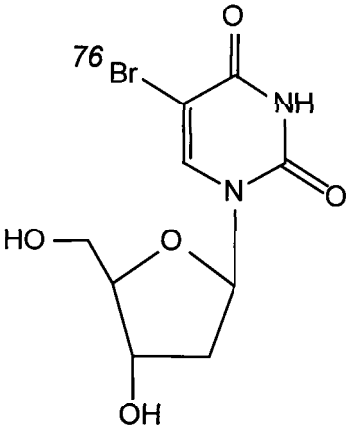
2[^{11}C]Thymidine



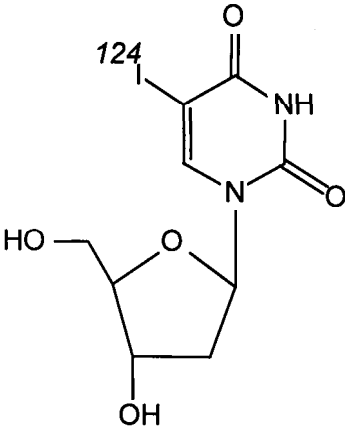
[^{18}F]FLT



[^{11}C] FMAU



[^{76}Br] BrdU



[^{124}I] IUdR

Clinical studies of methyl-labelled thymidine have been performed in non-Hodgkin's lymphoma (Martiat et al. 1988), neuroendocrine tumours, and head and neck cancer(van Eijkeren et al. 1992). The investigators found higher uptake in high grade tumours compared to low grade ones. Increased uptake was also noticed in the myocardium, kidney, and liver (which was attributed to blood pooling). Activity seen in the gut wall could have been due to the normal proliferation of bowel mucosa. 2-[11C] thymidine has been used to image brain tumours (Vander Borght et al. 1994; Eary et al. 1999), sarcomas, and lung cancers, with mixed results. In Vander Borght's study, an increased thymidine uptake (tumor-to-cortex ratio ≥ 1.2) in 11 of 14 untreated tumours and in 5 of 6 recurrent tumours was found. However, there was no correlation between thymidine uptake and tumour grade.

The study by Eary et al compared 2-[11C] thymidine with FDG PET and magnetic resonance imaging (MRI) in 13 patients with brain tumours (Eary et al. 1999). In two cases where lower 2-[11C] thymidine uptake than FDG, tumour progression was slower compared to tumours in 3 patients with high uptake of both tracers. For brain imaging the blood brain barrier is much more permeable to [11C]CO_2 than [11C]thymidine, necessitating data correction for high background activity (Wells et al. 2002).

2-[11C]thymidine-PET has also been used to image response to treatment. Shields et al studied the effect of chemotherapy on 2-[11C]thymidine and FDG uptake in 4 patients with small cell lung cancer and 2 with sarcoma(Shields et al. 1998). In the 4 responding patients decreases in uptake of both tracers were seen. In the 2 patients with progressive disease (1 metastatic small cell lung cancer, and 1 abdominal sarcoma) only small decreases (<10%) in KTdR (thymidine flux constant) were observed, the latter patient actually had a 69% increase in FDG SUV.

Drugs which target incorporation of deoxythymidinetriphosphate (dTTP) into DNA result in decreased DNA biosynthesis and repair. For many agents this is

mediated by inhibition of the enzyme thymidylate synthase (TS). TS is a key target in cancer therapeutics. It is a catalyst for the methylation of 2'-deoxyuridine-5'-monophosphate (UMP) into 2'-deoxythymidine-5'-monophosphate (TMP) in the de novo synthetic pathway of thymidine nucleotides. Drugs such as 5-fluorouracil (5-FU) inhibit this pathway resulting in depletion of intracellular thymidine pools. As a consequence of the decreased availability of intracellular thymidine, cells employ the salvage pathway where more thymidine is imported from the extracellular space and then phosphorylated by TK to form TMP. Increased extracellular thymidine leads to reduced activity of TS inhibitors, and conversely inhibition of thymidine transport results in enhanced activity of these agents.

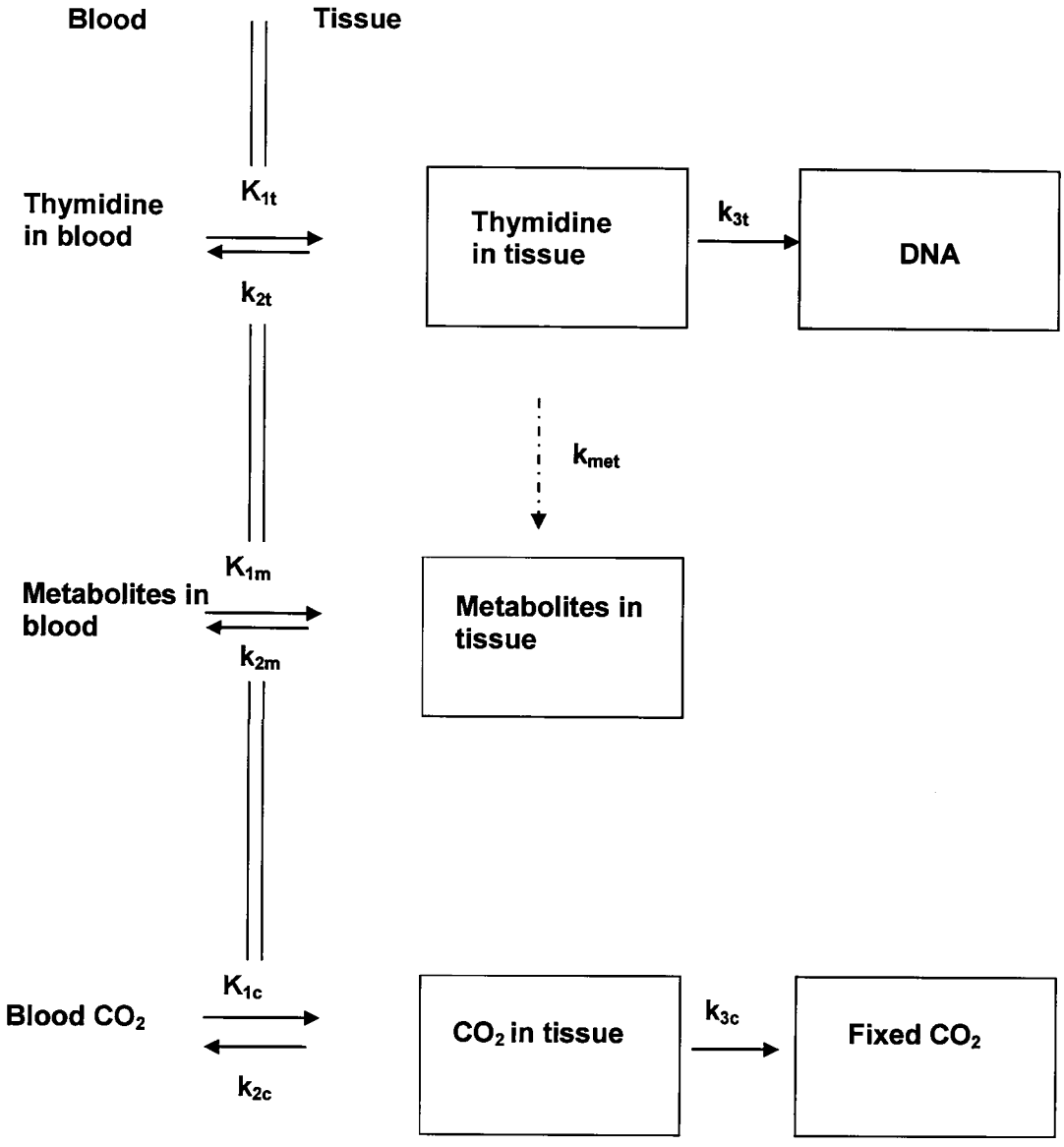
In the first study of its kind, Wells et al employed 2-[11C]thymidine PET to measure TS inhibition in patients with advanced gastrointestinal cancer before and 1 hour after treatment with a novel TS inhibitor, nolatrexed hydrochloride (AG337, THYMITAQ, Aguoron Pharmaceuticals, San Diego, CA, USA) (Wells et al. 2003). Five patients treated with the agent together with 7 untreated controls were scanned. Treatment was associated with increased fractional retention (FRT) and standardised uptake value (SUV, corrected for body weight) of 2-[11C]thymidine compared to the control group where no significant changes in uptake were seen. Plasma AG337 AUC measurements correlated with both plasma deoxyuridine levels (a pharmacodynamic marker of TS inhibition due to increased intracellular levels of uridine monophosphate)(Jackman et al. 1984) and 2-[11C]thymidine uptake in four and three patients respectively ($r=1$, $p=0.01$ for the two parameters).

The need for correction of metabolites in 2-[11C]thymidine studies was previously demonstrated by Wells et al in patients with advanced gastrointestinal cancer where it was found that semi-quantitative metabolite-uncorrected parameters SUV and AUC failed to correlate with Ki-67 labelling index, in contrast to FRT (Wells et al. 2002). The lack of correlation with the SUV method was later attributed to the presence of labeled metabolites and unincorporated thymidine(Wells et al. 2005). A

study comparing FDG and 2-[11C]thymidine –PET with computed tomography (CT) for response in metastatic renal cancer treated with interleukin 2 for 6 weeks found that responding tumors had decreases in both FDG and thymidine uptake, however, there were discrepancies in several tumour sites which showed an increase in thymidine uptake despite decreases in FDG and this correlated with ultimate tumor progression in these areas (Eary et al. 1999). This suggests that changes in [11C]thymidine uptake may be an earlier predictor of drug resistance than FDG.

One of the major metabolites of 2-[11C]thymidine is $[11C]CO_2$. The distribution of radiolabelled carbon dioxide $[11C]CO_2$ is pH dependent, therefore the contribution of $[11C]CO_2$ to the PET signal and pH of the blood are important when interpreting 2-[11C]thymidine-PET studies (Shields et al. 1992). For data analysis, a 5-tissue compartment model with 8 rate constants (see Figure 4) has been developed by Mankoff et al (Mankoff et al. 1998). The complexity of the analysis together with the short half-life of 20.4 min of [11C] present challenges for the widespread use of 2-[11C]thymidine-PET . Currently, clinical studies of 2-[11C]thymidine-PET are restricted to dedicated PET research centres with a cyclotron on-site. Most PET research centres have now switched from using [11C]thymidine to newer [18F]-radiolabelled pyrimidine analogues, which aim to be less complex in terms of analysis. The main advantage for [11C]-thymidine compared to some of these newer compounds is that it bears the most similarity to the target nucleoside substrate and thus should provide a more reliable estimate of the salvage pathway for DNA synthesis.

Figure 1.15: Tissue compartmental model for thymidine



(where K1t= transfer of thymidine from blood to tissue, k2t= transfer of thymidine from tissue to blood, k3t= incorporation of thymdine into DNA, kmet= rate of metabolism of intracellular thymidine, K1m= transfer of thymidine metabolites from blood to tissue, k2m= transfer of metabolites from tissue to blood, k1c= transfer of CO2 from blood to tissue, k2c= transfer of CO2 from tissue to blood, k3c= irreversible trapping of CO2 within tissue).

1.13.2 [18F]Fluorothymidine (FLT)

3'-deoxy-3'-[18F]fluorothymidine ([18F]FLT) is a thymidine analogue. Compared to 2-[11C]thymidine, the main advantages of [18F]FLT are its longer half-life of 109.8 minutes and resistance to degradation. FLT is transported intracellularly via an equilibrative nucleoside transport mechanism, after which it becomes phosphorylated by TK1 and trapped as the phosphate. Another set of sodium-dependent concentrative transporters also exists in normal tissues which mediate influx only(Belt et al. 1993). The transport of [18F]FLT follows biphasic kinetics, with rapid initial accumulation followed by a slower rate of accumulation. Unlike thymidine only minimal amounts of [18F]FLT are incorporated into DNA as it lacks the 3'-hydroxyl moiety(Lu et al. 2002; Krohn et al. 2005).

The rate of uptake of FLT into cells and phosphorylation by TK1 is approximately 30% of that of thymidine(Munch-Petersen et al. 1991). The expression of TK1 is tightly regulated with the cell cycle(Adler et al. 1974; Sherley et al. 1988; Sherley et al. 1988; Roehl et al. 1990) it increases in S phase(Toyohara et al. 2002):, and is targeted for degradation in M phase, such that newly divided cells have low levels of TK1. Unlike thymidine, and FMAU (discussed below) FLT is not a substrate for mitochondrial TK2 which is constitutively expressed throughout the cell cycle.

Rasey et al showed that [18F]FLT measures TK1 activity in A549 lung carcinoma cells *in vitro* (Rasey et al. 2002). High levels of TK is associated with an increased risk of relapse and reduced survival in patients with node-positive breast cancer(Romain et al. 1997). A preclinical study from our group has shown that [18F]FLT uptake decreases as early as 24hrs post cisplatin treatment in RIF-1 sarcoma bearing mice, and these changes correlated with decreases in proliferation cell nuclear antigen (PCNA), and preceded changes in tumour size(Leyton et al. 2005). Similar decreases were seen at 48hr in the same model treated with 5-fluorouracil(Barthel et al. 2003). Preclinical comparison of [3H]thymidine, [18F]FLT

and FDG-PET for monitoring response to radiotherapy in C3H/He mice bearing SCCVII tumours showed that the reduction in [18F]FLT uptake correlated with that of [3H]thymidine and Ki-67 LI. [18F]FLT uptake declined rapidly (6 hours) post-irradiation, whereas a significant decrease in FDG uptake was only noted at day 3, which may have reflected local radiation induced inflammatory changes (Sugiyama et al. 2004).

The first human study of [18F]FLT-PET was performed by Shields et al in a patient with sarcoma: high tumour localization was seen as well as high uptake in the bone marrow, liver, bowel, kidneys and the bladder(Shields et al. 1998). Low uptake was noted in the normal brain, muscle, heart, and lungs. In humans, FLT is metabolised by glucuronidation in the liver and excreted via the kidneys(Shields et al. 2005). FLT was originally used for the treatment of HIV, but stopped due to toxicities such as peripheral neuropathy, myelosuppression and hepatic failure (Kong et al. 1992; Flexner et al. 1994). Due to the above toxicities however, although typically only 10μg of FLT is injected for a single PET scan it is recommended that patients have adequate haematological and hepatic function prior to scanning(Been et al. 2004).

[18F]FLT can be produced with high specific activity, the production method and radiation dosimetry have been established (Grierson et al. 2000; Vesselle et al. 2003). Two different strategies have been developed for [18F] labeling of FLT(Been et al. 2004). The method of Grierson and Shields utilizes nosylate derivatives of thymidine (Grierson et al. 2000), and that of Machulla employs anhydrothymidine derivatives(Machulla 2000). The second method is easier to perform, but has low radiochemical yields of 5-14%. Cleij et al have further improved the yield by adding dimethyl sulphoxide to the precursor(Cleij 2001).

Prior to commencement of work reported in this thesis, [18F]FLT-PET had not been studied previously in breast cancer. The optimal parameter for describing [18F]FLT uptake had not been established. Although repeatability studies have been determined for [11C]thymidine(Wells et al. 2005) no studies have evaluated the

repeatibility within tumours of [18F]FLT, nor described the pharmacokinetic parameter which correlates best with tissue proliferation.

Buck et al compared the uptake of FDG and [18F]FLT in 26 patients with solitary lung nodules. The results showed that tumour uptake of FDG was higher than that of [18F]FLT, but that correlation of [18F]FLT SUV with proliferation was significantly better for FLT which was entirely specific for malignant tumours. There were two false negative cases for [18F]FLT, one in a metastatic colorectal lesion and the other in a non-small cell lung cancer with a low proliferation index(Buck et al. 2003). A second study which compared [18F]FLT uptake with proliferation in ten patients with non-small cell lung cancer found that the correlation was better for Patlak analysis of [18F]FLT retention than SUV, and a superior correlation for [18F]FLT uptake with Ki-67 labelling index than S-phase fraction (Vesselle et al. 2002). Dittman et al compared [18F]FLT and FDG-PET in sixteen patients with primary and metastatic thoracic tumours (non-small cell lung cancer, oesophageal carcinoma, sarcoma, Hodgkin's lymphoma, and renal carcinoma)(Dittmann et al. 2003). Whole-body imaging was performed 90minutes post tracer injection. There was no correlation with Ki-67 labelling index (LI) and [18F]FLT-PET, which the authors attributed to the diversity of tumour types which were imaged. The interval between biopsy and PET scans and method of calculating the Ki-67 LI was not stated. The [18F]FLT and FDG-PET results were similar, with one bone metastasis being missed due to high physiological FLT uptake.

[18F]FLT-PET has been shown to be inferior to FDG-PET for imaging liver metastases from colorectal tumours which is likely to be due to the high physiological background signal due to glucuronidation(Francis et al. 2003). Imaging of extrahepatic colorectal cancer metastases in the same study did have more promising results. Another study of colorectal tumours (primary and metastatic) by the same group demonstrated good correlation ($r=0.8$, $p<0.01$) between [18F]FLT SUV and corresponding MIB-1 proliferation indices(Francis et al. 2003).

[18F]FLT-PET has also been used to evaluate tumourous and non-tumourous cerebral lesions using static imaging one hour after injection. The results were compared to FDG uptake in the same patients. [18F]FLT-PET was superior to FDG in distinguishing tumours from grey matter (presumably due to the high rate of glycolysis in normal brain tissue causing an intense FDG signal). The sensitivity and specificity of [18F]FLT for diagnosing brain tumours was 79% and 63% respectively; there were three false negatives in grade II astrocytomas (Choi et al. 2005).

A study by Cobben et al evaluated the utility of [18F]FLT-PET for studying soft-tissue sarcoma in 19 patients, who had static imaging performed 1hr post-injection of [18F]FLT. The MIB-1 score (an antibody which recognises Ki-67) correlated with [18F]FLT uptake as measured by SUV(Cobben et al. 2004), however [18F]FLT-PET missed a 0.5cm diameter metastatic lymph node. Equivalent results for [18F]FLT and FDG have been reported for laryngeal cancer (Cobben et al. 2004), though as expected the tumour uptake of FDG was higher than that of [18F]FLT. In stage III melanoma, [18F]FLT-PET scans upstaged two out of ten patients with therapeutic consequences. The authors found [18F]FLT-PET had a threshold diameter of 6mm for detecting lymph node metastases and had a region based sensitivity of 88%(Cobben et al. 2003).

1.13.3 FMAU

2'-fluoro-5-methyldeoxyuracil-beta -D-arabinofuranoside (FMAU) can be labeled with [11C] or [18F] (Conti et al. 1995; Wang et al. 2002; Sun et al. 2003). FMAU resists degradation and is incorporated into DNA but not RNA or protein. It has been previously used as an antiviral agent and an anti-neoplastic agent as at high concentrations it acts to inhibit DNA synthesis. FMAU is a substrate for TK1 and TK2 and is incorporated into DNA by DNA polymerase. The level of uptake of FMAU in vitro is proportional to the rate of DNA synthesis and proliferation (Collins et al. 1999).

Studies in normal dogs show that there is increased uptake in proliferating tissues such as the bone marrow and intestine where 87% and 64% of the radioactivity was located in the DNA. In contrast, the radioactivity in non-proliferating tissues and organs such as the heart and kidneys was in the supernatant (Sun et al. 2005).

Sun et al studied the dosimetry of [18F]FMAU in 14 patients with a variety of cancers (prostate, glioma, metastatic colorectal, renal, breast, lung, and sarcoma) using PET(Sun et al. 2005). All tumours were visualised. At 60 min post-injection 70% of the administered radioactivity in the urine was due to intact [18F]FMAU. There was physiological uptake in the heart, liver and kidneys. Due to high uptake in the latter two regions two regions were visible as areas of decreased signal intensity (i.e. cold spots). Low uptake in the bone marrow may allow further study of this agent for imaging bone metastases. The elevated physiological uptake in the liver and renal regions in humans compared to dogs could be attributed to interspecies differences in nucleoside transporters and tracer metabolism.

1.13.4 Bromodeoxyuridine

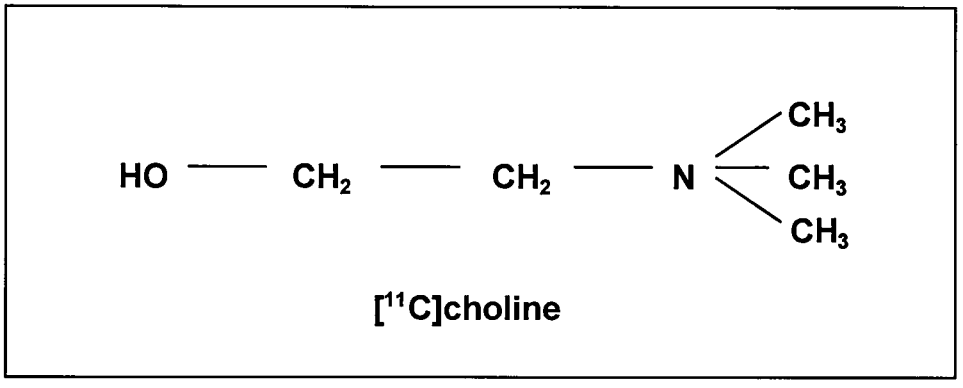
[76Br]Bromodeoxyuridine, [76Br]Du has also been suggested as an alternative to FDG. For years BrDu has been used in immunohistochemistry to assess proliferation in tissue sections. However despite encouraging results from preclinical studies with up to 70% of administered tracer detectable in tissue/tumour DNA, clinical evaluation of the tracer has proved disappointing. The main problems appear to be dehalogenation, resulting in high levels of [76Br] in plasma and non-proliferating tissues. Techniques in preclinical studies including forced diuresis with loop diuretics have been employed to circumvent this problem, but this would be an added burden for patients undergoing [76Br]Du scans(Lu et al. 1999). Data would require to be corrected for this high background activity as it needs to be distinguished from that of [76Br]Du. In a study of 8 patients with brain tumours on average only 9% of

radioactivity was found in tumour DNA (Gudjonssona et al. 2001). Cimetidine has also been used to decrease elimination and increase bioavailability of [76Br]Du (Borbath et al. 2002).[76Br] has a long t½ of 16 hours, which increases the dose of radiation to the patient.

1.14 Choline

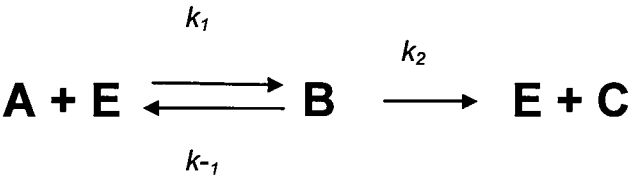
Choline is a quaternary saturated amine, an essential nutrient, and a precursor of i) phosphatidylcholine the major phospholipid component of cell membranes, ii) the neurotransmitter acetylcholine. The structure is shown below in Figure 1.16.

Figure 1.16 Structure of choline



Choline is transported intracellularly in human breast cancer cells by a Michaelis-Menten like mechanism, see Figure 1.17 (Katz-Brull et al. 1996).

Figure 1.17. Michaelis-Menten equation for enzyme catalysis

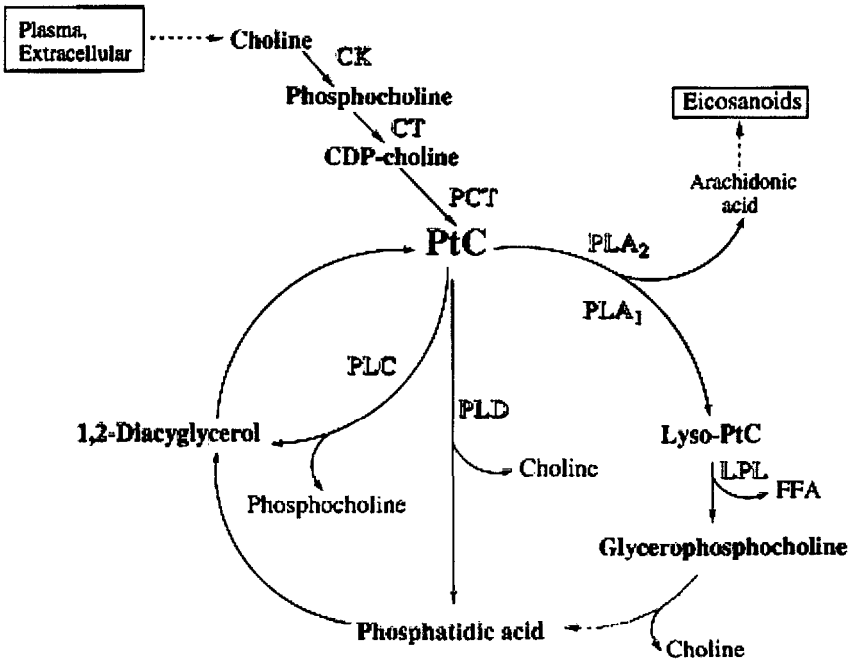


(where k_1 is the rate constant for the combination of the enzyme E with the substrate A, to form the enzyme subtrate complex, B, k-1 is the rate constant for the dissociation of the E and the unaltered substrate A and B (i.e. altered substrate), k_2 is the rate constant for formation of the product C and enzyme E).

Formation of phosphocholine results from the phosphorylation of choline by the enzyme choline kinase (CK) in the presence of ATP and Mg^{2+}. This reaction effectively commits choline to the Kennedy pathway for the formation of phosphatidylcholine (PtC), see Figure 1.18. Hydrolysis of PtC is effected by three major PtC-specific enzymes, phospholipase C (*PLC*), phospholipase D (*PLD*), and phospholipase A_1 and A_2 (PLA_1 and PLA_2). The rate of choline phosphorylation by CK has been found to be twice that of its transport across the cell membrane(Katz-Brull et al. 1996). Three isoforms of CK have been elucidated in mammalian cells(Aoyama et al. 2004). The α isoforms of the enzyme (CKα1, CKα2) contain 453 amino acids, and CKβ contains 394 amino acids. Studies in mouse liver have shown that most (60%) of active CK exists as the α/β heterodimer with the remainder as the homodimeric form (α/α or β/ β), this configuration changes to α/α as the predominating isoform when the cells are treated with the hepatotoxin CC14. The relative roles each of the isoforms plays in tumorigenesis and response to growth factors requires further evaluation.

Figure 1.18: Biosynthesis and hydrolysis of PtC.

(where cytidylyltriphosphate=CTP, phosphocholine cytidyltransferase=(CT), phosphocholine transferase (PCT), phospholipase C = PLC, phospholipase D (PLD), and phospholipase A1, A2 =PLA1and PLA2, and FFA, free fatty acid) Figure taken from Aboagye and Bhujwalla (Aboagye et al. 1999).



PtC is the major phospholipid constituent in cell membranes, and also acts as a source of lipid second messengers e.g diacylglycerol and lyso-phosphatidic acid. The rate-limiting step in PtC formation is the cytidylyltriphosphate(CTP):phosphocholine cytidylyltransferase reaction. CK is also thought to play a regulatory function in PtC synthesis as increased CK activity results in an increased rate of PtC synthesis. However, induction of CK by ras oncogene transfection, growth factors (eg PDGF-AA, basic FGF, EGF and phorbol esters) and chemical carcinogens can result in increased formation of phosphocholine which is independent of PtC synthesis(Cuadrado et al. 1993). Alterations in membrane choline phospholipid metabolism (MCPM) are evident in breast cancer tumorigenesis (Aboagye et al. 1999). In normal human mammary epithelial cells low levels of choline metabolites are present at steady state, with glycerophosphocholine (GPC) predominating, with benzo(a)pyrene-induced

immortialisation of the cells an early switch occurs such that the major metabolite changes to phosphocholine. Oncogenic transfection of erbB2 resulted in both an increase in the overall GPC:phosphocholine ratio and the total level of choline metabolites compared to the immortalised cells(Aboagye et al. 1999).

The change in MCPM induced by erbB2 is thought to be due to activation of the erb2 receptor tyrosine kinase and hence stimulation of the ras/raf/MAPK pathway (see Figure 6). The increased rate of growth and proliferation has been attributed as the cause of altered MPCM in tumour cells, however in normal proliferating mammary epithelial cells the level of choline metabolites remains low and MPCM is unaltered; suggesting that the change in MPCM is being driven by another mechanism such as enhanced receptor tyrosine kinase cascade, amplification of CK, phospholipase C/D/A genes during carcinogeneis, or differential induction of different CK isozymes.

In comparison with normal cells human breast tumour cells have been found to have an increase of CK activity of 38.5%(Ramirez de Molina et al. 2002). Inhibition of CK by RNA-interference (RNAi) mediated down-regulation of in nonmalignant and malignant human breast epithelial cell lines resulted in decreased proliferation (measured by PCNA and Ki-67) and formation of phosphocholine (measured by magnetic resonance spectroscopy spectroscopy (MRS)) and promoted cell differentiation (Glunde et al. 2005). The recently developed CK inhibitor, MN58b, also results in reduced formation of phosphocholine in breast cancer cells, with a decreased number of cells observed 48hrs after dosing (Al-Saffar et al. 2006).

The cytokine tumour necrosis factor alpha (TNFα) induces cell cycle arrest in G_0 and G_1/S phases of the cell cycle. When a human breast cancer cell line (MCF7) were treated with TNFα there was a resultant decrease in phosphocholine production, which was found to be due to decreased choline transport into the cell and an accompanying 2-fold increase in the activity of the enzyme cytidine triphosphate cytidylyltransferase (Bogin et al. 1998). These cellular changes in choline metabolism are thought to be a prelude to apoptosis.

Radiolabelled choline has been used to study the effect of inhibition of the Raf-1/MAP kinase pathway in a cell culture study using HT29 colon carcinoma cells. Geldanamycin, a benzoquinoid ansamycine antibiotic related to herbimycin A, binds to heat shock protein 90 (hsp90) in complex with co-chaperones, leading to degradation of Raf-1 and other oncogenic client proteins. When treated with geldanamycin, a decrease in methyl-[14C]choline uptake and phosphocholine production was observed, which was associated with a decrease in extracellular signal regulated kinase 1 and 2 phosphorylation (Liu et al. 2002). This effect was independent of PI3 kinase.

1.15 [18F]-AH111585

The focus of the final study in this thesis concerns a new [18F]-labelled RGD peptide,which is proposed to measure αvβ3 integrin levels. The first synthetic RGD peptide developed for imaging by Haubner et al [125I]-c(RGDyV) in mouse models of melanoma and osteosarcoma also had high liver signal due to hepatobiliary clearance(Haubner et al. 1999). To try and circumvent this problem van Hagen et al then coupled an RGD analogue to diethyleletriamepentaacetic acid (DTPA) which when labelled with [111In] resulted in renal clearance in a rat model, further advances of this compound were limited as the uptake and retention in the kidneys was 4-8 times that of any other tissue(van Hagen et al. 2000). Several RGD-based peptides have now been evaluated as imaging agents with both PET and SPECT. Studies focusing on the RGD binding site of the integrin receptor have utilised a peptide combined to a galacotose ring, which enables rapid uptake, distribution and excretion of the tracer.

Coupling of a sugar amino acid moiety (SAA) to a second generation derivative of the compound used by Haubner, [125I]-c[RGDyK(SAA)] yielded further improvements in tumour retention, tumour to blood ratios, decreased liver signal, and similar renal and blood clearance in murine models of melanoma and osteosarcoma.

Glycosylation resulted in the pentapeptide becoming more hydrophilic, which explains the alteration in pharmacokinetics (i.e. preferred renal to hepatobiliary excretion). However this modification also results in increased activity in lung, mycocardium, and liver compared to the non-glycosylated peptide(Haubner et al. 2001).

[18F]Galacto-RGD PET uptake measured by SUV in a variety of human malignant tumors correlated with tissue expression of αvβ3 measured by immunohistochemistry using the LM609 antibody and MVD(Beer et al. 2006). The alpha v integrins recognise Arginine-Glycine-Aspartate (RGD) as a determinant factor for binding to their cognate ligands. Pasqualini et al have shown that RGD-based peptides displayed on a probe designed to target alpha v integrins bind to those expressed on tumor neovasculature (Pasqualini et al. 1997) rather than that on tumor cells in a breast cancer model, using MDA-MB-435. The ratio of αvβ3/5 integrin expression on endothelial cells compared to human breast carcinoma cells *in vivo* in patients remains unknown.

Expression of membrane-type 1 matrix metalloproteinase in MCF-7 cells is associated by functional association of αvβ3 which initiates the first step in activation of the pro-angiogenic matrix metalloproteinase 2 (MMP2)(Deryugina et al. 2000). αvβ3 experession in a breast cancer cell line has also been shown to accelerate the development of osteolytic bone metastases(Pecheur et al. 2002). Abdollahi et al studied the effect of an αv integrin inhibitor, S247, combined with external beam radiotherapy in prostate cancer cells and human umbilical vascular endothelial cells (HUVEC) and found that the combination enhanced the anti-angiogenic effects of radiation by inhibiting the radiation induced up-regulation of αvβ3 expression and Akt activation (Abdollahi et al. 2005). Non-invasive imaging of αvβ3 status in the future could act as a predictive factor for choosing therapy.

In the clinical setting several αv integrin antagonists are in phase 1/2 trials, and can be classified into antibodies, endogenous peptides, synthetic peptides and peptidomimetics (Alghisi et al. 2006). Cilengitide is a cyclic RGD peptide which acts as

an αvβ3 and αvβ5 antagonist and is now undergoing Phase 2 clinical trials in patients with hormone-refractory prostate cancer, non-small cell lung cancer and pancreatic cancer. A Phase 1 study of cilengitide in patients with advanced solid tumors did not reach dose limiting toxicity, therefore the optimum dose for this agent remains to be determined (Eskens et al. 2003). Vitaxin is a humanised form of LM609, has also entered early stage clinical trials(Gutheil et al. 2000). Treatment with the anti-angiogenic agent AG-013736 (a small molecule inhibitor of VEGF/PDGF receptor kinases) has been shown to result in decreased integrin expression measured by an RGD-phage displayed peptide in a preclinical model (Yao et al. 2006) .

The final study is a first-in-man study of [18F]-AH111585 to determine its pharmacokinetics and utility as a radiotracer in patients with advanced breast cancer.

Thesis Outline

This thesis describes the biological processes which lead to tumour proliferation in cancer, the current methods for measuring response to treatment, theory and principles of PET, and rationale for new radiotracers (Chapter 1). The next chapter focuses on clinical studies of [18F]FLT-PET, including correlation of its retention and delivery with immunohistochemical markers of proliferation, generation of a cardiac input function for use as an alternative to sampling blood from the radial artery, repeatability in the absence of treatment, and examination of its potential as an early response marker in response to cytotoxic chemotherapy. The roles of different analysis techniques are compared, and tracer uptake in normal tissues is assessed. Finally the value of using [18F]FLT as a pharmacodynamic marker to thymidylate synthase by capecitabine is presented. Chapter 3 focuses on [11C]choline-PET, correlation with histological parameters of MAPK activity, repeatability of uptake, and early changes in response to HER2/neu inhibition by trastuzumab. The final chapter describes a phase 1 study of a new tracer ([18F]-AH111585) used to image tumour angiogenesis in metastatic breast cancer by detecting the αvβ3 integrin.

CHAPTER 2: [18F]Fluorothymidine ([18F]FLT)

2.0 Outline of [18F]FLT Projects

The first project examines how the uptake and retention of [18F]FLT correlates with Ki-67 LI, a commonly used immunohistochemical marker of cell proliferation, in a group of patients with primary and metastatic breast cancer. Previous studies have shown a correlation between [18F]FLT uptake and KI-67 LI in non-small cell lung cancer(Vesselle et al. 2002; Buck et al. 2003), but this is the first time that 1) the value of mathematically-modelled kinetic parameters and 2) the utility of [18F]FLT-PET in breast cancer will be studied. The use of the cardiac blood pool to derive a suitable arterial input function for [18F]FLT is then explored.

One of the essential characteristics of any test is that it lacks significant test-retest variability in the absence of any intervention. The same is true for the development of new radiotracers(Aboagye et al. 2003). The second study evaluates the repeatability of [18F]FLT and the pharmacokinetic parameters SUV, Ki, and FRT. The data will then be used to determine significance levels after intervention with FEC chemotherapy. This third study (response to treatment) will compare pre- and post-treatment [18F]FLT uptake and retention at one week to clinical response at 60 days post first treatment as is normal with clinical evaluation to chemotherapy. In responding tumour lesions it is expected that at one week a decrease in [18F]FLT uptake will be seen due to decreased tumour proliferation. The potential of [18F]FLT-PET for use as a pharmacodynamic marker to study the activity of the thymidine salvage pathway an early increase in [18F]FLT uptake is expected in response to successful inhibition of thymidylate synthase. The initial results of this [18F]FLT-PET study are presented at the end of this chapter.

2.1 [18F]FLT-PET Correlation with Proliferation in Breast Cancer

2.1.1 HYPOTHESIS

[18F]FLT uptake measured by PET corresponds with proliferation in breast cancer

Non-invasive left ventricular sampling provides a suitable surrogate arterial input function for [18F]FLT-PET to that obtained from radial artery sampling

2.1.2 AIMS

- To assess pharmacokinetic parameters which describe [18F]FLT uptake in breast cancer lesions in vivo using PET
- To determine if the parameters differ significantly from those in corresponding normal tissue
- To measure the correlation between [18F]FLT-PET in vivo and proliferation in the same tumours using the Ki-67 LI in tumour biopsies
- In patients where the heart is in the field of view of the PET scanner, to correlate the results derived from radial arterial sampling with non-invasive cardiac sampling.

2.1.3 INTRODUCTION

Tumour proliferation is a key target for modern cancer therapeutics. Breast cancer was chosen as a model system as i) there is an opportunity to correlate imaging findings in tumours in situ prior to surgery or treatment with biopsy findings, ii) outcomes for the treatment of breast cancer need to be improved, and iii) a successful, non-invasive marker of breast tumour proliferation could potentially be extrapolated to a large population of patients resulting in widespread diagnostic and therapeutic applications as there is a high incidence of breast cancer in the Western world.

Patients with larger breast tumours are increasingly being treated with neoadjuvant chemotherapy in an attempt to downstage the size of the tumour and make limited surgery a viable option(Buzdar 2007; Mieog et al. 2007). Despite any clear survival benefit from neoadjuvant treatment, the opportunity to test chemosensitivity in vivo and kill occult micrometastases remains attractive; however novel early predictors of response are required to validate this approach. Patients with relapsed and metastatic disease were included in the study to enable the utility for [18F]FLT-PET in these situations to be discovered. Primary tumours less than 2.5 cm were not included in this study, as currently there is no role for neoadjuvant treatment in this patient group and the standard initial treatment is surgical excision (except if the patient is medically unfit for surgery, or as part of a clinical trial).

Tumour expression of the Ki-67 antigen, an immunohistochemical marker of proliferation, is widely used to assess prognosis. In patients with breast cancer treated with neoadjuvant endocrine therapy changes in expression of Ki-67 after only 2 weeks of therapy were predictive of relapse free survival(Dowsett et al. 2007). Interestingly this study found that the baseline proliferation level did not affect prognosis, whereas if the level remained elevated at 2 weeks then prognosis was adversely affected. Rather

than performing repeat biopsies, [18F]FLT-PET has the potential to offer a non-invasive method of measuring tumour proliferation in serial studies.

For [18F]FLT to be a viable radiotracer for use in breast cancer, it is imperative that tumour uptake is significantly different from corresponding normal tissue. In planning this study the region of interest (ROI) analysis was for complete tumour ROIs in breast or metastatic regions to be compared with normal breast or (if normal breast was not in the field of view) lung on the contralateral side. The kinetics of the radiotracer in blood and tissue need to be ascertained, as it is unlikely that a tracer which is rapidly metabolised into multiple metabolites, or has a rapid washout from tissues is going to gain widespread acceptance outside research centres. The optimum time for PET scanning post intravenous injection for [18F]FLT is not known, therefore dynamic imaging over a reasonable time window should allow the optimal period of tumour uptake from the injection time point to be detected.

Radiotracer uptake and retention can be described by a variety of pharmacokinetic parameters - described in Chapter 1. Analytic methods used to describe "proliferation-related" PET parameters measured the kinetics of [18F]FLT simultaneously in arterial blood and tissues using dynamic PET scanning, such a protocol has not been reported previously. In planning this study, the PET parameters were compared in terms of correlation with Ki-67 LI in tumour samples.

To determine if arterial sampling was required for future studies, in patients where the heart was in the field of view of the PET scan, a region of interest was drawn manually on the cardiac blood pool and compared to the measured data obtained from the online blood sampling from the radial artery. This would facilitate future studies without the need for radial artery sampling, whilst not limiting the availability of measuring multiple pharmacokinetic parameters. The kinetic analysis presented in the [18F]FLT studies in this chapter relies upon continuous radial artery sampling to provide an accurate estimate of radiotracer concentration in plasma over time i.e. a dynamic arterial plasma input function; this is viewed as the gold standard

for PET imaging. Most PET centres do not have this facility, and are therefore restricted to semiquantitative parameters. Alternatives to arterial sampling do exist, such as arterialised-venous sampling which requires hand warming and continuous venous sampling. A less invasive option is the use of the cardiac blood pool drawn as an ROI over the left ventricle, which was explored in the patients in this study.

Compared to FDG, there should be little myocardial uptake of [18F]FLT as myocardial expression of TK1 is intrinsically low(Toyohara et al. 2002). Previous studies have employed the alternatives described above for FDG(Weinberg et al. 1988; Choi et al. 1991; Choi et al. 1993; Chen et al. 1994), but the use of alternatives for [18F]FLT has yet to be evaluated.

2.1.4 METHODOLOGY

2.1.4.1 Eligibility criteria and recruitment

Patients were recruited from medical oncology clinics in Charing Cross Hospital, London. The inclusion criteria for patients were as follows: 1) age ≥ 18 years and ≤ 80 years, 2) histologically or cytologically proven breast cancer, 3) at least one site of measurable disease ≥ 2.5cm (n.b. patients with liver and/or bone metastases were allowed to participate in the study provided the measurable lesion was not located at these sites as previous studies suggested high normal uptake in these regions(Shields et al. 1998)), 4) have a treatment-free interval of ≥ 3 weeks (for cytotoxic chemotherapy, hormonal therapy, or cytostatic agents), nb 4 weeks applied for radiotherapy to the imaging site - to give a satisfactory washout period and prevent measurement of an effect related to previous treatment, 5) life expectancy of ≥ 3 months, 6) haemoglobin of ≥ 10g/dL, granulocyte count of ≥ 1.5 x 10^9/L, platelet count of ≥ 100 x 10^9/L, 7) adequate creatinine clearance (calculated ≥ 50ml/min), 8) adequate hepatic function (bilirubin ≤ 1.5 ULN, serum transaminases ≤ 2.5 x the upper

limit of normal) 9)ECOG performance status 0 – 2 inclusive(Oken et al. 1982) – see Appendix 1, 10) be able to give fully informed consent and comply with the protocol. The exclusion criteria were: 1) pregnant or lactating patients, 2) sexually active patients who were not employing adequate contraception (pregnancy tests were performed in all women of childbearing potential, this population was strongly advised to avoid pregnancy in this study), 3) patients with uncontrolled medical conditions, 4) patients unable to lie flat, 5) patients with evidence or previous diagnosis of cerebral metastases.

Eligible patients were approached and given a study information leaflet to consider at their leisure. All research was performed according to the Declaration of Helsinki guidelines. Ethical approval for the studies was granted by the Hammersmith Hospitals NHS Trust Ethics Committee.

The plan was to recruit 10 patients, allowing for a dropout rate of 20% for a target of 8 patients. However, if after 3 patients it became apparent that with 3 scans there was excessive bruising, or the scans were not well tolerated, it was proposed to recruit 14 patients in total, allowing for a dropout rate of 21% for a target of 11 patients. The plan of the study would have been changed such that each of the further 8 patients would have 2 scans each, either baseline + repeatability, or baseline + post-treatment (there would be 4 patients in each of these groups). As the initial protocol was well tolerated in the first 3 patients, the study continued with 3 scans planned for each subject. A decision was made to study 15 patients in total to improve the robustness of the data, ethics and ARSAC appoved this amendment.

Fifteen patients with 13 primary tumour areas, 6 nodal metastatic regions, and 1 pulmonary metastasis were included. The histological types were as follows: 11 tumours were invasive ductal carcinomas, 3 were lobular carcinomas, and one was an inflammatory carcinoma.

For the cardiac blood pool analysis, eleven patients who participated in the [18F]FLT proliferation, repeatability and response to FEC chemotherapy studies were included as the heart was in the field of view.

2.1.4.2 Scanning procedure and [18F]FLT synthesis

An arterial cannula was inserted in the radial artery prior to the start of the scan (after an Allen's test to ensure satisfactory ulnar circulation) under local anaesthetic (2% bupivicaine) to allow arterial blood sampling during the scan. A second cannula was inserted into a suitable upper limb vein to allow intravenous administration of the radiotracer. Two transmission scans (~20 min) were performed to ensure that the patients were positioned correctly, i.e. the field of view was centred on the tumour of interest, and to facilitate attenuation correction.

Patients were scanned for 95 minutes following a bolus intravenous injection of a tracer dose of [18F]FLT over 30 seconds. Radiochemical purity and specific activity was determined by the quality control laboratory staff in Hammersmith Imanet® prior to injection. The dose injected ranged from 153 to 380MBq (specific activity 25-465 GBq/μmol, measured using high performance liquid chromatography (HPLC)). PET scans were performed using an ECAT962 HR+ tomograph (CTI/Siemens Knoxville, TN) within Hammersmith Imanet (GE Healthcare®) which allows simultaneous data acquisition to form 63 transaxial planes (axial field of view 15.7 cm). Images were reconstructed using 2D filtered back projection (FBP). In two patients reconstruction was performed using an iterative ordered subset expected maximisation algorithm to identify the tumour regions, the object maps drawn using this method were then applied to the images obtained by the filtered back projection method. This was attributed to the presence of high noise in the background region (due to the liver being in the field of view in 1 case, and the intravenous injection site in the second).

Data were binned into 31 discrete time intervals (referred to as frames) of varying length (30s x 10; 60s x 5; 120s x 5; 180s x 5; 600s x 6). The scanner dimensions are shown below in Table 2.1. The raw data count was transferred onto SPARC Ultra workstations (Sun Microsystems Inc., Mountain View, California, USA). Reconstruction into 3D images of radioactivity concentration was performed using CTI (Siemens, Knoxville) software.

Table 2.1: Dimensions of the ECAT 962 HR+ Tomograph

Scanner	962	
Reconstruction method	2D FBP	
Zoom	1.00	2.5
Pixel size (x-y) mm	5.23	2.09
Slice thickness	2.42	
Transaxial resolution (x-y) mm	8.5 ramp, brain mode off	
Axial resolution (z) mm	5.0	

All radiochemical synthesis of [18F]FLT was performed by the chemistry department within Hammersmith Imanet®. [18F]FLT was synthesised by a method which involves radioflorination of the 2,3'-anhydro-5'-O-(4,4'-dimethoxytrityl)-thymidine precursor described previously by Cleij et al (Cleij 2001). The maximum permissible cold activity was <10 micrograms per preparation. Radiochemical purity was > 95%. The pH range of the injectate was restricted to between 5.5 and 7.5.

2.1.4.3 Determination of Radioactivity in Blood and Plasma after Injection of [18F]FLT

In addition to the PET scanning, arterial blood sampling was performed continuously for the first 10 minutes post-injection; discrete arterial samples were taken at baseline, 2.5, 5, 10, 20, 30, 45, 60, 75, and 90 min. Total blood radioactivity was measured from the continuous sampling in an on-line radioactivity detector. The activity was compared to that in the discrete samples which was monitored by gamma counting; [18F]FLT plasma parent fraction (and metabolite, [18F]FLT-glucuronide)(Muzi et al. 2005) was determined by HPLC (Barthel et al. 2003).

The radioactivity in an aliquot of blood and plasma (1ml) was measured using a sodium iodide well counter. The remainder of blood (7ml) was centrifuged at 14,000 rpm to obtain plasma. The plasma samples (2ml) were deproteinised by solvent extraction (using 5 fold ice-cold acetonitrile, Fisher Scientific, Leicestershire UK) analysed using a reverse-phase HPLC. The column (C18, μ Bodapak, 30 x 0.78 cm id; 10 μm particle size) was washed with the mobile phase: a mixture of potassium di-hydrogen phosphate, pH 4.5 (10mM) and acetonitrile (85:15, v/v) at a flow rate of 3ml per min. The eluate was monitored for radioactivity. Both detectors were linked to a PC based integrator which recorded the radioactivity profile and enabled the correction for [18F]-radioactivity decay and background and integration of radioactive components. The amount of [18F]FLT and other radioactive components at each sample time was calculated as a percentage of each radioactive component in each analyte.

The [18F]-radioactivity profile in plasma showed parent [18F]FLT and another more polar radioactive component than [18F]FLT. [18F]FLT decreased slowly with time, whereas the polar radioactive component was observed to increase with time (see figure 2.2).

To assess the metabolism of [18F]FLT, 5 arterial plasma samples taken at 60 min were treated with β-glucuronidase (5000U/ml) for 30 min at 37 ^{0}C, or β-

glucuronidase (5000U/ml) and a β-glucuronidase inhibitor (saccharic acid –1,4,lactone (0.5M)) for 30min at 37 ^{0}C and analysed by HPLC using the method of Barthel et al(Barthel et al. 2003). The results of the metabolite analysis from this technique are shown in Table 2.1. The metabolite analysis was performed by Hammersmith Imanet staff under the supervision of Ms S Osman.

2.1.4.4 Pharmacokinetics and Data Analysis

Following reconstruction, the kinetic image data were analysed with the aid of Analyze® image analysis software (Biomedical Imaging Resource, Mayo Foundation Rochester, MN, USA). Images from the final 5 time frames were combined to form an "add image" on which an object map was defined. Regions of interest (ROIs) were drawn manually on tumour, normal breast, lung, and vertebral tissue. The object map was then applied to the complete dynamic image data set to derive tissue activity time curves (TACs). From these TACs, together with the blood data, the following methods of analysis were used to generate parameters, which describe delivery, washout, uptake and retention of the tracer.

SUV and AUC

The semiquantitative parameters SUV and AUC were calculated for each region from the TACs after correction for the injected dose of radioactivity and [18F] decay. The average (as opposed to peak) activity during specific time frames was used for calculation of both parameters. Weight and height were measured for each patient immediately prior to scanning.

$$\text{Corrected activity (t) } [m^2/ml] = \frac{\text{Measured activity at time (t) [kBq/ml] x } e^{\lambda t}}{\text{Injected dose [kBq] / BSA}}$$

λ = decay constant for [^{18}F] (1.053 x 10^{-4})
t = time in minutes
BSA = Body surface area (m^2) –this was calculated for each patient visit.
NB Corrected activity is equivalent to standardised uptake value (SUV).

SUV was corrected for body surface area (BSA) using the formula below:

BSA (m^2) = 0.20247 x Height(m)$^{0.725}$ x Weight(kg)$^{0.425}$ (DuBois D 1916)

For AUC the integral of each SUV value multiplied by the duration of the time frame in seconds for the 31 time frames was calculated.

Plasma Input Functions

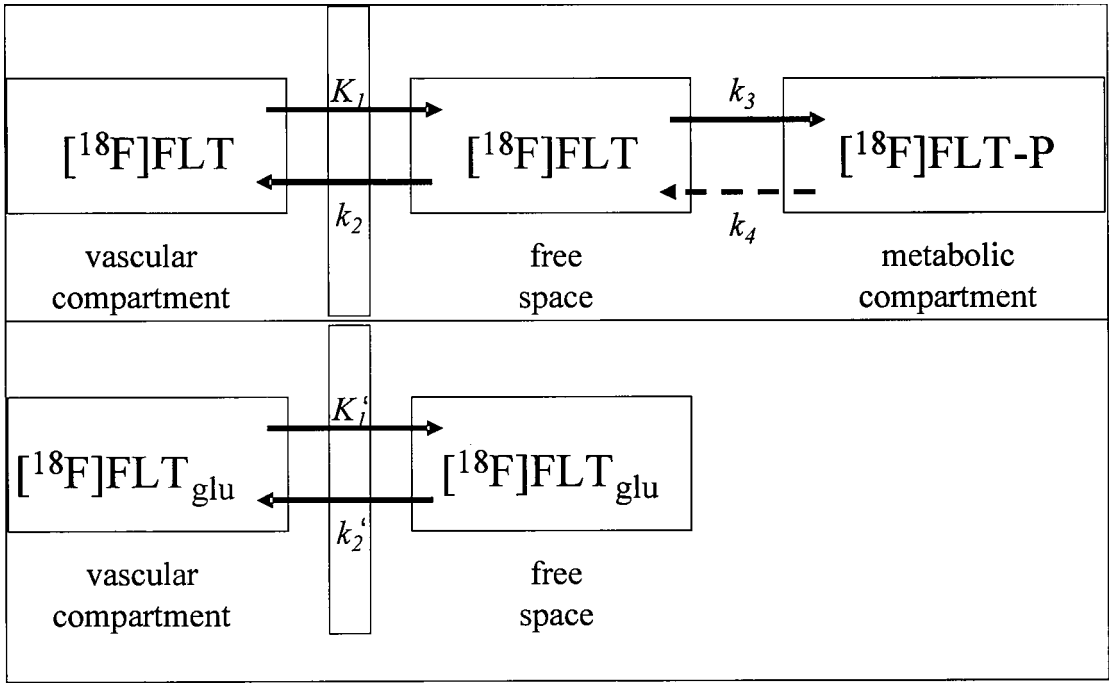
The ratio of radioactivity in whole blood to plasma measured in the discrete blood samples (described above) was fitted to a linear function and plotted against time. The proportion of radioactivity in plasma recovered in the non-metabolised, i.e. parent fraction, was fitted to a function describing an exponential approach to a constant. These two functions were then applied to the continuous on-line and discrete arterial data, which after cross-calibration with the camera gives a parent plasma input function for subsequent kinetic analyses (i.e. compartmental, spectral, and Patlak). The plasma input functions were generated using Matlab version6® with in-house software. Modifications of the arterial plasma input function were used for Patlak analysis and are described in the Patlak and spectral analysis section below.

Compartmental Modelling

A two tissue compartmental model, similar to the one described by Sokoloff for FDG, was used to derive the unidirectional delivery macro parameter K_1(Sokoloff L 1977)..This was possible for [18F]FLT as the proportion of metabolites in the delivery

phase is negligible (see chromatogram at 2 minutes shown in Figure 2.2A below). The proposed model for [18F]FLT is shown below in Figure 2.1. The process of glucuronidation of FLT blocks phosphorylation, as phosphorylation and glucuronidation occur at the same position.

Figure 2.1: Two Tissue Compartment Model for [18F]FLT



(where K1= unidirectional delivery of [18F]FLT from plasma to tissue, k2 = transfer back from tissue to plasma, k3 = trapping of [18F]FLT as the phosphorylated form within tissue by TK1, k4 = dephosphorylation of [18F]FLT within tissue, K1' = delivery of [18F]FLT-glucuronide into tissue, and k2'=transport of [18F]FLT-glucuronide back to plasma).

The time delay between tissue uptake and measurement of on-line blood radio activity of the tracer was chosen initially depending on the best fit of the mathematical model to the raw tissue data and selecting the delay with the lowest residual sum of

squares. During the project, an automated method of delay detection became available using Matlab® and the compartmental model shown above. This method for computing delay detection was then applied to all data in this thesis.

Patlak and Spectral Modelling

Three forms of Patlak analysis were undertaken in this study by using three different arterial input functions: i) classical Patlak using the parent plasma input function in which there is correction for the presence of metabolites in arterial plasma, ii) total Patlak in which there is no correction for metabolites in the plasma input function and iii) modified Patlak in which there was correction for metabolites in both tissue and plasma, see Chapter 1 for equations (Patlak et al. 1985; Mankoff et al. 1996).

Whilst Patlak analysis measures irreversible retention, the exact pharmacokinetics of [18F]FLT have not yet been described; therefore spectral analysis – a data-led approach with no a priori assumptions about radiotracer behaviour was undertaken. Spectral analysis was used to calculate the ratio of tracer uptake at sixty minutes and ninety minutes compared to that at 1 minute (FRT60:1 and FRT90:1).

Cardiac Blood Pool Analysis

The early time frames (2 to 5) were used to form a composite image from which the cardiac blood pool was identified as an ROI to minimise any possible spill over from myocardial uptake which should be minimal. The periphery of this was drawn manually to form an object map, which was then applied to the dynamic [18F]FLT image to generate TACs, and the area under the time activity curve (AUC $kBq.sec.ml^{-1}$) determined as an integral of the midframe uptake multiplied by the frame duration in seconds. The AUC of the total blood input function curve was also calculated for comparison, as in the heart ROI the measured activity was from total blood – i.e. it was not possible to separate arterial plasma for region analysis. The

peak activities for the heart ROI and total blood input functions, AUC at 60 minutes (AUC60), AUC at 90 minutes (AUC90), and total blood activity at 60 minutes were compared.

2.1.4.5 Ki-67 Immunohistochemistry

To determine the relationship between [^{18}F]FLT uptake and histological markers of proliferation patients with a suitable core biopsy taken within 3 months of the scan (median 18 days) were studied. Formalin fixed sections were sectioned and stained with an anti-Ki-67 monoclonal antibody, NCL-Ki-67-MM1 (Novocastra Laboratories, Newcastle Upon Tyne, UK). All staining was performed by David Peston, of the immunohistochemistry laboratory, Department of Histopathology, Charing Cross Hospital London.

The numbers of total and Ki-67 positive tumour cells were manually counted in 8 randomly selected fields of view using a BX51 microscope (Olympus Optical, Tokyo, Japan) at 400 X magnification with the aid of Sigma Scan Pro 5 (Aspire Software International, Leesburg, VA). The ratio of Ki-67-positive stained cells to the total number of tumour cells was then used to calculate the Ki-67 labelling index (LI).

2.1.4.6 Statistical Analysis

A paired t-test was used to assess the difference between tumour and normal tissue data (breast, or if normal breast tissue was not in the field of view normal lung tissue was used). The association between PET parameters and Ki-67 LI was determined using the Pearson correlation coefficient (95% confident, two-tailed). A p-value of ≤ 0.05 was considered significant. All statistical analysis in this thesis was performed using the aid of Graph Pad Prism ® version 3 (Graph Pad Software, San Diego, California, USA).

2.1.5 RESULTS

2.1.5.1 Patients

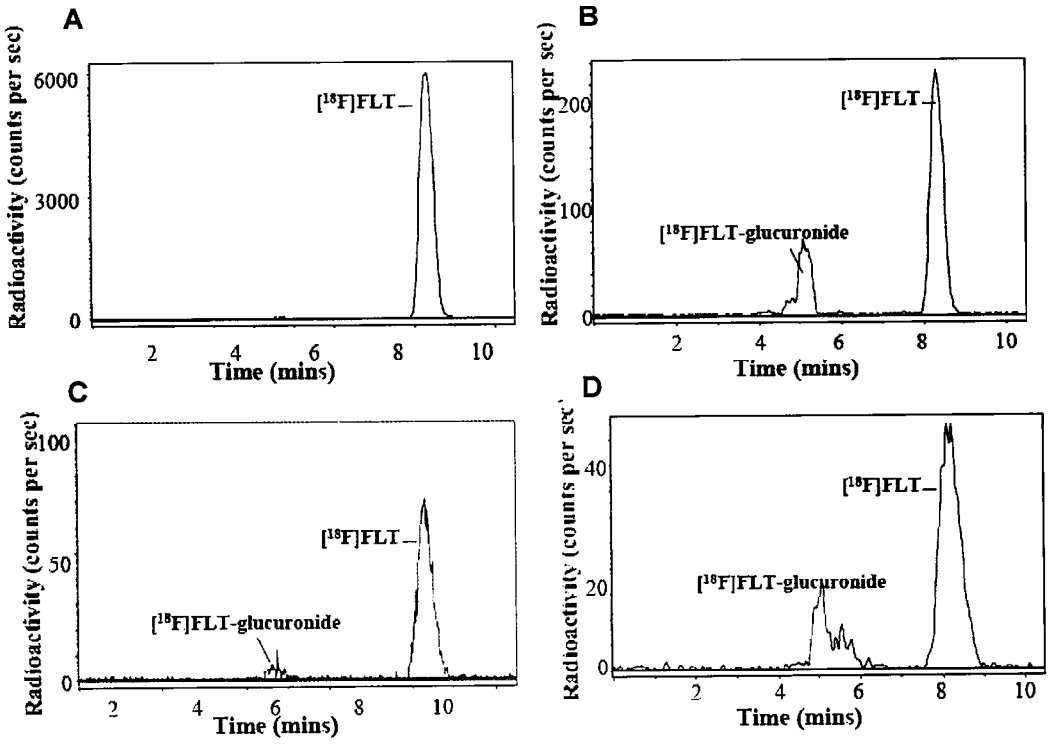
Fifteen female patients aged between 37 and 79 years participated in the study. The scans were well tolerated. The tumour phenotypes, regions studied, and results of the semi-quantitative analysis and modelled parameters are shown in Table 2.2 and Table 2.3 respectively. The majority of the patients had ductal carcinoma (73.3%), followed by lobular carcinoma (20%); inflammatory carcinoma was the least common (6.7%). This is in keeping with findings in the general population where ductal carcinoma represents the most common histological subtype of breast cancer affecting 75% of breast cancer patients (Veronesi et al. 2005).

Uptake was studied on a lesion by lesion basis – in large tumours (i.e. greater than 5cm) the ROIs covered a proportion of the tumour area as there was significant heterogeneity in uptake of [18F]FLT over large tumour areas. Regions which were obviously necrotic were not included within the tumour ROIs. In total, twenty nine tumour regions comprising of 22 primary tumours and 7 metastatic lesions were studied.

2.1.5.2 Metabolism of [18F]FLT and effect of β-glucuronidase

The results shown in Figure 2.2 and Table 2.1 (below) indicated that during the scanning period, [18F]FLT was metabolised into a single metabolite – [18F]glucuronide. This reaction was inhibited by the addition of β-glucuronidase leading to an increase in [18F]FLT, and the action of β-glucuronidase was subsequently inhibited by the addition of saccharic acid-1,4-lactone leading to a decrease in the percentage fraction of [18F]FLT detected in arterial plasma.

Figure 2.2: HPLC Chromatograms from arterial plasma showing [18F]FLT and metabolite



where A) 2 min arterial plasma sample showing a parent [^{18}F]FLT peak, B) 60 min arterial plasma (control) sample in which both [^{18}F]FLT and [^{18}F]FLT-glucuronide peaks are seen, C) 60 min arterial plasma sample incubated with β-glucuronidase, D) 60 min arterial plasma sample incubated with β-glucuronidase and (saccharic acid-1,4-lactone).

Table 2.1: Metabolism of [18F]FLT and effect of β-glucuronidase

	Percentage Radioactivity due to [18F]FLT		
	60 min plasma Sample	60 min plasma sample + β-glucuronidase*	60 min plasma sample + β-glucuronidase + saccharic acid 1,4 lactone§
Sample 1	80.61	93.59	88.97
Sample 2	80.05	94.55	77.16
Sample 3	76.85	93.78	77.12
Sample 4	84.80	90.39	ND
Sample 5	74.00	88.00	80

Tables 2.2 and 2.3: Kinetic parameters for primary tumours, metastatic tumours, and normal tissue (breast or lung).

* Intraductal carcinoma is represented by the letter D, invasive lobular carcinoma by the letter L, and inflammatory carcinoma by the letter I; the histological types are suffixed with the tumour grade (1-3). Ki, rate constant measured by the modified Patlak technique (ml plasma.ml tissue^{-1}. s^{-1}) x 10^{-4}. K1 – delivery constant (microL.s^{-1}.mL^{-1}). Larger tumours (> 5cm) were subdivided into separate regions for analysis. SUV_A = SUV at 21.5 min, and SUV_B = SUV at 90 min (m^2.ml^{-1}) x 10^{-5}. AUC – AUC measured at 90 minutes (m^2.ml.s^{-1}).

Table 2.2: Semiquantitative parameters of [18]FLT uptake

Patient#	Region, Type and Grade*	SUV_A	SUV_B	AUC 90
1	Tumour, L2	5.767	6.308	0.353
3	Tumour, D3	5.418	3.795	0.269
4	Tumour A, D2	7.868	9.164	0.467
4	Tumour B, D2	5.989	7.189	0.365
4	Tumour C, D2	9.515	10.749	0.571
4	Tumour D, D2	8.736	10.293	0.528
5	Tumour, L3	4.134	3.676	0.208
6	Tumour A, D3	9.286	11.189	0.560
6	Tumour B, D3	8.002	9.912	0.498
7	Tumour, D2	5.118	4.999	0.273
8	Tumour A, D2	5.863	6.296	0.348
8	Tumour B, D2	4.541	5.384	0.286
8	Tumour C, D2	5.030	5.736	0.314
8	Tumour D, D2	6.721	8.510	0.443
9	Tumour, D2	4.335	4.827	0.259
11	Tumour A, I3	5.063	4.373	0.280
11	Tumour B, I3	4.188	3.726	0.228
12	Tumour, L2	3.039	2.368	0.160
13	Tumour, D2	13.128	14.415	0.751
14	Tumour, D2	7.824	8.324	0.469
15	Tumour A, D2	6.929	7.583	0.401
15	Tumour B, D2	5.366	6.349	0.332
2	Lung metastasis, D3	5.721	6.369	0.353
5	Mammary node	7.171	7.232	0.387
5	Axillary node	3.950	6.188	0.299
6	Axillary node	8.076	9.159	0.479
10	Axillary node	13.728	19.983	0.927
10	Pretracheal node	10.124	12.184	0.621
13	Axilla	9.349	14.211	0.646
1	Normal breast	2.252	1.748	0.115
2	Normal lung	1.583	0.922	0.075
3	Normal breast	1.010	0.664	0.044
4	Normal breast	0.456	0.046	0.019
5	Normal breast	1.096	0.469	0.047
6	Normal breast	2.792	2.220	0.137
7	Normal breast	1.329	0.769	0.055
8	Normal breast	1.203	0.867	0.061
9	Normal breast	2.039	1.445	0.080
10	Normal lung	2.241	1.152	0.106
11	Normal breast	1.639	1.246	0.089
12	Normal breast	1.854	1.259	0.095
13	Normal breast	0.771	0.557	0.042
14	Normal breast	1.295	1.109	0.071
15	Normal breast	0.314	0.471	0.071

Table 2.3: Modelled pharmacokinetic parameters of [18]FLT uptake

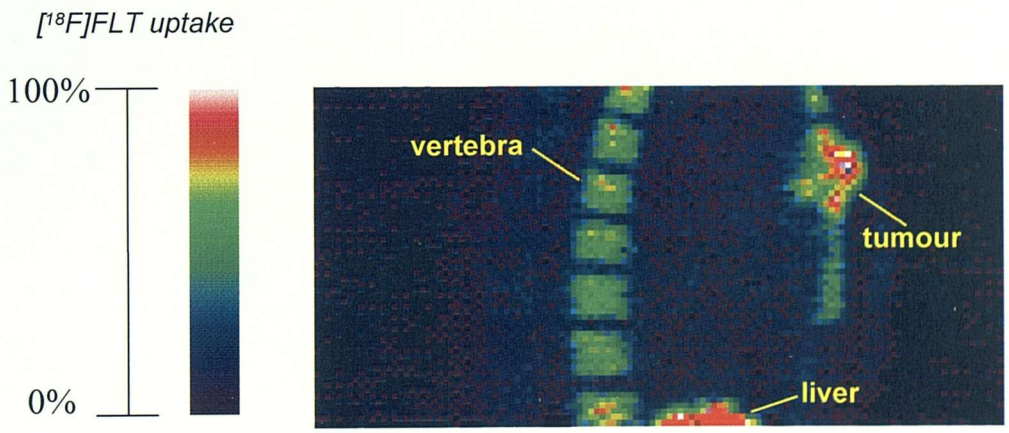
Patient#	Region, Type and Grade	Ki	FRT 90:1	K_1
1	Tumour, L2	2.987	0.192	1.815
3	Tumour, D3	1.953	0.120	2.051
4	Tumour A, D2	6.717	0.524	1.455
4	Tumour B, D2	5.462	0.536	1.237
4	Tumour C, D2	7.018	0.413	2.404
4	Tumour D, D2	7.895	0.444	2.021
5	Tumour, L3	2.269	0.179	2.051
6	Tumour A, D3	5.390	0.264	2.301
6	Tumour B, D3	5.362	0.305	1.887
7	Tumour, D2	1.767	0.194	1.314
8	Tumour A, D2	3.603	0.213	2.048
8	Tumour B, D2	3.135	0.231	1.641
8	Tumour C, D2	3.560	0.238	1.769
8	Tumour D, D2	5.476	0.324	1.982
9	Tumour, D2	2.233	0.183	1.518
11	Tumour A, I3	1.958	0.097	2.515
11	Tumour B, I3	1.615	0.113	1.978
12	Tumour, L2	0.627	0.098	0.964
13	Tumour, D2	3.581	0.367	3.820
14	Tumour, D2	3.534	0.322	1.639
15	Tumour A, D2	1.818	0.202	1.792
15	Tumour B, D2	1.550	0.209	1.399
2	Lung metastasis, D3	3.978	0.252	1.920
5	Mammary node	5.276	0.373	1.215
5	Axillary node	3.759	0.182	2.825
6	Axillary node	4.570	0.267	1.895
10	Axillary node	10.379	0.594	2.072
10	Pretracheal node	6.509	0.380	3.528
13	Axilla	10.311	0.467	2.266
1	Normal breast	0.448	0.087	0.374
2	Normal lung	0.408	0.089	0.659
3	Normal breast	0.468	0.178	0.245
4	Normal breast	< 0.03	0.005	0.448
5	Normal breast	0.000	0.001	1.184
6	Normal breast	0.570	0.151	0.514
7	Normal breast	0.190	0.081	0.397
8	Normal breast	0.226	0.096	0.539
9	Normal breast	0.514	0.222	0.290
10	Normal lung	0.549	0.053	0.625
11	Normal breast	0.348	0.084	0.571
12	Normal breast	0.235	0.099	0.369
13	Normal breast	0.472	0.019	0.315
14	Normal breast	0.484	0.213	0.272
15	Normal breast	0.010	0.033	0.355

2.1.5.3 [18F]FLT uptake in tumour and normal lesions

Twenty nine distinct tumour areas in the 15 patients were detected using [18F]FLT-PET. [18F]FLT-PET was able to visualise all of the breast tumour lesions in the study. All of the patients had measurable disease in the breast or axilla except for patient 2 who had a secondary lung metastasis (from breast cancer).

The mean activity injected was 302 MBq (range 153-381MBq, radiochemical purity 100%). [18F]FLT localised mainly in tumour, liver and vertebrae – see Figure 2.3. The uptake of [18F]FLT-PET was not reversible within the duration of the scanning period. [18F]FLT-PET images showed high tumour-to-background contrast. Uptake was also seen in the liver and bone marrow due to catabolism of the radiotracer, as well as its uptake by the proliferating bone marrow cells(Shields et al. 1998; Shields et al. 2002).

Figure 2.3 Sagittal view of [18F]FLT-PET image showing high uptake in a primary breast tumour, normal liver, and vertebrae.



The high physiological uptake in liver, bone, and the primary breast tumour compared to normal tissue depicted in the PET image above is further demonstrated by the SUV curve of the same patient shown below in Figure 2.4.

Figure 2.4: [18F]FLT-SUV in tumour and normal tissues

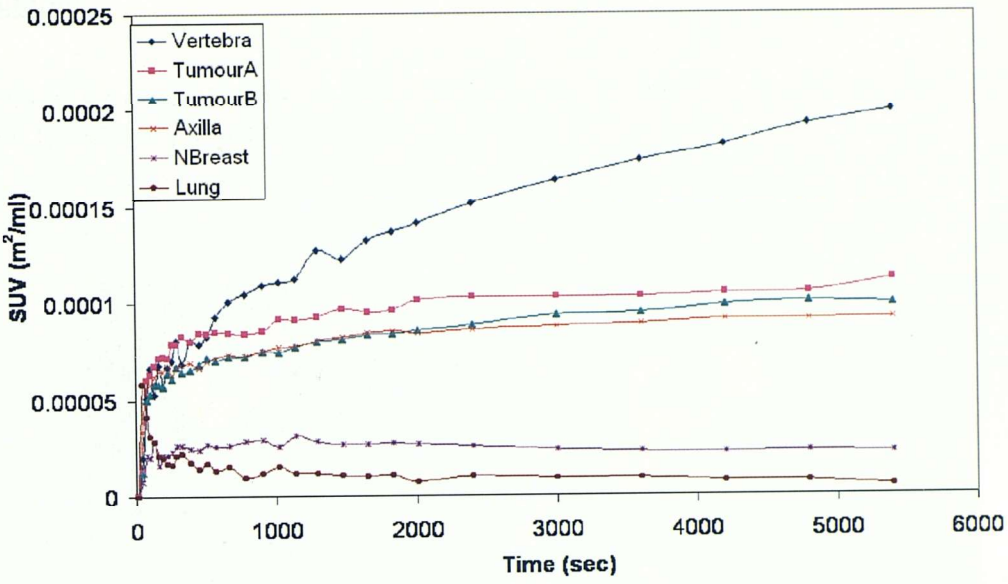
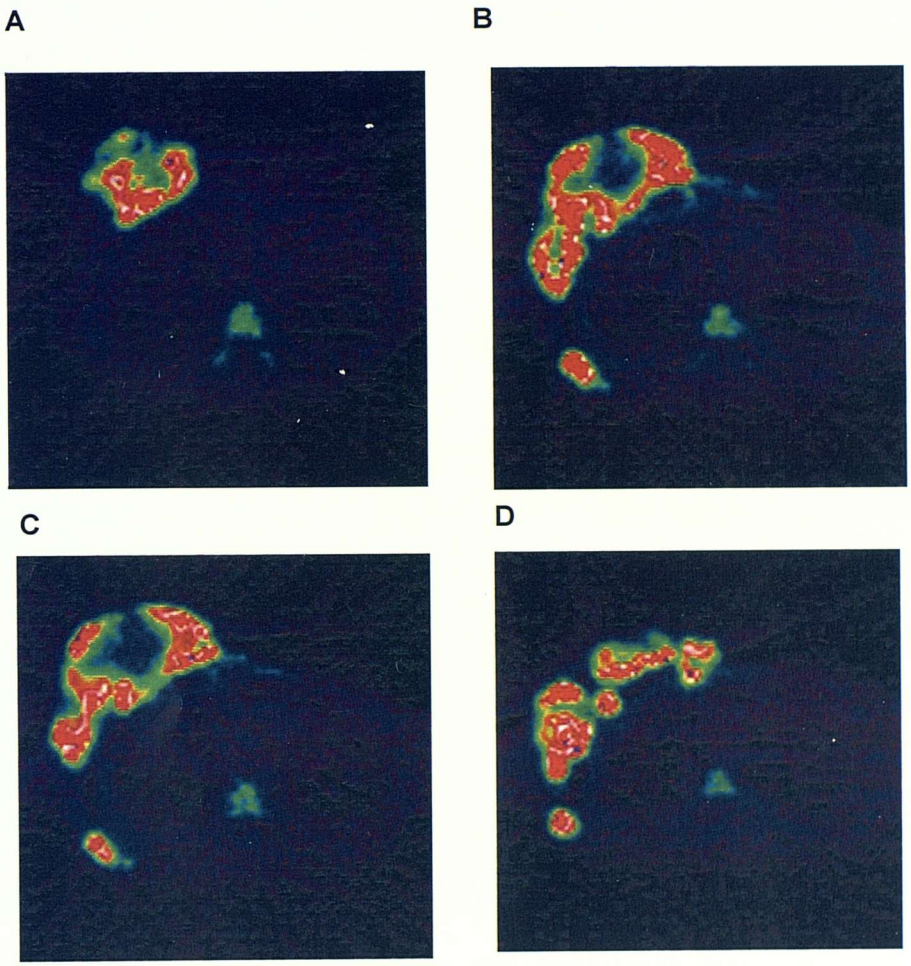


Figure 2.4 above shows the decay and BSA-corrected uptake for [18F]FLT in tumour and normal tissues, note the high uptake in normal vertebra and tumour regions (A,B, and axilla) compared to normal tissues such as breast and lung.

[18F]FLT-PET retention in larger tumours was heterogeneous; this could be due to differing proliferation rates within the same tumour and areas of tumour necrosis, possibly as a result from an altered blood supply in different regions. An example of heterogeneity is shown in Figure 2.5.

Figure 2.5: Heterogeneous uptake of [18F]FLT in a patient with a large primary tumour.

The slices labelled A, B, C, and D respectively, depict transverse sections moving from the superior to the inferior aspect of the tumour.



There was a significant difference in [18F]FLT kinetic parameters in tumour lesions compared to the corresponding normal tissue (breast or lung) for all of the tumour ROIs that were analysed. SUV was measured at 21.5 mins and 90 mins to determine if early measurement had any difference in correlation with Ki-67 LI. The latter time point was chosen as the transport of [18F]FLT should be at steady state, and the signal was due to the phosphorylated radiolabel, and not unphosphorylated [18F]FLT.

Measurement of the SUV at an early or late time point had no effect on this significance ($p<0.0001$ for both). Modelled parameters were equally effective as semiquantitative parameters for discriminating tumour lesions from normal tissue ($p < 0.0001$ for Ki, FRT, K1, and AUC). In patient 4 a hotspot of [18F]FLT uptake was clearly visible in a rib posteriorly on the PET scan, this corresponded with a hotspot in the same location on a Technetium ([99mTc]) bone scan (see Figure 2.5b above). There was a trend for [18F]FLT uptake to be higher in ductal tumours (mean SUV90 = $8.287 \pm 0.997 \times 10^{-5}$ $m^2.ml^{-1}$) than lobular tumours (mean SUV90 = $5.514 \pm 0.913 \times 10^{-5}$ $m^2.ml^{-1}$) though this was not statistically significant (Mann-Whitney $p=0.08$); the uptake was lowest in an inflammatory carcinoma (patient 11).

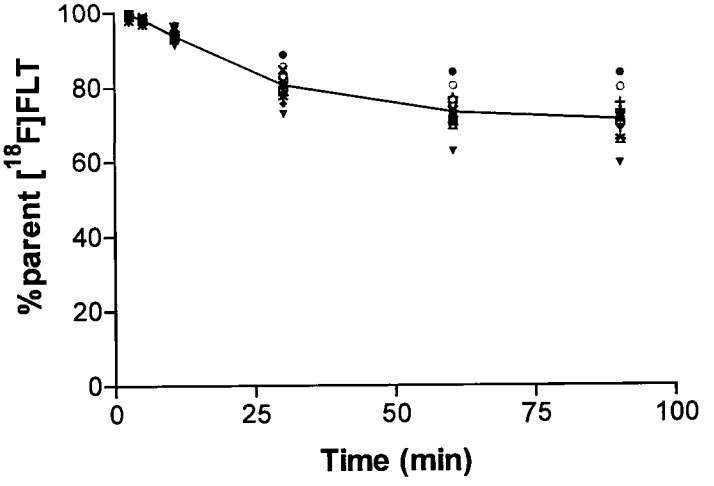
In large tumours (> 5 cm), there was marked heterogeneity (see Figure 2.5); regions of obvious necrosis were excluded from the analysis. Radiotracer localisation also differed between primary tumours and metastases from the same patient. Localisation of radioactivity in normal tissues such as breast and lung was generally low.

The proposed compartmental model for [18F]FLT is shown in Figure 2.1. In this model, [18F]FLT-glucuronide derived predominantly from the blood (transported from liver) can occupy an exchangeable space but does not contribute to the specific signal derived from the phosphorylation of [18F]FLT to [18F]FLT-phosphate. Determination of plasma-tissue exchange rate constants was made possible because of the ability to

perform online arterial sampling and HPLC profiling of parent [18F]FLT levels. [18F]FLT was slowly metabolised in all patients such that only 71.54±1.50 of [^{18}F]FLT remained unmetabolised at 90 min post injection (coefficient of variation =8.09%) (Figure 2.6).

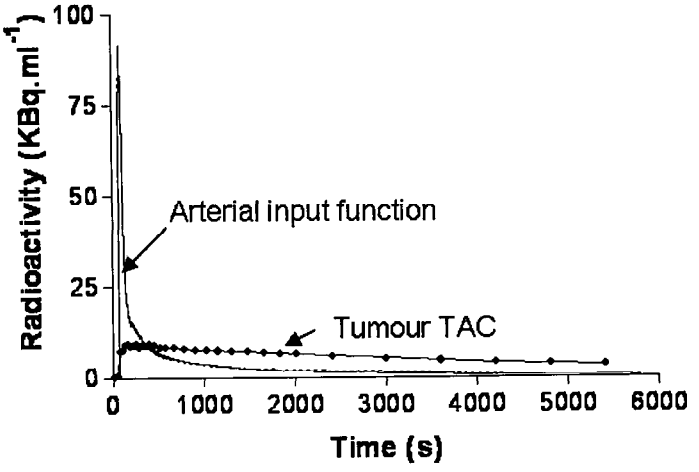
Figure 2.6: Metabolism of [18F]FLT

The percentage of parent compound [18F]FLT measured in arterial plasma for each of the patients during the scan is shown in Figure 2.6 below, with the mean value depicted by a trend line. At 90 minutes post-injection 71.54 ± 1.50% of [18F]FLT remained unmetabolised (coefficient of variation = 8.09%).



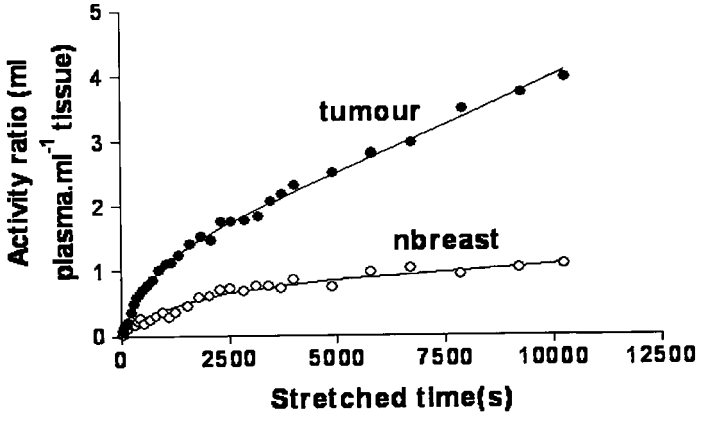
A non-decay corrected tumour activity (TAC) curve from patient 3 is shown below with the parent plasma input function (i.e. radioactivity present in arterial plasma due to unmetabolised [18F]FLT) in Figure 2.7.

Figure 2.7 Tumour TAC curve and arterial parent plasma input function



Using the modified Patlak approach, a linear phase of the curve was discernible indicating that there was unidirectional uptake of the radiotracer; the slope, Ki, was higher in tumour than in normal tissues. An example of this for patient 3 is shown below in Figure 2.8.

Figure 2.8 Comparison of tumour and normal breast [18F]FLT retention using modified Patlak analysis



The spectral model also fitted the data and showed that there was a retention component in tumour but less so in normal breast (asymptotic nature of the unit IRF in patient **4**, Figure 2.9). Use of this data-led modeling approach showed the existence of predominantly reversible kinetic components (bars to the right in Figure 2.10; the bars to the left represent irreversible components).

Figure 2.9 Comparison of the IRF for breast tumour and normal tissue

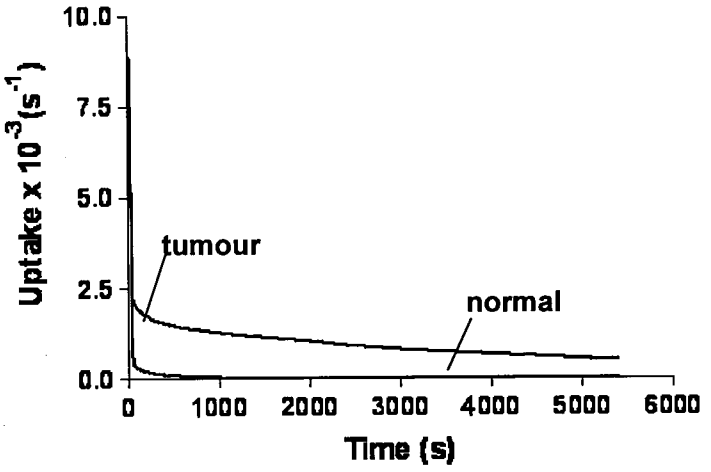
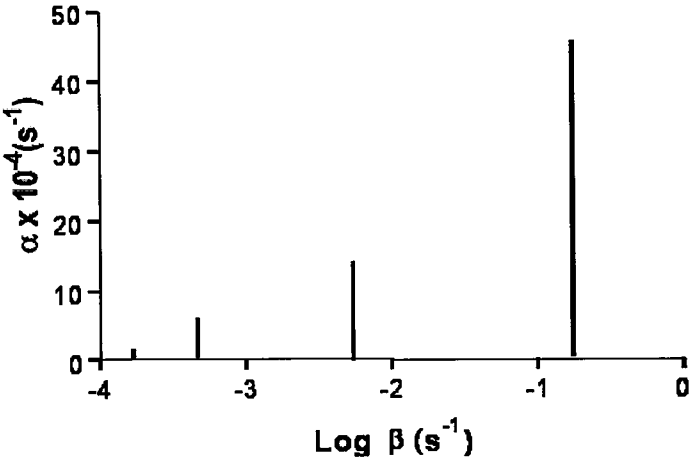


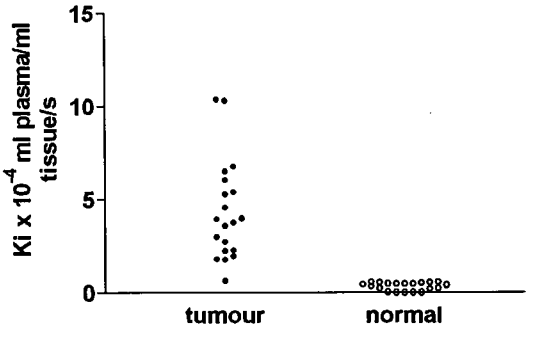
Figure 2.10 Spectrum of kinetic components in breast tumour



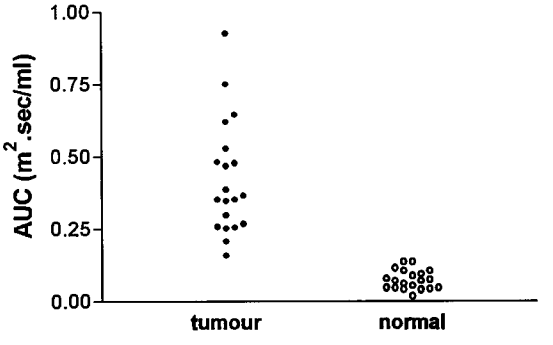
A summary of the parameters from all 29 individual tumour sites from 25 patients is shown above in Tables 2.2 and 2.3. In all cases, the delivery and retention of FLT was higher in tumours than in normal tissues (Ki ($p < 0.0001$), $SUV_{21.5}$ ($p < 0.0001$), SUV_{90} ($p < 0.0001$), AUC ($p < 0.0001$), FRT90 ($p = 0.0001$)), the delivery of FLT K_1, ($p < 0.0001$). K_1 values were low and similar to the low blood flow values seen previously in these tumours(Wilson et al. 1992). The results are depicted graphically in Figures 2.11. Overall, uptake was higher in nodal and metastatic regions in comparison with primary breast tumours. Retention of [18F]FLT was also lower in the inflammatory carcinoma in comparison with the other histological subtypes. There was a wider range for each parameter for tumour uptake in comparison with normal breast tissue.

Figure 2.11 Difference between tumour and normal tissue [18F]FLT pharmacokinetic parameters

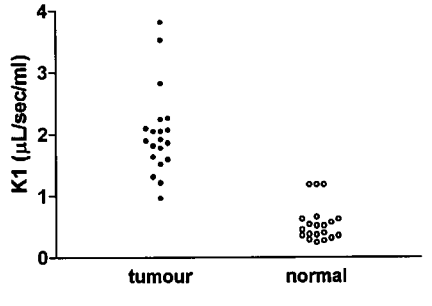
a) Modified Patlak Ki



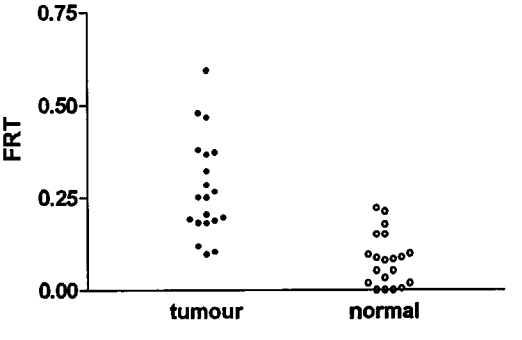
b) AUC



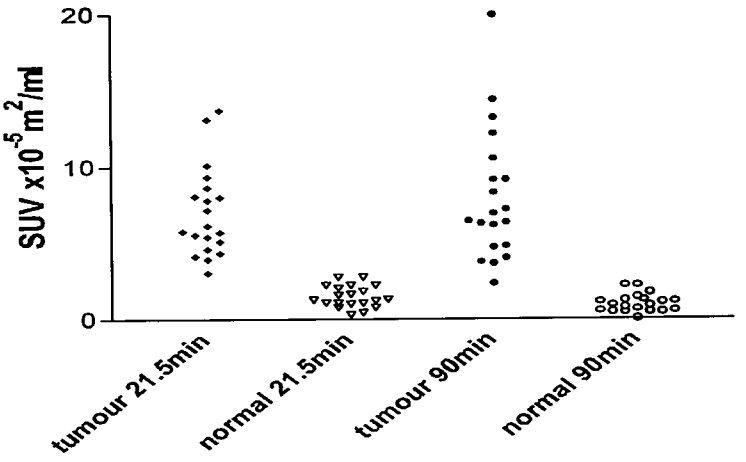
c) K1 compartmental



d) FRT



e) SUV (early: 21.5min, and late: 90mln)

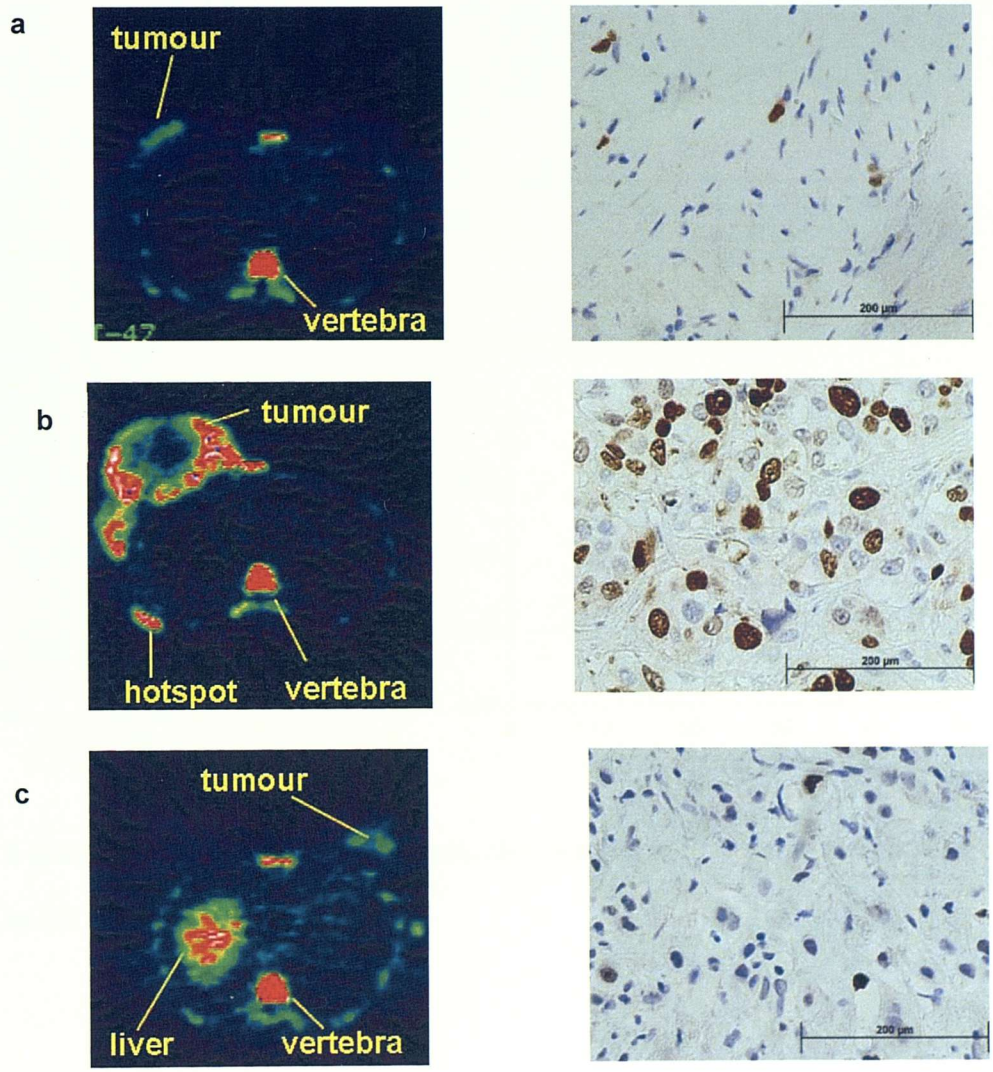


2.1.5.4 Correlation between [18F]FLT uptake and Ki-67 LI

Since [18F]FLT has the potential to be used as a surrogate marker of cell proliferation, it was important to examine the association between its kinetic parameters and a standard measure of proliferation, LI. Of particular interest are associations with the kinetic parameters that describe retention as these are related to phosphorylation of the radiotracer by TK1. Suitable histology was available in 12 of the 15 patients. An example of the difference in retention of [18F]FLT between tumours with low (patient 1 and 11) and high (patient 4) LI is shown in Figure 2.12.

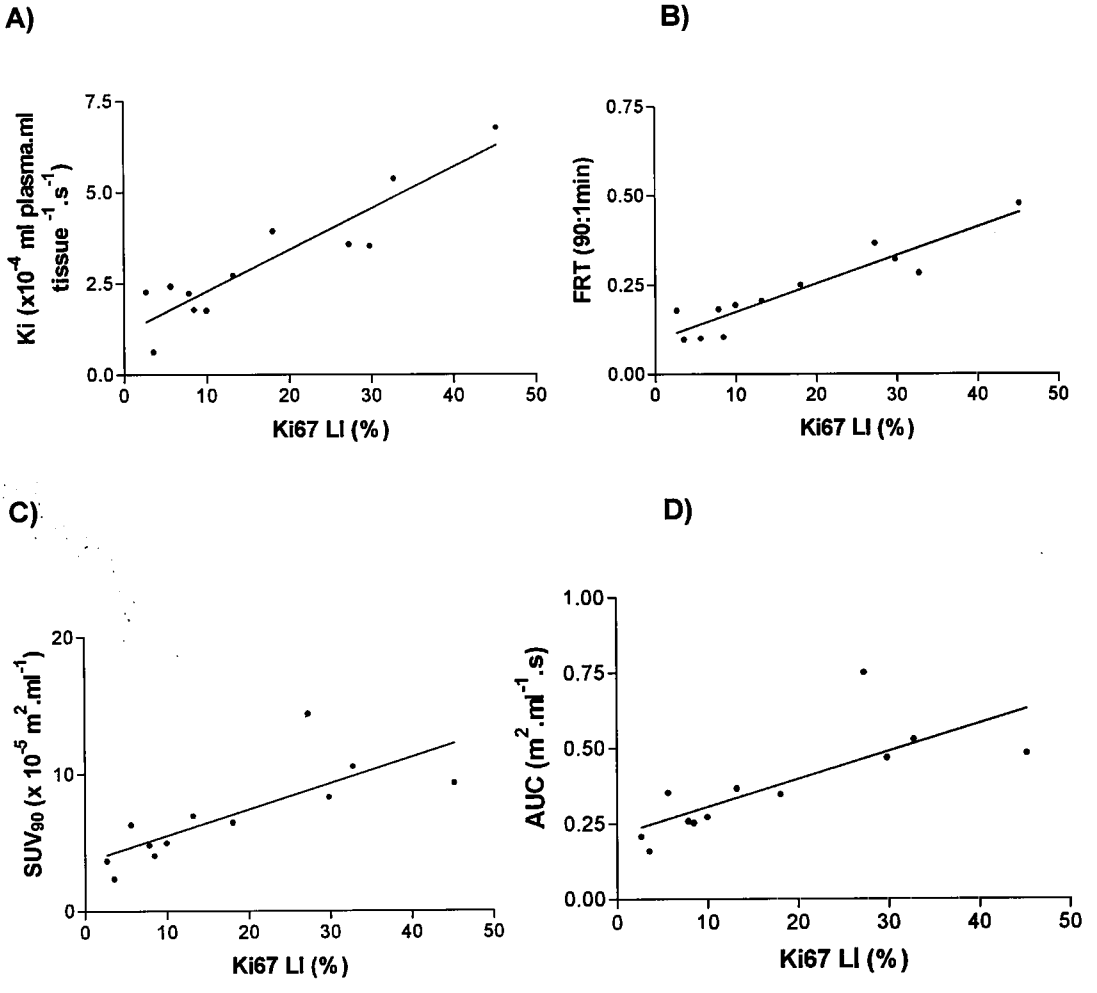
Figure 2.12: [18F]FLT PET images and corresponding Ki-67 immunohistochemistry sections

Where a) shows [18F]FLT retention in a lobular carcinoma and corresponding histological section stained for Ki-67 LI (4.9%), b) shows an [18F]FLT-PET image of a large primary ductal carcinoma with high uptake around the periphery of the tumour, central necrosis, and a hotspot on the sixth rib which was confirmed as a metastasis on a radioisotope bone scan; Ki-67 LI (45.2%) and c) an inflammatory breast carcinoma, and high uptake in the liver and the vertebra; Ki-67 LI (8.8%).



A strong correlation was found using Pearson's correlation coefficient between LI and Ki (r=0.92, p<0.0001), FRT (r=0.92, p<0.0001), $SUV_{21.5}$ (r=0.71, p=0.0098), SUV_{90} (r=0.79, p=0.002), and AUC (r=0.76, p=0.004) (Figure 2.13). There was a non-significant correlation between LI and K_1(r=0.28, p=0.38).

Figure 2.13 Correlation between Ki-67 LI and pharmacokinetic parameters



(where A is Modified Patlak Ki, B is FRT ratio (90:1min), C is SUV corrected for BSA at 90min, and D is AUC at 90min).

The results of the correlation and linear regression analysis for the various parameters and Ki67 LI are shown below in table 2.4.

Table 2.4: [18F]FLT-PET correlation with Ki-67 LI

Parameter	*Pearson r*	*p*	r^2
Patlak Ki (modified)	0.9195	<0.0001	0.8455
Patlak Ki (parent)	0.9413	<0.0001	0.8860
Patlak Ki (total)	0.9388	<0.0001	0.8813
FRT90:1	0.9149	<0.0001	0.8371
K1	0.2804	0.3773	0.0786
SUV 21.5 min	0.7094	0.0098	0.5032
SUV 90 min	0.7912	0.0022	0.6260
AUC 90 min	0.7626	0.0039	0.5815

The kinetics support a simple model of intracellular retention of the radiotracer by phosphorylation (Figure 2.1) (Barthel et al. 2003; Wagner et al. 2003; Barthel et al. 2004). The K_1 for [18F]FLT was of the same order of magnitude as blood flow in breast tumours and normal breast previously reported by Wilson *et al*(Wilson et al. 1992); the K_1 values were in general higher for tumour (range: 0.964 –3.82 ml plasma.s^{-1}.ml^{-1} tissue) than normal breast or lung (range: 0.315-1.18 x 10^{-3} ml plasma.s^{-1}.ml^{-1} tissue) but this did not reach statistical significance.

Since the proliferation-specific signal for [18F]FLT is the formation of [18F]FLT-phosphate, we hypothesised that retention of [18F]FLT will correlate with proliferation. Both reversible and irreversible kinetic components were observed in the [18F]FLT-derived spectrum of kinetic components. In this study irreversible uptake kinetics were demonstrated by graphical analysis. Spectral analysis of the data showed that there are both reversible and irreversible components. These two findings are not mutually

exclusive as the reversible component could be due to influx/efflux of FLT, as well as dephosphorylation of FLT. Another reversible component is the blood volume component that is seen as a large peak in the higher end of the spectrum (Figure 2.10).The Patlak model can determine the net irreversible transfer constant (Ki) in the presence of reversible components. Muzi et al suggest that use of a 3 parameter compartmental model leads to underestimation of K1 by 47%, as there is a significant k4 with [18F]FLT.

All the retention parameters for [18F]FLT correlated with LI determined by Ki-67 labelling. The correlations with Ki-67 increased in the order AUC< SUV<FRT, Ki. This is the first description of Ki for [18F]FLT calculated with full correction for plasma and tissue metabolites. The superior nature of this parameter may be due to implementation of these corrections. However correction for tissue metabolites may not be absolutely essential, correction for plasma metabolites did suffice, as witnessed by the higher correlation for Ki obtained using a parent plasma input function rather than the new modified Patlak analysis. There was no significant correlation between K1, tracer delivery, and Ki-67 which was to be expected as this parameter is largely dependent on tumour blood flow. An improvement in the estimation of K1 could have been obtained by using shorter time frames at the start of the scan; whether this would have affected the correlation is unknown.

Visvikis *et al.* performed Ki calculations for [18F]FLT uptake in colorectal cancer without correction for the space of exchangeable region occupied by metabolites(Visvikis et al. 2003). In this breast cancer study, this leads to overestimation of Ki by 12.2%, although the correlation with LI ($r=0.91$, $p<0.0001$) does not change substantially. Ignoring any contribution of metabolites, underestimates Ki (by 16.5%; $r=0.94$, $p<0.0001$). SUV90 and AUC were also highly correlated with LI. SUV is the parameter which has been used by most investigators in other tumour types including lung and colorectal cancer, and in general, correlation coefficients of 0.7 to 0.92 have been reported (Buck et al. 2002; Buck et al. 2003; Francis et al. 2003;

Wagner et al. 2003). In the only other breast tumour studies published so far, Smyczek-Gargya *et al* used [18F]FLT PET to image 12 patients with primary breast cancer (Smyczek-Gargya et al. 2004). In that study there was a lack of correlation between Ki-67 and [18F]FLT-derived SUV. However, in that study, the scanning protocol was different and the SUV value was not corrected for body surface area.

Proliferation as determined by [18F]FLT-derived Ki was higher in tumours than in normal breast or lung. The values differed between primary tumours and corresponding metastases. This is important from both a prognostic viewpoint, as well as for therapy monitoring given that all tumour masses can be studied at once. Shields *et al.*, have reported Ki values for a lymphoma and sarcoma in the dog (Shields et al. 2002). Their tumour-derived Ki values in the dog, where metabolism of [18F]FLT is lower, are in agreement with the metabolite-corrected Ki values in humans found in this study.

2.1.5.5 Results of cardiac blood pool analysis

The results for undecay corrected activity measured using both techniques are shown below in table 2.5, and results of Pearson's correlation and linear regression are shown in table 2.6. An example of the activity curve obtained by using the heart ROI and the total blood input curve from patient 6 are shown in Figure 2.13.

In general, there was a significant correlation between the cardiac blood pool ROI and that obtained from dynamic arterial sampling. As can be seen from the table 2.5 and Figure 2.14, the peak activity in the heart was significantly less than that in the total blood curve ($p<0.0001$ by paired t-test). This is likely to be due to the activity in the heart ROI being taken at a mid-frame timepoint and average counts rather than peak counts being used. The use of shorter time frames at the start of the scan could help to overcome this problem in the future.

Table 2.5 Results obtained using the cardiac blood pool ROI and dynamic radial artery sampling

Patient	*Activity injected (MBq)*	*AUC60 heart ROI*$^{+}$	*AUC60 total blood*$^{+}$	*AUC90 heart ROI*$^{+}$	*AUC90 total blood*$^{+}$	*peak activity blood**	*peak activity heart**	*Activity at 60min blood**
1	296.30	23062.01	23443.95	26664.50	27669.10	100.42	66.14	2.56
2	369.63	23945.07	27628.05	27621.99	31934.41	197.44	84.44	2.53
3	271.03	20220.79	15821.67	23152.55	17713.08	91.53	60.91	1.18
4	246.64	14417.38	13151.28	16503.29	14807.32	71.12	33.04	0.98
5	188.70	14500.52	11820.67	16794.26	13677.29	124.74	59.06	1.06
6	343.25	24879.13	22227.51	28983.71	25807.66	167.99	92.82	2.11
7	296.30	26745.99	26562.81	31380.20	30590.30	169.61	73.06	2.37
8	368.96	34760.56	25209.71	45010.74	29108.75	133.90	13.65	2.26
9	370.62	31686.27	25851.33	36932.66	29934.66	204.13	97.95	2.38
10	380.73	29227.03	22642.66	34387.48	26641.32	188.50	74.35	2.28
11	248.57	24044.85	20851.06	28012.93	24388.17	118.47	59.16	2.13

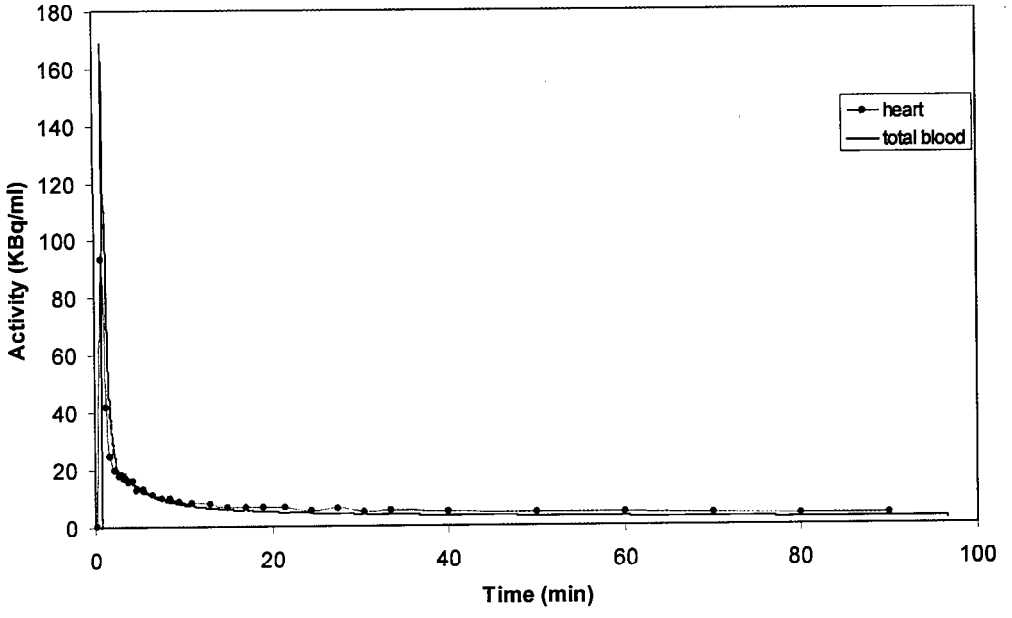
($^{+}$AUC in kBq.sec.ml^{-1}, *activity measured in kBq.ml^{-1})

One other factor which could be important for improving the correlations is the ability to sample only arterial blood from the cardiac ROI, as there may have been some spill over from the right ventricle. Smaller ROIs using an ellipse of 6 x 6 pixels may be suitable for this purpose rather than a larger, manually drawn ROI.

Table 2.6 Correlation between cardiac AUC and radial artery total blood AUC

	Pearson r	r^2
AUC60 heart ROI and total blood	0.82, p=0.0019	0.67
AUC90 heart and total blood	0.78, p=0.0049	0.60
AUC60 heart and total blood activity at 60min	0.77, p=0.0057	0.59
Peak heart and total blood activity	0.67, p= 0.0234	0.45

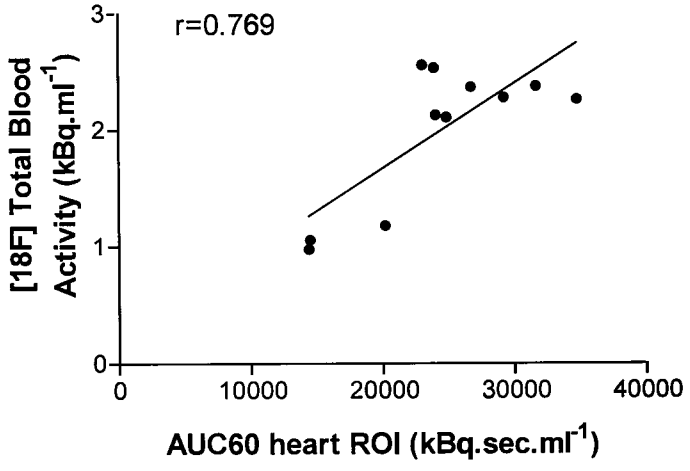
Figure 2.14 Relationship between cardiac ROI and total blood arterial input function



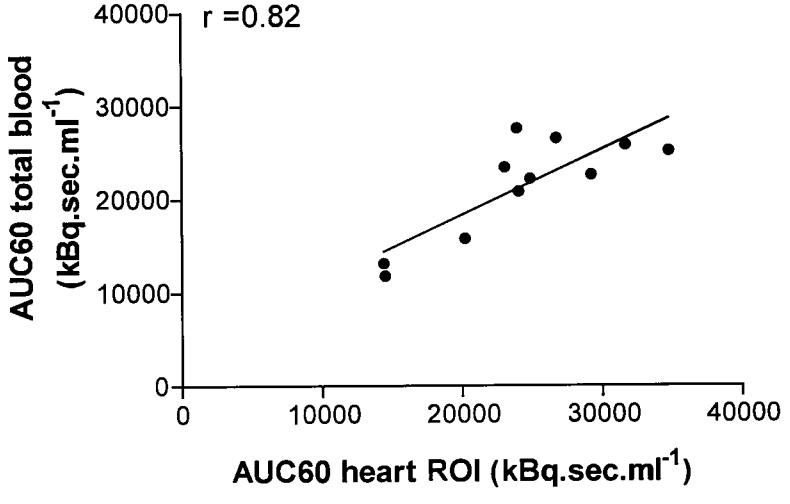
The correlation between the heart AUC60 and measured total blood activity at 60 min, and the correlation between AUC60 for both input functions are shown below in Figure 2.15 A) and B), respectively.

Figure 2.15 Correlation between two forms of input function

A) Relationship between radial artery total blood activity at 60 min and heart ROI AUC60.



B) Relationship between heart and radial artery AUC60



This demonstrates that it is possible to use a dynamic input function derived non-invasively from a cardiac ROI for [18F]FLT. Other alternatives to a cardiac ROI which have been investigated previously for FDG include use of the abdominal aorta, but this is prone to problems such as partial volume effects and spill over(Germano et al. 1992). The linear regression analysis of the peak activity in the heart and total

blood shows that it would be feasible to calculate a correction factor to the cardiac data in order that values closer to dynamic arterial sampling are obtained.

2.1.6 CONCLUSIONS

- At 60 mins post injection approximately 70% of [18F]FLT remained as the parent compound in humans, with the remainder metabolised to a single metabolite [18F]FLT-glucuronide.
- Both semiquantitative and modelled kinetic parameters describing uptake and retention of [18F]FLT correlated with tumour proliferation measured by Ki-67; though the correlation is superior for Ki and FRT than SUV or AUC
- There was a significant difference between breast tumour and normal tissue delivery, uptake, and retention of [18F]FLT for all parameters – SUV, AUC, Ki, FRT, K1 ($P<0.0001$)
- There was a wide intratumoural variation in [18F]FLT uptake in primary tumours and metastases illustrating a broad spectrum of tumour proliferative capacity
- Early (at 21.5 minutes post-injection of [18F]FLT) and late measurement of SUV (at 90 minutes) are equally useful
- [18F]FLT derived activity measurements in cardiac ROIs and total blood do correlate; the best correlation is for AUC60.

2.2 Repeatability of [18F]FLT Pharmacokinetic Parameters

2.2.1 HYPOTHESIS

Tumour uptake and retention of [18F]FLT is repeatable in the absence of treatment or other intervention

2.2.2 AIMS

- To compare the repeatability of [18F]FLT measurements in breast tumours in serial scans amongst patients with breast cancer
- To determine significant changes in [18F]FLT uptake which equate to a significant response

2.2.3 Introduction

For a novel tracer to be validated it is crucial that the intrinsic variability of tracer uptake in the absence of an intervention is established. This is a prerequisite for reliable response detection; i.e. it will enable significant levels of change in [18F]FLT uptake to be defined for the parameter under investigation.

Despite the considerable amount of papers citing the use of [18F]FDG for diagnosis and treatment response monitoring, only two relatively small studies have been produced concerning the repeatability of uptake of FDG in tumours (Minn et al. 1995; Weber et al. 1999). One study focused on lung cancer(Minn et al. 1995), and the other had a variety of tumour types and anatomical locations(Weber et al. 1999).

Whilst the early clinical [18F]FLT papers show promising results in terms of its correlation with tumour proliferation(Dittmann et al. 2003; Buck et al. 2005), and tumour specificity, the most robust pharmacokinetic parameter describing [18F]FLT uptake/retention remains to be defined. Standard semiquantitative measures (SUV and AUC) need to be compared with modelled parameters, for if [18F]FLT is to be widely utilised outside a research institution it is likely that semiquantitative parameters would be more pertinent in a clinical environment.

One could predict that a model with no inherent assumptions that includes both irreversible and reversible tracer kinetics i.e. spectral analysis is likely to be more susceptible to variation than the Patlak technique which assumes tracer uptake is irreversible. Therefore, repeatability analysis was performed for both techniques. Radiotracer delivery, K1, is subject to changes in tumour perfusion, which in turn is affected by factors such as blood flow, intracapillary pressure, tumour angiogenesis, and blood volume. Consequently, it is probable that K1 is not reproducible – but prior to making any such assumptions, the repeatability of this parameter was also assessed.

2.2.4 Methods

Nine of the patients entered in study 2.1 were able to have repeatability scans after an initial baseline scan. The entrance criteria, tumour demographics and scanning techniques were all as for study 2.1. The remainder of the patients did not have [18F]FLT repeatability scans due to failure of radiochemical synthesis, scanner breakdown, need to start treatment urgently, or, in the case of one patient, poor medical fitness. Every attempt was made to reposition the patient for the second scan in exactly the same position as the baseline one by measuring the distance from the top of the scanner field of view to an appropriate bony landmark. Patient rotation made placement of the baseline object map on the repeatability scan invalid, therefore the a new object map was drawn on each repeatability scan using the baseline object map as a reference guide.

Analysis of repeatability of SUV60, SUV90, Ki, K1, FRT ratio at 60 and 90 mins (FRT60 and FRT90), and AUC at 60 and 90 mins (AUC60 and AUC90) was performed on a lesion-by-lesion basis. Patient weight was recorded prior to each scan, and together with height, enabled SUV correction for BSA for each scan data set.

The coefficient of variation (cov) for each parameter was calculated as described previously and is shown below (Bland et al. 1995):

i) $s^2 =$ *Within subject variance* $= \dfrac{(\text{measurement A} - \text{measurement B})^2}{2}$

ii) m = *Mean value of 2 observations for each patient* $= \dfrac{(A+B)}{2}$

iii) $x =$ *mean (for all patients) of* s^2m^2

v) Coefficient of variation (cov) = square root of $x = \sqrt{x}$

For repeatability measurements individual parameter values for the two pre-treatment scans were plotted against each other; high repeatability was represented by all data distributed along a line of unity. A Pearson's correlation coefficient and Wilcoxon signed rank test were used to assess correlation and significant differences between the two scans, respectively. The normality of the data was also assessed as a probability plot of the ordered relative differences versus the normal probability (cumulative frequency of ranks) for each lesion; a curved line indicates deviation from normality. Relative differences in parameter estimates were defined as 2 x (Scan A – Scan B)/ (Scan A + Scan B).

To compare the repeatability of the various pharmacokinetic parameters, an intraclass correlation coefficient (IC) that describes the correlation between the two measurements of a parameter was calculated using SPSS® for Windows® version 12.0; if the two measurements were identical the IC will be 1. Random or systematic differences between the two measurements reduce the value of the IC. A 2 way random mixed model with absolute agreement was used. The difference in the variance of the relative difference for the different parameters was tested using the F-test that compares the standard deviations (SDs) of two normally distributed data sets.

The 95% normal ranges for spontaneous fluctuations in the parameters was calculated as 1.96 x SD of the relative difference in the two pre-treatment scans. [18F]FLT response was the relative difference between post-treatment and mean pre-treatment measurement parameters, i.e., $(Scan_{pre} - Scan_{post})/(Scan_{pre})$, where the pre-treatment scan is the mean of the two pre-treatment scans in the case of patients who completed the repeatability phase of the study.

2.2.5 Results

Ki obtained by using the modified Patlak method, FRT ratio at 60:1 min and 90:1 min (FRT60, FRT90), K1, SUV and AUC at 60 and 90 minutes (SUV60, SUV90, AUC60, AUC90) were used to assess repeatability of [18F]FLT uptake in 9 tumour lesions from 8 patients. The repeatability analysis was also assessed for the impulse response function values at 60 and 90 minutes, as there was a possibility that the FRT ratios were influenced by the presence of a blood volume component at 1 minute. The results are shown below in Table 2.7. One other patient's data was excluded from this analysis due to an anomaly in tissue radioactivity data (scanner head counts) compared to the administered dose.

The time between baseline scan and the repeatability scan ranged from 2-10 (median=4.5) days. There was no significant difference between the two scans for all of the imaging parameters (range p =0.13 (for FRT60) to p = 1.06 (for AUC60)). Regression analysis of the line of unity indicated good test-retest correlation for all the parameters studied, excluding K1. The standard deviations of the mean relative difference were 10.5 and 15.1% for SUV90 and Ki, respectively. This measure was much lower for IRF60 and IRF90 in comparison to the relevant FRT values (SD of mean relative difference = 12.6 and 24.6 for IRF60 for FRT60, respectively).

F-test values were 0.97 for SUV90 and 0.99 for Ki. These results indicate that both parameters (SUV90 and Ki) can be used repeatedly in serial scans. The 95% normal values for spontaneous fluctuations were determined from the SD of the relative difference are shown in table 2.7 below. AUC60 and AUC90 were slightly superior to SUV60 and SUV90. This was predictable as the AUC is a measure of uptake throughout the scan, as opposed to SUV which defines uptake at a single midframe timepoint and is subject to more noise. The timing of measurement of the

semiquantitative parameters (i.e. sixty minutes opposed to ninety minutes) had little effect on their repeatability – they were both equally good.

FRT 90:1 and 60:1 appeared less reproducible than the other parameters (but were superior to the relative IRFs by the F-test, see table 2.7 below), this was attributed to the presence of a blood volume component present causing intrinsic variability of the IRF in some of the lesions at 1 minute. For that reason the repeatability of the impulse response function at 60 and 90 minutes was calculated, as at that stage the tracer uptake has approached steady state. The IRF values proved to be more reliable, for example the SD of the mean relative difference was much lower for IRF60 and IRF90 were 12.65 and 15.29, respectively, compared to the relevant FRT60 and FRT90 values (24.6 and 32.7).

As expected K1, which represents unidirectional tracer delivery to the tumour, obtained by compartmental analysis was not reproducible and therefore would not be suitable for measuring response. This parameter is largely flow dependent, and this may be a major contributing factor for its lack of robustness in this study. This may not signify an adverse event, as the previous study (section 2.2) showed no correlation between K1 and Ki-67 LI, therefore it is unlikely that K1 would be an appropriate measure of tumour proliferative response to treatment.

Table 2.7 Repeatability of semi-quantitative and modelled parameters in tumour lesions

Parameter	COV	Pearson Correlation coefficient	r^2	Wilcoxon p value	ICC	SD of mean relative difference (%)	F-test
SUV 60	7.019	0.974	0.948	0.910	0.986	10.49	0.94
SUV 90	7.380	0.986	0.973	0.950	0.993	10.52	0.97
AUC60	5.990	0.987	0.975	1.055	0.994	8.98	0.97
AUC90	5.228	0.992	0.984	1.000	0.996	8.37	0.99
Ki	10.146	0.969	0.939	1.050	0.990	15.14	0.99
FRT60	17.278	0.905	0.819	0.129	0.948	24.56	0.80
FRT90	18.876	0.963	0.928	0.203	0.946	32.71	0.79
IRF60	9.577	0.965	0.932	0.203	0.977	12.65	0.68
IRF90	11.697	0.963	0.928	0.250	0.977	15.29	0.72
K1	31.564	-0.197	0.039	0.301	0.250	43.61	0.08

(where ICC = interclass correlation coefficient)

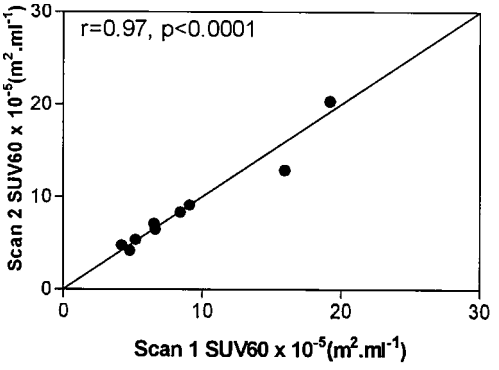
Table 2.8: Spontaneous fluctuation range for each [18F]FLT pharmacokinetic parameter

Parameter	95% Confidence Interval
SUV 60	$\pm 0.2056 \times 10^{-5}$ $m^2.ml^{-1}$
SUV 90	$\pm 0.2063 \times 10^{-5}$ $m^2.ml^{-1}$
AUC60	± 0.1761 $m^2.s.ml^{-1}$
AUC90	± 0.1536 $m^2.s.ml^{-1}$
Ki	$\pm 0.2968 \times 10^{-4}$ ml plasma. ml^{-1} tissue. s^{-1}
FRT60	±0.4810
FRT90	±0.5399
IRF60	± 0.2479 s^{-1}
IRF90	± 0.2998 s^{-1}
K1	± 0.8547 $\mu l.s^{-1}.ml^{-1}$

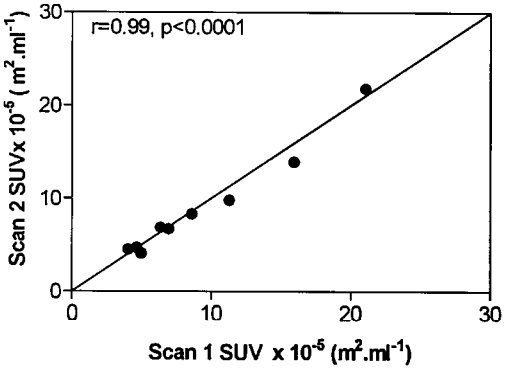
The results of Pearson's correlation coefficient for each parameter are depicted graphically in Figure 2.16 below.

Figure 2.16 Correlation of Baseline and Repeatability Scan Parameters for [18F]FLT uptake in breast tumour lesions.

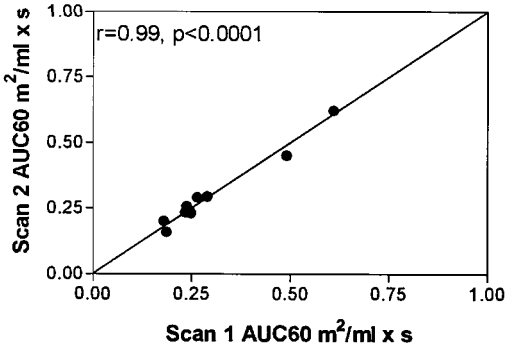
a) SUV60



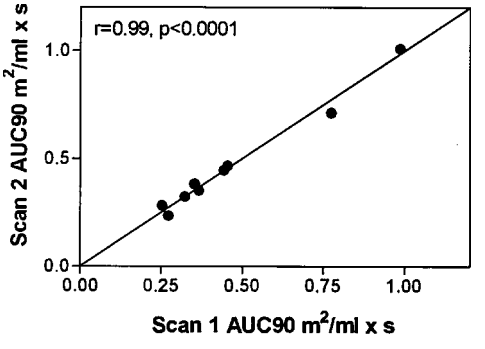
b) SUV90



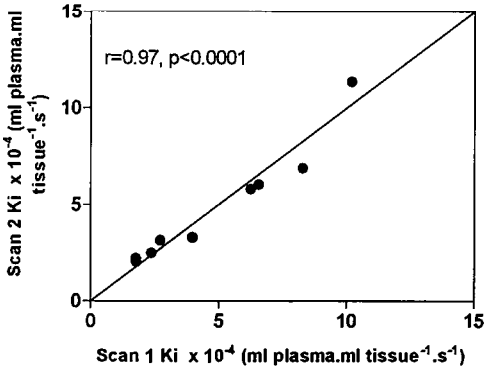
c) AUC60



d) AUC90



e) Ki



f) FRT60

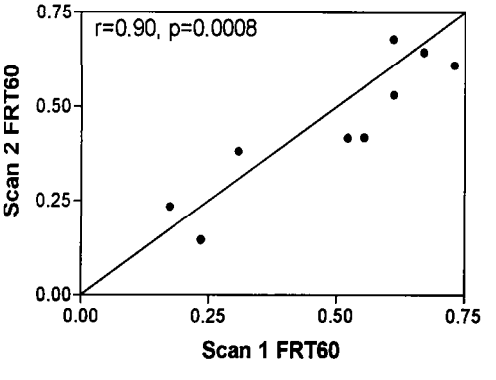
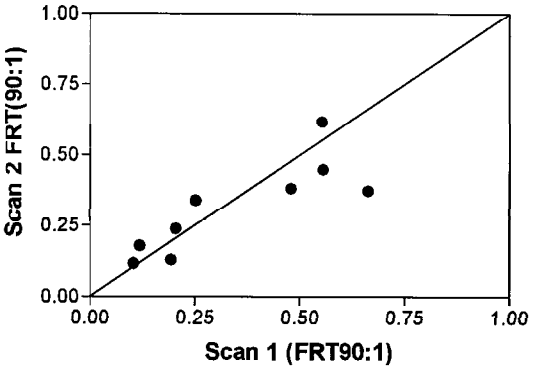
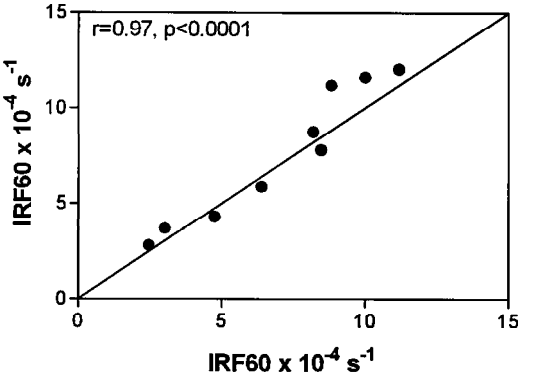


Figure 2.16 Correlation of Baseline and Repeatability Scan Parameters for [18F]FLT uptake in breast tumour lesions.

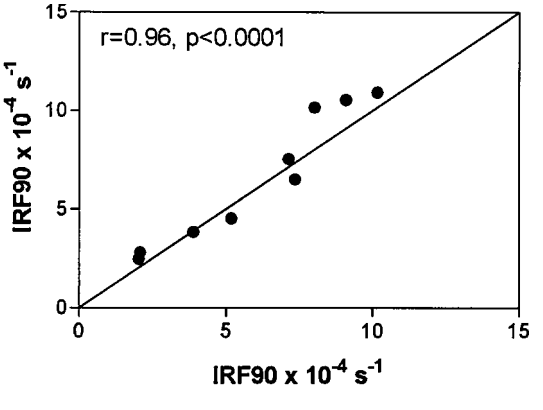
g) FRT90



h) IRF60



i) IRF 90



j) K1

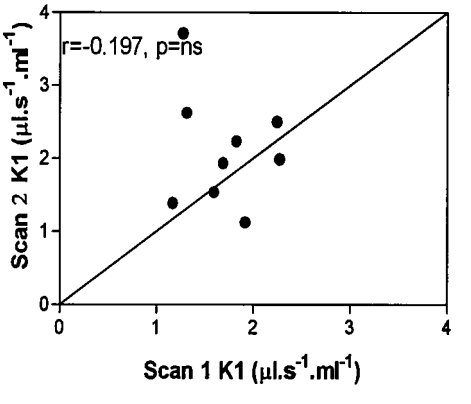


Figure 2.16 above shows the correlation between values for the baseline (scan 1) and repeatability scan (scan 2) plotted for each pharmacokinetic parameter along a superimposed line of unity; n=9 lesions..

2.2.6 Discussion

This study has shown that [18F]FLT uptake and retention is repeatable when measured by semiquantitative and metabolite-corrected modelling techniques. Spectral analysis data, in particular FRT60 and FRT90, is subject to noise thus it may be more appropriate to use the IRF values at these time points. This study provides objective criteria for determining true changes in [18F]FLT-PET imaging parameters during serial measurements. The data can also be used to define the sample size for larger [18F]FLT-PET trials.

The previous repeatability studies for FDG looked at SUV and Ki in ten and sixteen patients respectively(Minn et al. 1995; Weber et al. 1999). This is the first time that repeatability of human tumour [18F]FLT kinetics has been evaluated. The repeatability for spectral analysis and compartmental analysis for FDG in tumours has not been reported previously. It would be interesting to study the repeatability of FRT and K1 parameters for FDG to determine if they are as liable to fluctuation to the same degree as was observed in this study with [18F]FLT. However, as stated at the outset of this study, it was inherent in the spectral analysis model that there would be more noise in the data as a result of its intrinsic nature of calculation. The two tissue compartmental method chosen for calculation of K1 may be inappropriate for [18F]FLT due the presence of a significant k4 (i.e. dephosphorylation of FLT-monophosphate)(Muzi et al. 2005).

Repeatability studies are demanding on patients; ideally all the patients would have had the same tumour histological type, similar stage of disease, anatomical location, and preferably no previous treatment. Three of the eight patients had received previous chemotherapy or hormonal treatment; none had received radiotherapy to the imaging site. This repeatability study is exploratory by nature, perhaps in the future larger studies can be performed which can evaluate such factors more closely.

2.2.7 Conclusion

- [18F]FLT uptake and retention in breast cancer is repeatable when measured by PET using SUV, AUC, modified Patlak Ki, FRT, and IRF.
- Measurement of radiotracer uptake at 60 or 90 minutes post-injection are equally repeatable for SUV and AUC
- Response criteria have been derived for each parameter (i.e. significant changes in [18F]FLT are those which lie outside the 95% confidence interval listed in table 2.8).

2.3 [18F]FLT-PET Prediction of Early Response to Treatment in Breast Cancer

2.3.1 Hypothesis

[18F]FLT-PET will provide an accurate measure of the effect of anti-proliferative chemotherapy on breast cancer in vivo

2.3.2 Aims

- To assess the early changes in [18F]FLT-PET pharmacokinetic parameters in response to a commonly used cytotoxic chemotherapy regimen in patients with locally advanced and metastatic breast cancer

- To correlate the [18F]FLT-PET response at day 8 with clinical response to chemotherapy at 60 days

2.3.3 Introduction

Anti-cancer therapies work by disrupting the balance between tumour cell proliferation and cell death. Response assessment using the RECIST criteria relies upon detection of a decrease in physical tumour volume as a result of reduced cell proliferation or increased cell death due to necrosis or apoptosis(Therasse et al. 2000). However changes in tumour dimensions may take a long time to develop, and provide little information about cell viability. Consequently, some authors believe that the RECIST criteria are altogether inappropriate for monitoring response to novel cytostatic agents which may have minimal effect on tumour size (Korn et al. 2001; Michaelis et al. 2006).

The early detection of tumour chemosensitivity or chemoresistance has obvious advantages in terms of maximising patients' treatment response benefit i.e. by continuing with successful therapies, whilst simultaneously minimising patient exposure to ineffective and potentially toxic treatment regimens. A quantitative proliferative index measurement could provide a mechanism for chemosensitivity or chemoresistance to be detected in vivo. Histological Ki-67 immunostaining and analysis of cell cycle genes have shown changes in breast tumour proliferation status as early as 24h and certainly at 1-4 weeks after chemotherapy or hormone therapy; in some cases the early changes in proliferation were predictive of pathological response (Dowsett et al. 1999; Ellis et al. 2003; Ellis et al. 2003; van Diest et al. 2004; Vincent-Salomon et al. 2004).

Non-invasive molecular imaging technologies including FDG-PET have been explored as surrogates to the anatomical and histological or molecular approaches mentioned above due to a combination of factors including their ability to detect changes in tumour biochemistry in all tumour regions and good repeatability (Wahl et al. 1993; Weber et al. 1999). Decreases in FDG uptake as early as one week after starting chemohormonotherapy treatment have previously been reported in

breast tumours(Wahl et al. 1993). FDG uptake may, however, increase within the early period after treatment through mechanisms involving enhanced inflammatory response, making it unpredictable as a response marker (Dehdashti et al. 1999; Spaepen et al. 2003). Proliferation markers like [18F]FLT, are not susceptible to such inflammatory changes(van Waarde et al. 2004) and can potentially be used to measure early changes in response.

[18F]FLT can be used to measure proliferation in tumours of breast cancer patients (Kenny et al. 2005). This current study examines the role of [18F]FLT for determining response to therapy in breast cancer; in this specific instance a standard chemotherapy regime (5-fluorouracil, epirubicin, and cyclophosphamide (FEC)) was used. To ascertain if the reductions in [18F]FLT uptake post-treatment are significant, knowledge of the intrinsic variability of [18F]FLT-PET reported in the previous study above (section 2.2), was used to provide the objective criteria for early response assessment.

A previous [18F]FLT-PET study evaluated response of breast tumours to a variety of treatments (chemotherapy and endocrine therapy) at 5.5 weeks. (Pio et al. 2006). The timescale for post-treatment scans in that study were similar to that for RECIST(Therasse et al. 2000). We rationalised that, like the early FDG studies (Wahl et al. 1993), oncologists may benefit more from an earlier indication of response. Thus, this study investigated whether [18F]FLT-PET could be used to measure response as early as 1 week after initiation of FEC chemotherapy and compared the PET results with clinical response measured at 60 days.

2.3.4 Methods

The patients were those entered into study 2.1; eligibility criteria were as described previously. After at least one pre-treatment scan (two in the case of the nine patients who entered the repeatability study, 2.2) patients were treated with combination intravenous 5-fluorouracil (600mg/m^2), epirubicin (60 mg/m^2), and cyclophosphamide (600mg/m^2) (FEC) chemotherapy. The post-treatment PET scan was performed approximately 1 week later. Patients received FEC chemotherapy every 21 days up to a maximum of 8 cycles until surgery or disease progression.

Patients received a single bolus intravenous injection of [18F]FLT (153-381MBq, specific activity 15-227 GBq.μmol^{-1}) over 30 seconds. The scanning protocol, reconstruction, and arterial blood sampling were as described previously in study 2.1. The parameters SUV90, Ki (obtained by modified Patlak analysis), AUC90, and FRT90:1 were used to quantify [18F]FLT uptake and retention, respectively, in the pre- and post-treatment scans. In the nine patients who participated in the repeatability study, the mean of each parameter for the two scans was used as a baseline value.

Tumour response was defined using the RECIST criteria, see section 1.7, table 2 (Therasse et al. 2000). Tumours were measured using electronic callipers (AR/2001, Camlab Laboratory products, Cambridge, UK) on each of the PET scanning visits and at day 60 post-treatment by the same investigator. Radiological investigations (ultrasound, computed tomography) were used where clinically appropriate.

2.3.5 Results

15 patients with 19 discrete lesions due to breast cancer (all histological types; see study 2.1 for demographics) were entered into the study. Of these, 13 patients with a total of 17 lesions had at least one pre-treatment and a post-treatment scan (one patient withdrew from the study due to a viral illness and the other patient could not be scanned at 1 week). All of the patients tolerated the PET scanning protocol, and none suffered complications due to the study. With the exception of 3 patients (2 of whom had metastatic disease, and one locally advanced) who had received prior treatment for breast cancer, all patients were newly diagnosed.

Clinical and [18F]FLT-PET response

Thirteen patients completed both pre-treatment and post-treatment scans at the required study time. Clinical response (CR/PR) was evident in 6 patients at 60 days, the remaining 6 had stable disease, and one patient died from cerebral metastases. Therefore, no patient could be classified as having had progressive disease within the imaging region. In responding lesions the average decrease in FLT-PET was 41.3% for SUV90, and 52.9% for Ki; in non-responding lesions the average increase in FLT-PET was 3.1% for SUV90 and 1.9% for Ki.

The interval between commencement of chemotherapy and the post-treatment [18F]FLT-PET scanning ranged from 6 to 12 (median 8) days. Figures 2.17A and B show typical transverse PET images through the chest of patient 1 before and after receiving FEC chemotherapy; a reduction in [18F]FLT uptake was seen at 1 week post-treatment. This patient showed the most significant [18F]FLT-PET response with an 83% decrease in [18F]FLT uptake. Figures 2.17C and D are images of patient 8 who did not show a reduction in [18F]FLT uptake.

The average SUV90 and Ki from multiple slices of entire lesions were compared. Figure 2.18 shows the [18F]FLT-PET response pattern for all lesions.

Objective [18F]FLT response was defined as relative differences in imaging parameters that were below the normal ranges of spontaneous fluctuation; values higher than the range will constitute significantly increased proliferation. The normal ranges are the two solid lines on either side of the mean (bold solid line) in Figure 2.18. [18F]FLT-PET response (< 95% range) was seen in 12 of 17 (SUV90) and 11 of 17 (Ki and AUC90) lesions, but in only 2 of 17 lesions when assessed by FRT90. As there were no changes in tumour size at 1 week (Table 2.9), with the exception of the axillary metastasis in patient 6, we can state that the [18F]FLT-PET responses preceded tumour size changes.

Figure 2.17 Comparison of [18]FLT-PET response and non-response

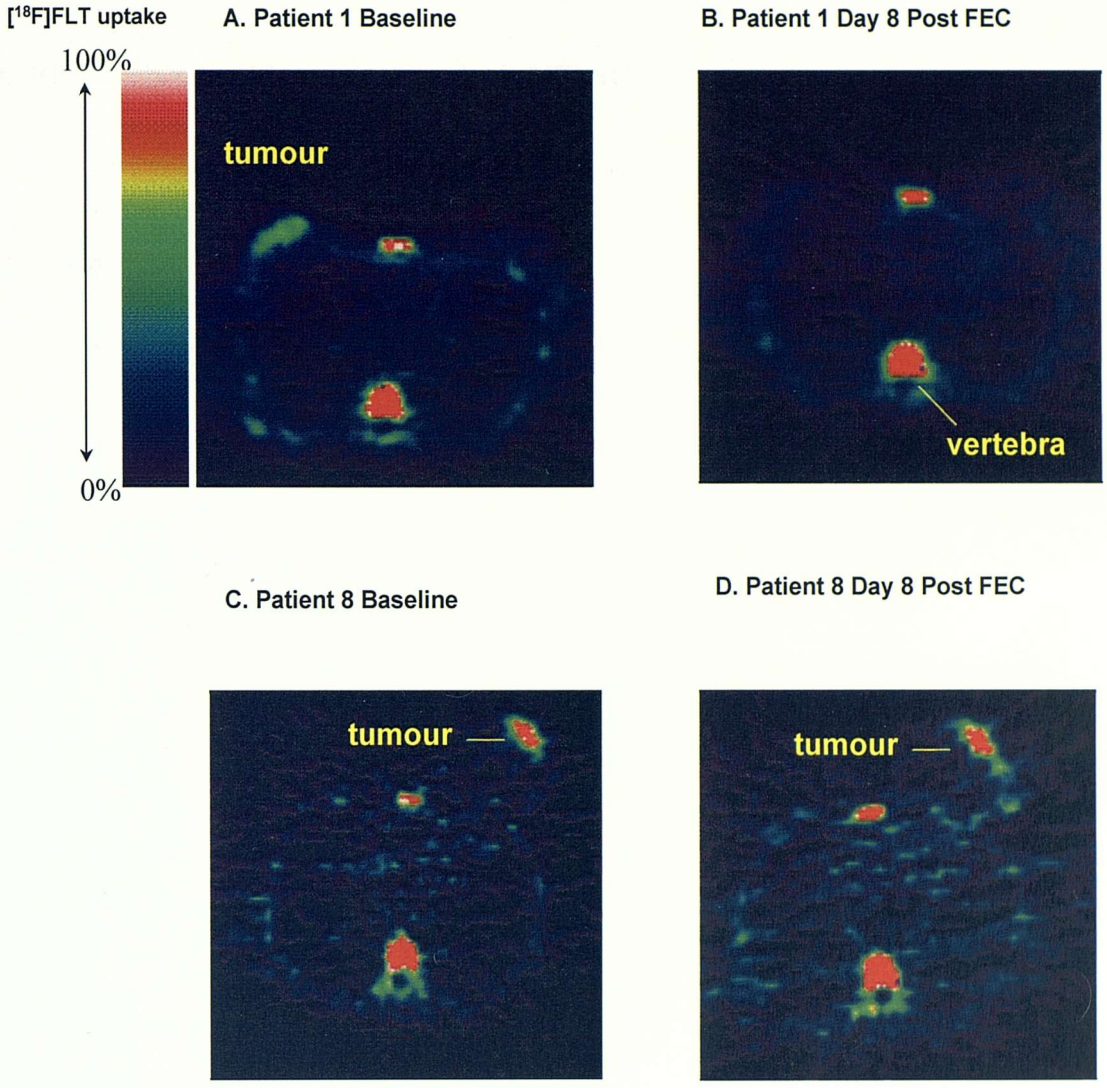
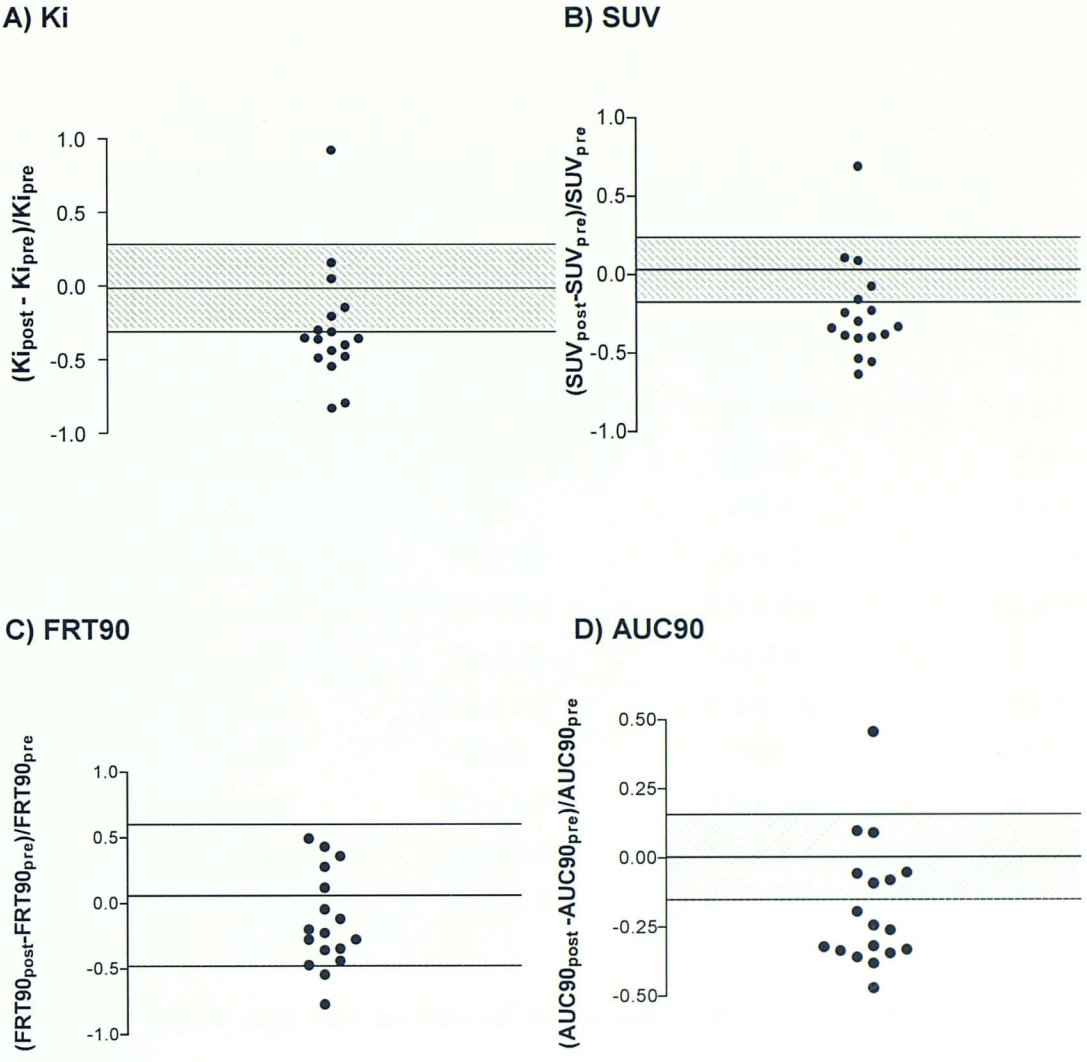


Figure 2.17 above shows [18F]FLT-PET images in transverse section of a breast tumour which was associated with both a clinical and [18F]FLT response (A and B), and a tumour which did not respond clinically or by [18F]FLT-PET criteria (C and D).

Figure 2.18 [18]FLT-PET response for all tumour lesions



(where values above the upper bold line represent significant increases in proliferation post-treatment, values below the lower bold line represent significant decreases in proliferation, and those between the two bold lines were associated with no significant change).

Table 2.9 Clinical response to FEC chemotherapy

Patient	Tumour Region Imaged	Baseline Dimensions (cm^2)	Day 8 Dimensions (cm^2)	Day 60 Dimensions (cm^2)
1	Breast	8.0 x 6.4	7.5 x 6.7	1 x 1
2	Lung met	3.0 x 3.0	ND	ND
3	Breast	7.7 x 10.1	6.7 x 10.7	6.5x 8.6
4	Breast	26 x 18	ND	16x 13
5*	Breast	19 x 18	19 x 18	19 x 18
5	Axilla	3 x 4	3 x 4	2 x 2
6	Breast	10.5 x 10	8.5 x 9	5 x 4
6	Axilla	4.5 x 4.5	2.5 x 3	CR
7	Breast	4x4	4 x 4	3 x1
8	Breast	10 x 13	10 x 13	12 x 13
9	Breast	3.7 x 3.4	3.5 x 2.8	3.5 x 3.2
10†	Axilla	3 x 2.9	3 x 2.9	3 x 3
11	Breast	9.0 x 7.8	8.9 x 7.9	8 x 8
12	Breast	6 x 3	ND	ND
13	Breast	2.7 x 3.5	2.6 x 2.9	2.2 x 2.2
14	Breast	5.8 x 7.8	5.7 x 7.7	3.5 x 3.5
15	Breast	3.1 x 3.2	3.1 x 2.4	ND

(5*: This patient also had an internal mammary node lesion which had not been detected by other imaging investigations, 10†: This patient also had a pretracheal node lesion which had not been detected previously. ND: Patient 2 developed brain metastases, Patient 4 could not attend at day 8, Patient 12 withdrew from study due to a viral illness, and Patient 15 proceeded to surgery due to an abscess).

All 6 patients who had a clinical response also had a significant reduction in [18F]FLT uptake as measured by Ki and SUV. Figure 2.18 (below) shows the relationship between [18F]FLT response and clinical response of individual lesions. Pre-treatment tumour size and tumour sizes at days 8 and 60 post-chemotherapy are

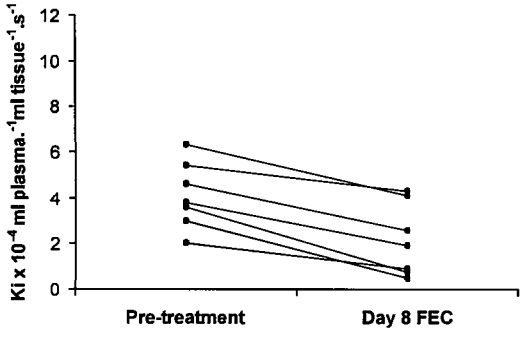
recorded in Table 2.9 (above). Only one of the patients (patient 2) in this study developed progressive disease after the first cycle of treatment days in the form of previously undiagnosed cerebral metastases and died as a result of this before day 60; the metastases were outside the field of view of the PET scanner used in this study. Patient 12 withdrew from study due to a viral illness, and patient 14 developed a breast abscess after the 1st cycle of chemotherapy and proceeded to mastectomy. These patients could not be assessed for clinical response to FEC at day 60. Patient 3 had a significant increase in Ki and SUV90 by 92.3 and 69.2%, respectively; this patient failed to achieve a partial response, and has had disease progression within 18 months following completion of chemotherapy.

Changes in [18F]FLT uptake were not always similar for different lesions in patients with more than one lesion, i.e. there was intra-patient variability in [18F]FLT response. This was evident in patients 5, 6, and 10 for both Ki and SUV90. For instance, patient 5 had a primary lobular carcinoma with axillary nodal and internal mammary metastasis (the internal mammary metastasis had not been detected on prior screening investigations, including computed tomography). Clinically the patient was classified as a non-responder due to lack of response in the primary tumour (although the axillary node showed a reduction in size) after two cycles of FEC and her treatment was changed to combination docetaxel-trastuzumab. With regard to [18F]FLT response, the primary tumour did not show a significant reduction in Ki or SUV90, whereas there was a significant reduction in SUV90 and Ki in the internal mammary node and the axillary nodal metastasis. Similarly, patient 6 had a reduction in both SUV90 and Ki in the axilla but not in the breast; this patient had a clinical response in both areas. The patient has subsequently relapsed in the breast despite completing 6 cycles of chemotherapy plus surgery and radiotherapy. It was interesting to note at the time of surgery that this patient had a pathological complete response in the axilla.

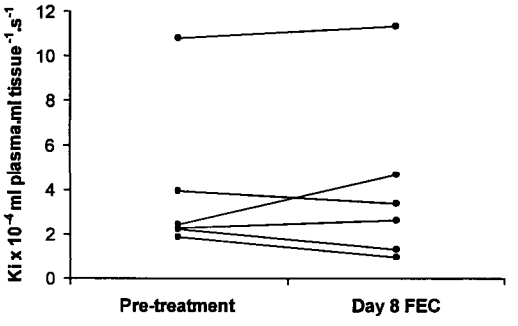
To evaluate the early predictive value of [18F]FLT-PET in breast cancer patients in this pilot study, i.e. the ability of PET at 1 week post-treatment to predict response at 60 days, the lesions were classified in this pilot study into CR/PR (n=7 lesions) and those with stable disease (n= 6 lesions), and compared with [18F]FLT-PET response. Figure 2.19 shows that there was a significant difference between the two groups for changes in [18F]FLT uptake for Ki ,SUV90, FRT90 and AUC90 (Mann-Whitney p=0.022 for both Ki and SUV90, p=0.026 for FRT90). The difference was not significant for AUC90 (p=0.366) which may reflect that changes in the total area under the curve at 90 minutes were relatively small and non-discriminatory for detecting response in this particular study.

Figure 2.19 Relationship between clinical response and changes in [18F]FLT-PET parameters.

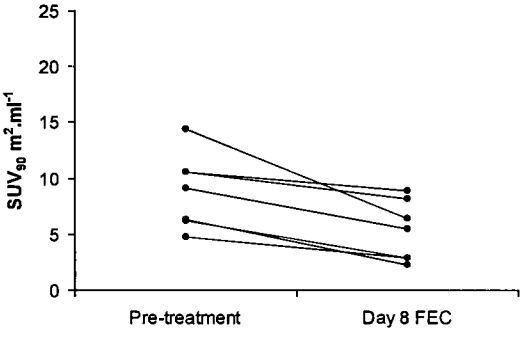
A) Ki in Responders



B) Ki in Stable Disease



C) SUV90 in Responders



D) SUV90 in Stable Disease

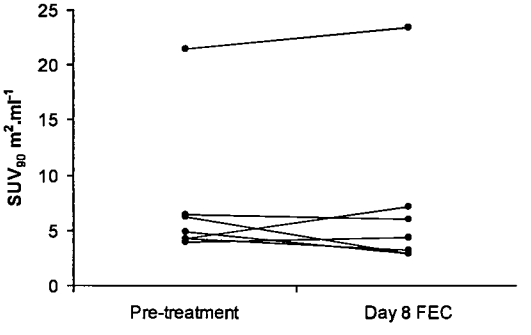


Figure 2.19 above shows the response pattern for modified Patlak Ki and SUV90 for responders (A and C), and lesions with stable disease (B and D), there was a significant difference between the 2 groups in terms of [18F]FLT-PET response, Mann-Whitney p=0.022.

2.3.6 Discussion

Data from the repeatability study had shown that a decrease in tumour [18F]FLT of ≥18% for SUV90, and/or ≥ 31% for Ki is required for a significant response. In this study, objective changes in [18F]FLT-PET were seen at 1 week after FEC chemotherapy. Given that [18F]FLT uptake highly correlated with proliferation in breast cancer in the previous study (Kenny et al. 2005) these present findings indicate that [18F]FLT-PET can be used to measure changes in proliferation as early as 1 week post-treatment. Since tumours can acquire drug resistance after 1 week of treatment, this time-point is not necessarily optimal for imaging but allows for early monitoring of chemosensitivity.

[18F]FLT-PET response was seen in a high proportion of tumours at this early time point (12 of 17 or 11 of 17 when assessed by SUV90/AUC90 or Ki) and importantly preceded tumour size changes. The results with FRT90 suggested only 2 patients had achieved a significant response, however the value of the IRF at 1 minute used to calculate the FRT90 may have been affected by fluctuations due to blood flow at the early part of the scan (as evidenced by the lack of repeatability of K1). The 30 second time frames used at the beginning of the dynamic imaging may have been suboptimal in this current study. The basis for choosing the selected time bins was based on our group's previous experience with [11C]thymidine(Wells et al. 2002; Wells et al. 2002; Wells et al. 2003), and is also backed by Mazoyer et al (Mazoyer et al. 1986) who showed that for FDG, differences in rate constants obtained from dynamic PET scanning are insignificant when the initial scan duration was <30 seconds.

Although this is a pilot study we sought to compare the [18F]FLT-PET lesion response to the patient's clinical response at 60 days. In general the patients who showed CR/PR had a change in SUV90 and Ki of -63.4 to -15.6 and -83.0 to -20.4% respectively. Early Ki-67-based proliferation studies have been performed in breast

cancer patients and in some cases predicted for pathologic response (Dowsett et al. 1999; Archer et al. 2003; Ellis et al. 2003; Ellis et al. 2003; van Diest et al. 2004; Vincent-Salomon et al. 2004). Studies by Dowsett et al. (1999) suggested that in breast cancer patients treated with tamoxifen, even to achieve disease stabilisation, a reduction in proliferation index of 50% and a 2-3-fold increase in apoptotic index will be required (Dowsett et al. 1999), i.e. some of the changes in proliferation below the lower limit of spontaneous fluctuation seen in our studies may be insufficient to cause clinical regression. If we had set >50% decrease in [18F]FLT uptake as necessary for significant response, 3 lesions out of 6 which showed a clinical response would have been detected. On the other hand, patients who failed to show changes in [18F]FLT-PET parameters or had an increase are less likely to show a clinical response. This is in keeping with one of the reports of [18F]FDG-PET in breast cancer(Wahl et al. 1993). In that study, Wahl and co-workers demonstrated that non-responding patients failed to show a decrease in [18F]FDG uptake at day 63 (Wahl et al. 1993). The ability to distinguish between patients that had stable disease and those that had complete or partial response by using SUV90 is encouraging. Future studies using [18F]FLT-PET could be enhanced by measuring other factors such as apoptosis that influence tumour regression(Dowsett et al. 1999).

The range of spontaneous fluctuations for Ki is slightly higher than that of SUV90. However, Ki is the more accurate parameter when correlated with Ki-67 labelling index(Kenny et al. 2005). Factors that can affect the SUV90 parameter include changes in radiotracer delivery and dephosphorylation within the tumour, as well as changes in systemic clearance after treatment. Hence, the more clinically applicable method, SUV, is robust but knowledge of the aforementioned factors needs to be obtained to justify its use.

In general, [18F]FLT-PET is likely to be more specific for measuring changes in proliferation than FDG, which can show an increased uptake in inflammatory regions (Buck et al. 2003; van Waarde et al. 2004). Pio et al have recently reported the

advantage of [18F]FLT-PET over FDG-PET for measuring treatment response in 14 patients with breast cancer including those with liver metastases(Pio et al. 2006). There are a number of differences between that study and this one. In their study, response assessment was done at ~ 5 weeks after treatment initiation. Also different treatment regimes were used; one-third of the patients were treated with hormonal therapy and the remaining with a variety of cytotoxic chemotherapy regimes. Of interest, the authors showed that the 10- or 45-min [18F]FLT SUV correlated with CA27.29 and late changes in tumour size. These studies did not, however, examine other kinetic parameters or the repeatability of the measurement parameters.

This pilot study is important in many respects. The response studies demonstrate that [18F]FLT-PET measurements can be done early, i.e., studies of the time course of drug effect can be performed with [18F]FLT-PET commencing at 1 week post treatment. The optimal time for predicting long term clinical response will depend on the dosing regime, pharmacokinetics and mechanism of action of the agent of interest. Of note in this study is the fact that some lesions which showed an early [18F]FLT-PET response failed to have a significant clinical response, which may be attributed to initial chemosensitivity followed by the development of tumour chemoresistance. This study may be important in the clinical trial of novel mechanism-based, relatively non-toxic, molecular therapeutics. The clinical trial evaluation of such agents is still based on maximum tolerated dose and tumour volume measurements(Parulekar et al. 2004). Maximum biological activity could occur at a lower dose than the maximum tolerated dose and using the RECIST criteria to define response may be inappropriate for some agents that are unlikely to cause early overt changes in tumour volume (Ratain et al. 2004). Imaging studies of the type reported here could shorten Phase I and II trials and provide important information on mechanism of action.

2.3.7 Conclusion

- [18F]FLT-PET can detect changes in proliferation at 1 week post treatment after FEC chemotherapy.

2.4 [18F]FLT-PET As A Pharmacodynamic Marker In Vivo

2.4.1 Hypothesis

Membrane nucleoside transport is enhanced following TS inhibition, therefore [18F]FLT-PET should be a suitable marker for monitoring the pharmacodynamics of tumour TS inhibition.

2.4.2 Aims

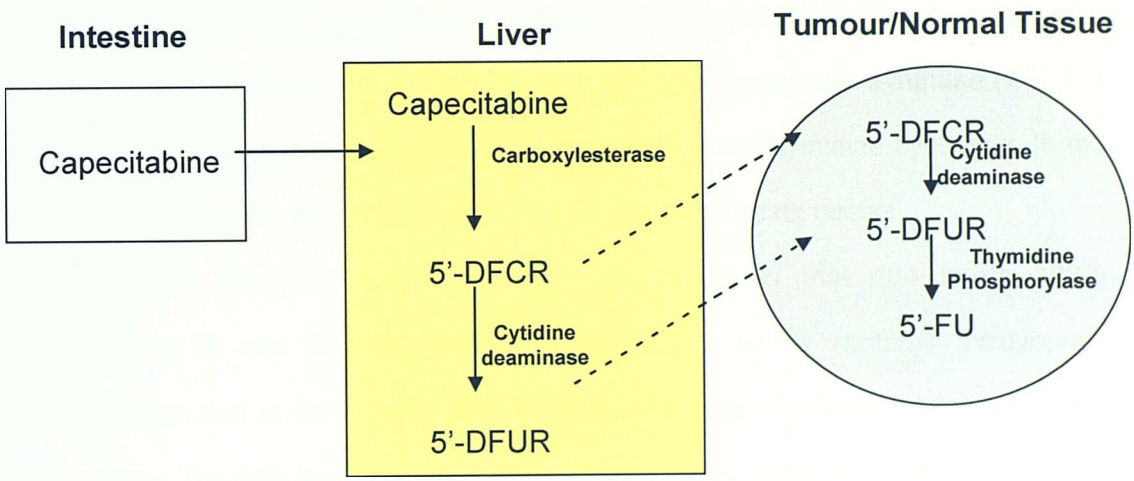
- To determine if [18F]FLT-PET can be used as a pharmacodynamic marker of early response of breast cancer to treatment with a thymidylate synthase inhibitor, capecitabine
- To study the pharmacokinetics of [18F]FLT by PET in tumour lesions before and after the 1st dose of capecitabine
- To examine the effect of blood flow on changes in [18F]FLT kinetic parameters by performing [15O]-labelled water scans
- To compare the changes in [18F]FLT-PET parameters to with clinical response

2.4.3 Introduction

Capecitabine is a fluoropyrimidine, and acts as a pro-drug of the commonly used anti-cancer drug 5-fluorouracil (5-FU). It is thought to be preferentially activated in tumour tissue, leading to improved intratumoural drug concentrations and less systemic toxicity than 5-FU. The tumour selectivity is due to the higher expression of thymidine phosphorylase (TP) in tumour tissue compared to normal tissue (Miwa et al. 1998). The active agent, 5-FU inhibits TS and, thus, DNA synthesis (it is also incorporated into RNA)(Miwa et al. 1998). The mechanism of action of capecitabine is depicted below in Figure 2.19.

Figure 2.20 Mechanism of action of Capecitabine

(where DFCR = deoxyfluorocytidine and DFUR = deoxyfluorouridine)

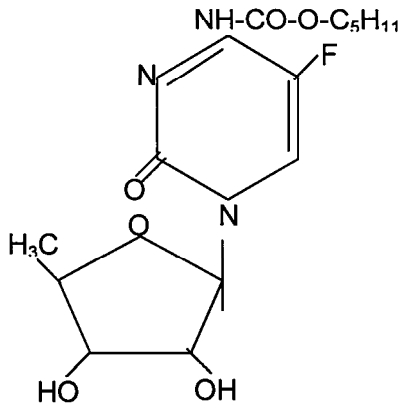


As shown in Figure 2.20 above, capecitabine is metabolised to 5-FU via 3 metabolic steps. After absorption in the intestine, carboxyl esterase converts it to 5'-deoxyfluorocytidine (DFCR). DFCR is then metabolised to deoxyfluorouridine (DFUR) by cytidine deaminase. The third and final steps involves conversion of DFUR to 5-FU by thymidine phosphorylase (TP) which is expressed in solid tumours at levels 3-10 times that of surrounding normal tissue(Schuller et al. 2000; Yarden et al. 2004). Intratumoural expression of TP has shown to be a predictive marker of 5-DFUR activity in breast cancer(Tominaga et al. 2002).

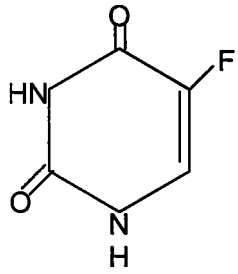
The structure of capecitabine and 5-FU are shown below in Figure 2.21. 5-FU either undergoes catabolism by dihydropyrimidine dehydrogenase (DPD) forming dihydrofluorouracil, which is subsequently metabolised to fluoro-β-alanine (FBAL) before urinary elimination, or anabolism by TP to form compounds responsible for its cytotoxic activity. Fluorodeoxyuridine monophosphate (FdUMP) is a product of phosphorylation of FU by thymidine kinase. FdUMP subsequently competes with uridine monophosphate to form a ternary complex with thymidylate synthase (TS) and folic acid, inhibiting TS in the rate limiting step of de novo thymidine synthesis. In the absence of thymidine, DNA synthesis is reduced and cell death occurs.

One of the main advantages of capecitabine is that due to its 100% bioavailability it can be given orally, unlike 5-FU which requires intravenous administration due to its variable absorption from the gastrointestinal tract and rapid degradation. The high first pass metabolism of 5-FU have resulted in patients receiving protracted infusions at home. Capecitabine has shown activity against a variety of tumour xenografts including colon, gastric, breast, cervical, bladder, ovarian, and prostate cancer; however the largest experience to date and current clinical indications are for metastatic breast and colorectal cancer.

Figure 2.21 Structures of Capecitabine and 5-FU



Capecitabine



5-FU

This study will evaluate whether [18F]FLT-PET can be used as an early pharmacodynamic marker of capecitabine activity. In contrast to the previous study, 2.3, where the antiproliferative effects of treatment led to a decrease in [18F]FLT, this study should show that early inhibition of the de novo thymidine synthesis pathway will lead to an early rise in [18F]FLT as the cells attempt to synthesize more thymidine monophosphate by the salvage pathway.

As the activity of TP is critical for capecitabine activation, then it would be interesting to study the intratumoural expression of this enzyme. Therefore, in patients with suitable lesions, the plan was to study the relationship between TP expression (from fine needle aspirates), [18F]FLT uptake and radiological response. Fine needle aspiration will be used as core biopsies are invasive, and tissue proliferation due to the inflammatory response after a biopsy could theoretically alter [18F]FLT uptake. Factors that could affect the relationship between TP expression and [18F]FLT include the rate of catabolism of 5-FU to inactive metabolites, a process that is initially catalysed by DPD, as well as the levels of the target enzyme,TS.

In an additional pharmacodynamic study, the levels of capecitabine and metabolite, deoxyuridine, dUrd, in plasma will be assessed at selected time points as indices of drug exposure. dUrd levels are a surrogate for global TS inhibition largely resulting from TS inhibition in normal tissues (de Jonge et al. 2002; Benepal et al. 2005). The PET scans will be commenced at 1 hour after the first oral dose of capecitabine. From the published plasma pharmacokinetics of capecitabine, it is expected that maximum tumour concentrations will be achieved within 1-2 hours after drug administration (Schuller et al. 2000).

Patients will be assessed for radiological and clinical response by the RECIST criteria (Therasse et al. 2000) during routine follow-up at medical oncology clinics as they continue their treatment with capecitabine. To mitigate any effect of altered drug/radiotracer delivery on [18F]FLT pharmacokinetics, a surrogate measure for blood supply using H_2[15O]-PET will be used prior to each [18F]FLT-PET scan. The basis for this is outlined below.

2.4.3.1 H_2[15O]

Tumours have a heterogeneous vascular architecture characterised by areas of angiogenesis, leaky vasculature, and areas of necrosis. Measurement of tumour blood flow has implications for both diagnosis and pharmacokinetics. In the diagnostic setting, altered blood flow patterns measured by H_2[15O] are able to differentiate breast tumour tissue from surrounding normal tissue(Hentschel et al. 2007). Tumour blood flow rates can affect drug pharmacokinetics by impairing the delivery of anticancer drugs in underperfused areas. It is commonly acknowledged that tumour hypoxia in areas of reduced blood supply is associated with resistance to both chemo- and radiotherapy via expression of a host of biological factors including HIF-1(Tredan et al. 2007).

Water is a chemically inert, freely diffusable tracer i.e. it has no net effect on tissue structure or function and is not modified or retained by tissue. This, together with its 100% first-pass extraction, makes it suitable for studying tumour blood supply. Most studies published using H_2[15O]-PET have been performed as part of neurological investigations of cerebral blood flow. Blood flow and the volume of distribution of water (Vd, the volume of water in tissue that exchanges with an equivalent volume of arterial blood during the time of the water scan) were studied in 20 patients with breast carcinoma and found to be significantly higher in tumour compared to normal breast tissue, the differences were explained in part by different tissue composition, i.e. the higher fat content of normal breast tissue (Wilson et al. 1992). Previously, Mankoff et al have shown that a low-ratio of glucose metabolism (measured by FDG) to blood flow is a positive predictive factor for complete response and disease free-survival in breast cancer patients treated with neoadjuvant chemotherapy(Mankoff et al. 2003), and that after 2 months of treatment in non-responding patients tumour blood flow increases by 48%.

In this study patients are planned to have a baseline water and [18F]FLT-PET scan on the same day, and then repeat scans on the day of starting capecitabine which is anticipated to be 2-10 days after the baseline scan. The [18F]FLT uptake will be corrected for changes in tumour blood flow (measured using H_2[15O]) to determine if changes in [18F]FLT signal reflect a genuine change in retention or are due to altered [18F]FLT delivery. The proposed method for measuring water flow and Vd is now outlined below.

The one compartment model developed by Kety in 1951 is most commonly used for modelling H_2[15O] data, and has mainly been used for neurology and cardiology studies(Kety 1951).

The behaviour of water within tissue is described by the following equation:

$$C(t) = f \times [Ca(t) \otimes \exp(-f / Vd \times t)]$$

(where C(t) is the radioactivity concentration in tissue at time t, $C_a(t)$ is the radioactivity concentration in arterial blood at time t, f is regional blood flow (per gram of perfused tissue) from plasma to tissue, V_d is the volume of distribution for water which is defined as the ratio of the water concentration in tissue to that in blood at equilibrium, and $\otimes$ denotes the convolution operator.)

One of the limitations of the water flow model is that assumes equivalent flow throughout the tumour – which may be inappropriate for larger lesions, especially those with areas of necrosis. For that reason, in this study, lesions larger than > 5cm will be subdivided into separate tumour areas, and necrotic areas will not be sampled.

2.4.4 Methods

Patients were recruited from the medical oncology clinics in Charing Cross Hospital, London. The inclusion criteria for this study were: age more than 18 years and less than or equal to 80 years, with a diagnosis of histologically or cytologically proven breast cancer, at least one site of measurable disease at least 2cm in diameter (nb patients with liver and/or bone metastases were allowed to participate in the study provided the measurable lesion is not located at these sites), a treatment-free interval of 3 weeks, nb 4 weeks applied for radiotherapy to the imaging site/1 week for patients previously on tamoxifen, a life expectancy of at least 3 months, a haemoglobin of at least 10g/dL, granulocyte count of at least 1.5 x 10^9/L, platelet count of at least 100 x 10^9/L, have adequate creatinine clearance (calculated at least 50ml/min), have adequate hepatic function (bilirubin not greater than 1.5 ULN, serum transaminases not greater than 2.5ULN), be able to consent and comply fully with the study protocol. The exclusion criteria were: pregnant or lactating patients, sexually active patients who

are not employing adequate contraception, pregnancy were performed in all women of childbearing potential, (this population was also strongly advised to avoid pregnancy in this study), patients with uncontrolled medical conditions, patients unable to lie flat, patients with evidence or previous diagnosis of cerebral metastases, patients with excessive bruising from a previous scan on the same side as the position of the new arterial line.

Eligible patients had a breast tumour or regional lymph node lesion or metastasis measuring ≥ 2.0cm, for which they were to receive treatment with capecitabine chemotherapy. All patients had AJCC stage III/IV breast cancer. Information sheets were given to all patients. All patients were given a minimum of 24 hours to make a decision about participation in the study. Consenting patients with suitable lesions were to have fine needle aspirates prior to PET scanning to assess TP enzyme levels. Full information was available to all patients' general practioners, and carers who requested it, after the patients' consent had been obtained.

Patients were scanned on two separate occasions, one baseline prior to treatment, and the second scanning session was within 1 hour of the first oral dose of capecitabine. Treatment was dosed at 1250mg/m^2, which is the standard dose for capecitabine monotherapy in metastatic breast cancer. Plasma samples were taken at 15 and 60 minutes post the 1st dose of capecitabine and stored for future analysis of capecitabine, and metabolite, FBAL.

Nine patients with locally advanced and metastatic breast cancer were recruited for the study, of whom 8 completed the two scanning sessions. The other patient could not be scanned due to radiochemistry failure to manufacture [18F]FLT on two occasions.

Details of the patients and sites of disease are shown in Table 2.10.

Table 2.10 Patients in the [18F]FLT Pharmacodynamic study

Patient	Imaging site	Sites of Disease	Histology	Response
1	Pelvis	Liver, bones, ovary	Grade III IDC ER-ve, PR-ve, c-erbB2 +++	Partial
2	Upper thorax	Supraclavicular fossa	Grade III IDC ER +, PR + c-erbB2 +++	Partial
3	Chest wall	Posterior thorax	Grade III IDC c-erb B2-ve	n/a
4	Breast, axilla	Bones, liver, lymph, breast	Grade II IDC	Partial
5	Supraclavicular fossa	Lymph nodes, liver	Grade II Lobular carcinoma ER-ve, PR-ve, c-erb –ve	n/a (RIP)
6	Breast and contralateral axilla	Breast, lymph nodes	Grade III IDC ER +++/ PR+++ c-erbB2 -ve	n/a (RIP)
7	Lungs	Lung, bones	Grade III IDC ER+++, PR+, c-erbB2 negative	n/a
8	Breast	Breast, bones	Grade III IDC	Partial

Scans were acquired in the following time frames for the dynamic water study:

Table 2.11: Dynamic water scans

Dy1: Dynamic $H_2[^{15}O]$				
No.	Duration	Type	Accumulated	
			Frames	Time (min:sec)
1	30s	Background	1	0:30
1	20s	Frames	2	0:50
22	5s	Frames	24	2:40
3	10s	Frames	27	3:10
5	30s	Frames	32	5:40
5	60s	Frames	37	10:40

For the [18F]FLT study the frames were acquired as follows:

Table 2.12: Dynamic [18F]FLT Imaging

Dy2 Dynamic Emission [^{18}F] FLT				
No.	Duration	Type	Accumulated	
			Frames	Time (min:sec)
1	30s	Background	1	00:30
6	10s	Frames	7	01:30
4	15s	Frames	11	02:30
4	30s	Frames	15	04:30
5	120s	Frames	20	14:30
4	180s	Frames	24	26:30
4	600s	Frames	28	66:30

2.4.4.1 Radiotracer Synthesis and Scanning Procedure

[15O] was generated by the action of deuteron beams in the same cyclotron which produces [18F], and was then reacted with hydrogen (H_2) to produce H_2[15O]. Due to the short half-life of 123 s, the gases are pumped directly to the scanner table to enable hydrogenation. [18F]FLT was manufactured as described previously in

section 2.1. The target radioactivity for injection was 600MBq for H_2[15O], and 222MBq for [18F]FLT. Prior to injection of both tracers a short, 2D, 2 minute transmission scan was performed; a second longer transmission scan lasting 20 minutes was performed for attenuation correction prior to injection of the H_2[15O] only. Both radiotracers were administered by bolus iv injection over 20-30 seconds. Patients were scanned for 10min 40sec for the H_2[15O] scan, and for 66 min 30 sec for the [18F]FLT scan. Images were reconstructed using 2D filtered back projection; reconstructed images had a spatial resolution of (x,y,z): 8.5, 8.5, 5 mm.

Arterial blood sampling was done from a cannula inserted into the radial artery (see section 2.2 for technique). Continuous sampling was performed at a rate of 5ml/minute for 1minute post-completion of the H_2[15O] scan and for the first 10 minutes of the [18F]FLT scan. Samples were taken for cross-calibration for measurement of activity due to [18F]FLT at the following time-points: baseline, 2min 30sec, 5min, 10min, 20min, 30min, 45min, and 60min. Measurement of activity due to the [18F]FLT metabolite, [18F]FLT-glucuronide was undertaken at 2min 30sec, 5min, 10min, 30min, and 60min to enable metabolite correction for mathematical modelling of [18F]FLT pharmacokinetics. Correction was made for delay and dispersion of the recorded arterial curve due to the time delay between the measured arterial input function and the imaging pixel, and dispersion due to the slower rate of flow through the edge of a laminar vessel.

ROIs were defined manually on the [18F]FLT scans as previously outlined in section 2.1. Definition of the ROIs on water images was very difficult when they were used alone, this was worse for tumours located near a region of high blood flow such as the liver. To avoid sampling error between the [18F]FLT scans and the water scans, the ROIs were identified on the [18F]FLT scan, and the same object map was applied to the dynamic water datasets.

Mathematical modelling and measurement of semiquantitative parameters for [18F]FLT was done as previously described in section 2.1. The following parameters

were obtained: SUV and AUC at 60 minutes (SUV60, AUC), modified Patlak Ki, parent plasma Patlak Ki, and FRT60:1.

The permeability surface area product (ps) for [18F]FLT was calculated as follows using K1 (delivery constant from compartmental analysis) and flow obtained from the water analysis:

$$K1 = \text{flow (f)} \times \text{extraction}$$

$$K1/f = 1 - e^{-ps/f}$$

$$e^{-ps/f} = 1 - K1/f$$

$$-ps/f = \ln (1-K1/f)$$

$$PS = -f \times \ln (1-K1/f)$$

2.4.4.3 Immunohistochemistry

Two patients consented for FNA. One sample was analysed for TP using 100ul of Anti-Thymidine Phosphorylase (TP) Antibody, antigen retrieval system, Roche® Diagnostics, UK. Staining was performed by Mr D Peston, Histopathology Department, Charing Cross Hospital, London as reported previously (Teo et al. 2003). The second sample was found not to contain tumour cells.

2.4.4.4 Statistics

The results for Ki, FRT, SUV, and AUC of [18F]FLT were determined to be significant based upon the variability for each parameter as described in section 2.2. A Wilcoxon matched-pairs test was used to determine if there was a significant difference in tumour blood flow, Vd, K1, and PS product, using GraphPad Prism version 3.

2.4.5 Results

The scans were well tolerated. The activity of [18F]FLT injected ranged from 147-234MBq, and that of H_2[15O] was 566-777MBq. Of the eight patients who completed the study, suitable PET images were obtained in six. This is because one patient with small-volume metastatic disease present in the larynx which was outside the field of view of the PET scan had a lesion suitable for imaging which was presumed to be a metastatic lymph node. On [18F]FLT-PET scan images there was no significant uptake; further investigation by fine needle aspiration and MRI imaging showed that this was non-invasive and not a metastatic lymph node. The other patient who had widespread liver disease was initially thought to have a metastatic lung lesion in the right apex, however detailed radiological review concluded that this was benign; there was no significant uptake in this region compared to normal lung tissue on the [18F]FLT-PET scan.

10 breast tumour lesions in total were imaged using [18F]FLT PET and H2[15O]. The lesion with the maximal change in [18F]FLT-PET SUV60 was a primary breast tumour which showed a 50% increase in SUV60 (see Figure 2.22). The smallest change was seen in a cervical node which showed a 1.35% decrease in uptake. With the exception of this lesion, all other lesions showed an increase in uptake measured by SUV60 at 1 hour post-capecitabine. Of these increases, 4 were significant as defined by the repeatability study in section 2.2: one in an ovarian metastasis, one in a breast tumour, and 2 in distinct regions within patient 8 with a large breast tumour (i.e. an increase in (SUVpre-SUVpost-SUV)/SUVpre of >95% confidence interval for variability); all of these 4 lesions had a partial clinical response. The changes in SUV60, AUC, FRT60, IRF60 and Ki are shown in Figure 2.23. The two lesions from patient 4 (breast and axilla) are depicted with white circles, and the four lesions from patient 8 are depicted with grey symbols and lines.

The significance of responses is shown in Figure 2.24 (significant response is above the upper solid line). Four lesions were deemed to have responded using SUV60 and AUC60 (identical lesions for both parameters). For modelled data, the changes in modified Patlak Ki and IRF60 were significant for all but 2 lesions. The significant changes matched those obtained by SUV60, in the additional 2 lesions one had a clinical response, and the other could not be assessed.

In contrast, FRT60 suggested a significant response in an axillary lymph node which was deemed not to have responded by any of the other parameters; FRT60 showed no significant response for the remainder of the lesions. Although faster time frames at the start of this study compared to those in study 2.3 were used to improve the assessment of delivery of [18F]FLT, the difference in spectral analysis results suggest that the FRT60 is still influenced by blood flow at one minute. IRF60 may be a more reliable parameter than FRT60 as suggested previously by the repeatability analysis in study 2.2. The lower response rate for FRT60 may be explained by its wider confidence interval for this parameter obtained using the repeatability data of 0.078±0.48, however there are no data for the repeatability of FRT60 with the new time frames used in this study.

The mean blood flow before therapy (± SE) was 0.55±0.07 ml/min/ml, and post-capecitabine this increased to 0.76 ± 0.17 ml/min/ml. However this was not significant as would be expected as scans were performed on average 6 days apart (range = 3-13).

Figure 2.22 [18F]FLT-PET Images Pre and Post Capecitabine

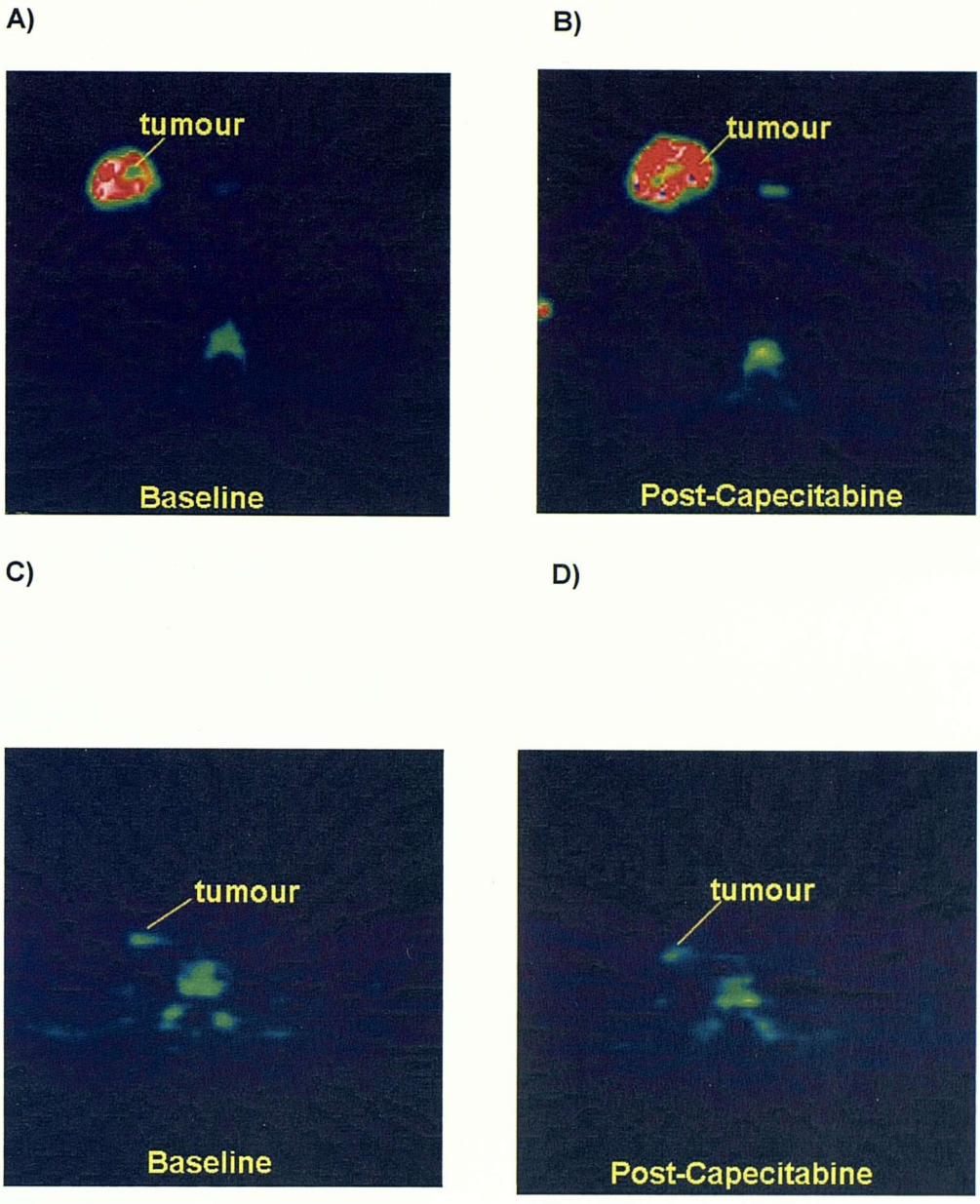
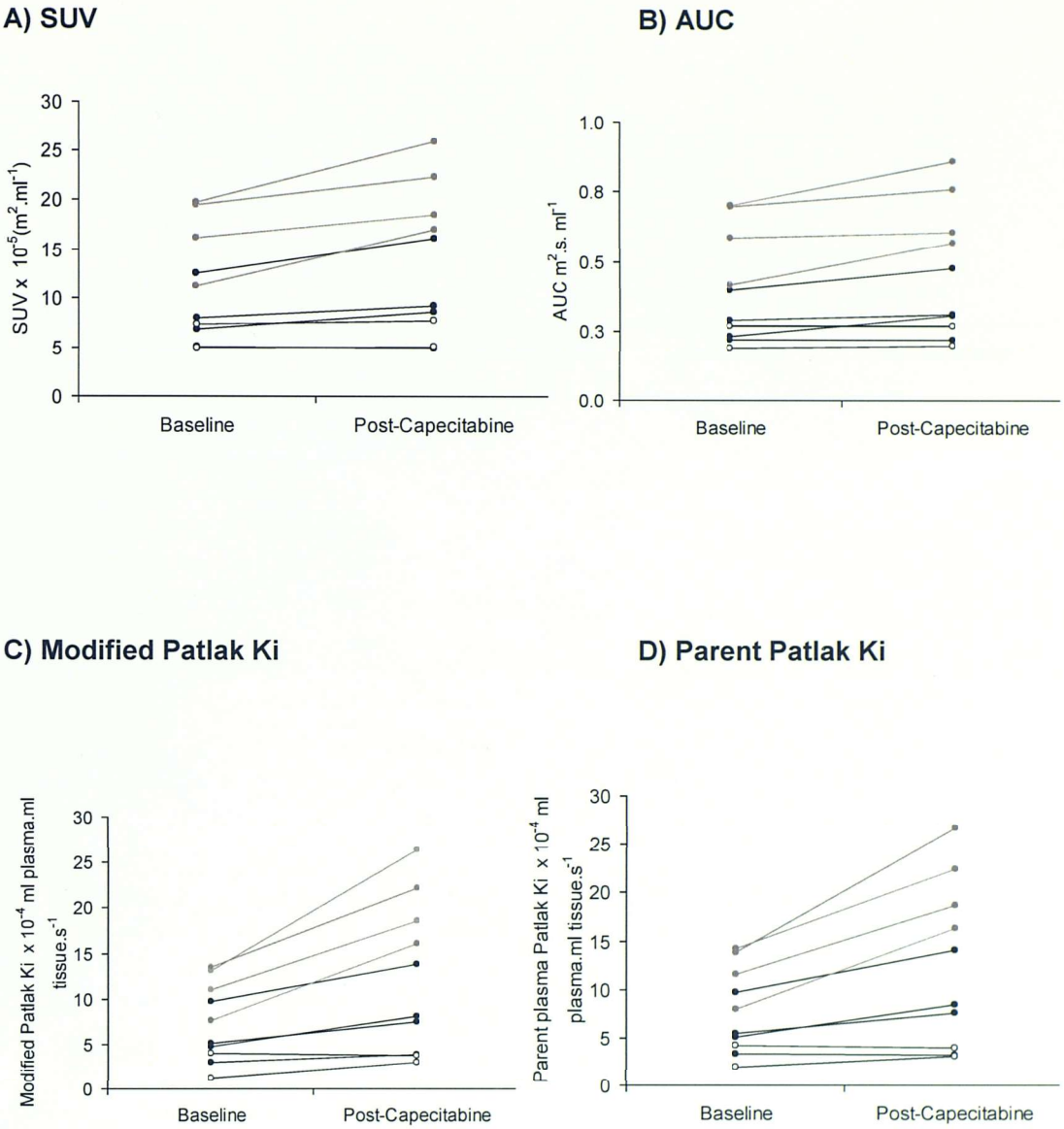
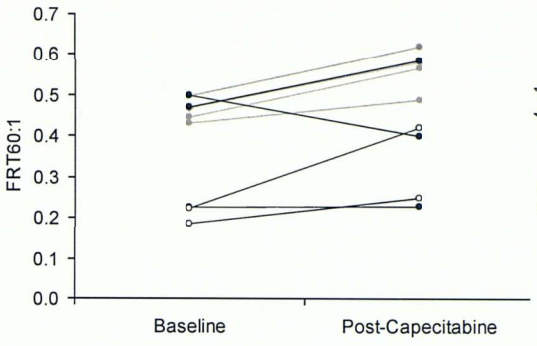


Figure 2.22. Images of the tumour with the maximum increase in [18F]FLT SUV post-capecitabine are shown in above in a primary breast tumour, 2.22 a) and b), compared to the tumour with the minimal change which are shown in c) and d).

Figure 2.23 Changes in [18F]FLT Pharmacokinetic Parameters Post-Capecitabine



2.23E) FRT



F) IRF60

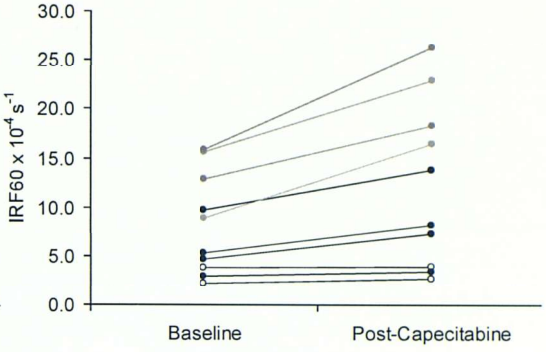


Figure 2.24 Significance of [18F]FLT response to capecitabine for all lesions

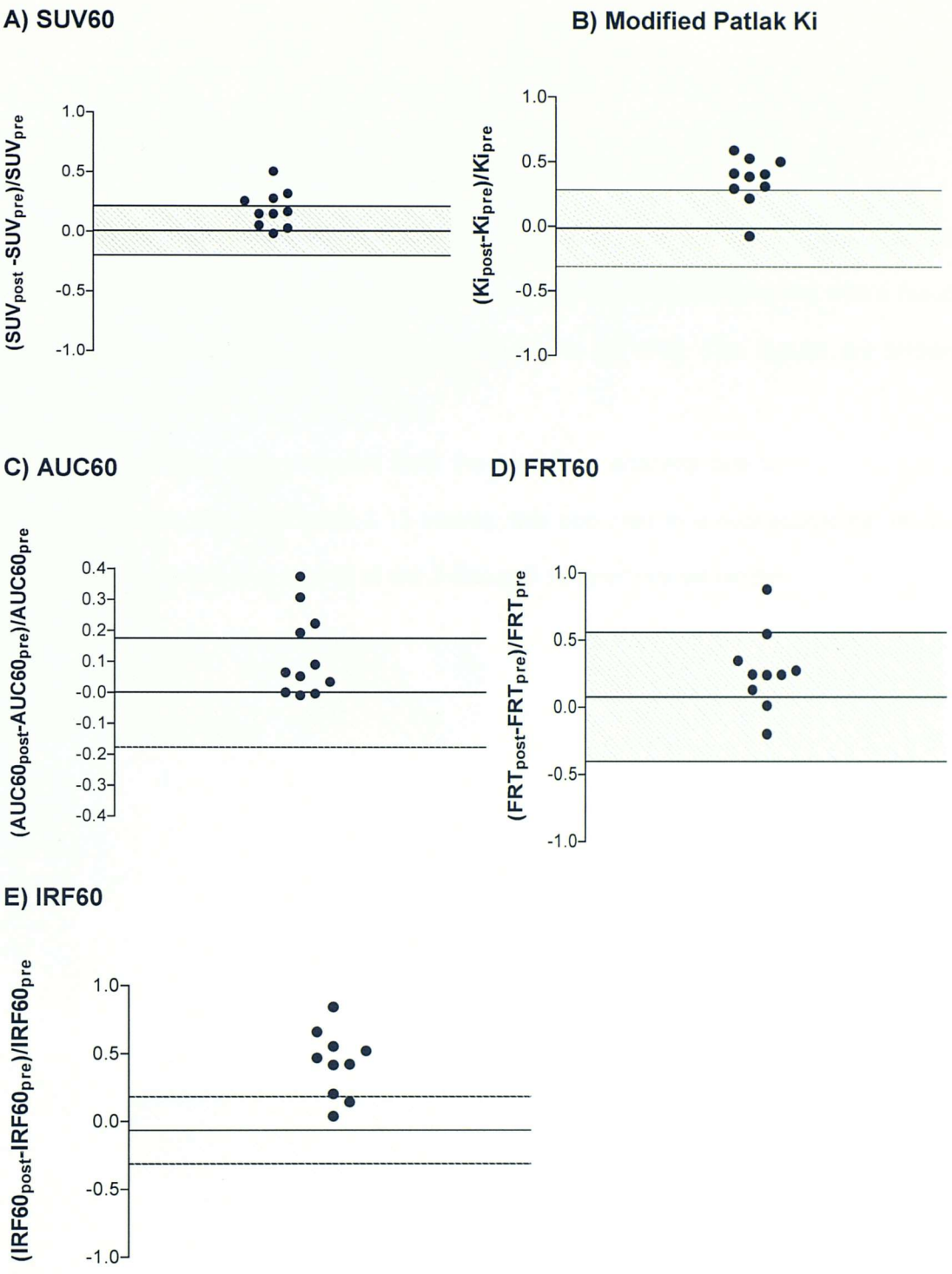


Figure 2.24 above shows the response pattern for all lesions for each of the pharmacokinetic parameters, values within the shaded area show no significant change in [18F]FLT uptake compared to baseline, those above the upper border of the

area represent a significant increase, and those below the lower border represent a significant decrease).

2.4.5.1 Tumour perfusion, Vd, and PS product

This was assessed in 9 out of 10 lesions, the remainder could not be assessed as there was a delay in commencing continuous blood sampling with a result in loss of counting of the peak radioactivity due to $H_2[15O]$. The results are shown below in table 2.13.

One case was excluded from the statistical analysis due to the data being subject to noise (line 3 in table 2.13 below), this occurred in a supraclavicular lymph node which resulted in a poor fit of the 2-tissue 3 compartmental model.

Table 2.13: Comparison of tumour Vd, K1, and PS product pre- and post-capecitabine.

Region	Pre flow	Post flow	AUC pre	AUC post	Vd	Vd	K1 $x10^{-3}$	K1 $x10^{-3}$	Preps	Post ps
Tumour	0.52	0.52	0.076	0.090	0.93	0.97	2.60	2.62	3.10	2.62
Tumour	0.98	0.34	0.036	0.050	0.32	0.47	1.14	2.55	1.18	2.56
Tumour	0.31	0.26	0.056	0.054	0.54	0.60	1.71	6.13	2.07	6.17
Tumour	0.25	0.14	0.050	0.038	0.57	0.59	1.53	1.30	1.91	1.30
Axilla	**	**	0.069	0.064	0.64	0.57	7.08	0.92	10.64	0.92
Tumour a	0.50	0.71	0.075	0.064	0.76	0.71	3.77	3.24	5.00	3.25
Tumour b	0.44	1.46	0.049	0.067	0.46	0.65	2.33	2.98	2.81	2.99
Tumour c	0.58	0.95	0.063	0.076	0.63	0.80	5.05	4.49	7.12	4.50
Tumour d	0.61	0.90	0.075	0.071	0.75	0.74	4.05	4.86	5.16	4.87

(where columns in grey represent values post-capecitabine and units are: flow ml/min/ml tissue, AUC m^2sec/ml, Vd ml blood/ml tissue, K1 for [18F]FLT from compartmental analysis µl/s/ml, ps product ml/s/m, ** was not included due to a poor fit of the model).

Statistical analysis by the Wilcoxon matched-pairs test showed that there was no significant difference for tumour blood flow (p=0.25), AUC (p=0.16), Vd (p=0.16), K1 (p=0.65), or ps product (p=0.74) between baseline and post-capecitabine scans.

Clinical Response

This was assessed in 5 patients. Two patients died before response assessment could be performed (one due to brain metastases and the other had an unexplained death at home). In the remaining patients one was not assessed as the imaging site had not contained tumour due to the FNA findings. None of the patients had a complete response.

Therefore, as there were a small number of patients in this study, and only one response category it is difficult to correlate the PET findings with clinical response.

Immunohistochemistry

Only one sample was suitable for analysis, 100% of cells stained positive for thymidine phosphorylase at a 1:500 dilution. This patient also had a significant response as determined by Modified Patlak Ki and IRF60 but not by SUV60 or AUC60. The patient had a partial clinical response.

2.4.6 Discussion

Drug metabolism is subject to a large interpatient variability; due to a combination of genetic e.g. allotypes of dihydropyrimidine dehydrogenase, environmental e.g. age, and disease factors e.g. reduced renal clearance. Whilst it is possible to measure some of these affects, most require invasive studies and some are difficult to quantify. Early pharmacodynamic monitoring with [18F]FLT could allow non-invasive individualisation of drug therapy. This small pilot study attempted to quantify early (mins to hours) changes in [18F]FLT-PET uptake post-treatment with the TS inhibitor, capecitabine.

Previously, [18F]FLT has been used as a marker of the pharmacokinetics of cisplatin in a radiation-induced (RIF-1) fibrosarcoma model. In that study, decreased [18F]FLT at 24 hours was associated with cell cycle arrest, reduced TK-1 and co-factor ATP(Leyton et al. 2005). Another in vivo study has shown a decrease in [18F]FLT uptake in the same model in response to 5-FU treatment after an interval of 24 hours and 48 hours, reflecting decreased proliferation at these later timepoint (Barthel et al. 2003).

The early pharmacodynamic response to TS inhibition with 5-FU has also been measured preclinically using [18F]FLT-PET in the RIF-1 model. The early increases in [18F]FLT uptake at 1-2h hours post-dosing were due to an increased number of membrane equilibrative nucleoside transporter, ENT1. This was due to redistribution of the transporter from the cytoplasm to the cell membrane, induced by 5-FU and surprisingly not due to increased TK1, the TK1 co-factor ATP, incorporation of [18F]FLT into DNA, or increased binding affinity of ENT1(Perumal et al. 2006).

In this current study, although the patient numbers are small, the fact that there was no significant increase in PS product suggests that the effect was not due to increased permeability at the tumour cell membrane and/or increased numbers of the nucleoside transporter binding sites. The PS product is derived by from the delivery of

[18F]FLT, K1 obtained by compartmental analysis, and the blood flow (obtained by the water study). In the previous study, section 2.2, to assess repeatability of pharmacokinetic parameters, the repeatability of K1 was poor (r^2= 0.039), however this is likely to have been optimised in this study due to an increased number of rapid time frames at the start of the dynamic imaging post [18F]FLT injection. One possible explanation for the increase in [18F]FLT uptake post-capecitabine is that the transport mechanism has not reached full saturation, and that there is an absolute increase in [18F]FLT extraction from the plasma into the tumour cells. The underlying process which drives the increased [18F]FLT extraction post TS inhibition remains to be verified in human breast tumour cells *in vivo*.

The timing of [18F]FLT-scans is crucial and depends upon the pharmacokinetics of the drug involved, therefore pharmacodynamic studies with 5-FU should be performed early as later studies may result in decreased [18F]FLT uptake due to an anti-proliferative effect. Whilst the alternative pharmacodynamic marker, 2-deoxyuridine, has been used as an index of 5-FU activity, its level is not tumour specific, and reflects the anti-proliferative of 5-FU in non-tumour cells as well as tumours. The action of capecitabine is however, thought to be more tumour specific than 5-FU due to the presence of TP, however systemic effects do occur such as palmar plantar erythema, so although 2-deoxyurdine levels in capecitabine treatment should be more predictive of intratumoural TS inhibition, they are likely not to be 100% specific. One of the future objectives from this study is to correlate the levels of 2-deoxyuridine measured in plasma on the capecitabine treatment day with [18F]FLT.

Mankoff's previous breast study showed a mean tumour blood flow of 0.3 ± 0.14 ml/min/g of tissue, and a 2 month post-treatment value of 0.23 ± 0.19 ml/min/g of tissue(Mankoff et al. 2002). The timing of that study at 2 months makes comparison with the current one difficult, as at that time the changes are likely to be treatment related, whereas in this one the changes in blood flow were used as a correction factor for [18F]FLT uptake and are unlikely to be treatment related given that they were

measured within an hour of taking the first dose of treatment. The reported Vd for breast tumours has been reported previously as 0.56± 0.15 $ml_{blood}.ml_{tissue}^{-1}$, which compares favorably to this study where the Vd was 0.622±0.06 $ml_{blood}.ml_{tissue}^{-1}$; that of normal breast tissue has been established as 0.14±0.05 $ml_{blood}.ml_{tissue}^{-1}$ (Wilson et al. 1992). The changes for Vd and blood flow were non-significant, suggesting that future pharmacodynamic studies with [18F]FLT-PET could be done without the need for prior scanning with [15O] water.

The major limitation with this study was the small number of patients which was contributed to by poor patient recruitment, radiochemical failure, and the limited number of imaging sites (i.e. exclusion of liver metastases). Despite this, the novel finding of increased [18F]FLT post-capecitabine at such an early time interval warrants further investigation.

CONCLUSION

- [18F]FLT-PET in breast tumour lesions demonstrates early changes in response to treatment with the TS inhibitor capecitabine

- The increases in tumour uptake of [18F]FLT are not due to increased blood flow or permeability surface product

CHAPTER 3: CHOLINE

3.1 Hypothesis

- The uptake of [11C]Choline will be significantly different in human breast cancer compared to normal tissue
- [11C]Choline uptake measured by PET is repeatable in breast cancer
- [11C]Choline-PET is a marker of MAPK activity in vivo
- Inhibition of MAPK via a c-erb-b2 inhibitor will lead to a decrease in [11C]Choline signal

3.2 Aims

- To determine the difference in uptake in [11C]choline measured by PET in breast tumour lesions and metastases compared to normal tissue
- To study the repeatability of [11C]choline-PET in breast tumour lesions and metastases
- To study the relationship between [11C]choline and immunohistochemical markers of signal transduction in breast cancer biopsies
- To determine the effect of a MAPK inhibitor, trastuzumab, on [11C]choline pharmacokinetics

3.3 Introduction

The focus of this chapter is another PET radiotracer, [11C]choline and its potential to characterise intracellular signalling events within breast tumours. In contrast to the previous studies where [18F]FLT focused on proliferation – a result of increased signalling through growth factor pathways, the aim with this study is to concentrate on events upstream within the cell signalling mechanism where upregulation of MAPK acts as a precursor to cell proliferation. As cancer treatments become more target-specific, then a non-invasive method of detecting pathway activation and/or inhibition by treatment would have clear advantages and help to achieve individualisation of cancer therapy.

To date there have been no published clinical studies investigating the potential of [11C]choline-PET in breast cancer. Most of the published PET studies using [11C]choline have focused on the diagnosis of primary and regional lymph node metastatic prostate cancer (Hara et al. 1998; de Jong et al. 2003; de Jong et al. 2003; Yamaguchi et al. 2005; Yoshida et al. 2005; Fanti et al. 2007). Although other tumours e.g. glioma and lung, have been studied to a lesser extent(Pieterman et al. 2002; Khan et al. 2003; Khan et al. 2004).

Recently, the uptake of the PET tracers [18F]FLT, [11C]Choline, FDG, [11C]acetate, and [11C]methionine were compared in a preclinical study of treatment-induced effects on a breast tumour model (multicellular tumour spheroids (MTS) produced from the MCF-7 cell line of breast tumour cells). The level of reduction in choline uptake was insignificant for two cytotoxic agents – paclitaxel and docetaxel, inappropriately low for the degree of inhibition induced by doxorubicin, and gave a false index of efficacy with imatinib (i.e. decrease in uptake when an increase in tumour growth was observed)(Monazzam et al. 2007). [18F]FLT was the best tracer for

detecting growth related effects. These results may be partially explained by the fact that [11C]choline is not specific for proliferation, the use of a non-standard model (MTS) which may require further validation as there have only been a limited number of published reports (6) of its use to date, and timing of the experiments (3 or 5 days).

Most previous studies analysing choline and choline related metabolites in breast cancer have utilised MR spectroscopy with either [31]P or [1]H. One such study found , increased phosphocholine levels in tumour xenografts of the MCF-7 and MDA-mb-231 cell lines compared to normal tissue, which decreased post-treatment with the microtubule stabilising agent, docetaxel (Morse et al. 2007). The timing of imaging in relation to drug administration is crucial, as although a decrease in phosphocholine levels in breast carcinoma cells in response to choline kinase inhibition can be seen as early as 4 hours after dosing, (Al-Saffar et al. 2006).

As with [18F]FLT in chapter 2, the validity of [11C]choline must be established by determining if there is a significant difference in breast tumour/metastases compared to the corresponding normal tissue in patients, which is expected given the low levels of membrane phosphocholine metabolites in normal mammary cells compared to breast tumour cells(Aboagye et al. 1999), and if the tracer pharmacokinetics are reproducible by performing serial scans in the absence of treatment. Trapping of choline within the cell is dependent on the phosphorylating action of choline kinase (CK) forming phosphocholine. Malignant transformation in mammary cells has been shown preclinically to result in an altered phenotype with increased phosphocholine relative to glycerocholine(Aboagye et al. 1999). Therefore the first aspect of the study will be to detect if this is also true for human breast cancer in vivo, by seeking to establish a difference in tumour lesion uptake from normal tissue uptake.

There is clearly a need to demonstrate repeatability of [11C]choline uptake in breast cancer as the normal variability of this radiotracer in the absence of treatment has not been previously determined. As with [18F]FLT, absolute quantification of the

repeatability of each pharmacokinetic parameter describing [11C]choline uptake and retention will allow accurate definition of treatment-induced PET response.

The third aspect of the study will determine the correlation of [11C]choline with immunohistochemical testing of tumour biopsies for MAPK, pMAPK, and proliferation (using Ki-67). [11C]Choline is not a proposed marker of cell proliferation, but of membrane phospholipid choline metabolism and MAPK activation upstream of mitosis, therefore correlation with proliferation may be inferior to [18F]FLT.

Finally, it seems appropriate to employ molecular imaging to determine if a molecular therapy is exerting its desired effect of MAPK inhibition via the c-erbB2 receptor. Thus, in the absence of a licensed mitogen activated protein kinase kinase (MEK) inhibitor, trastuzumab was used in a group of suitable patients with locally advanced and metastatic breast cancer. Measurement of [11C]choline uptake was performed at baseline and after treatment with trastuzumab which acts by inhibiting the the c-erbB2 receptor.

3.4 Methods

3.4.1 Patients

Ethical approval for the study was granted by the Hammersmith Hospitals NHS Trust Research Ethics Committee. The administration of radioactivity for the PET scans was approved by the Administration of Radioactive Substances Advisory Committee, UK. The patient recruitment for the study was divided into two arms: A) to determine the repeatability of [11C]choline, patients had a baseline scan followed by a second one within 1 week in the absence of treatment, and B) a treatment arm in which patients had a baseline scan followed by treatment with trastuzumab and a post-treatment scan within 1 month of initiating treatment.

Patients were recruited from the medical oncology clinics in Charing Cross Hospital, London. The inclusion criteria for the study were as follows: age $\geq$ 18 years and $\leq$ 80 years, histological or cytological evidence of breast cancer with at least one site of measurable disease $\geq$ 2.5cm, a treatment-free interval of $\geq$ 3 weeks (for cytotoxic chemotherapy, hormonal therapy, or cytostatic agents), nb 4 weeks applied for radiotherapy to the imaging site, a life expectancy of $\geq$ 3 months, haemoglobin of $\geq$ 10g/dL, granulocyte count of $\geq 1.5 \times 10^9$/L, platelet count of $\geq 100 \times 10^9$/L, adequate creatinine clearance (calculated $\geq$ 50ml/min), adequate hepatic function (bilirubin $\leq$ 1.5 ULN, serum transaminases $\leq$ 2.5ULN),ECOG performance status 0 – 2 inclusive, able to give fully informed consent and comply with the protocol. In addition those patients in Group B had to have breast tumours which had c-erbB2 receptor positivity grade 3+ by immunohistochemistry, or positive by a fluorescent in situ hybidisation test (FISH).

Subject exclusion criteria were as follows: pregnant or lactating patients, sexually active patients who were not employing adequate contraception (pregnancy tests were performed in all women of childbearing potential, this population were also strongly advised to avoid pregnancy in this study), patients with uncontrolled medical

conditions, patients unable to lie flat, and patients with evidence or previous diagnosis of cerebral metastases.

The initial recruitment to the study was poor, so for that reason an application for an amendment was made to the ethics committee and subsequently granted to include: patients with primary breast cancer (not just locally advanced or metastatic) in group A, measurable lesions greater or equal to 2cm in diameter, and to perform the post-treatment scan in Arm B at the earlier timepoint of 2-5 days post-trastuzumab, rather than the original timepoint of 1 month. The reason for this final amendment was that trastuzumab is often combined with cytotoxic agents in patients with metastatic breast cancer, and this would provide the opportunity for those patients who were suitable to enter the study and have cytotoxic chemotherapy as soon as possible after the post-trastuzumab scan.

3.4.2. Radiotracer synthesis and scanning

[11C]Choline was synthesized via the reaction of [11C]methyliodide with 2-dimethylaminoethanol (DMAE) and isolated and purified by solid-phase extraction (SPE) method(Zheng et al. 1996).The target radioactivity was 370MBq for each scan which is equivalent to 1.036 mSv(Kobori et al. 1999). A short transmission scan lasting 2 minutes for subject positioning, and a second longer transmission scan for attenuation correction were performed prior to radiotracer injection. All patients were scanned on a CTI/Siemens HR+ ECAT962 tomograph as described in chapter 2.

[11C]Choline was administered via bolus intravenous injection over 10-30 seconds followed by a 6ml normal saline flush. Patients were scanned for approximately 65 minutes in 2D; the data were reconstructed by filtered back projection and binned into time frames as shown below in table 3.1.

Table 3.1 Reconstruction of [11C]choline time frames (version 1)

dy1 Dynamic Emission				
No.	Duration	Type	Accumulated	
			Frames	Time (min:sec)
1	30s	Background	1	00:30
9	30s	Frames	10	5:00
5	60s	Frames	15	10:00
5	120s	Frames	20	20:00
5	180s	Frames	25	35:00
6	300s	Frames	31	65:00

The scans were initially reconstructed into the following time frames as shown above, however after our previous experience with [18F]FLT it was thought that faster frames at the start of dynamic imaging would be optimal for discerning radiotracer delivery, the new protocol was devised and is shown below in table 3.2. This resulted in a 10s extra duration in scanning time post-radiotracer injection. The second reconstruction format was employed 9 months after the study was initiated, and only the first 3 patients in the study were scanned using the protocol in Table 3.1.

Table 3.2 Reconstruction of [11C]choline time frames (version 2)

No.	*Duration*	*Type*	*Accumulated*	
			Frames	Time (min:sec)
1	30s	Background	1	00:30
5	10s	Frames	6	1:30
2	20s	Frames	8	2:10
2	30s	Frames	10	3:10
5	60s	Frames	15	8:10
3	120s	Frames	18	14:10
2	180s	Frames	20	20:10
3	300s	Frames	23	35:10
3	600s	Frames	26	65:10

3.4.3 Blood sampling and [11C]Choline metabolite analysis

Continuous arterial blood sampling was performed at a rate of 300ml/hr for the first 10 minutes via a 22G arterial cannula inserted in the radial artery (as described in chapter 2). Discrete samples were taken for cross-calibration of radioactivity and

metabolite analysis as shown below in table 3.3. Therefore the total volume of blood taken per scan was 150ml. Patients had haemoglobin levels checked routinely after the study to ensure that there was no anaemia.

Table 3.3 Blood sampling protocol for [11C]Choline-PET study

Syringe	Isotope	Scan No.	Volume	Time	
BL	[11C]	Dy1	5ml	Baseline	
1	[11C]	Dy1	10ml	2:30	Metabolites
2	[11C]	Dy1	10ml	3:30	Metabolites
3	[11C]	Dy1	10ml	5:00	Metabolites
4	[11C]	Dy1	10ml	7:30	Metabolites
5	[11C]	Dy1	10ml	10:00	Metabolites
6	[11C]	Dy1	10ml	15:00	Metabolites
7	[11C]	Dy1	5ml	20:00	
8	[11C]	Dy1	10ml	30:00	Metabolites
9	[11C]	Dy1	10ml	45:00	Metabolites
10	[11C]	Dy1	5ml	50:00	
11	[11C]	Dy1	10ml	60:00	Metabolites

To measure the contribution of [11C]-radiolabelled metabolites the radioactivity in an aliquot of blood and plasma (1ml) was measured using a sodium iodide well counter. The remainder of blood (7ml) was centrifuged at14,000 rpm to obtain plasma. The radioactivity profile in plasma was determined with a reverse-phase HPLC linked to radioactivity and absorbance detectors and connected to a PC based integrator. The plasma samples were deproteinised by solvent extraction, concentrated by rotary evaporation, re-suspended in mobile phase and an aliquot (1ml) analysed using a reverse-phase HPLC. The column (Luna, 250 x 4.6mm; 10um diameter; Phenomenex) was washed with the mobile phase: a mixture of sodium di-hydrogen phosphate (0.25M) and methanol (80:20, v/v) at a flow rate of 3 ml per min. The eluate was monitored for radioactivity. Both detectors were linked to a PC based integrator which

recorded the radioactivity profile and enabled the correction for [11C]-radioactivity decay and background and integration of radioactive components. The amount of [11C]choline and other radioactive components at each sample time was calculated as a percentage of each radioactive component in each analyte. The blood radioactivity and metabolite analysis was supervised by Ms S Osman of Hammersmith Imanet Ltd ®.

3.4.4. Image and Data Analysis

The images from time frames 12-20 were added together to form an 'add image' using Analyze® software, on which tumour and normal regions were identified. The perimeter of each suitable lesion was drawn manually and used to form an object map. Lesion identification was also attempted using earlier time frames, however this was unsatisfactory due to a poor signal to noise ratio so the strategy was abandoned. The object map was then applied to the complete dynamic image as described in previous chapters, and combined with a timing file to form time activity curves. The TACs were decay corrected for Carbon-11, weight, and body surface area (see chapter 1 for analysis techniques). Modelling and semiquantitative analysis was used to generate SUV at 60 minutes, AUC at 60 minutes, Modified Patlak Ki, Parent Plasma Ki, IRF60, and FRT (ratio of the IRF at 60 mins to that at 1 minute).

3.4.5 Immunohistochemistry

Patients who had suitable, recently taken biopsies were approached for consent for use of tissue. All immunohistochemistry was performed by Dr Jie Jiang, Histopathology Department, Charing Cross Hospital, London - apart from Ki-67 immunostaining (which was done by Dr David Peston from the same Department (using the same method as described in chapter 2)).

4 µm thick sections were cut from formalin-fixed, paraffin-embedded archival tissue blocks and mounted on 3-aminopropyltriethoxysilane (APES; Sigma) treated slides and dried overnight at 37 °C. The sections were placed in a 60 °C oven for 1 h prior to being dewaxed in xylene and rehydrated through graded alcohols. Endogenous peroxidase was blocked by immersing in 2% hydrogen peroxide in methanol for 10 min. Antigen retrieval was carried out by pressure cooking, using 10 mM citrate buffer pH 6.0 and immunohistochemistry (IHC) was performed as previously described(Taylor et al. 1998) and according to the manufacturers' instructions using mouse monoclonal antibodies for oestrogen receptor P-S118 (cat. no. 2511; New England Biolabs, Herts, UK), total MAPK (cat no 4696 New England Biolabs, Herts, UK) phosphorylated MAPK (pMAPK, cat. no. 4376; New England Biolabs), progesterone receptor (cat. no. MU328-UC; Biogenex, USA), phosphorylated c-erbB2 (cat no 2249, New England Biolabs), mouse AKT-1 (cat. no 2967, New England Biolabs), and rabbit antibodies for pAKT (cat no 3787, New England Biolabs) and c-erbB2 (cat. no. A0485; Dako). The rest of staining procedure followed the streptavidin-biotin-peroxidase complex of the ABC protocol, which was described previously (Zidan et al. 1997). One previous positive sample was used as a positive control.

ER (phosphorylated serine 118) and pMAPK levels were scored by a trained histopathologist, using the modified McCarty's H-scoring system, which was based on the percentage of positive cells and the intensity of staining to provide a total score varying from 0 to 300. The staining was designated as negative (H-score <50), weakly positive (+; H-score of 51–100), moderately positive (++; 101–200) or strongly positive (+++, 201–300)(McCarty et al. 1984). The staining pattern of TMAPK, P-AKT and AKT1 are cytoplasmic and nuclear, therefore they were scored as + if there was only cytoplasmic staining, and as ++ if both of nuclear and cytoplasmic staining were present. The areas showing the representative Ki-67 expression in each section were chosen, and the minimum of 1,000 tumor cells were counted manually under light

microscopic fields (× 400) using a computer-assisted image-analyzing system (VM-30; Olympus, Tokyo, Japan)

c-erbB2 and phospho-c-erbB2 were scored using the universal method recommended in the Dako HercepTest™ evaluation system and shown in table 3.4 below.

Table 3.4: Grading of c-erbB2 staining intensity in tissue

Negative:	No immunostaining of the cytoplasmic membrane identified; or faint or blush staining involving a portion of the circumference of the cytoplasmic membrane in less than 10% of the neoplastic cell population.
Low positive (+):	Weak but definitive staining of the membrane over 100% of the cytoplasmic circumference in 11- 30% of the neoplastic cell population
Medium positive (++):	Strong positive staining of the membrane over 100% of the cytoplasmic circumference in 31-50% of the neoplastic cell population
High positive (+++):	Strong positive staining of the membrane over 100% of the cytoplasmic circumference in 51-100% of the neoplastic cell population

3.4.6 Statistical analysis

The difference between tumour and normal tissue uptake was evaluated on a lesion by lesion basis using the Wilcoxon matched pairs test.

Repeatability was analysed using the same tests as outlined in secion 2.3 using GraphPad prism version 4.0 and Microsoft Excel. Pearson's correlation coefficient was used to determine if there was a significant correlation between the immunohistochemistry tests and the [11C]choline-PET parameters. The Mann-Whitney test was used to determine if there was any significant difference between the PET

parameter values for those scored +1 or +2 by immunohistochemistry; except for phosphoHer-2, where the Kruskal-Wallis one way analysis of variance was used as there were three different immunohistochemical groups (0, +2, and +3).

3.5 Results

3.5.1. Patient Characteristics

22 patients aged between 39 and 71 yrs entered the study in total, of whom 21 had at least one [11C]choline scan; the other patient could not be scanned due to radiochemistry production failures on two occasions. The scans were well tolerated. The mean radioactivity administered per scan was 347.43 ± 6.29 MBq. The patient characteristics for the two studies are summarised in Tables 3.5-3.6 below, respectively.

Table 3.5 [11C]Choline Repeatability Study Patients

Pt	Tumour Type	AJCC Clinical stage*	Histological Grade	Oestrogen receptor staining	No. of scans
1	Lobular	II	II	Er ++	2
2	Inflammatory	IV	III	Negative	2
3	Ductal	II	III	Negative	2
4	Ductal	II	III	Negative	2
5	Ductal	IV	II	Er +	1
6	Ductal	IV	II	Er ++	2
7	Mucinous	II	II	Er +++	1
8	Ductal	III	II	Er +++	2
9	Ductal	IV	II	Er ++	2
10	Ductal	IV	III	Negative	2
11	Ductal	LII	III	Negative	2
12	Ductal	LI	II	Er +++	2
13	Ductal	LI	III	Negative	2
14	Ductal	LI	III	Er +	2

*(*AJCC clinical staging of breast cancer – see Appendix 2).*

Table 3.6 [11C]Choline Response to Treatment Study Patients

Pt	Tumour Type	AJCC Clinical stage*	Histological Grade	Oestrogen receptor staining	No. of scans
15	Ductal	LI	III	Negative	1
16	Ductal	III	III	Negative	1
17	Ductal	LII	II	Negative	2
18	Ductal	LII	III	Negative	2
19	Ductal	III	III	Er +++	2
20	Ductal	IV	III	Negative	2
21	Ductal	IV	III	Er ++	2

3.5.2 [11C]Choline Analysis in Arterial Plasma

The [11C]-radioactivity profile in plasma showed [11C]choline and one other radioactive component more polar than [11C]Choline. It is highly likely that the metabolite in this case was [11C]betaine, although conclusive experiments were not done in this study to prove this, evidence that this is the main metabolite of choline in humans has been published elsewhere (Barak et al. 1983; Roivainen et al. 2000). The metabolism analysis of arterial plasma samples in 19 patients showed that [11C]Choline decreased rapidly post-injection such that at 60 mins the mean radioactivity in arterial plasma due to choline was 15.15 ± 2.16% (range 7.98 - 41.99%).The polar radioactive components were observed to increase with time. A typical profile of [11C]choline concentration in arterial plasma is shown below in Figure

3.1, followed by HPLC chromatograms illustrating the metabolism of choline are shown in Figure 3.2.

Figure 3.1: Plasma concentration of [11C]Choline and metabolite post-injection

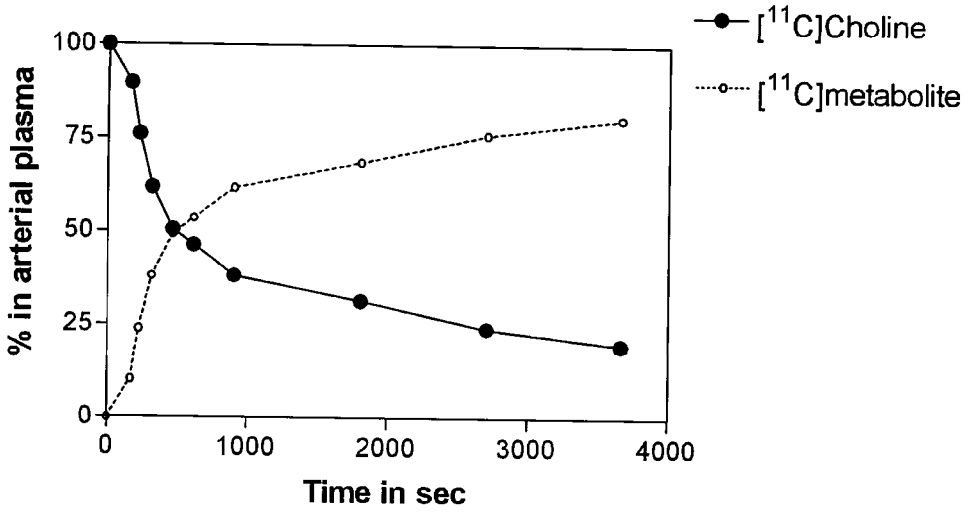
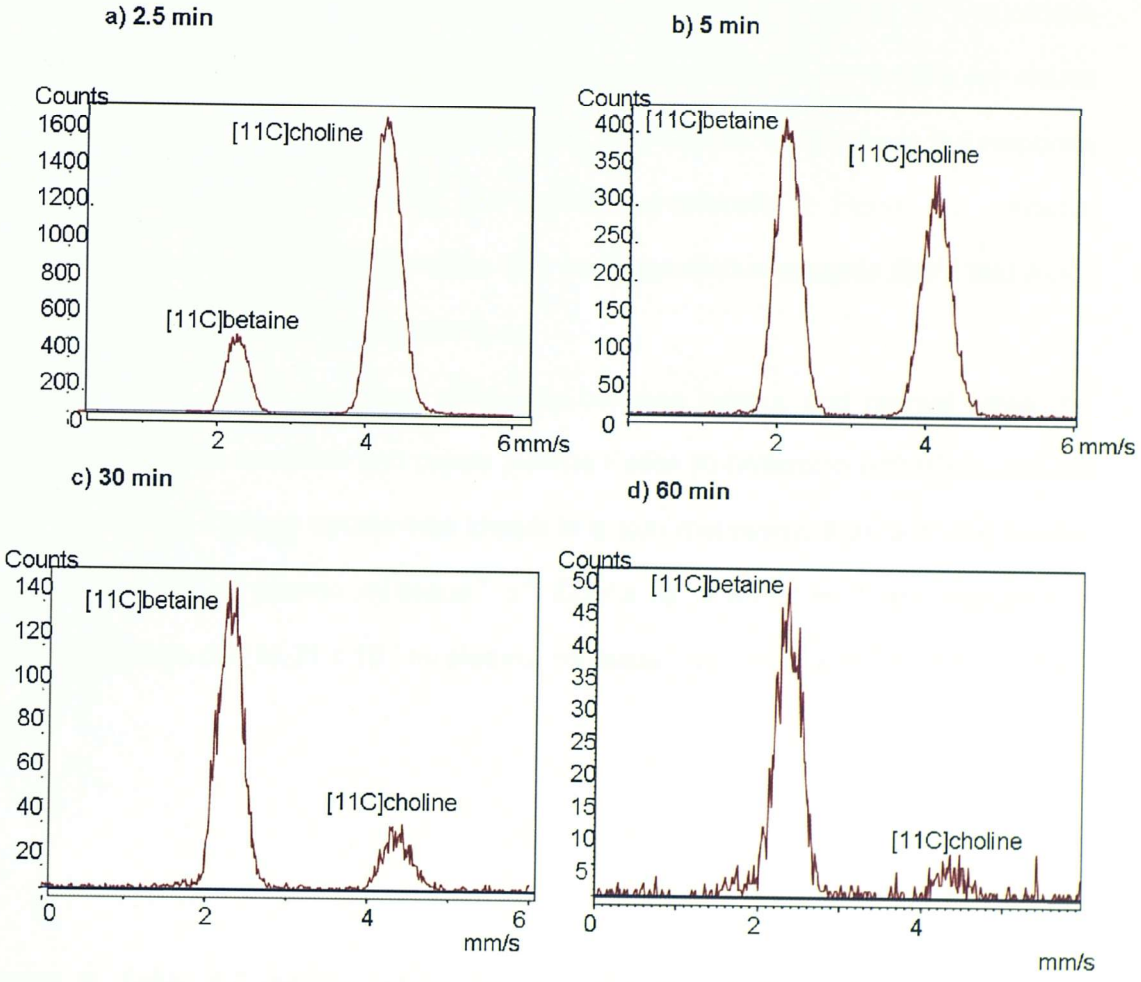


Figure 3.1 above shows the metabolite profile of [11C]choline post-injection. [11C]-derived radioactivity due to [11C]choline is seen to decrease over time, with a corresponding increase in concentration of an [11C]radiolabelled metabolite (most likely to be [11C]betaine. At 60mins post-injection the mean radioactivity due to [11C]choline was 15.1%.

Figure 3.2. HPLC Chromatograms of Arterial Plasma Post-Injection with [11C]Choline

Figure 3.2 above shows the relative contributions of [11C]choline and major metabolite, [11C]betaine to the [11C]radioactivity in arterial plasma during the 60min scanning period. The HPLC chromatograms displayed above were kindly provided by Ms S Osman of Hammersmith Imanet®.



3.5.3. Comparison of tumour and normal tissue uptake of [11C]Choline

All 21 patients were included in this part of the analysis which sought to evaluate the differences in pharmacokinetic parameters describing [11C]choline uptake and retention between breast tumours/metastases and normal tissues on a lesion by lesion basis (total no. of tumour lesions = 25). Tracer uptake was visible in all tumour lesions; no new lesions were identified by [11C]choline-PET which had not been previously identified by other radiological methods. The results for the various parameters in breast tumour/metastases and corresponding normal tissues are shown in Table 3.7 (patients in the repeatability study are in italics, and those in the response study are shown in normal font); and depicted graphically in Figure 3.3. Arterial sampling failed in patient 20; therefore only semiquantitative analysis (SUV and AUC) was performed in this particular patient.

There was a significant difference between tumour and normal breast for SUV, AUC, IRF60, modified and parent plasma Patlak Ki (Wilcoxon $p<0.0001$), but not FRT ($p=0.204$). Tumour uptake was lowest in a skin metastasis from a ductal tumour ($Ki = 4.08 \times 10^{-4}$ ml plasma..ml tissue^{-1}. s^{-1}, SUV x 10^{-5} 2.86 m^2.ml^{-1}), and highest in a lung metastasis ($Ki=18.21 \times 10^{-4}$ ml plasma..ml tissue^{-1}. s^{-1}, ,SUV x 10^{-5} 12.89 m^2.ml^{-1}).

Index to Table 3.7 (below), where SUV=SUV x 10^{-5} m^2/ml, AUC=AUC at 60min m^2.sec/ml, Ki= modified Patlak Ki x 10-4 (ml plasma/ml tissue/s), Ki parent = Patlak Ki from parent plasma x 10-4 (ml plasma/ml tissue/s), FRT= ratio of the IRF at 60min to 1min, IRF60= IRFx10^{-3} /s).

Table 3.7 Tumour and normal tissue uptake of [11C]Choline

Patient	Region	SUV	AUC	Ki	Ki Parent	FRT60	IRF60
1	*breast tumour*	*4.598*	*0.210*	*5.658*	*8.216*	*0.496*	*10.370*
	Nbreast	*1.068*	*0.056*	*3.694*	*4.600*	*0.358*	*2.182*
2	*breast tumour*	*4.620*	*0.184*	*5.063*	*6.486*	*0.388*	*6.581*
	Nbreast	*2.493*	*0.067*	*2.474*	*1.620*	*0.322*	*1.803*
3	*breast tumour*	*2.806*	*0.107*	*4.077*	*5.285*	*0.602*	*7.159*
	Lung	*2.020*	*0.052*	*4.018*	*4.291*	*0.724*	*3.761*
4	*breast tumour*	*6.771*	*0.262*	*7.843*	*9.148*	*0.455*	*9.936*
	Nbreast	*1.470*	*0.074*	*1.671*	*1.889*	*0.366*	*2.079*
5	*breast tumour*	*5.537*	*0.209*	*5.694*	*6.106*	*0.540*	*6.690*
	Nbreast	*4.601*	*0.155*	*4.094*	*4.244*	*0.265*	*3.545*
6	*lung met.*	*9.798*	*0.387*	*12.947*	*14.042*	*0.591*	*12.530*
	Lung	*1.834*	*0.084*	*2.758*	*3.396*	*0.266*	*1.385*
7	*breast tumour*	*6.359*	*0.173*	*8.928*	*9.555*	*0.825*	*8.829*
	Nbreast	*1.476*	*0.036*	*1.873*	*1.957*	*0.827*	*1.892*
8	*breast tumour*	*7.492*	*0.330*	*11.098*	*9.705*	*0.323*	*9.057*
	Nbreast	*1.303*	*0.063*	*2.075*	*2.506*	*0.369*	*2.041*
9	*axillary node 1*	*12.890*	*0.504*	*18.212*	*17.389*	*0.474*	*20.260*
	cervical node 2	*11.026*	*0.434*	*16.122*	*18.554*	*0.492*	*16.630*
	cervical node 3	*10.910*	*0.440*	*16.025*	*16.565*	*0.529*	*17.570*
	Lung	*2.290*	*0.100*	*3.637*	*4.674*	*0.382*	*3.345*
10	*lung met*	*8.587*	*0.332*	*12.778*	*14.309*	*0.540*	*14.220*
	Lung	*1.733*	*0.071*	*2.129*	*2.780*	*0.377*	*2.698*
11	*breast tumour*	*7.362*	*0.199*	*10.967*	*12.402*	*0.523*	*11.390*
	Nbreast	*1.127*	*0.036*	*1.828*	*2.180*	*0.350*	*1.890*
12	*breast tumour*	*9.931*	*0.266*	*13.456*	*14.896*	*0.595*	*14.740*
	axillary node	*4.151*	*0.173*	*6.214*	*7.403*	*0.271*	*5.879*
	Nbreast	*1.437*	*0.052*	*0.441*	*1.853*	*0.412*	*1.911*
13	*breast tumour*	*7.067*	*0.305*	*15.972*	*18.462*	*0.488*	*14.900*
	Nbreast	*2.215*	*0.089*	*3.939*	*4.316*	*0.540*	*4.513*
14	axillary node	7.874	0.183	11.547	12.812	0.600	13.260
	Muscle	1.651	0.051	3.816	3.799	0.728	3.806
15	breast tumour	7.782	0.316	8.886	12.056	0.467	12.460
	Nbreast	2.260	0.087	3.199	3.550	0.511	3.376
16	axillary node	9.818	0.403	12.666	13.906	0.511	13.350
	Lung	2.868	0.091	2.867	3.081	0.576	3.188
17	cervical node	7.328	0.307	7.882	10.871	0.347	10.150
	axillary node	6.182	0.234	4.115	7.039	0.326	7.511
	Muscle	2.340	0.103	2.901	3.723	0.487	3.133
18	breast tumour	5.728	0.243	5.409	6.087	0.323	6.351
	Nbreast	0.831	0.045	1.015	1.154	0.196	0.903
19	breast tumour	8.1067	0.3196	17.97	20.797	0.447	19.73
	Nbreast	0.816	0.0357	2.717	2.9062	0.3288	1.917
20	Lung met 1	7.589	0.345	n/a	n/a	n/a	n/a
	Lung met 2	6.451	0.311	n/a	n/a	n/a	n/a
	Lung	2.319	0.121	n/a	n/a	n/a	n/a
21	lymph node	10.430	0.395	15.074	16.847	0.634	16.150
	Lung	3.567	0.152	5.262	6.530	0.490	5.455

Figure 3.3 Comparison of tumour and normal tissue [11C]choline uptake

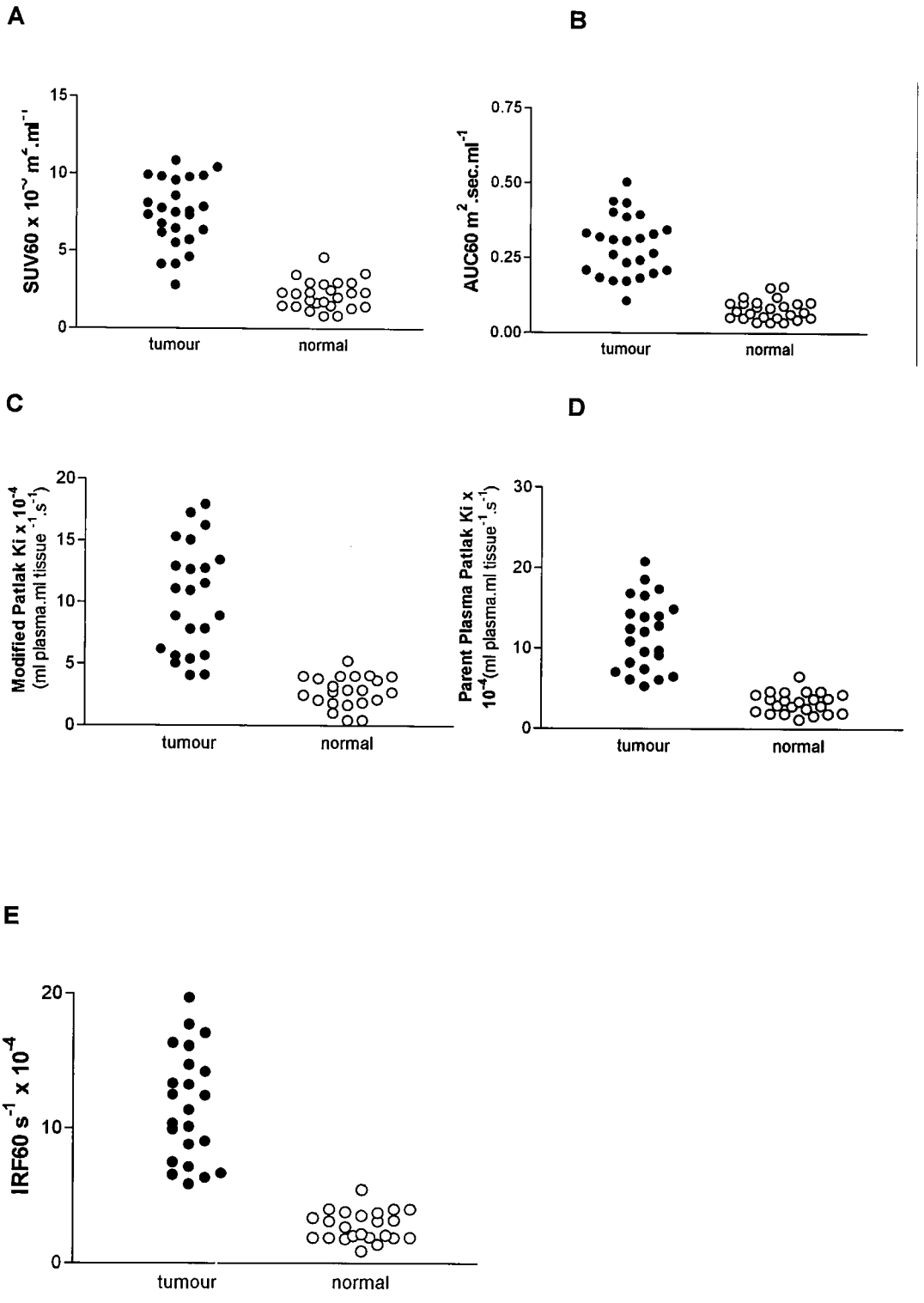


Figure 3.3 above shows the difference between tumour and normal tissue pharmacokinetic parameters describing [11C]choline uptake, where A) is SUV at 60min, B) is AUC at 60min, C) is Ki obtained by modified Patlak analysis, D) is Ki obtained by classical (i.e. parent plasma) Patlak analysis, and E) is the IRF at 60min. The Wilcoxon p was <0.0001 for all of the above parameters, but not significant for FRT.

Overall, tissue uptake of choline was of the order lung ≤ normal breast < tumour < spleen ≤ liver. Typical examples of TAC curves (corrected for activity and body surface area) in tissues from patient 4 and patient 9 are shown in Figure 3.4.

Figure 3.4. Time Activity Curves for [11C]choline in different tissues

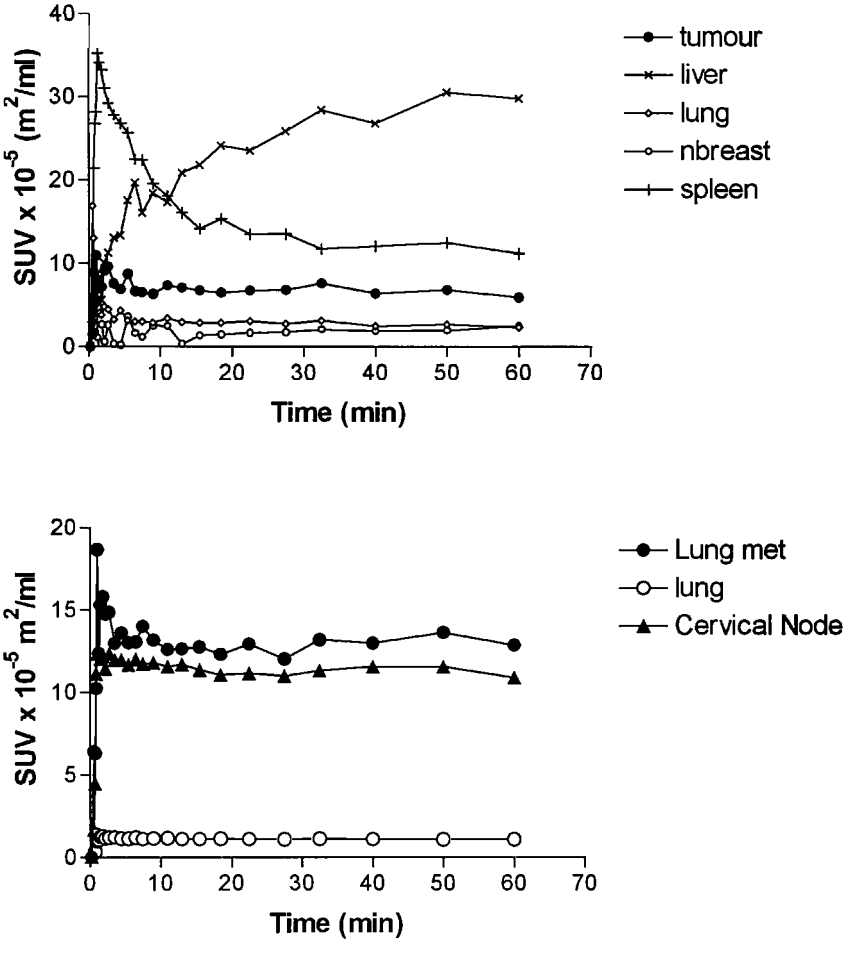


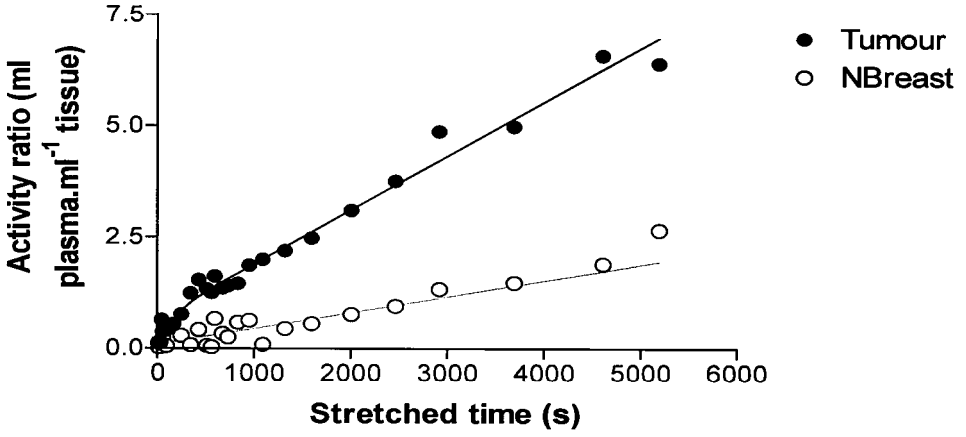
Figure 3.4 – top panel shows the activity (corrected for decay and BSA) measured in different tissue regions in patient 4 who had a primary breast tumour, and bottom panel shows the uptake in a lung metastasis and metastatic cervical node in patient 9.

There was a good fit of the Patlak and spectral models to the raw tumour data (Figure 3.5). Tumour Patlak Ki calculated using parent plasma as an input function was 17.9% higher than Ki calculated using modified Patlak analysis (see chapter 1 – mathematical modelling section for an explanation of the Patlak-Rutland plot).

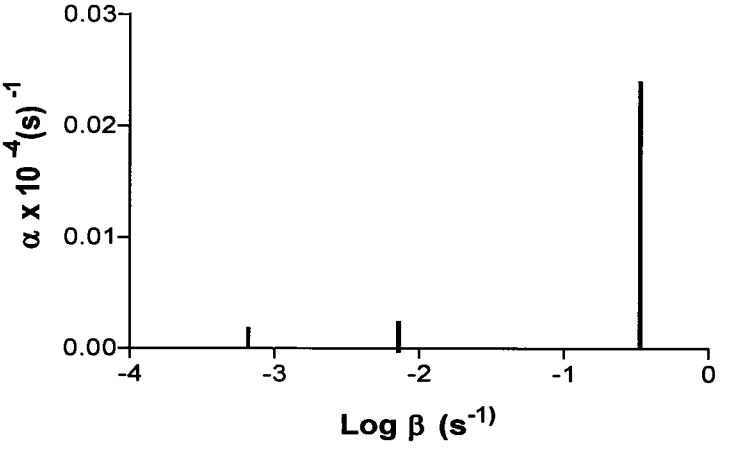
Whilst the TAC curves suggest that uptake of [11C]choline reaches steady state early in the scan (see asymptotic nature of TAC curves in Figure 3.4 after 5 mins), the linear phase of the Patlak plots in Figure 3.5 below suggest that a net irreversible retention component of the tracer is present. The increasing slope towards the end of the Patlak plot is likely to be due to rapid elimination of [11C]choline from the blood. Dynamic imaging for a longer duration would help clarify whether indeed irreversible retention is indeed saturable, in which case a plateau in the Patlak plot would be expected.

Figure 3.5 Patlak and Spectral models of choline uptake

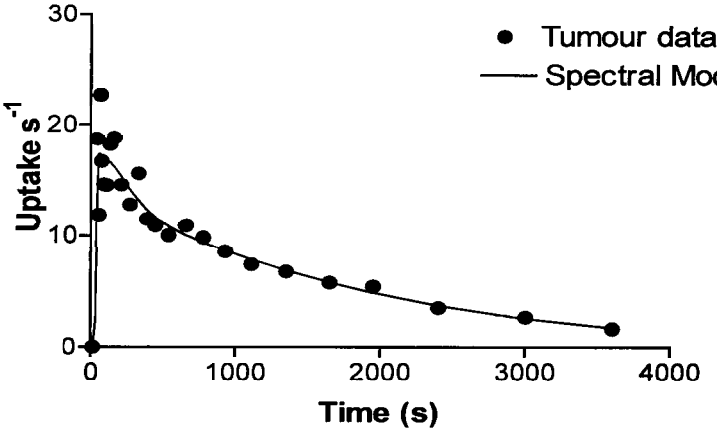
a) Comparison of Modified Patlak fits in tumour and normal breast tissue from patient 4



b) Spectral analysis of data from patient 4 showing range of kinetic components in a breast tumour lesion – values to the right of the graph represent irreversible components, and those to the left represent trapped components.



c) Kinetic behaviour of tumour data compared to spectral analysis model in the same patient



3.5.4 Repeatability of [11C]Choline PET

Thirteen patients were entered into this section of the study, of which 10 had repeatability scans. Of the remaining three patients, one patient did not return for a repeatability scan due to back pain, and there was a radiochemical production failure for the other 2 patients. Repeatability was assessed on a lesion-by-lesion basis for a total of 12 lesions. The mean (± SD) gap between repeatability scans was 3.75 ± 1.75 days, during which none of the patients received any treatment. Most (70%) of the patients had relapsed disease; the remainder were newly diagnosed.

[11C]Choline uptake was found to be reproducible for all the parameters under investigation the exception of FRT60 and the IRF value @ 1 minute. The Pearson correlation coefficient (r) for Ki (modified Patlak) was 0.89, $p<0.0001$, for parent plasma Patlak: $r=0.85$, $p=0.0003$, and SUV $r=0.945$, $p<0.0001$ – see results in full in table 3.8, below. The results are also depicted graphically in Figure 3.6, below.

Table 3.8 Repeatability of semi-quantitative and modelled parameters in tumour lesions

Parameter	COV	Pearson Correlation coefficient	r^2	Wilcoxon p value	SD of mean relative difference (%)	F-test
SUV 60	8.439	0.945	0.892	0.542	12.37	0.695
AUC60	9.396	0.928	0.861	0.685	14.78	0.570
Ki	14.664	0.894	0.798	0.787	21.21	0.787
Parpat Ki	14.430	0.845	0.714	0.946	26.06	0.849
FRT60	14.426	0.587	0.345	0.946	21.00	0.894
IRF60	13.380	0.894	0.799	0.542	19.52	0.964
IRF1	15.078	0.477	0.200	1.000	21.45	0.937

From table 3.8 above, it is evident that semiquantitative measures (SUV and AUC) appeared to be more robust than modelled data which are heavily dependent

upon the arterial plasma input function for their calculation. The spontaneous fluctuation range – i.e. mean variability value calculated by:

$$\frac{(\text{value for scan 2} - \text{value for scan 1}) \times 2}{(\text{value for scan 1} + \text{value for scan 2})}$$

is shown in below in Table 3.9.

Table 3.9: Spontaneous fluctuation range for each [11C]Choline pharmacokinetic parameter

Parameter	Mean variability ± 95% Confidence Interval
SUV 60	$-0.01129 \pm 2.038 \times 10^{-5}$ $m^2.ml^{-1}$
AUC60	$-1.16 \times 10^{-2} \pm 8.92$ $m^2.s.ml^{-1}$
Ki	$-3.80 \times 10^{-2} \pm 4.22 \times 10^{-4}$ ml plasma. ml^{-1} tissue. s^{-1}.
Parpat Ki	$-1.46 \times 10^{-2} \pm 4.98 \times 10^{-4}$ ml plasma. ml tissue. s^{-1}.
FRT60	0.030 ± 0.412
IRF60	$-0.025 \pm 4.380 \times 10^{-4}$ s^{-1}

Figure 3.6 Repeatability of choline PET parameters in tumour lesions

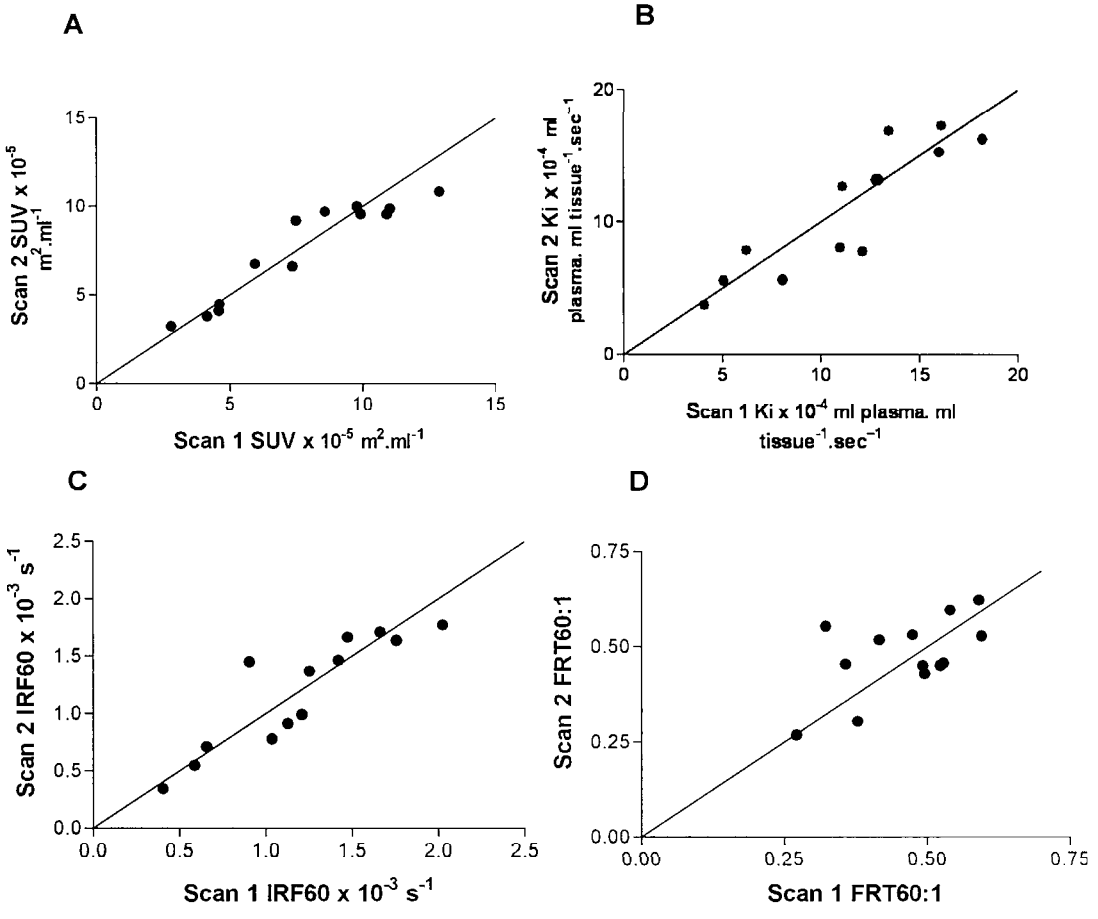


Figure 3.6 above shows the repeatability for 13 lesions identified in 10 patients for A) SUV, B) Modified Patlak Ki, C) IRF60, and D) FRT60:1, see table 3.8 for statistical analysis results.

3.5.5 Correlation of [11C]Choline–PET parameters with immunohistochemistry of breast tumour lesions

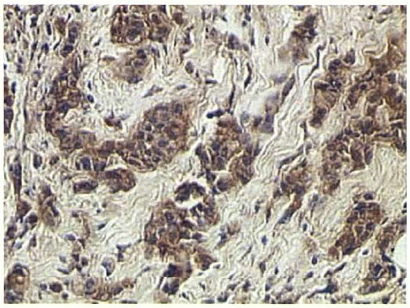
This was examined in 10 patients from both the repeatability and the response to trastuzumab studies. Six of the patients were newly diagnosed with breast cancer. With the exception of one biopsy which was taken 8 months prior to the scan all other biopsies were performed within 4 weeks of the baseline scan. The results of the immunohistochemistry are shown in Table 3.10, and Figure 3.7 (kindly provided by Dr Jiao).

Table 3.10. Immunohistochemistry analysis of tumour samples

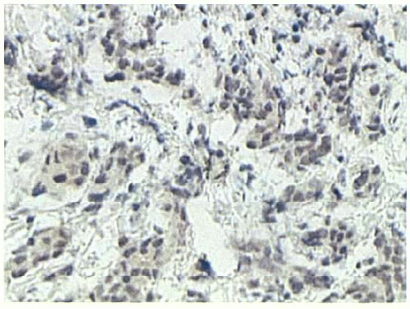
Patient	New (N) or Relapse (R)	Biopsy Site	ER	Her2	P-Her2	P-MAPK	T-MAPK	P-AKT	AKT1
1	N	Breast	+++	+	-	+++	++	++	++
2	N	Breast	+++	+++	-	++	+	+	++
3	R	Breast	-	-	-	++	++	+	+
4	N	Breast	-	++	+++	+++	+	++	++
5	N	Breast	-	+++	+++	+++	+	++	++
6	R	Axilla	++	+++	+++	++	+	++	++
7	R	Breast	+++	+	++	+++	+	+	+
8	N	Node	-	+++	-	+++	+	++	++
9	N	Breast	-	+++	-	++	+	+	++
10	N	Breast	+++	-	-	+++	+	++	+

Figure 3.7 Immunohistochemistry of tumour biopsies.

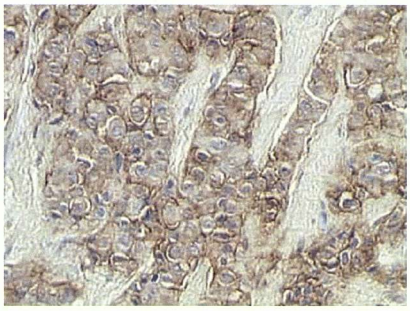
a) CerbB2 –grade III



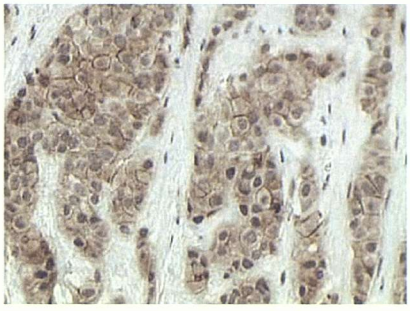
b) Phospho-CerbB2: negative



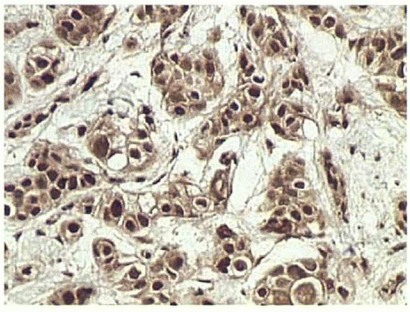
c) CerbB2 –grade III



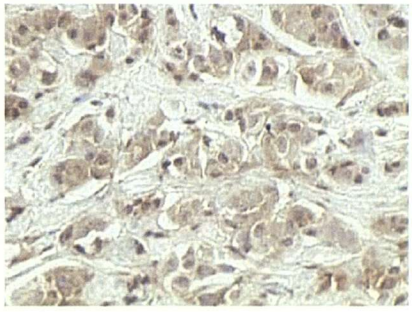
d) Phospho-CerbB2 grade III



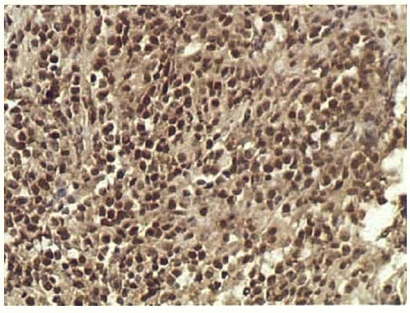
e) PMAPK-grade III



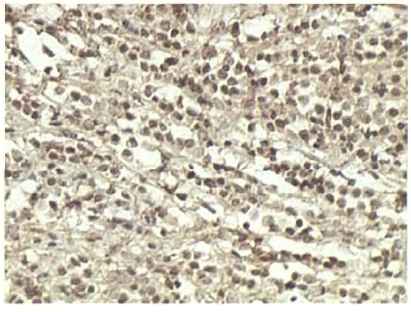
f) TMAPK-showing cytoplasmic staining only



g) PMAPK-grade +++ McCartys



h) TMAPK-showing nuclear and cytoplasmic staining



The results of the Pearson's correlation analysis are shown below in Table 3.11. No significant correlations were found for any of the parameters with the immunohistochemistry.

Table 3.11 Pearson's Correlation between pharmacokinetic parameters and tumour immunohistochemistry

	SUV60	*Modified Patlak Ki*	*FRT60:1*	*IRF@60min*
PhosphoMAPK	0.3526	-0.1708	0.2209	-0.3184
Total MAPK	0.2276	0.06205	-0.2400	0.01702
PhosphoAkt	0.1366	-0.2699	0.2043	-0.3082
Total Akt	-0.1213	0.3169	-0.4119	0.3911
PhosphoHer2	0.2491	0.07406	0.3725	0.02239
Ki-67 LI	0.2342	0.3771	-0.04731	0.04863

As a secondary measure, Spearman's correlation coefficient was also employed; however the results were also non-significant for all of the parameters. The results of the Mann Whitney test and Kruskal-Wallis test (used for phosphoher2) are shown below in table 3.12.

Table 3.12 Assessment of differences in McCarty score by [11C]Choline-PET parameters

	SUV60	*Modified Patlak Ki*	*FRT60:1*	*IRF@60min*
PhosphoMAPK	0.76	0.61	0.35	0.48
Total MAPK	0.71	0.89	0.71	0.89
PhosphoAkt	0.91	0.35	0.49	0.61
Total Akt	1.00	0.52	0.38	0.27
PhosphoHer2	0.23	0.85	0.33	0.81

(values represent p values obtained from the Mann-Whitney test for PhosphoMAPK, total MAPK, PhosphoAkt, and Total Akt; the Kruskal-Wallis test was used to calculate p values to separate the three categories of PhosphoHer2 staining).

The table above suggests that [11C]choline-PET was unable to distinguish between different McCarty's scores of the various immunostains used in the study; however it is worth noting the fact that the McCarty's score is not fully quantitative and encompasses a range of possible values of stain intensity. The difference between a high +2 score and a low +3 score may in fact be minimal, which is not translated into the statistical analysis comparing the two groups' correlation with [11C]choline-PET parameters. To date, quantitation of breast cancer MAPK activity has only been reported in vitro(Nurcombe et al. 2000).

The final study in this chapter investigates the effect of a known MAPK inhibitor, trastuzumab, on [11C]choline uptake and retention.

3.5.6 Measurement of response to trastuzumab with [11C]Choline

Eight patients entered this study, of which two could not be scanned post-trastuzumab due to radiochemical production failure in one and a change in treatment (addition of cytotoxic chemotherapy) in the other. Of the remaining six patients, eight lesions were imaged using [11C]choline-PET.

Full pharmacokinetic parameter analysis was possible in all but one of the six patients who refused to have arterial sampling. Scans were performed between 2 days and 4 weeks of the most recent trastuzumab injection. Only one patient had a complete response clinically, this occurred in a clinically palpable axillary node which became impalpable. The changes in pharmacokinetic parameters post-trastuzumab compared to baseline are shown below.

Due to the concerns about the validity of FRT as a suitable parameter for this study (namely poor repeatability data seen in the previous study, and the inability to distinguish between tumour and non-tumour tissue) IRF60 was employed as the spectral analysis parameter to measure response. The percentage decrease and increase in parameters and corresponding clinical response is shown below in Table 3.13.

Table 3.13 Comparison of Changes in Pharmacokinetic Parameters and Clinical Response

Patient[&]	*Lesion*	*SUV*	*AUC*	*Ki*	*IRF60*	*Clinical response**
14	Axilla	-47.58	-45.70	-47.57	-42.50	CR
17	Cervical Node	-26.72	-52.96	5.71	-11.66	PR
17	Axilla	-62.15	-126.77	-29.50	-58.29	PR
18	Breast	-17.30	-14.08	12.01	-6.47	PD
19	Breast	13.88	11.59	0.09	2.23	SD
20	Lung met1	-47.75	-29.48	n/a	n/a	PD
20	Lung met 2	-39.90	-65.20	n/a	n/a	PD
21	Lymph node	18.23	15.09	48.64	43.41	PD

*(where: [&] patients as described previously in Table 3.7. *Clinical response: CR = complete response, PR = partial response, SD = stable disease, and PD = progressive disease as defined in the RECIST criteria.)*

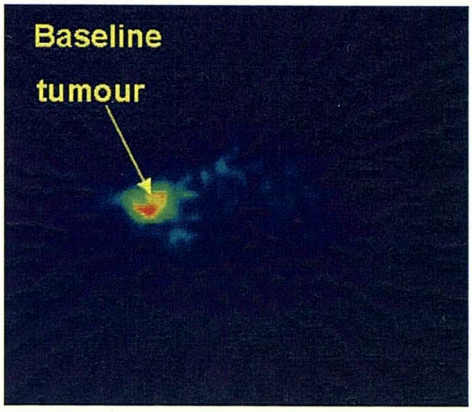
Typical changes in PET images in a patient with a partial clinical response (#17), and one with progressive disease (#21) are shown below in Figure 3.8. All the lesions which had a clinical response (complete or partial) had a decrease in SUV, AUC, and IRF60. However lesions which progressed were also associated with a decrease in one patient (#20) and an increase in another (#21). The small number of lesions in this study prohibits any definitive statistical analysis to assess if [11C]choline-PET parameters change post-trastuzumab is different between responders and non-responders.

The repeatability data was used to determine if the changes for individual lesions post-transtuzumab were statistically significant. The Bland-Altman plots for these results are shown in Figure 3.9. Many of the changes in the kinetic parameters were non-significant post-trastuzumab. In summary: for SUV there were 5 lesions

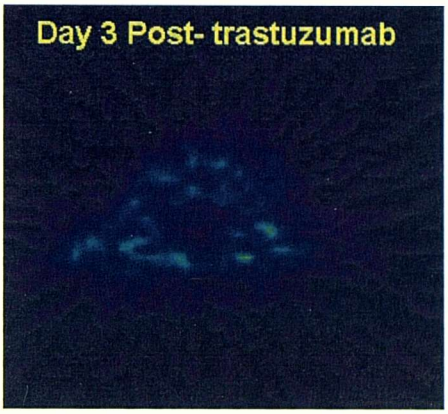
which showed a significant decrease; in comparison the clinical responses in these lesions were: 1 CR, 2 PRs, and 2 PD; for AUC there were 3 significant decreases in 2 lesions with PR and one with a PD. Most of the changes for the modelled parameters were nonsignificant except for one lesion which had a significant increase; this was associated with a clinical PD.

Figure 3.8 [11C]Choline-PET Images of response and non-response to trastuzumab

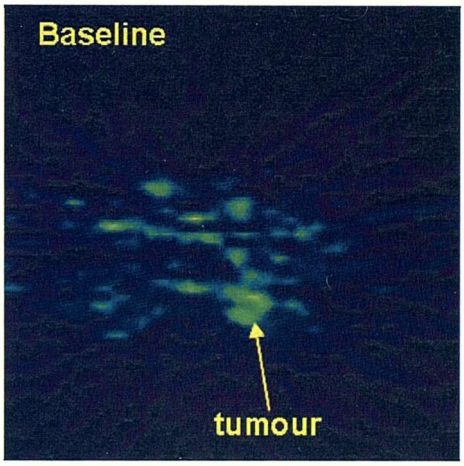
a) Patient 17 Cervical node



b) clinical response



c) Apical pleural node in patient 21



d) No significant change

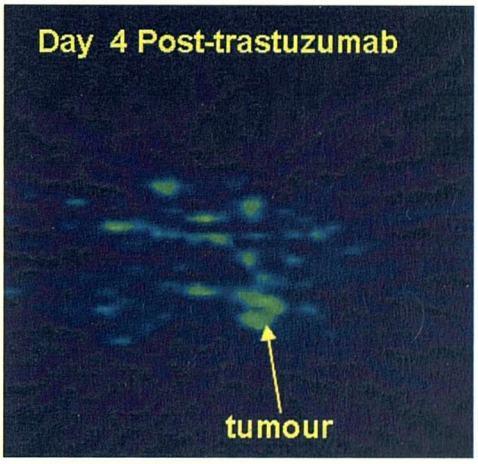


Figure 3.9 Significance Plots for [11C]Choline-PET Pharmacokinetic Response

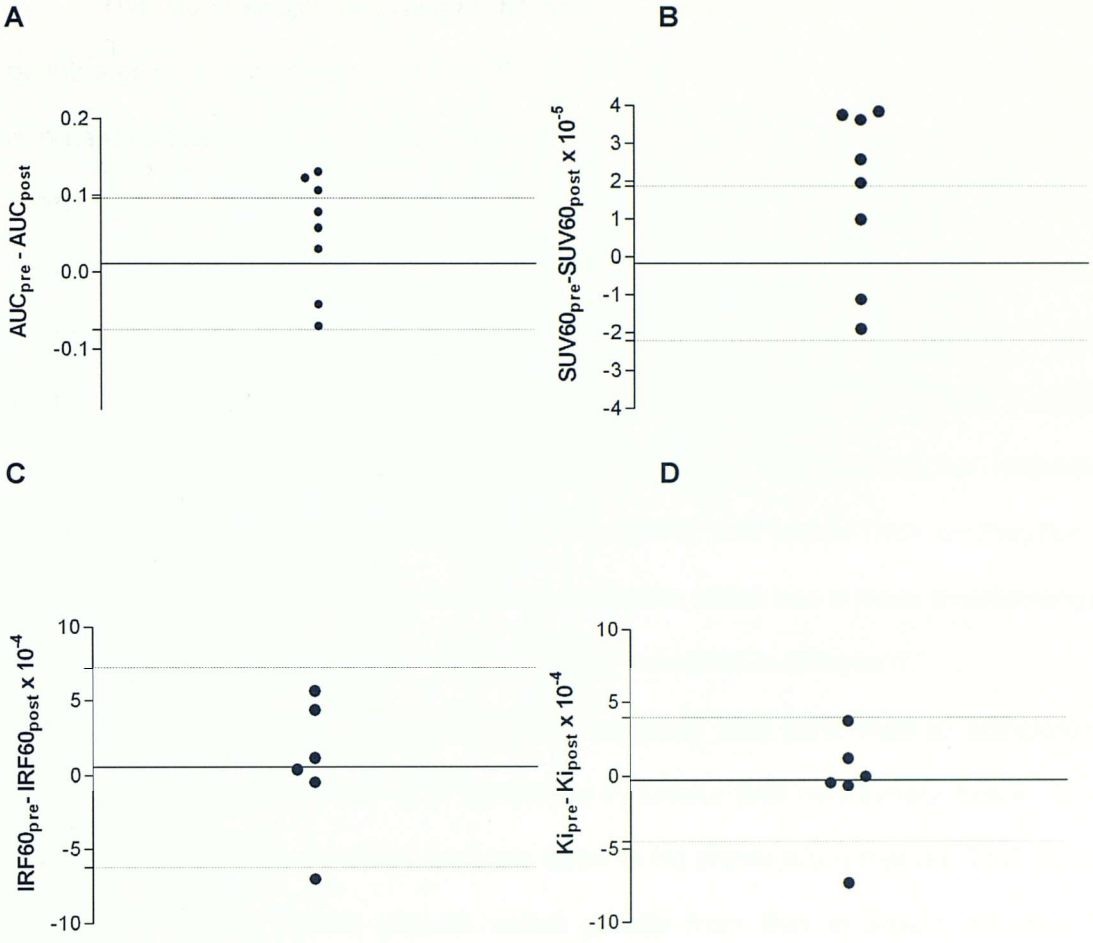


Figure 3.9 above shows the differences in parameters pre and post trastuzumab treatment, values inferior to the lower dotted line represent a significant increase, those above the upper dotted line represent a significant decrease, and those within in the dotted lines represent no significant change where A) is AUC at 60 mins (in m^2.sec/ml), B) is SUV x10^{-5} m^2/ml, C) is IRF value at 60 mins/s, and D) is modified Patlak Ki ml plasma/ ml tissue/s). Ki and IRF was not possible in one patient with two lesions as this patient refused arterial blood sampling.

3.6 Discussion

This study sought to evaluate the potential of [11C]choline as a potential PET radiotracer in breast cancer. No prior reports of the clinical utility of [11C]choline-PET in breast cancer have been published previously. This study has provided a detailed analysis of the differences in pharmacokinetics of uptake in [11C]choline in tumour compared to normal tissue, measured the metabolism of [11C]choline, assessed the repeatability for each parameter, assessed correlations with ex-vivo immunohistochemistry analyses; and finally examined the effects of the c-erbB2 inhibitor, trastuzumab. Compared to the focus of the previous chapter, (namely [18F]FLT which is a proposed marker of TK1 activity and hence DNA proliferation), [11C]choline is a proposed marker of phosphocholine which has a more diverse range of biological functions within the cell which were described in Chapter 1.

Dynamic imaging with arterial blood sampling was performed to completely assess the pharmacokinetics of [11C]choline in tumour and non-tumour tissue. The arterial sampling was necessary as it has been found previously i) that the TAC curve for [11C]choline in venous plasma varies greatly from that in arterial plasma in humans, and ii) the input function derived from arterial blood does not adequately represent the true input function into tissue due to peripheral metabolism of choline (Roivainen et al. 2000). The finding of higher [11C]choline in tumour tissue compared to normal, suggests that the malignant phenotype is associated with similar altered membrane choline phospholipid metabolism in human breast cancer to that seen in vitro studies(Aboagye et al. 1999). The uptake of [11C]choline was found to be significantly higher in human breast cancer compared to corresponding normal tissue for all of the parameters except FRT60. Possible explanations for this include the dependence of FRT60 on the IRF value @ 1 minute, which is subject to variations in the timing of frame acquisition, delivery and extraction from plasma of the radiotracer from plasma. We had sought to improve the frame acquisition, and shorter frames

(10s) were performed for the majority of patients, but this has had little impact on the results. As an alternative the IRF value at 60 minutes was used, which, at this late timepoint, represents a surrogate for radiotracer retention and hence [11C]choline phosphorylation. It was not surprising therefore that the repeatability of FRT60 was disappointing. As described above, the dependence on the IRF value at 1 minute seems to be the major contributing factor, and this was confirmed by the even poorer repeatability data for this parameter. Shorter time frames were used at the start of dynamic imaging to try and prevent this being due to frame acquisition; therefore the method to correct this problem remains unclear. The other contributing factors could be variation in blood flow between scans which would affect delivery of [11C]choline. The fact that FRT60 was not reproducible suggests that this parameter should not be used in future comparisons.

The repeatability for the other parameters, SUV, AUC, Ki, and IRF60 was much superior inferring that they should be used for quantitation of [11C]choline uptake and retention. Whether the modelled pharmacokinetic parameters (Ki, IRF60) are advantageous to semiquantitative techniques for [11C]choline remains to be validated; both can be used to differentiate tumour from normal tissue with a Wilcoxon p of <0.0001 but in a radiotracer which exhibits rapid metabolism such as this, it would seem preferable to use a method that is relies upon metabolite-corrected data.

To determine if [11C]choline-PET was a marker of MAPK activity, immunohistochemical indices were correlated with the pharmacokinetic parameters. This section of the study was ambitious, however unfortunately it was hindered by the low number of tumour biopsies and the time taken between the biopsy and the PET scan. No significant correlations were found for any of the PET parameters with the immunohistochemical stains. Overall, one third of patients in the study had metastatic disease, effectively precluding a biopsy as the lesions were in inaccessible areas, of the remainder many patients were not rebiopsied due to progression through initial treatment. The optimal time interval between a biopsy and [11C]choline-PET is

unknown as MAPK activity may change over time, and if the biopsy is done too close to the time of the PET scan changes due to the biopsy procedure itself could occur within the ROI. Increased [11C]choline uptake has been reported in animal models of muscle inflammation where it was unable to be differentiated from a C6 rat tumour glioma model; suggesting even worse tumour selectivity than [18F]FDG(van Waarde et al. 2006). Indeed, [11C]choline-PET has been proposed as a useful marker of inflamed synovium in patients with arthritis (Roivainen et al. 2003). Increased uptake of radiolabelled choline is a marker of CK activity in breast cancer cells(Al-Saeedi et al. 2007), and this can be down regulated by ERK inhibition(Liu et al. 2002); however further study of the dynamic relationship between CK and phosphoMAPK *in vivo* is required.

The final study sought to determine changes post-treatment with trastuzumab. Whilst changes in [11C]choline-PET were viewed post-treatment in responders, the repeatability data showed that the vast majority of these were non-significant, as decreases also occurred in a patient with PD. Perhaps detection of non-response by the quantitative parameters, modified Patlak Ki and IRF60, warrants further investigation as both of these parameters were able to detect a significant increase in a patient with PD. Clearly more patients are needed to ascertain whether [11C]choline is a useful marker of MAPK inhibition.

In summary, [11C]choline is useful for differentiating breast tumour from normal tissue, and is reproducible for the majority of pharmacokinetic parameters, but requires careful consideration of factors such as inflammation for selection of ROIs, correction for metabolites in arterial plasma, and needs a larger sample size to conclusively determine its future role as an in vivo biomarker for activation and treatment-induced inhibition of MAPK.

CHAPTER 4: Study of [18F]-AH111585-PET Pharmacokinetics, Efficacy, and Sensitivity in Patients with Metastatic Breast Cancer.

4.1 Hypothesis

[18F]-AH111585-PET can detect human metastatic breast cancer lesions *in vivo*.

4.2 Aims

i) To quantify the uptake and retention of [18F]-AH111585 in breast tumour lesions using SUV and mathematical modelling techniques

ii) To compare the uptake in tumour lesions with that of the corresponding normal tissue

iii) To compare the PET data with images obtained using computed tomography (CT)

iv) To determine if using the heart as an ROI would provide the same results as an arterial input function obtained from radial artery sampling during the scan.

4.3 Introduction

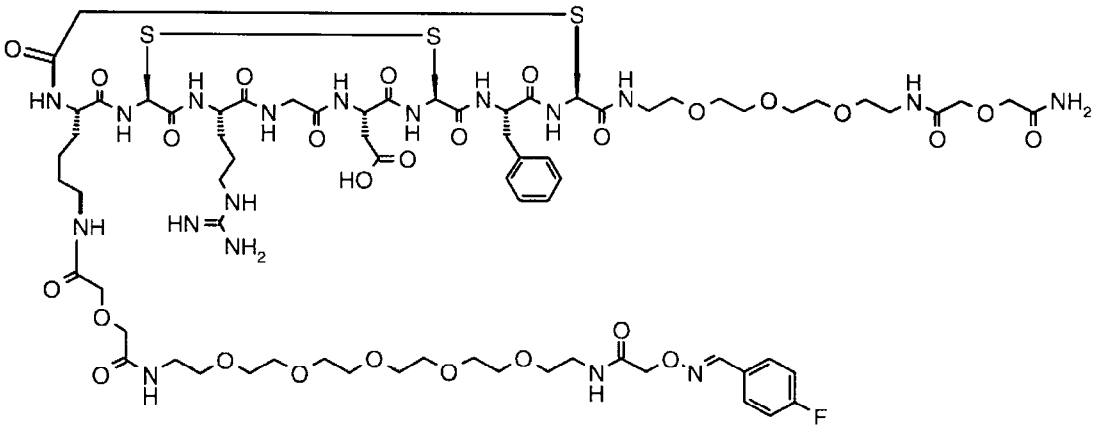
As angiogenesis is essential for the development of metastases and sustained tumour growth, a radiotracer which has been designed to bind to angiogenesis-associated integrins upregulated in tumours should have increased signal in tumour lesions compared to normal tissue. As Gasparini et al have shown an association between expression of the αvβ3 integrin and relapse-free survival in both node-positive and node-negative breast cancer, metastatic breast cancer was chosen as a model system in this study. A successful novel radiotracer for use in oncology should have applications for detecting common tumour types such as breast cancer.

As this was a first-in-man study, a healthy volunteer study was performed prior to the patient study to assess the safety, biodistribution, and radiodosimetry of [18F]-AH111585.

4.4 Methods

The structure of the [18F]-AH111585 radiotracer used in the study has been described by Indrevoll et al(Indrevoll et al. 2006), and is shown in Figure 4.1 below. [18F]-AH111585 was synthesised by Hammersmith Imanet Ltd ® on an automated module (TRACERlab FX_{F-N}; GE Healthcare) by coupling of an aminoxyfunctionalized precursor of [18F]-AH111585 with 4-[18F}-fluorobnezaldehyde at pH 3.5 to form the oxime [18F]-AH111585; a full description of the radiosynthesis has been published elsewhere by Glaser et al (Glaser et al. 2008) .

Figure 4.1. Structure of AH111585 as described by Indervoll et al.



Prior to patient studies, a series of 3 in vitro competition binding assays with [125I]Echisatin (a disintegrin derived from snake venom which binds to RGD dependent integrins) on membrane fractions EA/Hy 926 (a hybrid of human umbilical vein endothelial cells and A549 human lung cancer epithelial cells) was performed by GE Healtcare Ltd ®. The results showed that the affinity of this peptide for the αvβ3/ αvβ5 integrins was 8.2 (± 2.4) nM (Indrevoll et al. 2006).

4.4.1 Ethical Approval

The Hammersmith Hospitals NHS Trust Research Ethics Committee (London, UK) granted ethical approval for the study. The administration of the radioactivity was approved by the Administration of Radioactive Substance Advisory Committee United Kingdom. The Medical Health Regulations Authority sanctioned the use of [18F]-AH111585.

4.4.2 Procedure for radioactivity counting in blood and urine

Discrete blood samples (5ml) were taken at 5, 10, 15, 30, 60, 90 and 150 min post-injection of [18F]-AH111585. The radioactivity in an aliquot blood and plasma (1ml) was measured using a sodium iodide well counter. The remainder of blood (7ml) was centrifuged at 14,000 rpm to obtain plasma. The radioactivity profile in plasma was determined using an on-line system with a solid phase sample enrichment column linked to a reverse-phase HPLC radioactivity and absorbance detectors connected to a PC based integrator. The plasma samples were de-proteinised by solid phase sample enrichment column washed with 0.01M di-ammonium hydrogen phosphate (13.5ml) and further analysed using a reverse-phase HPLC. The column (Gemini, 250 x 10mm id) was washed with the mobile phase: a mixture of potassium di-hydrogen phosphate, pH4.0 (10mM) and methanol (45:55, v/v) at a flow rate of 3 ml per min.

The eluate was monitored for radioactivity. Both detectors were linked to a PC based integrator which recorded the radioactivity profile and enabled the correction for [18F]-radioactivity decay and background and integration of radioactive components. The amount of [18F]-AH111585 and other radioactive components at each sample time was calculated as a percentage of each radioactive component in each analyte. The radioactivity in 1 ml aliquots of blood and plasma were counted on a sodium iodide well counter and used to calculate the plasma/blood ratio.

4.4.3 Biodistribution and Radiation Dosimetry in Healthy Volunteers

The biodistribution and radiation dosimetry was determined by physicists from GE Healthcare®. Briefly, absolute values of [18F]activity in 10 organs were determined directly from qualitative analysis of the PET images together with the in vitro measurements of [18F]activity in whole blood, plasma, and urine following MIRD schema of a 70kg hermaphrodite using Organ Level Internal Dose Assessment (OLINDA®) software(Stabin et al. 2005) .

4.4.4 Breast Cancer Patient study

The study of patients with advanced breast cancer started enrolment after the study of the 8 healthy volunteers had been completed. The patients for the study were recruited from the oncology clinics in Charing Cross Hospital (part of Hammersmith Hospitals NHS Trust) under the supervision of Professor Coombes. All patients were given a study information leaflet and had at least 24 hours prior to deciding about participating in the study.

Patients eligible for the study were aged > 25 years with a diagnosis of metastatic breast cancer – histological confirmation of the primary tumour was required in all patients. The other inclusion criteria were as follows: post-menopausal/surgically sterile/ or had a negative pregnancy test (i.e. urinary human chorionic gonadotrophin, HCG, test) on the day of scanning, and be able to consent/comply with the study protocol. One metastasis had to measure at least 1 cm in diameter, and not have been irradiated previously – new lesion in a previously irradiated field were allowed. The patient had to have clinically satisfactory haematological and biochemical serum test results and Eastern Co-operative Oncology Group Performance Status of 0-2 (see Appendix 1) (Oken et al. 1982).

The exclusion criteria were: lactation, previous inclusion in the study, receipt of another investigational medicinal product within 30 days prior to the study, administration of chemotherapy within 3 weeks of the study, and occupational monitoring of ionising radiation exposure. All patients had a CT scan and other relevant imaging (e.g. a bone scan) of the metastatic site of interest within 4 weeks of the [18F]-AH111585-PET scan. The CT scans were reported by an independent consultant radiologist. Study recruitment was difficult for patients as there was no incentive to participate, and because most patients with advanced metastatic breast cancer were receiving chemotherapy.

4.4.5 Scan procedure- Patients

Prior to scanning a size 24G cannula was inserted into the radial artery under 2% lignocaine local anaesthetic. A size 22G cannula was inserted into an antecubittal vein in the contralateral arm to allow radiotracer administration.

All patients were imaged on the same Siemens/CTI ECT962/HR+ tomograph in Hammersmith Imanet® that had a 15.5 cm axial field of view (transaxial, 58cm). The field of view was centred on the tumour lesion of interest. A short transmission scan lasting 2 minutes was performed using rotating [68Ge] sources to check the position of the field of view. This was followed by a longer transmission scan lasting 20 minutes which was used for attenuation correction.

Following release of the radiolabelled isotope by the quality control department in Hammersmith Imanet, the dose vial was inspected in the PET scanning room to confirm the contents, pH, presence of impurities, and activity of the injectate. [18F]-AH111585 was injected as an intravenous bolus over 30 seconds in a volume of between 6-10mls followed by a 6ml normal saline flush. The amount of radioactivity in arterial blood was measured for 10 min using a continuous on-line radioactivity detector. Discrete samples

were taken for i) cross calibration of the blood radioactivity detection system with the PET camera ii) assay of the partition of the label between red cells and plasma, iii) assay of the parent compound and labelled metabolites in plasma, and iv) assay of the free fraction of the [18F]-AH111585 in plasma. The timing of the discrete samples is shown in table 4.1 below.

Table 4.1 Discrete Blood Sampling Protocol for the Patient Study

Syringe	Volume	Time	Pots		Haematocrit
			Blood	Plasma	
Baseline*	4ml	Baseline			haematocrit
1	10ml	2:30	1	2	metabolites
2	10ml	5:00	3	4	metabolites
3	10ml	10:00	5	6	metabolites
4	4ml	15:00	7	8	
5	10ml	30:00	9	10	metabolites
6	4ml	45:00	11	12	
7	10ml	60:00	13	14	metabolites
8	10ml	1:30:00	15	16	metabolites
9	10ml	2:30:00	17	18	metabolites

The HPLC eluates were collected, the total volume was recorded and the radioactivity aliquots (2 x 5 ml) were counted. Data were all decay corrected to start of injection. Peak areas for [18F]-AH111585 were analyzed and expressed as a ratio of total radioactivity in the original plasma samples. A model-based algorithm was used to correct for loss of parent [18F]-AH111585 on the solid support. For this, metabolite data were fitted to a straight line to derive a slope and intercept. These parameters were then used to scale the data such that the Y-intercept was 1. The analysis was done in MatLab version 6.

4.4.6 PET Imaging of Patients

Images were acquired in 3D over 61.5 minutes and reconstructed using both iterative and filtered back projection, according to the following time frames.

Table 4.2 Frame acquisition for the Patient Study

No.	Duration (s)	Type	Accumulated	
			Frames	Time (min: sec)
1	30	Background	1	00:30
6	10	Frames	7	01:30
4	15	Frames	11	02:30
4	30	Frames	15	04:30
6	120	Frames	21	16:30
5	180	Frames	26	31:30
3	600	Frames	29	61:30

Physical examination, and monitoring of the patients' heart rate, blood pressure, temperature, oxygen saturation, injection site, ECG, and other safety analyses were performed prior to, during, and after the study as shown in table 4.3. Patients were well hydrated during and after the scan to promote adequate renal excretion of the isotope.

Table 4.3. Study Schedule of Events for Subjects with Late Stage Breast Cancer

	Baseline	-5 min	Dose	+5 min	+10 min	+15 min	+30 min	+45 min	+1 h	+1 h 30 min	+2 h 30 min	+4 h	+24 h
Informed Consent	•												
Study Entry Criteria	•												
Demographic Information	•												
Medical History	•												
Prior/Concomitant Medication	•												
Physical Examination	•									•	•		•
Injection Site Monitoring		•					•			•	•		•
Pregnancy Test (Pre-Menopausal Females)	•												
ECG [1]	•	•		•	•	•	•	•		•	•		•
Pulse Oximetry	•	•		•	•	•	•	•		•	•		•
Vital Signs [2]	•	•		•	•	•	•	•		•	•		•
Blood Samples (Serum Biochemistry, Haematology)[3]	•						•			•	•		•
Blood Sample for Coagulation[3]	•									•	•		•
Urinalysis [4]	•									•	•		•
Pre-treatment Events	•												
Transmission Scan	•												
AH111585 (^{18}F) Injection			•										
Post-treatment Events (Adverse Events)[4]													
Dynamic imaging													
Blood and Plasma for Activity Counting				•	•	•	•		•	•	•		
Urine for Activity Counting[3]													

[1] Continuous ECG performed from –5 min to +15 min. Lead II was used for continuous monitoring.

[2] At baseline, before vital signs and pulse oximetry were measured, the subjects were resting for at least 5 minutes.

[3] Blood samples of subjects with late stage breast cancer were taken from arterial blood.

[4] Time points indicated were preferred time points, urine was collected as voided.

Shaded areas depict where continuous monitoring was performed

4.4.7 Patient Characteristics

7 female patients with metastatic breast cancer aged between 37 and 68 years (mean=51.9) were enrolled in the study. The initial plan had been to study 8 patients in total, however it was decided to conclude the trial after 7 patients had been enrolled as no additional benefit was perceived from studying 1 more patient, and the study objectives had been completed.

Patient characteristics are shown in table 4.3. All patients except 1 (who had received endocrine treatment only) had received chemotherapy previously for breast cancer. On reviewing the histology of the original breast tumours, all except 1 were oestrogen receptor (ER) positive, and all were c-erbB2 negative.

Table 4.4 Patient Characteristics

Patient no	Time from original diagnosis (years)	Primary tumour removed	No. of previous chemo$ regimes	Previous endocrine treatment	Histology *
1	7	Y	5	Y	Grade 2 IDC, ER 210/300, PR 60/300, c-erbB2 –ve.
2	1	N	0	Y	Grade 2 IDC, ER 300/300,PR 120/300, c-erbB2 –ve.
3	2	Y	2	Y	Grade 2 IDC, ER 300/300 PR 300/300 c-erbB2 -ve
4	8	Y	1	Y	Grade 2 IDC, ER 300/300,PR 210/300, c-erbB2 -ve
5	2	Y	4	N	Grade 3 IDC, ER –ve, PR –ve, c-erbB2 -ve
6	9	Y	2	Y	Grade 2 IDC, ER 210/300, PR -ve, c-erbB2-ve
7	8	Y	1	Y	Grade 2 IDC, ER 220/300, PR 60/300, c-erbB2-ve

(where $= chemotherapeutic, * IDC = invasive ductal carcinoma).

4.4.8 Activity injected for the Patient Study

The maximum permitted dose to be administered for the patient study was 370MBq (compared to 165MBq for healthy volunteers). After discussion with the physics team in Hammersmith Imanet®, it was decided that the target activity for the upper limit should be lowered for patients to 200MBq if the heart was in the field of view. This was to prevent count saturation of the scanner as the acquisition was in 3D. The activity administered to the individual patients are shown below in Table 4.10.

Table 4.5 Activity of [18F]-AH111585 Administered to Patients with Advanced Breast Cancer

Patient	*Dose of [18F]-AH111585 Injected (MBq)*	*Specific Activity(MBq/μmol)*	*Radiochemical purity*
1	198.85	101141	100%
2	214.12	134208	100%
3	244.32	128534	95%
4	277.85	150936	100%
5	202.70	129697	100%
6	210.12	135117	100%
7	292.02	170585	100%

4.4.9 Region of Interest Analysis

Regions of interest were manually drawn on entire tumour lesions and corresponding normal tissues using the computed tomography scans for guidance where appropriate, on the iterative images, to create object maps. In tumour regions where there was obvious central necrosis then the periphery was sampled as a ring-shaped region, and the central core was sampled as a sphere. Sampling of the cardiac contents was performed as a separate study and is described at the end of this chapter. The maps were then applied to the complete dynamic filtered back projection PET data set to obtain time

activity curves for each region using the Analyze® image analysis software (Biomedical Imaging Resource, Mayo Foundation Rochester, MN, USA).

The utility of the cardiac ROI as an arterial input function was assessed in three patients where the heart was in the field of view (patient 2 – breast lesion, patient 5 lung metastases, and patient 6 pleural and lymph node metastases) a combined image of frames 3 to 6 was formed. A region of interest (assumed to be the left ventricle) was placed on 4 consecutive slices, to form an object map. This was then applied to the dynamic data set to obtain a radioactivity versus time curve.

To avoid arterial blood sampling in future studies, the total blood input function obtained from radial artery sampling with that of the heart was compared. The total blood input function was used as the data obtained from the PET scan reflected activity in whole blood, as opposed to plasma alone. The tumour regions which were identified and used for analysis and corresponding CT slice numbers are shown below in Table 4.6.

Table 4.6. Regions of Interest for the Patient Study

Patient	Region name on PET scan	PET Slice no.	Total no. of slices object drawn in	Corresponding CT slice no.
1	Muscle	31-34	4	2/29
1	Vessel	31-34	4	2/29
1	*Tumour (SCF node)*	*31-34*	*4*	*2/29*
2	Normal liver	3-7	5	2/25
2	Normal spleen	3-7	5	2/25
2	Heart	26-30	5	2/18
2	Normal breast	31-41	11	n/a
2	Normal bone (vertebra)	16-19	4	See bone scan
2	*Breast tumour*	*31-41*	*11*	*n/a*
2	*Bone metastasis*	*34-37*	*4*	*See bone scan*
3	Normal liver (liver)	50-53	4	3/10
3	Normal spleen (spleen)	50-53	4	3/10
3	Right kidney cortex	19-22	4	3/18 to 3/19

Table 4.6. Regions of Interest for the Patient Study (contd)

Patient	Region name on PET scan	PET Slice no.	Total no. of slices object drawn in	Corresponding CT slice no.
3	*Liver metastasis Right anterior (Rant)*	*36-40*	*5*	*3/14*
3	*Liver metastasis Right middle (Rmid)*	*55-58*	*4*	*3/11*
3	*Liver metastasis Left middle (lmid)*	*46-49*	*4*	*3/10*
3	*Liver metastasis Right lateral (Rlat)*	*45-57*	*13*	*3/10 to 3/12*
3	*Liver metastasis Right superior post (Rsuppost)*	*50-56*	*7*	*3/10-3/11*
3	*Liver metastasis Left superior (lsup)*	*54-59*	*6*	*3/7-3/9*
4	Normal liver (liver)	23-27	5	5/10
4	Normal spleen (spleen)	23-27	5	5/10
4	*Liver metastasis*	*23-27*	*5*	*5/10*
5	Normal lung	37-39	3	2/11
5	*Lung metastasis 1(tumour1)*	*20-24*	*5*	*2/16*
5	*Lung metastasis 2 (tumour2)*	*37-39*	*3*	*2/11*
5	*Lung metastasis 3 (tumour3)*	*37-39*	*3*	*2/11*
5	*Lung metastasis 4 (tumour4)*	*18-21*	*4*	*2/21*
6	Normal lung	38-42	5	3/10
6	*Right ant tumour (Rant)*	*25-32*	*8*	*3/11-3/15*
6	*Inferior anterior tumour*	*12-19*	*8*	*3/18-3/19*
6	*Mediastinal lymph node Periphery = plymphnode Central necrotic region= centre lymph node*	*10-14*	*5*	*3/16-3/18*
7	Liver	36-38	3	3/5
7	*Liver met*	*36-38*	*3*	*3/5*

4.5 Results

4.5.1 Healthy volunteer radiation dosimetry and biodistribution

5 males and 3 females aged between 53 and 63 years (mean=59.9) were enrolled. The mean administered dose of radioactivity was 163.7±6.2 MBq. The study was well tolerated. There were no serious adverse events.

The [18F]-radioactivity profile in plasma showed [18F]-AH111585 and other more polar radioactive components than [18F]-AH111585. [18F]-AH111585 decreased slowly from 95% at 5 min to 47% of the radioactivity at 150 min. The polar radioactive components were observed to increase with time.

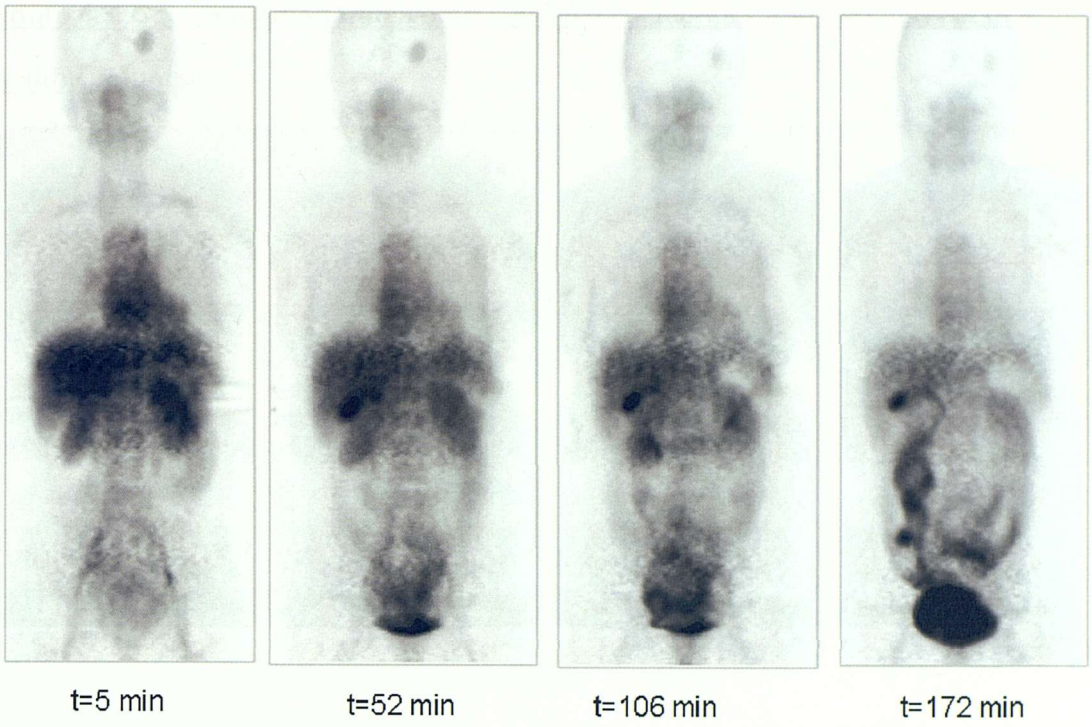
Images of the biodistribution study in a healthy volunteer are shown in Figure 4.2. There was no significant difference between male and female subjects for biodistribution of [18F]-AH111585. 57±15% of administered [18F] activity was excreted, 37±14% via the urinary pathway, and 20±5% via the gastrointestinal tract. The highest mean initial activity was seen in the liver (15±1%), walls of the upper and lower intestines (11±7%), kidneys (9±2%), lungs (7±1%), and contents of the cardiac chambers (5±1%).

The organs with highest normalised cumulative activities were (in order from highest to lowest): urinary bladder contents and bladder wall > liver > walls of the small and large intestines > contents of the small intestines > the kidneys. The mean effective dose was calculated as 26±4 μSv/MBq (Miller and McParland, unpublished data).

There was an unexpected finding in the first healthy volunteer, an area of increased uptake within the left fronto-temporal region of the brain. This area had been included in the scan due to the patient's short stature. There was no history to suggest an intracranial lesion; neurological and physical examination had been normal. An urgent MRI

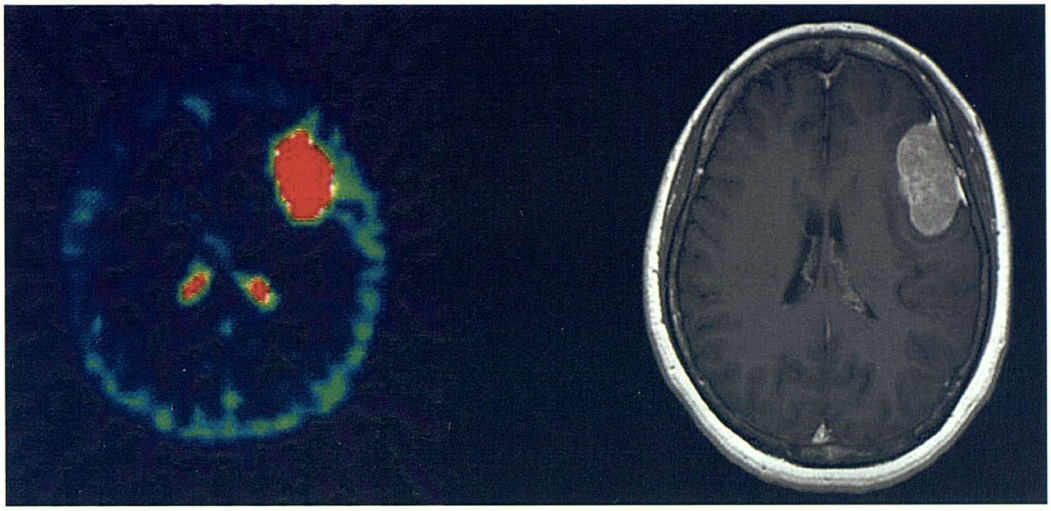
scan was requested which revealed a 4cm contrast-enhancing lesion in keeping with the [18F]-AH111585 PET scan, suggestive of a meningioma (see Figure 4.3). The volunteer was referred for a neurosurgical opinion, and the lesion was completely resected. Histology confirmed that the lesion was a meningioma, and the patient has now made a full recovery without any residual neurological deficit.

Figure 4.2. [18F]-AH111585 PET Images over time in a Healthy Volunteer



Coronal PET images of a healthy volunteer above, where t= time post injection of [18F]-AH111585, showing high initial uptake in the liver, kidneys, heart, and intestines, followed by progressive increases in activity in the gall bladder, urinary bladder contents and bladder wall. An abnormal focus of high uptake is seen in the left temporal region.

Figure 4.3. Corresponding transverse [18F]-AH111585-PET and MRI images of a healthy volunteer.



Transverse [18F]-AH111585-PET image (left) and contrast-enhanced MRI image (right) of the healthy volunteer shown previously in Figure 4.2, clearly reveal a mass lesion in the left temporal region, this was an unexpected incidental finding which was confirmed as a meningioma after surgical resection.This is likely to have been non-specific due to blood-brain barrier breakdown. Note also the high uptake centrally due to the vascular nature of the choroid plexus.

4.5.1 Advanced Breast Cancer Study Patients and Regions of Interest

The study was well tolerated in all patients. No serious adverse event occurred. All of the enrolled patients were able to complete the study. 232.5± 37.6MBq (range= 198.8 to 292.3) of [18F]-AH111585 was injected. 18 out of 19 possible lesions were imaged with both [18F]-AH111585-PET and CT. The remaining lesion was a clinically enlarged supraclavicular lymph node which had indefinite uptake on the PET scan and was not identified using CT (patient no.1). Due to concern about the validity of this region on the PET image, SUV analysis was performed only, and the lesion was not included in the overall summary statistics. Except for this lesion, there was good correlation between the CT and PET images, all lesions that were visible on CT (within the same field of view as the PET scanner) were visible on the PET scans and vice-versa (see Figure 4.4).

There was also good correlation between a [99m]Technetium-labelled bone scan and the [18F]-AH111585-PET scan of patient 2 who had bone metastases. In addition to detecting metastatic bone lesions, tumour uptake was visible in the primary grade II ductal carcinoma which had not been removed in the same patient (see Figure 4.5). [18F]-AH111585 clearly identified metastatic breast lesions in regions where the normal tissue background activity was low (lung, breast) as areas of increased activity; however metastases in areas with high background activity such as the liver were seen as regions of hypointensity. The areas of hypointensity in the liver on the [18F]-AH111585-PET scan did correspond with the CT images of the same region (see example in Figure 4.4) in all patients imaged with liver metastases.

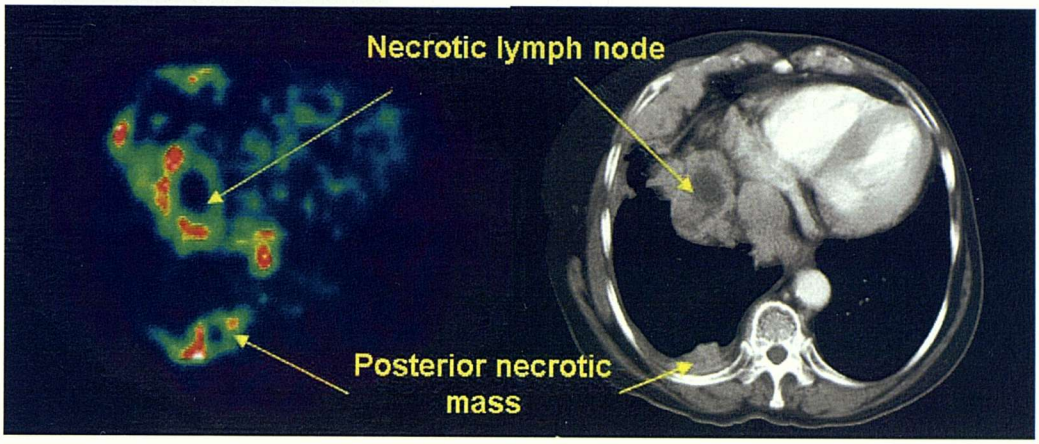
There was significant heterogeneity in uptake within single lesions, particularly those with necrotic centres, where the peripheral ring-enhancement is in keeping with active angiogenesis – see Figure 4.4. In patient no.6 there was obvious decreased uptake in the centre of a posterior pleural metastasis (see Figure 4.4a) which was not obviously identifiable as necrosis on the corresponding CT scan. There was also significant variation in uptake between different tumour lesions within the same patient, and between patients (see Table 4.7).

The time for [18F]-AH111585 to reach peak activity was dependent on the site of the metastatic lesion. Shorter times (less than 10 minutes) were seen in regions which are well perfused such as the lungs (Figure 4.7) and liver (Figure 4.9) and longer times (approximately 30 minutes) were seen in a primary breast tumour and bone metastasis. No patients in the study had central nervous system metastases, however the fact that there was uptake in a meningioma in a healthy volunteer suggests that [18F]-AH111585 also has potential for imaging this site.

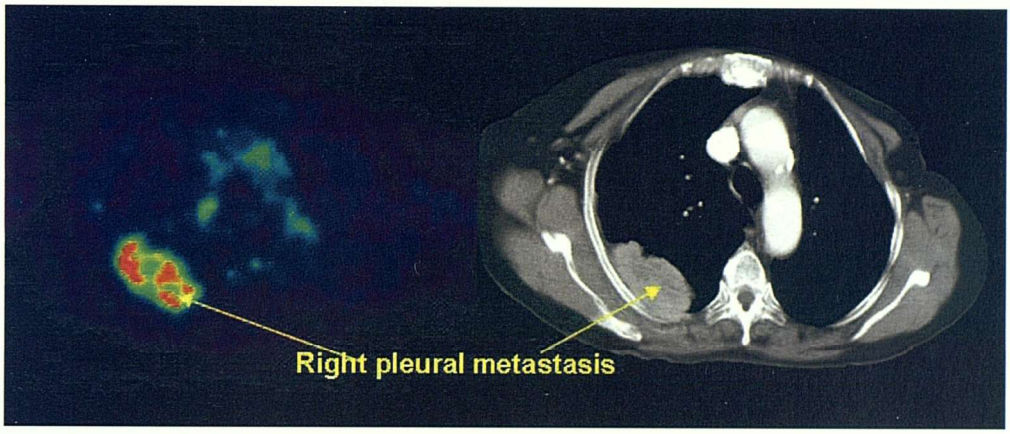
The Patlak and spectral analysis results indicate that there is a degree of irreversible binding of [18F]-AH111585 within lesions, dissociation of the radiolabelled ligand within the region was not seen within the time duration of the study (61.5mins). The slow metabolism of the agent compares favorably to that seen with other [18F]labelled PET probes (Kenny et al. 2005). Of the 15 patients and healthy volunteers, only one had developed an antibody to [18F]-AH111585. Further evaluation of this immunological response is currently being performed.

Figure 4.4 Transverse [18F]-AH111585 PET Images and CT Images in Patients

4.4a) Patient no.6: Increased peripheral enhancement in necrotic metastases



4.4b) Heterogeneity of [18F]-AH111585 uptake within a pleural metastasis



4.4c) Liver metastases seen as regions of hypointensity

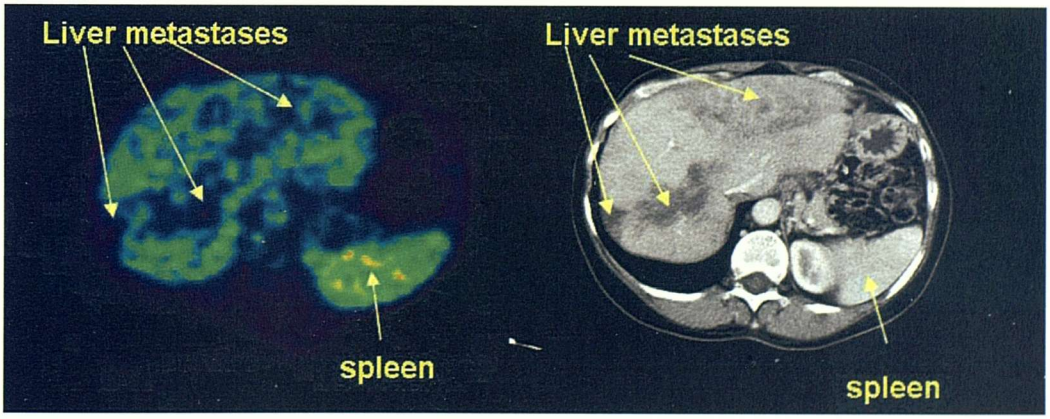
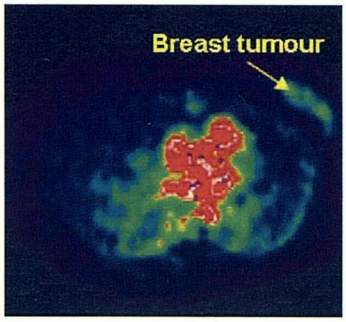
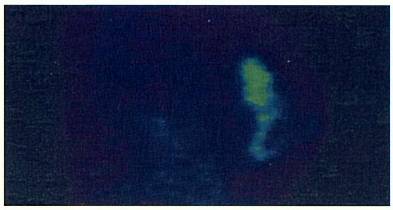
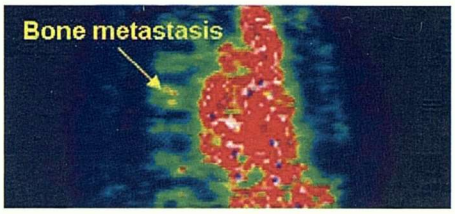


Figure 4.5. [18F]-AH111585 PET in a Primary Breast Tumour with Bone Metastases

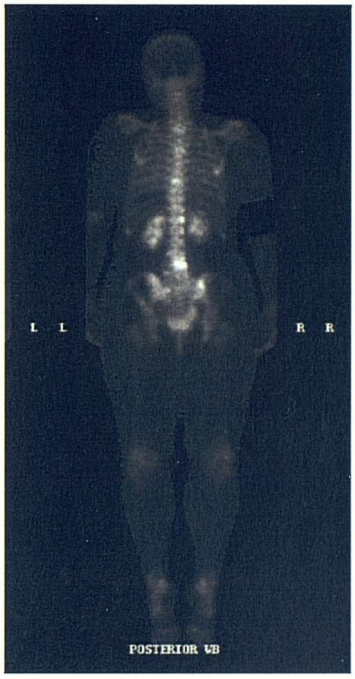




Sagittal and transverse views of a left breast tumour (grade 2 intraductal carcinoma) in patient 2.



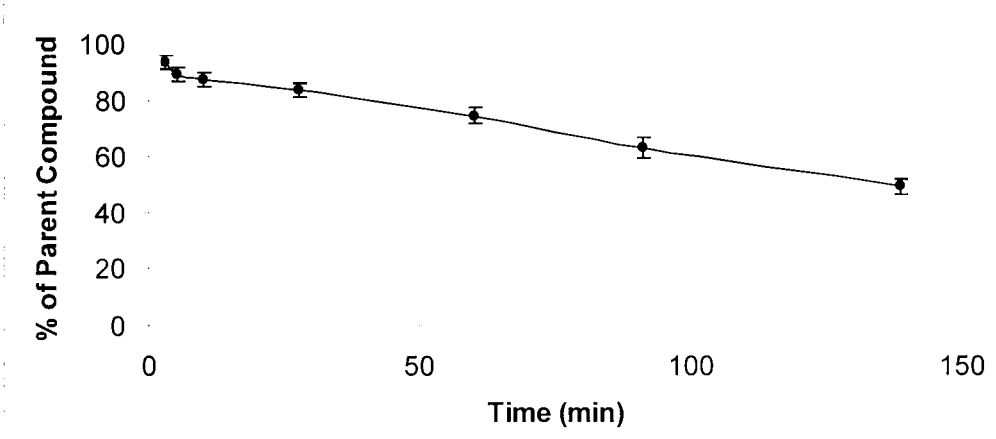
Sagittal section of [18F]AH-111585 PET image and corresponding Technetium [^{99}MTc] bone scan showing thoracic bone metastases



4.5.2 Metabolism of [18F]-AH111585

The compound was slowly metabolised. At 60 mins post intravenous injection the percentage of measured radioactivity in arterial plasma due to [18F]-AH111585 (± SEM) was 74.48± 3.18%, with the remainder due to metabolites.

Figure 4.6 Summary of [18F]-AH111585 metabolism data for patients

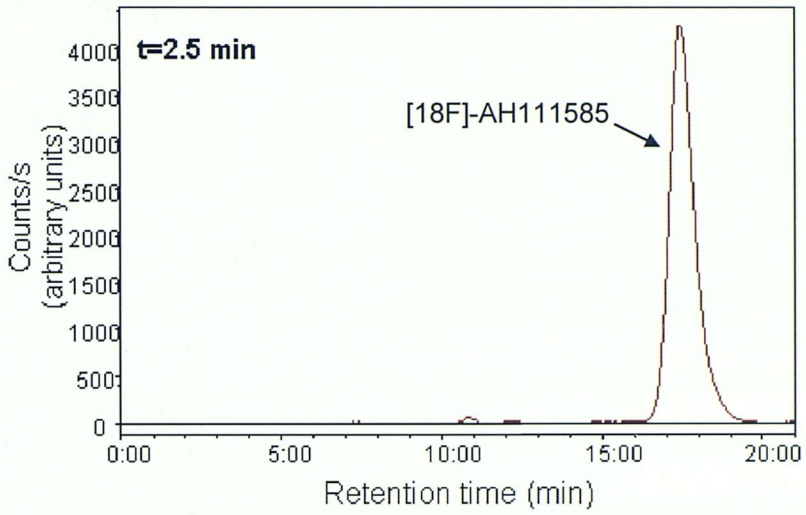


Proportion of unmetabolised [18F]-AH111585 to total [18F]-radioactivity in plasma as a function of time, measured as described in the methods section; bars are ± SEM, n = 7 patients.

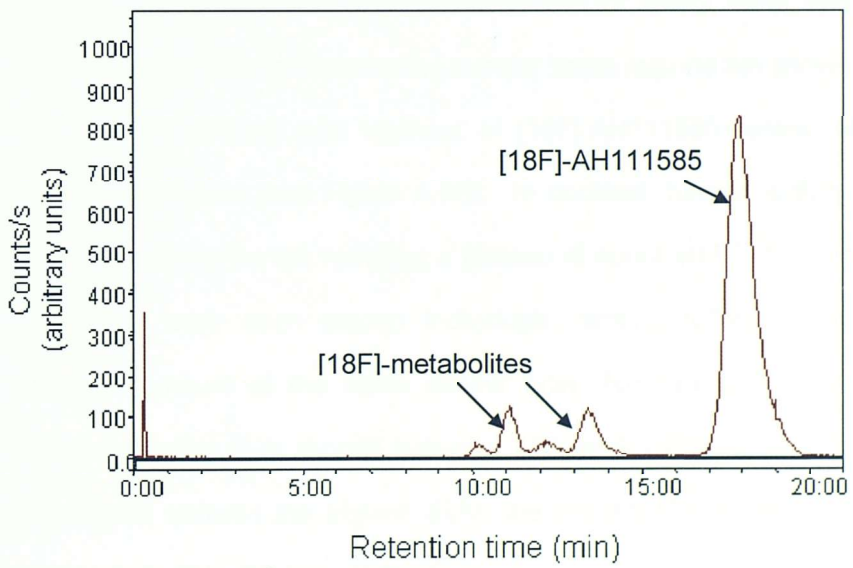
An example of the HPLC analysis of the metabolites and parent compound for patient in the study analysis are shown in Figure 4.7, the number of polar metabolites and contribution to overall radioactivity was seen to increase overtime. The exact nature of the metabolites was not characterised in this study, but could in future be analysed using techniques such as mass spectrometry.

Figure 4.7 HPLC Analysis of [18F]-AH111585 and Metabolites in Arterial Plasma.

A)



B)



Radiochromatograms of [18F]-AH111585-derived radioactivity in arterial plasma, assessed at 2.5min (A) and at 60min (B) after injection of the radioligand.

The slow metabolism of this compound is a favorable factor, as it suggests that static studies could be commenced at 30-60 minutes post injection of the radiotracer and is beneficial for mathematical modelling as sophisticated correction algorithms are unlikely to be necessary.

4.5.3 Mathematical analysis results

The results of the semiquantitative analyses and quantitative (i.e. modelled) analyses are shown in Tables 4.7, 4.8, and 4.9. Tumour regions are highlighted in bold, necrotic regions in grey, and normal tissue regions are white.

The data presented are analyses of radioligand uptake in 19 tumour regions from 18 CT-detectable lesions and 1 supraclavicular fossa lymph node. In the first patient only SUV and area under the curve calculations were performed because of concern about the validity of ROI definition as the lesion was detected on physical examination but not by CT. Graphical comparison of uptake corrected for decay, dose, and body surface area, in selected tumour and corresponding normal tissue regions are shown in Figures 4.8-4.10.

Rapid delivery and washout of [18F]-AH111585-derived activity was evident in normal lung tissue (see Figure 4.8B). In contrast, tumour activity increased continually over the imaging period, reaching a plateau at about 40-60 min. Large variations in [18F]-AH111585 were seen among individuals, among different tumour types, and even between tumours of the same cancer type. For example, inpatient 5 (with four lung metastases) the SUV ranged between 5.31 and 106.57 x 10^{-5} (m^2/ml). In general, lung metastases showed the highest SUV; the primary tumour and liver metastases showed lower uptake than the lung metastases.

Table 4.7 Results of SUV and AUC Analysis in Tumour and Non-Tumour Tissue

Patient	Region	SUV	AUC
1	**tumour**	**3.737**	**0.122**
	muscle	2.372	0.078
2	**tumour**	**5.313**	**0.129**
	nbreast	1.503	0.044
3	**Rant**	**8.980**	**0.262**
	Lmid	**9.911**	**0.295**
	Lsup	**8.008**	**0.212**
	Rmid	**8.853**	**0.241**
	Rlat	**3.680**	**0.110**
	Rsuppost	**8.868**	**0.246**
	Liver	11.417	0.044
4	**tumour**	**7.468**	**0.276**
	Liver	10.039	0.425
5	**Tumour1**	**96.251**	**2.768**
	Tumour2	**6.870**	**0.290**
	Tumour3	**5.309**	**0.147**
	Tumour4	**106.57**	**3.406**
	Lung	2.464	0.100
6	**ranttum**	**18.189**	**0.472**
	rposttum	**16.796**	**0.454**
	centrelnode	3.897	0.100
	infantmet	**17.882**	**0.477**
	outerpost	**14.105**	**0.373**
	plymphnode	**14.034**	**0.386**
	postcentre	7.803	0.207
	lung	2.750	0.104
7	**livermet**	**9.371**	**0.346**
	liver	9.841	0.348

(where SUV = SUV corrected for body surface area measured at 60 minutes post-injection x 10^{-5} $m_2.ml^{-1}$, and AUC= area under the curve at 60 minutes in $m^2.sec.ml^{-1}$).

Table 4.8 Results of Patlak Analysis in Tumour and Non-Tumour Tissue

Patient	Region	Ki	Ki (parent)
1	**tumour**	**n/a**	**n/a**
	muscle	n/a	n/a
2	**tumour**	**3.817**	**4.430**
	nbreast	1.601	1.658
3	**Rant**	**9.399**	**9.876**
	Lmid	**11.760**	**10.048**
	Lsup	**9.367**	**9.640**
	Rmid	**10.156**	**10.480**
	Rlat	**3.748**	**3.950**
	Rsuppost	**9.656**	**10.048**
	Liver	9.812	10.794
4	**tumour**	**3.747**	**4.370**
	Liver	4.730	5.818
5	**Tumour1**	**68.761**	**72.682**
	Tumour2	**2.350**	**3.038**
	Tumour3	**3.960**	**4.155**
	Tumour4	**72.547**	**78.084**
	Lung	1.036	1.263
6	**ranttum**	**27.490**	**28.687**
	rposttum	**21.820**	**23.824**
	centrelnode	1.688	3.305
	infantmet	**24.585**	**26.472**
	outerpost	**17.396**	**19.183**
	plymphnode	**22.145**	**21.066**
	postcentre	11.760	12.339
	lung	2.403	2.967
7	**livermet**	**7.424**	**9.971**
	liver	6.875	9.442

(where Ki= Irreversbile retention obtained using Modified Patlak analysis (x 10^{-5} ml plasma. ml tissue $^{-1}$. s $^{-1}$). Ki (parent) = Irreversbile retention obtained using parent plasma input function analysis i.e. Classical Patlak (x 10^{-5} ml plasma. ml tissue $^{-1}$. s $^{-1}$.)

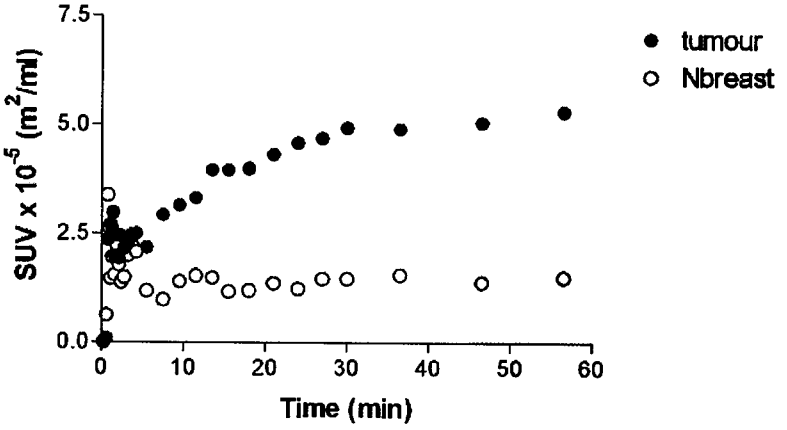
Table 4.9 Results of Spectral Analysis in Tumour and Non-Tumour Tissue

Patient	Region	IRF 1min	IRF 56.5	FRT	VD	K1	MRT
1	**tumour**	**n/a**	**n/a**	**n/a**	**n/a**	**n/a**	**n/a**
	muscle	n/a	n/a	n/a	n/a	n/a	n/a
2	**tumour**	**11.75**	**5.413**	**0.461**	**0.534**	**6.354**	**840.415**
	nbreast	5.56	1.470	0.264	0.183	1.325	1381.132
3	**Rant**	**62.97**	**7.207**	**0.114**	**1.653**	**16.434**	**1005.842**
	Lmid	**59.10**	**8.180**	**0.138**	**0.842**	**29.358**	**286.804**
	Lsup	**26.61**	**6.980**	**0.262**	**0.688**	**5.655**	**1216.622**
	Rmid	**28.65**	**9.046**	**0.316**	**2.206**	**23.200**	**950.862**
	Rlat	**41.270**	**3.191**	**0.077**	**0.365**	**10.085**	**361.924**
	Rsuppost	**56.450**	**7.735**	**0.137**	**0.802**	**13.691**	**585.786**
	Liver	123.400	5.777	0.047	0.853	93.173	91.550
4	**tumour**	**72.380**	**3.424**	**0.047**	**0.478**	**27.962**	**170.946**
	Liver	86.700	0.829	0.010	0.357	18.373	194.307
5	**Tumour1**	**353.000**	**60.250**	**0.171**	**15.018**	**313.732**	**47.869**
	Tumour2	**54.270**	**2.218**	**0.041**	**0.290**	**12.801**	**226.545**
	Tumour3	**.200**	**3.290**	**0.155**	**0.344**	**4.816**	**714.286**
	Tumour4	**313.200**	**58.290**	**0.186**	**13.859**	**62.227**	**2227.168**
	Lung	19.660	1.050	0.053	0.139	4.168	333.493
6	**ranttum**	**101.000**	**25.120**	**0.249**	**5.668**	**23.467**	**2415.307**
	rposttum	**93.580**	**21.430**	**0.229**	**4.632**	**22.788**	**2032.649**
	centrelnode	9.621	4.800	0.499	0.469	0.974	4815.195
	infantmet	99.980	23.350	0.233	2.579	17.686	1458.216
	outerpost	56.880	18.310	0.322	4.116	66.872	615.504
	plymphnode	68.210	16.030	0.265	4.096	14.834	2761.224
	postcentre	74.130	10.250	0.138	1.102	10.600	1039.623
	lung	23.520	2.470	0.105	0.298	6.612	450.696
7	**livermet**	**14.490**	**5.967**	**0.041**	**0.767**	**44.405**	**172.728**
	liver	14.490	5.566	0.037	0.828	42.263	195.916

(where *IRF1min = Impulse response function at 1 minute x 10^{-5}, IRF56.5min= Impulse response function at 56.5 minutes x 10^{-5}, FRT= fractional retention of the tracer = IRF56.5min/IRF1min). VD= Relative volume of distribution (ml plasma/ml of tissue). K1= Rate of delivery of [18F]-AH111585 obtained by spectral analysis x 10^{-4} (µl plasma/ml tissue/sec). MRT = Mean residence time of tracer in tissue region (in sec).*

Figure 4.8 Typical Time versus Radioactivity Curves from Tumour Regions and Corresponding Normal Tissue

4.8A



4.8B

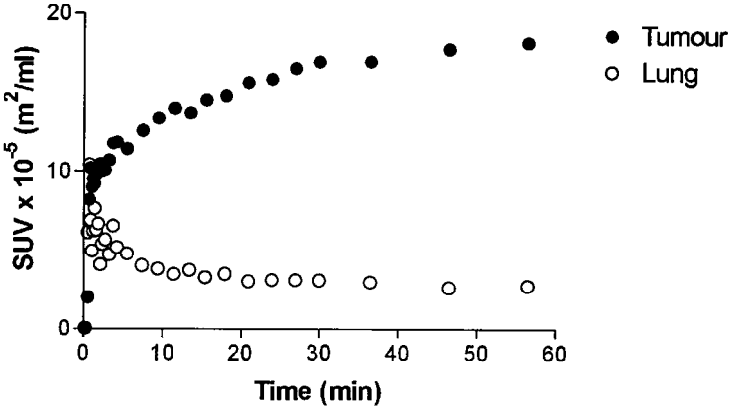


Figure 4.8: A, shows the uptake of [18F]-AH111585 in a primary breast tumour and normal breast tissue in patient 2; B, shows a lung metastasis and normal lung in patient no.5. In both the figures above, the higher uptake in the breast tumour and a lung metastasis is clearly discernible from that of normal tissue.

Figure 4.9 Heterogeneity of uptake within a single tumour lesion

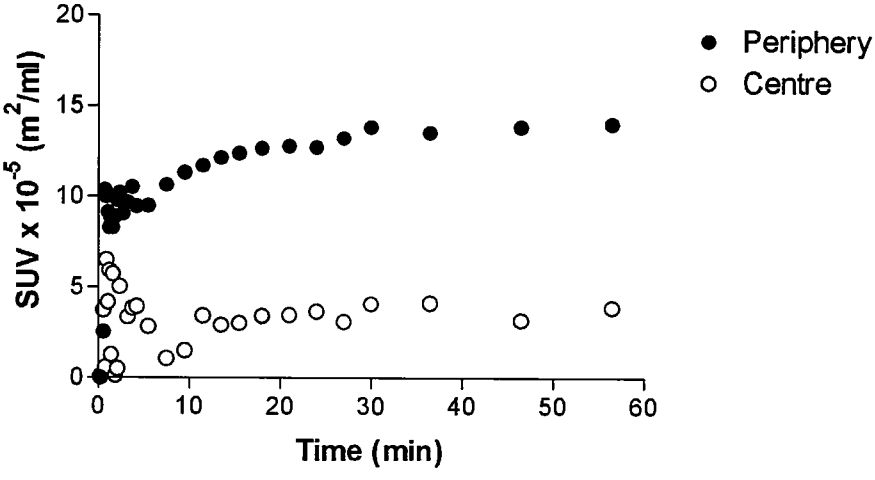


Figure 4.9 shows the difference in [18F]-AH111585 uptake between the necrotic centre of a lymph node, and the periphery of the same lesion from patient 6.

Figure 4.10. [18F]-AH111585 uptake in a liver metastasis and normal liver

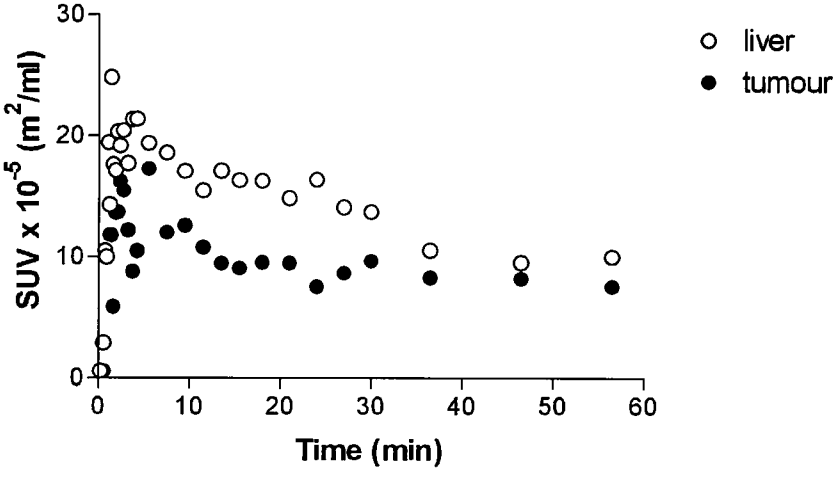


Figure 4.10. In contrast to the previous lesions the liver metastasis has low uptake compared to the normal liver (data presented from patient 2).

[18F]-AH111585 derived activity cleared rapidly from both blood and plasma with a half-life of about 10 min; the plasma-to-blood activity ratio was greater than 1 at all time points (see Figure 4.11). Analysis of the kinetic data indicated that the radioligand was irreversibly trapped in tumours within the imaging time during the scanning period (1h).

Figure 4.11 [18F]-Radioactivity in Arterial Blood and Plasma

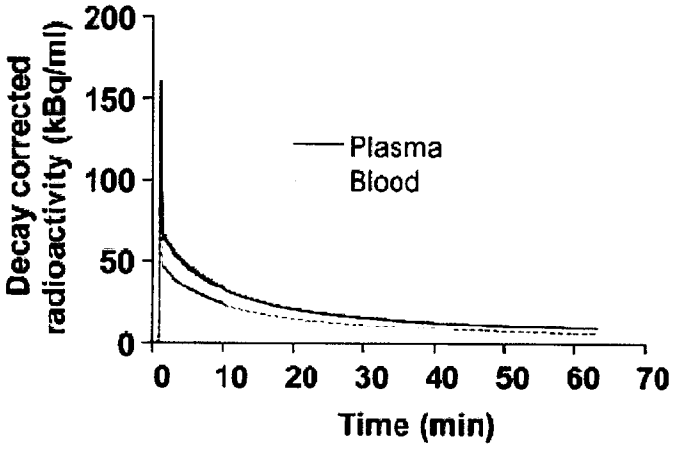


Figure 4.11 above shows a typical example (from patient 6) of the [18F]-derived radioactivity measured in arterial blood and plasma. The terminal half-lives of blood and plasma were 9.30 and 10.95 min, respectively indicating rapid clearance of the radiotracer to tissue.

In the Patlak plots of tumour lesions, an exponential phase followed by a discernible linear phase was seen, indicating irreversible trapping; the slope (Ki) was

higher than normal tissue (see Figure 4.12). The results were similar for both the Modified Patlak and Classical Patlak analyses (see Figure 4.13 and table 4.13).

Figure 4.12 Modified Patlak analysis of a tumour lesion compared to normal tissue

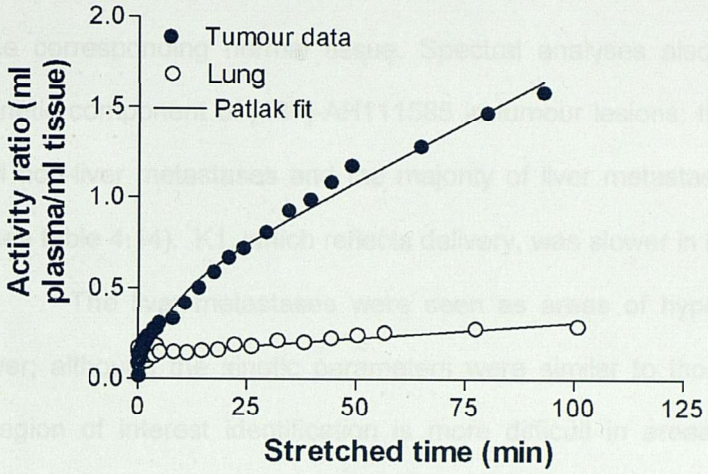


Figure 4.12 above shows the difference in [18F]-AH111585 Patlak slopes for a lung metastasis from patient 6, compared to normal lung tissue in the same patient. The values for Ki were 21.8 and 2.4 x 10^{-5} ml plasma/ml tissue/sec, respectively.

Figure 4.13 Classical Patlak analysis in a tumour lesion

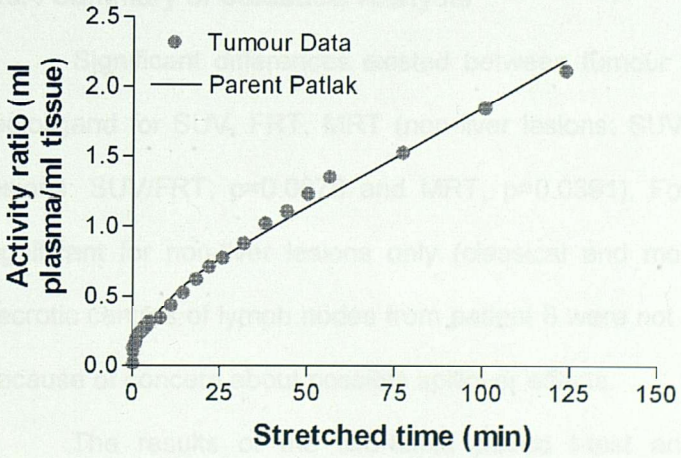


Figure 4.13 above shows a Classical Patlak analysis performed for the same tumour lesion as that illustrated in Figure 4.12; the value for Ki was 23.8 x 10^{-5} ml plasma/ml tissue/sec.

Ki was higher for non-liver metastatic lesions and the primary breast tumour than the corresponding normal tissue. Spectral analyses also demonstrated an irreversible kinetic component of [18F]-AH111585 in tumour lesions; the FRT results were higher for all non-liver metastases and the majority of liver metastases compared to normal tissue (see table 4.14). K1, which reflects delivery, was slower in metastases than normal liver.

The liver metastases were seen as areas of hypointensity compared to normal liver; although the kinetic parameters were similar to those in other metastatic lesions. Region of interest identification is more difficult in areas of hypointensity, and due to concern about spillover from normal liver tissue the statistical analysis were performed separately for liver and non-liver tissue. Similarly, there were potential errors for quantifying uptake in necrotic regions which are surrounded by a high-uptake tumour rim; hence the necrotic regions were not included in the statistical analyses of tumours.

4.5.4 Summary of Statistical Analysis

Significant differences existed between tumour and normal tissue uptake of the radioligand for SUV, FRT, MRT (non-liver lesions: SUV, p=0.002, FRT, p =0.0039; liver lesions: SUV/FRT, p=0.0078 and MRT, p=0.0391). For Ki analysis the difference was significant for non-liver lesions only (classical and modified Patlak; Ki p =0.002). The necrotic centres of lymph nodes from patient 6 were not included in the statistical analysis because of concern about possible spillover effects.

The results of the two-tailed paired t-test and Wilcoxon matched pairs test comparing uptake in tumour lesions versus normal tissues for all the parameters detailed

in the results tables (4.7 and 4.9 above) are shown below. As the normal uptake in the liver was high, the lesions were analysed in the following groups: 1) all tumour lesions, 2) non-liver tumour lesions, and 3) liver-only metastases.

Table 4.10 Difference between tumour and normal tissue uptake for all parameters

Parameter	No. of Lesions	Lesion type	T-test p value	Wilcoxon p value
SUV	19	All (incl pt 1)	0.076	0.0549
	18	Not incl pt 1	0.0777	0.049
	11	Non-liver (incl pt 1)	0.0466	0.0010
	10	Non-liver (not incl pt 1)	0.0469	0.0020
	8	Liver	0.0640	0.0078
AUC	19	All (incl pt 1)	0.1234	0.1747
	18	Not incl pt 1	0.1262	0.1738
	11	Non-liver (incl pt 1)	0.0597	0.0010
	10	Non-liver (not incl pt 1)	0.0607	0.0020
	8	Liver	0.0011	0.0078
Ki	18	All	0.0215	0.0088
	10	Non-liver	0.0127	0.0020
	8	Liver	0.4596	0.6406
Ki parent	18	All	0.0266	0.0358
	10	Non-liver	0.0135	0.0020
	8	Liver	0.111	0.0234
IRF @ 1 min	18	All	0.3675	0.4705
	10	Non-liver	0.033	0.0059
	8	Liver	0.002	0.0156
IRF @ 56.5 min	18	All	0.0099	0.0008
	10	Non-liver	0.0095	0.0020
	8	Liver	0.0765	0.1094
FRT	18	All	<0.0001	0.0003
	10	Non-liver	<0.0001	0.0039
	8	Liver	0.0189	0.0078
VD	18	All	0.0184	0.0052
	10	Non-liver	0.0170	0.0020
	8	Liver	0.4028	0.9453
K1	18	All	0.9068	0.9566
	10	Non-liver	0.1299	0.0020
	8	Liver	0.0048	0.0391
MRT	18	All	0.0031	0.0068
	10	Non-liver	0.0322	0.0645
	8	Liver	0.0190	0.0391

The Wilcoxon test shows that the [18F]-AH111585 uptake parameters SUV, AUC, IRF@1min, FRT, Ki obtained by parent Patlak analysis, and K1 were able to differentiate between tumour and normal tissue in both liver and non-liver lesions when the sites of metastases were grouped separately. The difference between tumour and non-

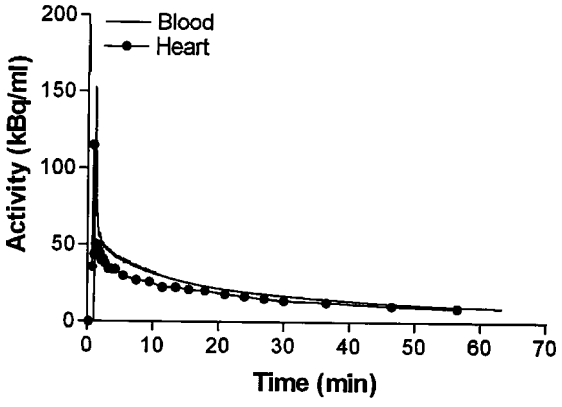
tumour uptake was significant for non-liver lesions but not for liver metastases for the following parameters: Ki obtained by Modified Patlak analysis, VD, and FRT@56.5 min. The converse was true for MRT where there was a significant difference between liver lesions and normal lesions, i.e. increased MRT in lesions compared to normal liver, but there was a lack of significance for non-liver lesions.

4.5.5 Comparison of the heart and radial artery sampling

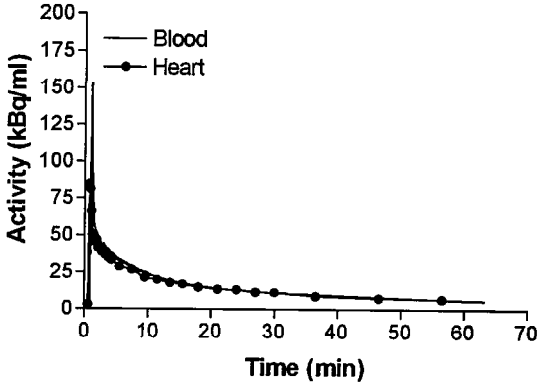
This was assessed in three patients (nos. 2, 5, and 6). As the ROI obtained from the heart represents total blood (i.e. there was no separation for plasma), the input function generated was compared to the total blood curve obtained by radial artery sampling performed during the scan. The results are depicted below in Figure 4.14, and suggest that there was good correlation between the two types of datasets; however definitive statistical analysis of the correlation was not performed due to the small sample size (n=3).

Figure 4.14 Comparison of Heart ROI and Total Blood Input Function

A



B



C

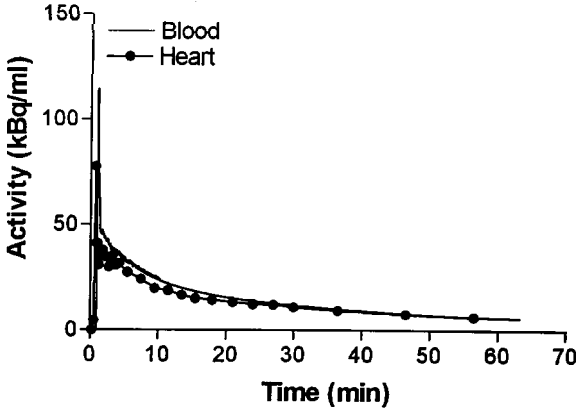


Figure 4.14 above, shows the [18F]-derived activity measurements in radial artery blood (labelled Blood) compared to the surrogate cardiac ROI (labelled heart) from patients 2 (Figure A), 5 (Figure B), and 6 (Figure C).

4.6 DISCUSSION

This study has for the first time shown that the RGD-containing integrin receptor binding ligand, [18F]-AH111585, demonstrates irreversible uptake in metastatic breast cancer; is stable in vivo, and rapidly cleared from blood. The power to separate potential areas of tumour angiogenesis from necrotic areas could aid treatment e.g. for planning radiotherapy, and selection of targeted agents. The ability of [18F]-AH111585 to non-invasively quantify $\alpha v\beta 3$ and $\alpha v\beta 5$ associated neovascularisation may become both a prognostic and predictive factor for treatment response in cancer patients.

The ideal qualities for a radiotracer which targets angiogenesis-associated integrins include: suitability for imaging common cancers (e.g. breast, lung, colorectal), high tumour-background ratio, fast-blood clearance to minimise non-target radioactivity. The time taken for the radiotracer to reach its target should be rapid, dissociation should be slow, so that maximal accumulation in the tumour is achieved(Liu 2006). This tracer fulfils most of the above criteria. There was a significant difference for both semi-quantitative and modelled parameters between tumour uptake and normal tissue uptake in non-liver lesions.

[18F]-AH111585 was found to be safe and well tolerated, with no adverse events in the 7 patients studied. All lesions identified by CT were visualised by the radiotracer (within the corresponding field of view). The one exception was in a clinically palpable supraclavicular lymph node which was not conclusively seen on the CT scan; the high density of vessels in this region and anatomic location are likely to have been contributing factors. The high in vivo stability of the radioligand together with its retention in tissue may have been reflected in the fact that most tumours (excluding liver lesions) demonstrated hyperintense uptake. Although there is potential for partial volume effects with lung

lesions, all of the tumours analyzed in this study were greater than 1cm, which obviates significant partial volume effects.

[18F]-AH111585 was found to be homogeneously distributed in the tumours or appeared within the tumour rim; this finding is consistent with the general principles regarding the distribution of angiogenesis within the outer zones of breast tumours, where viable regions exist (Fox et al. 1995; Fox et al. 1995; Koukourakis et al. 2000). The high liver background activity may have been due to the densely vascularised nature of the sinusoidal vessels, rapid blood flow which was identified in the preliminary biodistribution study where very high initial activities were seen in the liver, and the metabolism of [18F]-AH111585 by the liver. The exact nature of the metabolites is yet to be elucidated, as is the binding capability of the metabolites of [18] AH111585 to with αvβ3/ αvβ5 integrins.

K1, which reflects delivery, was slower in metastases than normal liver. MRT was higher in metastases than normal liver in the majority of lesions (6 out of 8). The fact that the liver has a dual blood supply from the hepatic artery and the portal vein, could mean that the systemic arterial input function overestimated the true tissue input function, therefore affecting the pharmacokinetic parameters. Prominent accumulation of RGD peptide ligand in the liver has also previously been reported in humans(Chen et al. 2004). Statistical noise in spectral analysis can also affect both K1 and MRT. The spleen also showed high uptake, this is thought to be due to blood pooling.

However, it has also been shown previously that liver metastases from breast cancer do not exhibit marked angiogenesis and instead rely on co-opting existing blood vessels (Stessels et al. 2004). Stessels et al, found that the median level of carbonic anhydrase 9, CA9, (a well known marker of hypoxia) was 0 in the 45 metastases which were examined; this was in contrast to colorectal liver metastases where the level of CA9 was much higher and suggests that liver metastases from breast carcinoma lack hypoxia-driven activation of their pro-angiogenic switch. However it should be remembered that

CA9 is not itself a direct biomarker of angiogenesis per se, rather, it is seen as a hypoxia marker. The values for the pharmacokinetics for [18F]-AH111585 uptake in this study in liver metastases are comparable to those in non-liver lesions (see tables 4.12-4.14). The high background signal in the liver presents challenges for use of this agent in patients with liver metastases and requires further study.

This study summarises the radioligand kinetics of an RGD peptide in humans. The rise in SUV over time in tumours compared with the rapid clearance in blood and normal lung tissue is consistent with selective high-affinity receptor binding and adequate pharmacokinetic properties. Both primary and metastatic lesions showed radioligand uptake which was higher than that of the corresponding normal tiisues ($p=0.002$) with the exception of liver metastases, which were still detectable but with reversed contrast. Nonetheless, the absolute values (SUV values corrected for body weight between 2 and 39 g/ml; or Ki between 2 and 69 x 10^{-5} ml plasma/ml tissue/s) were high enough for clinical use.

The variable uptake between tumour lesions in the same patient may be due to differences in angiogenesis in the tumour microenvironment; this finding warrants further investigation. The kinetic modelling allowed quantitative assessment of the radioligand-receptor interactions. The linear phase of the Patlak plots implied a net-irreversible binding of the radioligand to tumours within the imaging time. The values for Ki from modified Patlak analysis were lower than those obtained by classical Patlak; which suggests that some of the [18F]-AH111585 metabolites may exhibit receptor-binding properties. Compartmental analysis of the data would help discern the magnitude of reversible or irreversible binding components with the tissues.

Secondary to the net-irreversible trapping of the radioligand in tumours during the imaging period, the residence time of [18F]-AH111585 was higher in tumours than adjacent normal tissues; suggesting that a later imaging time (e.g. 60 min post-injection)

would be suitable for clinical studies of breast cancer. In contrast, a study by Beer et al in patients with squamous carcinoma of the head and neck found that uptake of the [18F]galacto-RGD peaked at 10-15min, then plateaued or had a slight decrease over 60 min; and was associated with reversible kinetics(Beer et al. 2007).

The biodistribution of [18F]galacto-RGD is similar to [18F]-AH111585(Beer et al. 2006). As there is high background in the liver and the spleen with both of these radiotracers, imaging of angiogenesis in these regions will be challenging. Only one breast carcinoma was included in the Beer study. If the SUV values for that tracer (corrected for body weight) are compared to [18F]-AH111585 in the patient primary breast cancer lesions – the values are quite similar – 3.1 in the Beer study compared to 2.1 in this study(Beer et al. 2006). This current study did not perform correlations with tumour levels of the target integrins as the metastases were deep-seated, therefore biopsies would have involved an invasive procedure for patients with advanced breast cancer.

Whilst the possibility of [18F]-AH111585-PET detecting both tumour cells and tumour neovasculature cannot be completely excluded in this study, in the epithelial breast cancer cell line, MCF-7, the level of expression of the $\alpha v\beta 3$ integrin was as low as 0.88%(Beauvais et al. 2004). It is important to remember that $\alpha v\beta 3/5$ expression on tumor cells and endothelial cells are both considered as therapeutic targets.

The results using the heart as an ROI to derive an arterial input function did underestimate the initial peak radioactivity as measured by the on-line arterial blood sampling. This may be explained by lack of a fully reliable definition of the left ventricle, so that some right ventricular blood may also have been sampled with venous mixing leading to an overall decreased activity per unit volume, or a partial volume effect, or the use of averaged counts over a time frame for the heart data rather than complete dynamic set as was used for the whole blood. Normally the arterial input function obtained by arterial sampling is subject to delay and dispersion effects between the arrival of the arterial blood

in the tissue of interest and the corresponding point of assay (Cunningham et al. 1994). A correction factor could be calculated from a larger dataset to detect a trend, which would be suitable for larger clinical studies that use image-based derived input functions.

[18F]-AH111585 has shown promising activity in this study, and may be useful for monitoring the response to antiangiogenic agents, including anti-VEGF, anti-VEGFR, and anti-αvβ3 receptor agents.

Future studies of this agent should i) correlate uptake of [18F]-AH111585 with tumour expression of αvβ3 measured by immunohistochemistry, ii) assess the utility to detect angiogenic growth in other particular tumour types, iv) assess the effect of novel anti-angiogenic agents, and iv) predict tumour response within an individual patient to a particular therapy.

In conclusion, [18F]-AH111585 is safe, well tolerated, can detect primary and metastatic tumour lesions, and is only minimally metabolised *in vivo*. These findings should promote [18F]-AH111585 as a novel PET radiotracer, and warrant further evaluation as a predictive factor and an agent in monitoring treatment response.

Chapter 5: CONCLUSION

This thesis has evaluated the potential of three novel PET radiotracers in breast cancer. Each of the radiotracers is proposed as biomarkers for diverse biological processes within the cell which contribute to the hallmarks of cancer; namely proliferation, activation of growth factor pathways, and development of an autologous blood supply. The main focus of the studies has been to provide an in-depth pharmacokinetic analysis of the radiotracers in tumour tissue using dynamic PET imaging and mathematical modelling techniques. Whilst the number of patients involved in the studies means that they are pilot in nature, some definitive conclusions have been reached.

For [18F]Fluorothymidine one can state that i) this is a marker of proliferation in breast cancer; ii) that quantitative parameters are superior to semi-quantitative in terms of correlation with Ki-67 LI,(Kenny et al. 2005) iii) that tumour uptake of [18F]FLT is reproducible, iv) that early decreases in [18F]FLT can discriminate between responders and non-responders to treatment with FEC chemotherapy (Kenny 2007), and v) that cardiac blood pool sampling is a promising non-invasive alternative to radial arterial sampling, but may need shorter early time frames to determine peak activity.

[11C]Choline was the focus of the second chapter. From these studies the results show that i) [11C]choline-PET can distinguish between breast tumour lesions and normal tissue; ii) uptake of [11C]choline is repeatable in breast tumours; iii) early changes in [11C]choline uptake can be observed post-treatment with the c-erbB2 inhibitor, trastuzumab. The results of the analysis to correlate [11C]choline uptake with phosphoMAPK may have been affected by the timing of the tumour biopsies. In relation to response to treatment with trastuzumab the results suggest that significant clinical

responses are associated with a decrease in [11C]choline retention; further larger studies are clearly required.

Finally, the potential of [18F]-AH111585 was evaluated in a first in man phase 1/2 study. This study showed that i) there was irreversible retention of the radiotracer in breast cancer; ii) that uptake was significantly higher in tumour compared to normal tissue; and iii) that cardiac blood pool analysis is a useful surrogate to radial artery sampling to provide an arterial plasma input function(Kenny 2008).

PUBLICATIONS, PRESENTATIONS, AND PRIZES ASSOCIATED WITH THIS THESIS

Abstracts and Posters

American Society of Clinical Oncolgy Annual Meeting, 2007: 14067

L. M. Kenny, E. Aboagye, P. S. Cohen, M. Miller, F. Turkheimer, A. Al-Nahhas, D. Blunt, R. C. Coombes. Imaging of angiogenesis in metastatic breast cancer by positron emission tomography (PET) using [18F]-AH11585, an [18F]- labeled alphaVbeta3 (αvβ3) peptide.

San Antonio Breast Cancer Symposium, 2006: 4127

Kenny LM, Aboagye EO, Al-Nahhas A, Charles L, Coombes RC. [^{11}C]choline-PET in human breast cancer: utility, repeatability and effect of receptor tyrosine kinase inhibition by trastuzumab.

American Society of Clinical Oncolgy Annual Meeting, 2006:613

L. M. Kenny, R. C. Coombes, A. Al-Nahhas, S. Osman, C. Lowdell, E. Aboagye. A feasibility study of [11C]choline for the molecular imaging of human breast cancer *in vivo* using positron emission tomography (PET).

American Society of Clinical Oncolgy Annual Meeting, 2005: 2084

L. M. Kenny, D. M. Vigushin, R. C. Coombes, S. Osman, S. Shousha, A. Al-Nahhas, E. Aboagye. Early assessment of response to treatment in breast cancer by [18F]fluorothymidine-positron emission tomography.

European Association of Nuclear Medicine, 2004.

Kenny LM, Al Nahhas A, Vigushin D, Coombes RC, Aboagye EO. [18F]Fluorothymidine Retention in Breast Cancer Measured by PET - Initial Results From A Pilot Study.

Oral Presentations

AACR 2007 Los Angeles. Special Session for Late-Breaking Phase 1 Clinical Trials. Phase 1 Clinical Study of [18F]-AH111585 PET Imaging of Angiogenesis in Human Breast Cancer.

UKRO Annual Meeting 2007: Novel Agents for Imaging Cancer Using PET

NCRI Meeting 2006: McElwain Prize Lecture [^{18}F]Fluorothymidine Positron Emission Tomography - A Novel Method to Study Cell Proliferation *In Vivo*.

Publications

1. Laura M Kenny, R Charles Coombes, Inger Oulie et al. Phase 1 Trial of the Positron-Emitting Arg-Gly-Asp (RGD) Peptide Radioligand ^{18}F-AH111585 in Breast Cancer Patients. J Nucl Med. 2008 Jun;49(6):879-862.

2. Kenny L, Coombes RC, Vigushin DM, Al-Nahhas A, Shousha S, Aboagye EO. Imaging early changes in proliferation at 1 week post chemotherapy: a pilot study in breast cancer patients with 3'-deoxy-3'-[18F]fluorothymidine positron emission tomography. Eur J Nucl Med Mol Imaging. 2007 Sep; 34(9):1339-47.

3. Kenny LM, Vigushin DM, Al-Nahhas A, Osman S, Luthra SK, Shousha S, Coombes RC, Aboagye EO. Quantification of cellular proliferation in tumor and normal

tissues of patients with breast cancer by [18F]fluorothymidine-positron emission tomography imaging: evaluation of analytical methods. Cancer Res. 2005 Nov 1;65(21):10104-12.

4. Kenny LM, Price P, Aboagye E. PET Imaging of Cell Proliferation. *Clin. Oncol.* 2004;16(3):176-185.

Prizes

September 2006	**McElwain Medical Oncology Prize**
June 2005	**American Society of Clinical Oncology Merit Award**
February 2004	**Westminster Medical School Oncology Trustees Research Fellowship**
September 2003	**Cancer Research UK Translational Research Prize**

APPENDIX 1

Eastern Co-operative Oncology Group Performance Status (ECOG)

Grade	ECOG
0	Fully active, able to carry on all pre-disease performance without restriction
1	Restricted in physically strenuous activity but ambulatory and able to carry out work of a light or sedentary nature, e.g., light house work, office work
2	Ambulatory and capable of all self-care but unable to carry out any work activities. Up and about more than 50% of waking hours
3	Capable of only limited self-care, confined to bed or chair more than 50% of waking hours
4	Completely disabled. Cannot carry on any self-care. Totally confined to bed or chair
5	Dead

APPENDIX 2: American Joint Committee on Cancer: Breast Cancer Staging

(Singletary et al. 2002)

Stage I

- T1*, N0, M0

Stage IIA

- T0, N1, M0
- T1*, N1, M0
- T2, N0, M0

Stage IIB

- T2, N1, M0
- T3, N0, M0

Stage IIIA

- T0, N2, M0
- T1*, N2, M0
- T2, N2, M0
- T3, N1, M0
- T3, N2, M0

Stage IIIB

- T4, N0, M0
- T4, N1, M0
- T4, N2, M0

Stage IIIC

- Any T, N3, M0

Stage IV

- Any T, Any N, M1

* [Note: T1 includes T1mic]

REFERENCES

Abdollahi, A., D. W. Griggs, H. Zieher, A. Roth, K. E. Lipson, R. Saffrich, et al. (2005). "Inhibition of alpha(v)beta3 integrin survival signaling enhances antiangiogenic and antitumor effects of radiotherapy." Clin Cancer Res **11**(17): 6270-9.

Abele, M. C., G. Valente, S. Kerim, R. Navone, P. Onesti, L. Chiusa, et al. (1997). "Significance of cell proliferation index in assessing histological prognostic categories in Hodgkin's disease. An immunohistochemical study with Ki67 and MIB-1 monoclonal antibodies." Haematologica **82**(3): 281-5.

Aboagye, E. O. and Z. M. Bhujwalla (1999). "Malignant transformation alters membrane choline phospholipid metabolism of human mammary epithelial cells." Cancer Res **59**(1): 80-4.

Aboagye, E. O. and P. M. Price (2003). "Use of positron emission tomography in anticancer drug development." Invest New Drugs **21**(2): 169-81.

Adjei, A. A., A. Mauer, L. Bruzek, R. S. Marks, S. Hillman, S. Geyer, et al. (2003). "Phase II study of the farnesyl transferase inhibitor R115777 in patients with advanced non-small-cell lung cancer." J Clin Oncol **21**(9): 1760-6.

Adler, R. and B. R. McAuslan (1974). "Expression of thymidine kinase variants is a function of the replicative state of cells." Cell **2**(2): 113-7.

Agiostratidou, G., I. Sgouros, E. Galani, A. Voulgari, N. Chondrogianni, E. Samantas, et al. (2001). "Correlation of in vitro cytotoxicity and clinical response to chemotherapy in ovarian and breast cancer patients." Anticancer Res **21**(1A): 455-9.

Al-Saeedi, F., T. Smith and A. Welch (2007). "[Methyl-3H]-choline incorporation into MCF-7 cells: correlation with proliferation, choline kinase and phospholipase D assay." Anticancer Res **27**(2): 901-6.

Al-Saffar, N. M., H. Troy, A. Ramirez de Molina, L. E. Jackson, B. Madhu, J. R. Griffiths, et al. (2006). "Noninvasive magnetic resonance spectroscopic pharmacodynamic markers of the choline kinase inhibitor MN58b in human carcinoma models." Cancer Res **66**(1): 427-34.

Alghisi, G. C. and C. Ruegg (2006). "Vascular integrins in tumor angiogenesis: mediators and therapeutic targets." Endothelium **13**(2): 113-35.

Antoch, G., J. Kanja, S. Bauer, H. Kuehl, K. Renzing-Koehler, J. Schuette, et al. (2004). "Comparison of PET, CT, and dual-modality PET/CT imaging for monitoring of imatinib (STI571) therapy in patients with gastrointestinal stromal tumors." J Nucl Med **45**(3): 357-65.

Aoyama, C., H. Liao and K. Ishidate (2004). "Structure and function of choline kinase isoforms in mammalian cells." Prog Lipid Res **43**(3): 266-81.

Archer, C. D., M. Parton, I. E. Smith, P. A. Ellis, J. Salter, S. Ashley, et al. (2003). "Early changes in apoptosis and proliferation following primary chemotherapy for breast cancer." Br J Cancer **89**(6): 1035-41.

Bailey, D. L. (1998). "Transmission scanning in emission tomography." Eur J Nucl Med **25**(7): 774-87.

Bailey, D. L., T. Jones and T. J. Spinks (1991). "A method for measuring the absolute sensitivity of positron emission tomographic scanners." Eur J Nucl Med **18**(6): 374-9.

Bailey, D. L., M. P. Miller, T. J. Spinks, P. M. Bloomfield, L. Livieratos, H. E. Young, et al. (1998). "Experience with fully 3D PET and implications for future high-resolution 3D tomographs." Phys Med Biol **43**(4): 777-86.

Barak, A. J. and D. J. Tuma (1983). "Betaine, metabolic by-product or vital methylating agent?" Life Sci **32**(7): 771-4.

Bartelink, H., A. C. Begg, J. C. Martin, M. van Dijk, L. Moonen, L. J. van 't Veer, et al. (2000). "Translational research offers individually tailored treatments for cancer patients." Cancer J Sci Am **6**(1): 2-10.

Barthel, A., S. T. Okino, J. Liao, K. Nakatani, J. Li, J. P. Whitlock, Jr., et al. (1999). "Regulation of GLUT1 gene transcription by the serine/threonine kinase Akt1." J Biol Chem **274**(29): 20281-6.

Barthel, H., M. C. Cleij, D. R. Collingridge, O. C. Hutchinson, S. Osman, Q. He, et al. (2003). "3'-deoxy-3'-[18F]fluorothymidine as a new marker for monitoring tumor response to antiproliferative therapy in vivo with positron emission tomography." Cancer Res **63**(13): 3791-8.

Barthel, H., M. Perumal, J. Latigo, Q. He, F. Brady, S. K. Luthra, et al. (2004). "The uptake of 3'-deoxy-3'-[(18)F]fluorothymidine into L5178Y tumours in vivo is dependent on thymidine kinase 1 protein levels." Eur J Nucl Med Mol Imaging.

Barthel, H., H. Wilson, D. R. Collingridge, G. Brown, S. Osman, S. K. Luthra, et al. (2004). "In vivo evaluation of [18F]fluoroetanidazole as a new marker for imaging tumour hypoxia with positron emission tomography." Br J Cancer **90**(11): 2232-42.

Beauvais, D. M., B. J. Burbach and A. C. Rapraeger (2004). "The syndecan-1 ectodomain regulates alphavbeta3 integrin activity in human mammary carcinoma cells." J Cell Biol **167**(1): 171-81.

Been, L. B., A. J. Suurmeijer, D. C. Cobben, P. L. Jager, H. J. Hoekstra and P. H. Elsinga (2004). "[18F]FLT-PET in oncology: current status and opportunities." Eur J Nucl Med Mol Imaging **31**(12): 1659-72.

Beer, A. J., A. L. Grosu, J. Carlsen, A. Kolk, M. Sarbia, I. Stangier, et al. (2007). "[18F]galacto-RGD positron emission tomography for imaging of alphavbeta3 expression on the neovasculature in patients with squamous cell carcinoma of the head and neck." Clin Cancer Res **13**(22 Pt 1): 6610-6.

Beer, A. J., R. Haubner, M. Sarbia, M. Goebel, S. Luderschmidt, A. L. Grosu, et al. (2006). "Positron emission tomography using [18F]Galacto-RGD identifies the level of integrin alpha(v)beta3 expression in man." Clin Cancer Res **12**(13): 3942-9.

Beer, A. J., R. Haubner, I. Wolf, M. Goebel, S. Luderschmidt, M. Niemeyer, et al. (2006). "PET-based human dosimetry of 18F-galacto-RGD, a new radiotracer for imaging alpha v beta3 expression." J Nucl Med **47**(5): 763-9.

Belt, J. A., N. M. Marina, D. A. Phelps and C. R. Crawford (1993). "Nucleoside transport in normal and neoplastic cells." Adv Enzyme Regul **33**: 235-52.

Benepal, T., A. Jackman, L. Pyle, S. Bate, A. Hardcastle, W. Aherne, et al. (2005). "A phase I pharmacokinetic and pharmacodynamic study of BGC9331 and carboplatin in relapsed gynaecological malignancies." Br J Cancer **93**(8): 868-75.

Benjamin, L. E., I. Hemo and E. Keshet (1998). "A plasticity window for blood vessel remodelling is defined by pericyte coverage of the preformed endothelial network and is regulated by PDGF-B and VEGF." Development **125**(9): 1591-8.

Benson, S. R., J. Blue, K. Judd and J. E. Harman (2004). "Ultrasound is now better than mammography for the detection of invasive breast cancer." Am J Surg **188**(4): 381-5.

Bland, J. M. and D. G. Altman (1995). "Calculating correlation coefficients with repeated observations: Part 1--Correlation within subjects." Bmj **310**(6977): 446.

Blomley, M. J. and R. J. Eckersley (2002). "Functional ultrasound methods in oncological imaging." Eur J Cancer **38**(16): 2108-15.

Bogin, L., M. Z. Papa, S. Polak-Charcon and H. Degani (1998). "TNF-induced modulations of phospholipid metabolism in human breast cancer cells." Biochim Biophys Acta **1392**(2-3): 217-32.

Bokel, C. and N. H. Brown (2002). "Integrins in development: moving on, responding to, and sticking to the extracellular matrix." Dev Cell **3**(3): 311-21.

Borbath, I., V. Gregoire, M. Bergstrom, D. Laryea, B. Langstrom and S. Pauwels (2002). "Use of 5-[(76)Br]bromo-2'-fluoro-2'-deoxyuridine as a ligand for tumour proliferation: validation in an animal tumour model." Eur J Nucl Med Mol Imaging **29**(1): 19-27.

Boss, D. S., R. V. Olmos, M. Sinaasappel, J. H. Beijnen and J. H. Schellens (2008). "Application of PET/CT in the development of novel anticancer drugs." Oncologist **13**(1): 25-38.

Boyle, P. and J. Ferlay (2005). "Cancer incidence and mortality in Europe, 2004." Ann Oncol **16**(3): 481-8.

Brady, F., S. K. Luthra, G. Brown, S. Osman, R. J. Harte, W. A. Denny, et al. (1997). "Carbon-11 labelling of the antitumour agent N-[2-(dimethylamino)ethyl]acridine-4-carboxamide (DACA) and determination of plasma metabolites in man." Appl Radiat Isot **48**(4): 487-92.

Bravo, R., R. Frank, P. A. Blundell and H. Macdonald-Bravo (1987). "Cyclin/PCNA is the auxiliary protein of DNA polymerase-delta." Nature **326**(6112): 515-7.

Brooks, P. C., R. A. Clark and D. A. Cheresh (1994). "Requirement of vascular integrin alpha v beta 3 for angiogenesis." Science **264**(5158): 569-71.

Brooks, P. C., A. M. Montgomery, M. Rosenfeld, R. A. Reisfeld, T. Hu, G. Klier, et al. (1994). "Integrin alpha v beta 3 antagonists promote tumor regression by inducing apoptosis of angiogenic blood vessels." Cell **79**(7): 1157-64.

Brown, G. D., S. K. Luthra, C. S. Brock, M. F. Stevens, P. M. Price and F. Brady (2002). "Antitumor imidazotetrazines. 40. Radiosyntheses of [4-11C-carbonyl]- and [3-N-11C-methyl]-8-carbamoyl-3-methylimidazo[5,1-d]-1,2,3,5-tetrazin-4(3H) -one (temozolomide) for positron emission tomography (PET) studies." J Med Chem **45**(25): 5448-57.

Buck, A. K., G. Halter, H. Schirrmeister, J. Kotzerke, I. Wurziger, G. Glatting, et al. (2003). "Imaging proliferation in lung tumors with PET: 18F-FLT versus 18F-FDG." J Nucl Med **44**(9): 1426-31.

Buck, A. K., M. Hetzel, H. Schirrmeister, G. Halter, P. Moller, C. Kratochwil, et al. (2005). "Clinical relevance of imaging proliferative activity in lung nodules." Eur J Nucl Med Mol Imaging **32**(5): 525-33.

Buck, A. K., H. Schirrmeister, M. Hetzel, M. Von Der Heide, G. Halter, G. Glatting, et al. (2002). "3-deoxy-3-[(18)F]fluorothymidine-positron emission tomography for noninvasive assessment of proliferation in pulmonary nodules." Cancer Res **62**(12): 3331-4.

Burgering, B. M. and P. J. Coffer (1995). "Protein kinase B (c-Akt) in phosphatidylinositol-3-OH kinase signal transduction." Nature **376**(6541): 599-602.

Burke, P. A., S. J. DeNardo, L. A. Miers, K. R. Lamborn, S. Matzku and G. L. DeNardo (2002). "Cilengitide targeting of alpha(v)beta(3) integrin receptor synergizes with radioimmunotherapy to increase efficacy and apoptosis in breast cancer xenografts." Cancer Res **62**(15): 4263-72.

Buzdar, A. U. (2007). "Preoperative chemotherapy treatment of breast cancer-A review." Cancer.

Byzova, T. V., W. Kim, R. J. Midura and E. F. Plow (2000). "Activation of integrin alpha(V)beta(3) regulates cell adhesion and migration to bone sialoprotein." Exp Cell Res **254**(2): 299-308.

Calderwood, D. A., B. Yan, J. M. de Pereda, B. G. Alvarez, Y. Fujioka, R. C. Liddington, et al. (2002). "The phosphotyrosine binding-like domain of talin activates integrins." J Biol Chem **277**(24): 21749-58.

Carmeliet, P. (2005). "Angiogenesis in life, disease and medicine." Nature **438**(7070): 932-6.

Carson, R. E., M. A. Channing, R. G. Blasberg, B. B. Dunn, R. M. Cohen, K. C. Rice, et al. (1993). "Comparison of bolus and infusion methods for receptor quantitation: application to [18F]cyclofoxy and positron emission tomography." J Cereb Blood Flow Metab **13**(1): 24-42.

Chalmers, C. R., S. W. Fenwick, G. J. Toogood and M. A. Hull (2006). "Immunohistochemical measurement of endothelial cell apoptosis and proliferation in formalin-fixed, paraffin-embedded human cancer tissue." Angiogenesis **9**(4): 193-200.

Chang, J., G. M. Clark, D. C. Allred, S. Mohsin, G. Chamness and R. M. Elledge (2003). "Survival of patients with metastatic breast carcinoma: importance of prognostic markers of the primary tumor." Cancer **97**(3): 545-53.

Chassevent, A., M. L. Jourdan, S. Romain, F. Descotes, M. Colonna, P. M. Martin, et al. (2001). "S-phase fraction and DNA ploidy in 633 T1T2 breast cancers: a standardized flow cytometric study." Clin Cancer Res **7**(4): 909-17.

Chen, K., S. C. Huang and D. Feng (1994). "New estimation methods that directly use the time accumulated counts in the input function in quantitative dynamic PET studies." Phys Med Biol **39**(11): 2073-90.

Chen, X., Y. Hou, M. Tohme, R. Park, V. Khankaldyyan, I. Gonzales-Gomez, et al. (2004). "Pegylated Arg-Gly-Asp peptide: 64Cu labeling and PET imaging of brain tumor alphavbeta3-integrin expression." J Nucl Med **45**(10): 1776-83.

Choi, S. J., J. S. Kim, J. H. Kim, S. J. Oh, J. G. Lee, C. J. Kim, et al. (2005). "[18F]3'-deoxy-3'-fluorothymidine PET for the diagnosis and grading of brain tumors." Eur J Nucl Med Mol Imaging **32**(6): 653-9.

Choi, Y., R. A. Hawkins, S. C. Huang, S. S. Gambhir, R. C. Brunken, M. E. Phelps, et al. (1991). "Parametric images of myocardial metabolic rate of glucose generated from

dynamic cardiac PET and 2-[18F]fluoro-2-deoxy-d-glucose studies." J Nucl Med **32**(4): 733-8.

Choi, Y., S. C. Huang, R. A. Hawkins, C. K. Hoh, J. Krivokapich, D. B. Buxton, et al. (1993). "A refined method for quantification of myocardial oxygen consumption rate using mean transit time with carbon-11-acetate and dynamic PET." J Nucl Med **34**(11): 2038-43.

Christman, D., E. J. Crawford, M. Friedkin and A. P. Wolf (1972). "Detection of DNA synthesis in intact organisms with positron-emitting (methyl- 11 C)thymidine." Proc Natl Acad Sci U S A **69**(4): 988-92.

Citri, A. and Y. Yarden (2006). "EGF-ERBB signalling: towards the systems level." Nat Rev Mol Cell Biol **7**(7): 505-16.

Cleaver, J. E. (1967). "The relationship between the rate of DNA synthesis and its inhibition by ultraviolet light in mammalian cells." Radiat Res **30**(4): 795-810.

Cleij, M. S., CJ. Brady, F. Ell, PJ. (2001). "An improved synthesis of 3'-deoxy-3'[18F]fluorothymdiine ([18F]FLT) and the fate of the precursor, 2,3'-anydro-5'-O-(4,4'-dimethoxytrityl)-thymidine." J Labelled Cod Radiopharm **44**: S871-3.

Cobben, D. C., P. H. Elsinga, A. J. Suurmeijer, W. Vaalburg, B. Maas, P. L. Jager, et al. (2004). "Detection and grading of soft tissue sarcomas of the extremities with (18)F-3'-fluoro-3'-deoxy-L-thymidine." Clin Cancer Res **10**(5): 1685-90.

Cobben, D. C., P. L. Jager, P. H. Elsinga, B. Maas, A. J. Suurmeijer and H. J. Hoekstra (2003). "3'-18F-fluoro-3'-deoxy-L-thymidine: a new tracer for staging metastatic melanoma?" J Nucl Med **44**(12): 1927-32.

Cobben, D. C., B. F. van der Laan, B. Maas, W. Vaalburg, A. J. Suurmeijer, H. J. Hoekstra, et al. (2004). "18F-FLT PET for visualization of laryngeal cancer: comparison with 18F-FDG PET." J Nucl Med **45**(2): 226-31.

Coleman, R. E. (1991). "Single photon emission computed tomography and positron emission tomography in cancer imaging." Cancer **67**(4 Suppl): 1261-70.

Collins, J. M., R. W. Klecker and A. G. Katki (1999). "Suicide prodrugs activated by thymidylate synthase: rationale for treatment and noninvasive imaging of tumors with deoxyuridine analogues." Clin Cancer Res **5**(8): 1976-81.

Conti, P. S., M. M. Alauddin, J. R. Fissekis, B. Schmall and K. A. Watanabe (1995). "Synthesis of 2'-fluoro-5-[11C]-methyl-1-beta-D-arabinofuranosyluracil ([11C]-FMAU): a potential nucleoside analog for in vivo study of cellular proliferation with PET." Nucl Med Biol **22**(6): 783-9.

Coombes, R. C., L. Gibson, E. Hall, M. Emson and J. Bliss (2003). "Aromatase inhibitors as adjuvant therapies in patients with breast cancer." J Steroid Biochem Mol Biol **86**(3-5): 309-11.

Coombes, R. C., E. Hall, L. J. Gibson, R. Paridaens, J. Jassem, T. Delozier, et al. (2004). "A randomized trial of exemestane after two to three years of tamoxifen therapy in

postmenopausal women with primary breast cancer." N Engl J Med **350**(11): 1081-92.

Cooney, M. M., W. van Heeckeren, S. Bhakta, J. Ortiz and S. C. Remick (2006). "Drug insight: vascular disrupting agents and angiogenesis--novel approaches for drug delivery." Nat Clin Pract Oncol **3**(12): 682-92.

Cooper, C. R., C. H. Chay and K. J. Pienta (2002). "The role of alpha(v)beta(3) in prostate cancer progression." Neoplasia **4**(3): 191-4.

Coqueret, O. (2002). "Linking cyclins to transcriptional control." Gene **299**(1-2): 35-55.

Cosgrove, D. and M. Blomley (2004). "Liver tumors: evaluation with contrast-enhanced ultrasound." Abdom Imaging **29**(4): 446-54.

Cross, D. A., D. R. Alessi, P. Cohen, M. Andjelkovich and B. A. Hemmings (1995). "Inhibition of glycogen synthase kinase-3 by insulin mediated by protein kinase B." Nature **378**(6559): 785-9.

Cuadrado, A., A. Carnero, F. Dolfi, B. Jimenez and J. C. Lacal (1993). "Phosphorylcholine: a novel second messenger essential for mitogenic activity of growth factors." Oncogene **8**(11): 2959-68.

Cui, X., R. Schiff, G. Arpino, C. K. Osborne and A. V. Lee (2005). "Biology of progesterone receptor loss in breast cancer and its implications for endocrine therapy." J Clin Oncol **23**(30): 7721-35.

Cully, M., H. You, A. J. Levine and T. W. Mak (2006). "Beyond PTEN mutations: the PI3K pathway as an integrator of multiple inputs during tumorigenesis." Nat Rev Cancer **6**(3): 184-92.

Cunningham, V. J. and T. Jones (1993). "Spectral analysis of dynamic PET studies." J Cereb Blood Flow Metab **13**(1): 15-23.

Cunningham, V. J. and A. Lammertsma (1994). "Radioligand studies in brain: Kinetic analysis of PET data." Medicinal Chemistry Research **5**: 79-96.

Czernin, J. and M. E. Phelps (2002). "Positron emission tomography scanning: current and future applications." Annu Rev Med **53**: 89-112.

d'Argy, R., R. Paul, L. Frankenberg, C. G. Stalnacke, H. Lundqvist, L. Kangas, et al. (1988). "Comparative double-tracer whole-body autoradiography: uptake of 11C-, 18F- and 3H-labeled compounds in rat tumors." Int J Rad Appl Instrum B **15**(5): 577-85.

Davis, P. L., M. J. Staiger, K. B. Harris, M. A. Ganott, J. Klementaviciene, K. S. McCarty, Jr., et al. (1996). "Breast cancer measurements with magnetic resonance imaging, ultrasonography, and mammography." Breast Cancer Res Treat **37**(1): 1-9.

de Jong, I. J., J. Pruim, P. H. Elsinga, W. Vaalburg and H. J. Mensink (2003). "11C-choline positron emission tomography for the evaluation after treatment of localized prostate cancer." Eur Urol **44**(1): 32-8; discussion 38-9.

de Jong, I. J., J. Pruim, P. H. Elsinga, W. Vaalburg and H. J. Mensink (2003). "Preoperative staging of pelvic lymph nodes in prostate cancer by 11C-choline PET." J Nucl Med **44**(3): 331-5.

de Jonge, M. J., C. J. Punt, A. Sparreboom, A. S. Planting, M. E. Peters, J. van De Schraaf, et al. (2002). "Phase I and pharmacologic study of oral ZD9331, a novel nonpolyglutamated thymidylate synthase inhibitor, in adult patients with solid tumors." J Clin Oncol **20**(7): 1923-31.

Dehdashti, F., F. L. Flanagan, J. E. Mortimer, J. A. Katzenellenbogen, M. J. Welch and B. A. Siegel (1999). "Positron emission tomographic assessment of "metabolic flare" to predict response of metastatic breast cancer to antiestrogen therapy." Eur J Nucl Med **26**(1): 51-6.

Del Pozo, M. A., W. B. Kiosses, N. B. Alderson, N. Meller, K. M. Hahn and M. A. Schwartz (2002). "Integrins regulate GTP-Rac localized effector interactions through dissociation of Rho-GDI." Nat Cell Biol **4**(3): 232-9.

Delbeke, D., R. E. Coleman, M. J. Guiberteau, M. L. Brown, H. D. Royal, B. A. Siegel, et al. (2006). "Procedure guideline for tumor imaging with 18F-FDG PET/CT 1.0." J Nucl Med **47**(5): 885-95.

Delpassand, E. S., K. Homayoon, T. Madden, M. Mathai and D. A. Podoloff (2000). "Determination of glomerular filtration rate using a dual-detector gamma camera and the geometric mean of renal activity: correlation with the Tc-99m DTPA plasma clearance method." Clin Nucl Med **25**(4): 258-62.

Deryugina, E. I., M. A. Bourdon, K. Jungwirth, J. W. Smith and A. Y. Strongin (2000). "Functional activation of integrin alpha V beta 3 in tumor cells expressing membrane-type 1 matrix metalloproteinase." Int J Cancer **86**(1): 15-23.

Di Paolo, S., A. Teutonico, E. Ranieri, L. Gesualdo and P. F. Schena (2007). "Monitoring antitumor efficacy of rapamycin in Kaposi sarcoma." Am J Kidney Dis **49**(3): 462-70.

Dimitrakopoulou-Strauss, A., L. G. Strauss, P. Schlag, P. Hohenberger, M. Mohler, F. Oberdorfer, et al. (1998). "Fluorine-18-fluorouracil to predict therapy response in liver metastases from colorectal carcinoma." J Nucl Med **39**(7): 1197-202.

Dittmann, H., B. M. Dohmen, F. Paulsen, K. Eichhorn, S. M. Eschmann, M. Horger, et al. (2003). "[18F]FLT PET for diagnosis and staging of thoracic tumours." Eur J Nucl Med Mol Imaging **30**(10): 1407-12.

Dowsett, M., C. Archer, L. Assersohn, R. K. Gregory, P. A. Ellis, J. Salter, et al. (1999). "Clinical studies of apoptosis and proliferation in breast cancer." Endocr Relat Cancer **6**(1): 25-8.

Dowsett, M., I. E. Smith, S. R. Ebbs, J. M. Dixon, A. Skene, R. A'Hern, et al. (2007). "Prognostic value of Ki67 expression after short-term presurgical endocrine therapy for primary breast cancer." J Natl Cancer Inst **99**(2): 167-70.

DuBois D, D. E. (1916). "A formula to estimate the approximate surface area if height and weight be known. ." Arch Intern Medicine. 1916; **17**: 863-71.

Dyson, N. (1998). "The regulation of E2F by pRB-family proteins." Genes Dev **12**(15): 2245-62.

Eary, J. F., D. A. Mankoff, A. M. Spence, M. S. Berger, A. Olshen, J. M. Link, et al. (1999). "2-[C-11]thymidine imaging of malignant brain tumors." Cancer Res **59**(3): 615-21.

Eary, J. F., D. A. Mankoff, J. Thompson, G. Philli and K. Krohn (1999). Tumor Metabolism and Proliferation Using Quantitative PET Imaging in Renal Cell Carcinoma Patients Treated with IL-2. . ASCO Annual Meeting.

EBCTCG (1992). "Systemic treatment of early breast cancer by hormonal, cytotoxic, or immune therapy. 133 randomised trials involving 31,000 recurrences and 24,000 deaths among 75,000 women - Early Breast Cancer Trialists' Collaborative Group." Lancet **339**(8785): 71-85.

Eberhard, A., S. Kahlert, V. Goede, B. Hemmerlein, K. H. Plate and H. G. Augustin (2000). "Heterogeneity of angiogenesis and blood vessel maturation in human tumors: implications for antiangiogenic tumor therapies." Cancer Res **60**(5): 1388-93.

Eberl, S., A. R. Anayat, R. R. Fulton, P. K. Hooper and M. J. Fulham (1997). "Evaluation of two population-based input functions for quantitative neurological FDG PET studies." Eur J Nucl Med **24**(3): 299-304.

Eliceiri, B. P., R. Klemke, S. Stromblad and D. A. Cheresh (1998). "Integrin alphavbeta3 requirement for sustained mitogen-activated protein kinase activity during angiogenesis." J Cell Biol **140**(5): 1255-63.

Ellis, M. J., A. Coop, B. Singh, Y. Tao, A. Llombart-Cussac, F. Janicke, et al. (2003). "Letrozole inhibits tumor proliferation more effectively than tamoxifen independent of HER1/2 expression status." Cancer Res **63**(19): 6523-31.

Ellis, M. J., E. Rosen, H. Dressman and J. Marks (2003). "Neoadjuvant comparisons of aromatase inhibitors and tamoxifen: pretreatment determinants of response and on-treatment effect." J Steroid Biochem Mol Biol **86**(3-5): 301-7.

Elstrom, R. L., D. E. Bauer, M. Buzzai, R. Karnauskas, M. H. Harris, D. R. Plas, et al. (2004). "Akt stimulates aerobic glycolysis in cancer cells." Cancer Res **64**(11): 3892-9.

Eskens, F. A., H. Dumez, R. Hoekstra, A. Perschl, C. Brindley, S. Bottcher, et al. (2003). "Phase I and pharmacokinetic study of continuous twice weekly intravenous administration of Cilengitide (EMD 121974), a novel inhibitor of the integrins alphavbeta3 and alphavbeta5 in patients with advanced solid tumours." Eur J Cancer **39**(7): 917-26.

Fanti, S., C. Nanni, V. Ambrosini, M. D. Gross, D. Rubello and M. Farsad (2007). "PET in genitourinary tract cancers." Q J Nucl Med Mol Imaging **51**(3): 260-71.

Fearon, E. R. and B. Vogelstein (1990). "A genetic model for colorectal tumorigenesis." Cell **61**(5): 759-67.

Flemington, E. K., S. H. Speck and W. G. Kaelin, Jr. (1993). "E2F-1-mediated transactivation is inhibited by complex formation with the retinoblastoma susceptibility gene product." Proc Natl Acad Sci U S A **90**(15): 6914-8.

Flexner, C., C. van der Horst, M. A. Jacobson, W. Powderly, F. Duncanson, D. Ganes, et al. (1994). "Relationship between plasma concentrations of 3'-deoxy-3'-fluorothymidine (alovudine) and antiretroviral activity in two concentration-controlled trials." J Infect Dis **170**(6): 1394-403.

Foekens, J. A., H. A. Peters, N. Grebenchtchikov, M. P. Look, M. E. Meijer-van Gelder, A. Geurts-Moespot, et al. (2001). "High tumor levels of vascular endothelial growth factor predict poor response to systemic therapy in advanced breast cancer." Cancer Res **61**(14): 5407-14.

Folkman, J. (1971). "Tumor angiogenesis: therapeutic implications." N Engl J Med **285**(21): 1182-6.

Folkman, J. (2002). "Role of angiogenesis in tumor growth and metastasis." Semin Oncol **29**(6 Suppl 16): 15-8.

Follen, M. and D. Schottenfeld (2001). "Surrogate endpoint biomarkers and their modulation in cervical chemoprevention trials." Cancer **91**(9): 1758-76.

Fox, S. B., R. D. Leek, M. P. Weekes, R. M. Whitehouse, K. C. Gatter and A. L. Harris (1995). "Quantitation and prognostic value of breast cancer angiogenesis: comparison of microvessel density, Chalkley count, and computer image analysis." J Pathol **177**(3): 275-83.

Fox, S. B., G. D. Turner, R. D. Leek, R. M. Whitehouse, K. C. Gatter and A. L. Harris (1995). "The prognostic value of quantitative angiogenesis in breast cancer and

role of adhesion molecule expression in tumor endothelium." Breast Cancer Res Treat **36**(2): 219-26.

Francis, D. L., A. Freeman, D. Visvikis, D. C. Costa, S. K. Luthra, M. Novelli, et al. (2003). "In vivo imaging of cellular proliferation in colorectal cancer using positron emission tomography." Gut **52**(11): 1602-6.

Francis, D. L., D. Visvikis, D. C. Costa, T. H. Arulampalam, C. Townsend, S. K. Luthra, et al. (2003). "Potential impact of [18F]3'-deoxy-3'-fluorothymidine versus [18F]fluoro-2-deoxy-D-glucose in positron emission tomography for colorectal cancer." Eur J Nucl Med Mol Imaging **30**(7): 988-94.

Gagliardi, A. and D. C. Collins (1993). "Inhibition of angiogenesis by antiestrogens." Cancer Res **53**(3): 533-5.

Gagliardi, A. R., B. Hennig and D. C. Collins (1996). "Antiestrogens inhibit endothelial cell growth stimulated by angiogenic growth factors." Anticancer Res **16**(3A): 1101-6.

Gallagher, B. M., A. Ansari, H. Atkins, V. Casella, D. R. Christman, J. S. Fowler, et al. (1977). "Radiopharmaceuticals XXVII. 18F-labeled 2-deoxy-2-fluoro-d-glucose as a radiopharmaceutical for measuring regional myocardial glucose metabolism in vivo: tissue distribution and imaging studies in animals." J Nucl Med **18**(10): 990-6.

Garber, K. (2006). "Energy deregulation: licensing tumors to grow." Science **312**(5777): 1158-9.

Gasparini, G., P. C. Brooks, E. Biganzoli, P. B. Vermeulen, E. Bonoldi, L. Y. Dirix, et al. (1998). "Vascular integrin alpha(v)beta3: a new prognostic indicator in breast cancer." Clin Cancer Res **4**(11): 2625-34.

Germano, G., B. C. Chen, S. C. Huang, S. S. Gambhir, E. J. Hoffman and M. E. Phelps (1992). "Use of the abdominal aorta for arterial input function determination in hepatic and renal PET studies." J Nucl Med **33**(4): 613-20.

Geworski, L., B. O. Knoop, M. de Wit, V. Ivancevic, R. Bares and D. L. Munz (2002). "Multicenter comparison of calibration and cross calibration of PET scanners." J Nucl Med **43**(5): 635-9.

Giancotti, F. G. and E. Ruoslahti (1999). "Integrin signaling." Science **285**(5430): 1028-32.

Ginos, J. Z., A. J. Cooper, V. Dhawan, J. C. Lai, S. C. Strother, N. Alcock, et al. (1987). "[13N]cisplatin PET to assess pharmacokinetics of intra-arterial versus intravenous chemotherapy for malignant brain tumors." J Nucl Med **28**(12): 1844-52.

Glaser, M., M. Morrison, M. Solbakken, J. Arukwe, H. Karlsen, U. Wiggen, et al. (2008). "Radiosynthesis and biodistribution of cyclic RGD peptides conjugated with novel [18F]fluorinated aldehyde-containing prosthetic groups." Bioconjug Chem **19**(4): 951-7.

Glunde, K., V. Raman, N. Mori and Z. M. Bhujwalla (2005). "RNA interference-mediated choline kinase suppression in breast cancer cells induces differentiation and reduces proliferation." Cancer Res **65**(23): 11034-43.

Gomez-Lazaro, M., F. J. Fernandez-Gomez and J. Jordan (2004). "p53: twenty five years understanding the mechanism of genome protection." J Physiol Biochem **60**(4): 287-307.

Gort, E. H., A. J. Groot, T. L. Derks van de Ven, P. van der Groep, I. Verlaan, T. van Laar, et al. (2006). "Hypoxia-inducible factor-1alpha expression requires PI 3-kinase activity and correlates with Akt1 phosphorylation in invasive breast carcinomas." Oncogene.

Goss, P. E., J. N. Ingle, S. Martino, N. J. Robert, H. B. Muss, M. J. Piccart, et al. (2005). "Randomized trial of letrozole following tamoxifen as extended adjuvant therapy in receptor-positive breast cancer: updated findings from NCIC CTG MA.17." J Natl Cancer Inst **97**(17): 1262-71.

Graflund, M., B. Sorbe, M. Bryne and M. Karlsson (2002). "The prognostic value of a histologic grading system, DNA profile, and MIB-1 expression in early stages of cervical squamous cell carcinomas." Int J Gynecol Cancer **12**(2): 149-57.

Grierson, J. R. and A. F. Shields (2000). "Radiosynthesis of 3'-deoxy-3'-[(18)F]fluorothymidine: [(18)F]FLT for imaging of cellular proliferation in vivo." Nucl Med Biol **27**(2): 143-56.

Groot-Wassink, T., E. O. Aboagye, M. Glaser, N. R. Lemoine and G. Vassaux (2002). "Adenovirus biodistribution and noninvasive imaging of gene expression in vivo by positron emission tomography using human sodium/iodide symporter as reporter gene." Hum Gene Ther **13**(14): 1723-35.

Grootoonk, S., T. J. Spinks, D. Sashin, N. M. Spyrou and T. Jones (1996). "Correction for scatter in 3D brain PET using a dual energy window method." Phys Med Biol **41**(12): 2757-74.

Group, E. B. C. T. C. (1992). "Systemic treatment of early breast cancer by hormonal, cytotoxic, or immune therapy. 133 randomised trials involving 31,000 recurrences and 24,000 deaths among 75,000 women." Lancet **339**(8785): 71-85.

Gudjonssona, O., M. Bergstrom, S. Kristjansson, F. Wu, G. Nyberg, K. J. Fasth, et al. (2001). "Analysis of 76Br-BrdU in DNA of brain tumors after a PET study does not support its use as a proliferation marker." Nucl Med Biol **28**(1): 59-65.

Gutheil, J. C., T. N. Campbell, P. R. Pierce, J. D. Watkins, W. D. Huse, D. J. Bodkin, et al. (2000). "Targeted antiangiogenic therapy for cancer using Vitaxin: a humanized monoclonal antibody to the integrin alphavbeta3." Clin Cancer Res **6**(8): 3056-61.

Haas, R. L., D. de Jong, R. A. Valdes Olmos, C. A. Hoefnagel, I. van den Heuvel, S. F. Zerp, et al. (2004). "In vivo imaging of radiation-induced apoptosis in follicular lymphoma patients." Int J Radiat Oncol Biol Phys **59**(3): 782-7.

Hall P.A, L. D. A., Wright N.A (1991). Assessment of Cell Proliferation in Clinical Practice, Springer-Verlag.

Hall, P. A., D. A. Levison, A. L. Woods, C. C. Yu, D. B. Kellock, J. A. Watkins, et al. (1990). "Proliferating cell nuclear antigen (PCNA) immunolocalization in paraffin sections: an index of cell proliferation with evidence of deregulated expression in some neoplasms." J Pathol **162**(4): 285-94.

Hanahan, D., G. Bergers and E. Bergsland (2000). "Less is more, regularly: metronomic dosing of cytotoxic drugs can target tumor angiogenesis in mice." J Clin Invest **105**(8): 1045-7.

Hanahan, D. and R. A. Weinberg (2000). "The hallmarks of cancer." Cell **100**(1): 57-70.

Hansen, S., D. A. Grabau, F. B. Sorensen, M. Bak, W. Vach and C. Rose (2000). "The prognostic value of angiogenesis by Chalkley counting in a confirmatory study design on 836 breast cancer patients." Clin Cancer Res **6**(1): 139-46.

Hara, T., N. Kosaka and H. Kishi (1998). "PET imaging of prostate cancer using carbon-11-choline." J Nucl Med **39**(6): 990-5.

Harbour, J. W. and D. C. Dean (2000). "The Rb/E2F pathway: expanding roles and emerging paradigms." Genes Dev **14**(19): 2393-409.

Haubner, R., W. A. Weber, A. J. Beer, E. Vabuliene, D. Reim, M. Sarbia, et al. (2005). "Noninvasive visualization of the activated alphavbeta3 integrin in cancer patients by positron emission tomography and [18F]Galacto-RGD." PLoS Med **2**(3): e70.

Haubner, R., H. J. Wester, F. Burkhart, R. Senekowitsch-Schmidtke, W. Weber, S. L. Goodman, et al. (2001). "Glycosylated RGD-containing peptides: tracer for tumor targeting and angiogenesis imaging with improved biokinetics." J Nucl Med **42**(2): 326-36.

Haubner, R., H. J. Wester, U. Reuning, R. Senekowitsch-Schmidtke, B. Diefenbach, H. Kessler, et al. (1999). "Radiolabeled alpha(v)beta3 integrin antagonists: a new class of tracers for tumor targeting." J Nucl Med **40**(6): 1061-71.

Henson, E. S. and S. B. Gibson (2006). "Surviving cell death through epidermal growth factor (EGF) signal transduction pathways: Implications for cancer therapy." Cell Signal.

Hentschel, M., T. Paulus, M. Mix, E. Moser, E. U. Nitzsche and I. Brink (2007). "Analysis of blood flow and glucose metabolism in mammary carcinomas and normal breast: a H2(15)O PET and 18F-FDG PET study." Nucl Med Commun **28**(10): 789-97.

Herbst, R. S., K. R. Hess, H. T. Tran, J. E. Tseng, N. A. Mullani, C. Charnsangavej, et al. (2002). "Phase I study of recombinant human endostatin in patients with advanced solid tumors." J Clin Oncol **20**(18): 3792-803.

Hoffman, R. M. (1986). PET Principles and Quantitation, Raven Press, New York, USA.

Hoffman, R. M. (1999). "Orthotopic metastatic mouse models for anticancer drug discovery and evaluation: a bridge to the clinic." Invest New Drugs **17**(4): 343-59.

Hortobagyi, G. N. (2005). "Trastuzumab in the treatment of breast cancer." N Engl J Med **353**(16): 1734-6.

Humphries, J. D., A. Byron and M. J. Humphries (2006). "Integrin ligands at a glance." J Cell Sci **119**(Pt 19): 3901-3.

Iida, H., C. G. Rhodes, R. de Silva, L. I. Araujo, P. M. Bloomfield, A. A. Lammertsma, et al. (1992). "Use of the left ventricular time-activity curve as a noninvasive input function in dynamic oxygen-15-water positron emission tomography." J Nucl Med **33**(9): 1669-77.

Indrevoll, B., G. M. Kindberg, M. Solbakken, E. Bjurgert, J. H. Johansen, H. Karlsen, et al. (2006). "NC-100717: a versatile RGD peptide scaffold for angiogenesis imaging." Bioorg Med Chem Lett **16**(24): 6190-3.

Inoue, T., E. E. Kim, S. Wallace, D. J. Yang, F. C. Wong, P. Bassa, et al. (1996). "Positron emission tomography using [18F]fluorotamoxifen to evaluate therapeutic responses in patients with breast cancer: preliminary study." Cancer Biother Radiopharm **11**(4): 235-45.

Isakoff, S. J., J. A. Engelman, H. Y. Irie, J. Luo, S. M. Brachmann, R. V. Pearline, et al. (2005). "Breast cancer-associated PIK3CA mutations are oncogenic in mammary epithelial cells." Cancer Res **65**(23): 10992-1000.

Jackman, A. L., G. A. Taylor, A. H. Calvert and K. R. Harrap (1984). "Modulation of anti-metabolite effects. Effects of thymidine on the efficacy of the quinazoline-based thymidylate synthetase inhibitor, CB3717." Biochem Pharmacol **33**(20): 3269-75.

Jacquemier, J. D., F. M. Penault-Llorca, F. Bertucci, Z. Z. Sun, G. F. Houvenaeghel, J. A. Geneix, et al. (1998). "Angiogenesis as a prognostic marker in breast carcinoma with conventional adjuvant chemotherapy: a multiparametric and immunohistochemical analysis." J Pathol **184**(2): 130-5.

Johnston, S. R. (2006). "Clinical efforts to combine endocrine agents with targeted therapies against epidermal growth factor receptor/human epidermal growth factor receptor 2 and mammalian target of rapamycin in breast cancer." Clin Cancer Res **12**(3 Pt 2): 1061s-1068s.

Katz-Brull, R. and H. Degani (1996). "Kinetics of choline transport and phosphorylation in human breast cancer cells; NMR application of the zero trans method." Anticancer Res **16**(3B): 1375-80.

Kaufmann, M., G. N. Hortobagyi, A. Goldhirsch, S. Scholl, A. Makris, P. Valagussa, et al. (2006). "Recommendations from an international expert panel on the use of neoadjuvant (primary) systemic treatment of operable breast cancer: an update." J Clin Oncol **24**(12): 1940-9.

Kempson, R. L. (1976). "Editorial: Mitosis counting--II." Hum Pathol **7**(4): 482-3.

Kenny, L., Coombes, R.C., Vigushin, D.M., Al-Nahhas, A., Shousha, S., Aboagye, E.O. (2007). "Imaging early changes in proliferation at 1 week post chemotherapy: a pilot study in breast cancer patients with 3'-deoxy-3'-[(18)F]fluorothymidine positron emission tomography." Eur J Nucl Med Mol Imaging **34**(9): 1339-47.

Kenny, L. M., Coombes, R.C., Oulie, I. et al (2008). "Phase 1 Trial of the Positron-Emitting Arg-Gly-Asp (RGD) Peptide Radioligand 18F-AH111585 in Breast Cancer Patients. ." JNM

Kenny, L. M., D. M. Vigushin, A. Al-Nahhas, S. Osman, S. K. Luthra, S. Shousha, et al. (2005). "Quantification of cellular proliferation in tumor and normal tissues of

patients with breast cancer by [18F]fluorothymidine-positron emission tomography imaging: evaluation of analytical methods." Cancer Res **65**(21): 10104-12.

Kety, S. (1951). "The theory and applications of exchange of inert gas at the lungs and tissues." Pharmacol Res **3**: 1-41.

Keyes, J. W., Jr. (1995). "SUV: standard uptake or silly useless value?" J Nucl Med **36**(10): 1836-9.

Khan, N., N. Oriuchi, H. Ninomiya, T. Higuchi, H. Kamada and K. Endo (2004). "Positron emission tomographic imaging with 11C-choline in differential diagnosis of head and neck tumors: comparison with 18F-FDG PET." Ann Nucl Med **18**(5): 409-17.

Khan, N., N. Oriuchi, H. Zhang, T. Higuchi, M. Tian, T. Inoue, et al. (2003). "A comparative study of 11C-choline PET and [18F]fluorodeoxyglucose PET in the evaluation of lung cancer." Nucl Med Commun **24**(4): 359-66.

Kim, R. H., M. Peters, Y. Jang, W. Shi, M. Pintilie, G. C. Fletcher, et al. (2005). "DJ-1, a novel regulator of the tumor suppressor PTEN." Cancer Cell **7**(3): 263-73.

Kjaer, A. (2006). "Molecular imaging of cancer using PET and SPECT." Adv Exp Med Biol **587**: 277-84.

Klos, K. S., S. L. Wyszomierski, M. Sun, M. Tan, X. Zhou, P. Li, et al. (2006). "ErbB2 increases vascular endothelial growth factor protein synthesis via activation of mammalian target of rapamycin/p70S6K leading to increased angiogenesis and

spontaneous metastasis of human breast cancer cells." Cancer Res **66**(4): 2028-37.

Knudsen, E. S. and K. E. Knudsen (2006). "Retinoblastoma tumor suppressor: where cancer meets the cell cycle." Exp Biol Med (Maywood) **231**(7): 1271-81.

Kobayashi, S., T. J. Boggon, T. Dayaram, P. A. Janne, O. Kocher, M. Meyerson, et al. (2005). "EGFR mutation and resistance of non-small-cell lung cancer to gefitinib." N Engl J Med **352**(8): 786-92.

Kobori, O., Y. Kirihara, N. Kosaka and T. Hara (1999). "Positron emission tomography of esophageal carcinoma using (11)C-choline and (18)F-fluorodeoxyglucose: a novel method of preoperative lymph node staging." Cancer **86**(9): 1638-48.

Kong, X. B., Q. Y. Zhu, P. M. Vidal, K. A. Watanabe, B. Polsky, D. Armstrong, et al. (1992). "Comparisons of anti-human immunodeficiency virus activities, cellular transport, and plasma and intracellular pharmacokinetics of 3'-fluoro-3'-deoxythymidine and 3'-azido-3'-deoxythymidine." Antimicrob Agents Chemother **36**(4): 808-18.

Korkolopoulou, P., M. Angelopoulou, M. Siakantari, F. Mitropoulos, T. Vassilakopoulos, H. Zorzos, et al. (2001). "Evaluation of DNA topoisomerase IIalpha expression provides independent prognostic information in non-Hodgkin's lymphomas." Histopathology **38**(1): 45-53.

Korn, E. L., S. G. Arbuck, J. M. Pluda, R. Simon, R. S. Kaplan and M. C. Christian (2001). "Clinical trial designs for cytostatic agents: are new approaches needed?" J Clin Oncol **19**(1): 265-72.

Koukourakis, M. I., A. Giatromanolaki, E. Sivridis and I. Fezoulidis (2000). "Cancer vascularization: implications in radiotherapy?" Int J Radiat Oncol Biol Phys **48**(2): 545-53.

Krasna, L., I. Netikova, A. Chaloupkova, E. Taislova, M. Zimovjanova, P. Vesely, et al. (2003). "Assessment of in vitro drug resistance of human breast cancer cells subcultured from biopsy specimens." Anticancer Res **23**(3B): 2593-9.

Krohn, K. A., D. A. Mankoff, M. Muzi, J. M. Link and A. M. Spence (2005). "True tracers: comparing FDG with glucose and FLT with thymidine." Nucl Med Biol **32**(7): 663-71.

Kyzer, S. and P. H. Gordon (1997). "Determination of proliferative activity in colorectal carcinoma using monoclonal antibody Ki67." Dis Colon Rectum **40**(3): 322-5.

Lajtha, L. (1963). "On the concept of the cell cycle." J Cell Comp Physiol **60 (Suppl 1)**: 143-145.

Lane, D. P. (1992). "Cancer. p53, guardian of the genome." Nature **358**(6381): 15-6.

Larson, S. M. and L. H. Schwartz (2006). "18F-FDG PET as a candidate for "qualified biomarker": functional assessment of treatment response in oncology." J Nucl Med **47**(6): 901-3.

Leyton, J., J. R. Latigo, M. Perumal, H. Dhaliwal, Q. He and E. O. Aboagye (2005). "Early detection of tumor response to chemotherapy by 3'-deoxy-3'-[18F]fluorothymidine positron emission tomography: the effect of cisplatin on a fibrosarcoma tumor model in vivo." Cancer Res **65**(10): 4202-10.

Liu, D., O. C. Hutchinson, S. Osman, P. Price, P. Workman and E. O. Aboagye (2002). "Use of radiolabelled choline as a pharmacodynamic marker for the signal transduction inhibitor geldanamycin." Br J Cancer **87**(7): 783-9.

Liu, S. (2006). "Radiolabeled multimeric cyclic RGD peptides as integrin alphavbeta3 targeted radiotracers for tumor imaging." Mol Pharm **3**(5): 472-87.

Livieratos, L., K. Rajappan, L. Stegger, K. Schafers, D. L. Bailey and P. G. Camici (2006). "Respiratory gating of cardiac PET data in list-mode acquisition." Eur J Nucl Med Mol Imaging: 1-5.

Lu, L., M. Bergstrom, K. J. Fasth, F. Wu, B. Eriksson and B. Langstrom (1999). "Elimination of nonspecific radioactivity from [76Br]bromide in PET study with [76Br]bromodeoxyuridine." Nucl Med Biol **26**(7): 795-802.

Lu, L., L. Samuelsson, M. Bergstrom, K. Sato, K. J. Fasth and B. Langstrom (2002). "Rat studies comparing 11C-FMAU, 18F-FLT, and 76Br-BFU as proliferation markers." J Nucl Med **43**(12): 1688-98.

MacCallum, D. E. and P. A. Hall (1999). "Biochemical Characterization of pKi67 with the Identification of a Mitotic-Specific Form Associated with Hyperphosphorylation and Altered DNA Binding." Experimental Cell Research **252**(1): 186-198.

Machulla, H. J. B., A. Kuntzsch, M. Piert, M. Wei, R. Grierson, JR. (2000). "Simplified labeling approach for syntehsizing 3'-deoxy-3'-[18F]fluorothymidine ([18F]FLT." J Radioanal Nucl Chem **243**: 843-6.

Maehama, T. and J. E. Dixon (1998). "The tumor suppressor, PTEN/MMAC1, dephosphorylates the lipid second messenger, phosphatidylinositol 3,4,5-trisphosphate." J Biol Chem **273**(22): 13375-8.

Malumbres, M. and M. Barbacid (2001). "To cycle or not to cycle: a critical decision in cancer." Nat Rev Cancer **1**(3): 222-31.

Mankoff, D. A., L. K. Dunnwald, J. R. Gralow, G. K. Ellis, A. Charlop, T. J. Lawton, et al. (2002). "Blood flow and metabolism in locally advanced breast cancer: relationship to response to therapy." J Nucl Med **43**(4): 500-9.

Mankoff, D. A., L. K. Dunnwald, J. R. Gralow, G. K. Ellis, E. K. Schubert, J. Tseng, et al. (2003). "Changes in blood flow and metabolism in locally advanced breast cancer treated with neoadjuvant chemotherapy." J Nucl Med **44**(11): 1806-14.

Mankoff, D. A., A. F. Shields, M. M. Graham, J. M. Link, J. F. Eary and K. A. Krohn (1998). "Kinetic analysis of 2-[carbon-11]thymidine PET imaging studies: compartmental model and mathematical analysis." J Nucl Med **39**(6): 1043-55.

Mankoff, D. A., A. F. Shields, M. M. Graham, J. M. Link and K. A. Krohn (1996). "A graphical analysis method to estimate blood-to-tissue transfer constants for tracers with labeled metabolites." J Nucl Med **37**(12): 2049-57.

Mankoff, D. A., A. F. Shields, J. M. Link, M. M. Graham, M. Muzi, L. M. Peterson, et al. (1999). "Kinetic analysis of 2-[11C]thymidine PET imaging studies: validation studies." J Nucl Med **40**(4): 614-24.

Marshall, C. (1999). "How do small GTPase signal transduction pathways regulate cell cycle entry?" Curr Opin Cell Biol **11**(6): 732-6.

Martiat, P., A. Ferrant, D. Labar, M. Cogneau, A. Bol, C. Michel, et al. (1988). "In vivo measurement of carbon-11 thymidine uptake in non-Hodgkin's lymphoma using positron emission tomography." J Nucl Med **29**(10): 1633-7.

Matsunaga, T., S. Kotamraju, S. V. Kalivendi, A. Dhanasekaran, J. Joseph and B. Kalyanaraman (2004). "Ceramide-induced intracellular oxidant formation, iron signaling, and apoptosis in endothelial cells: protective role of endogenous nitric oxide." J Biol Chem **279**(27): 28614-24.

Mazoyer, B. M., R. H. Huesman, T. F. Budinger and B. L. Knittel (1986). "Dynamic PET data analysis." ournal of Computer Assisted Tomography **10**: 645-653.

McCarty, K. S., Jr. and K. S. McCarty, Sr. (1984). "Histochemical approaches to steroid receptor analyses." Semin Diagn Pathol **1**(4): 297-308.

McCormick, D. and P. A. Hall (1992). "The complexities of proliferating cell nuclear antigen." Histopathology **21**(6): 591-4.

Meikle, S. R., J. C. Matthews, C. S. Brock, P. Wells, R. J. Harte, V. J. Cunningham, et al. (1998). "Pharmacokinetic assessment of novel anti-cancer drugs using spectral

analysis and positron emission tomography: a feasibility study." Cancer Chemother Pharmacol **42**(3): 183-93.

Michaelis, L. C. and M. J. Ratain (2006). "Measuring response in a post-RECIST world: from black and white to shades of grey." Nat Rev Cancer **6**(5): 409-14.

Mieog, J. S., J. A. van der Hage and C. J. van de Velde (2007). "Neoadjuvant chemotherapy for operable breast cancer." Br J Surg **94**(10): 1189-200.

Migliaccio, A., M. Di Domenico, G. Castoria, A. de Falco, P. Bontempo, E. Nola, et al. (1996). "Tyrosine kinase/p21ras/MAP-kinase pathway activation by estradiol-receptor complex in MCF-7 cells." Embo J **15**(6): 1292-300.

Migliaccio, A., D. Piccolo, G. Castoria, M. Di Domenico, A. Bilancio, M. Lombardi, et al. (1998). "Activation of the Src/p21ras/Erk pathway by progesterone receptor via cross-talk with estrogen receptor." Embo J **17**(7): 2008-18.

Miller, J. C., H. H. Pien, D. Sahani, A. G. Sorensen and J. H. Thrall (2005). "Imaging angiogenesis: applications and potential for drug development." J Natl Cancer Inst **97**(3): 172-87.

Minn, H., K. R. Zasadny, L. E. Quint and R. L. Wahl (1995). "Lung cancer: reproducibility of quantitative measurements for evaluating 2-[F-18]-fluoro-2-deoxy-D-glucose uptake at PET." Radiology **196**(1): 167-73.

Miwa, M., M. Ura, M. Nishida, N. Sawada, T. Ishikawa, K. Mori, et al. (1998). "Design of a novel oral fluoropyrimidine carbamate, capecitabine, which generates 5-fluorouracil

selectively in tumours by enzymes concentrated in human liver and cancer tissue." Eur J Cancer **34**(8): 1274-81.

Mochen, C., R. Giardini, A. Costa and R. Silvestrini (1997). "MIB-1 and S-phase cell fraction predict survival in non-Hodgkin's lymphomas." Cell Prolif **30**(1): 37-47.

Molinari, M. (2000). "Cell cycle checkpoints and their inactivation in human cancer." Cell Prolif **33**(5): 261-74.

Monazzam, A., R. Josephsson, C. Blomqvist, J. Carlsson, B. Langstrom and M. Bergstrom (2007). "Application of the multicellular tumour spheroid model to screen PET tracers for analysis of early response of chemotherapy in breast cancer." Breast Cancer Res **9**(4): R45.

Morse, D. L., N. Raghunand, P. Sadarangani, S. Murthi, C. Job, S. Day, et al. (2007). "Response of choline metabolites to docetaxel therapy is quantified in vivo by localized (31)P MRS of human breast cancer xenografts and in vitro by high-resolution (31)P NMR spectroscopy of cell extracts." Magn Reson Med **58**(2): 270-80.

Mortimer, J. E., F. Dehdashti, B. A. Siegel, J. A. Katzenellenbogen, P. Fracasso and M. J. Welch (1996). "Positron emission tomography with 2-[18F]Fluoro-2-deoxy-D-glucose and 16alpha-[18F]fluoro-17beta-estradiol in breast cancer: correlation with estrogen receptor status and response to systemic therapy." Clin Cancer Res **2**(6): 933-9.

Munch-Petersen, B., L. Cloos, G. Tyrsted and S. Eriksson (1991). "Diverging substrate specificity of pure human thymidine kinases 1 and 2 against antiviral dideoxynucleosides." J Biol Chem **266**(14): 9032-8.

Murohara, T., B. Witzenbichler, I. Spyridopoulos, T. Asahara, B. Ding, A. Sullivan, et al. (1999). "Role of endothelial nitric oxide synthase in endothelial cell migration." Arterioscler Thromb Vasc Biol **19**(5): 1156-61.

Muzi, M., H. Vesselle, J. R. Grierson, D. A. Mankoff, R. A. Schmidt, L. Peterson, et al. (2005). "Kinetic analysis of 3'-deoxy-3'-fluorothymidine PET studies: validation studies in patients with lung cancer." J Nucl Med **46**(2): 274-82.

Nabel, E. G. (2002). "CDKs and CKIs: molecular targets for tissue remodelling." Nat Rev Drug Discov **1**(8): 587-98.

Nahta, R. and F. J. Esteva (2003). "HER-2-targeted therapy: lessons learned and future directions." Clin Cancer Res **9**(14): 5078-84.

Namba, R., L. J. Young, C. K. Abbey, L. Kim, P. Damonte, A. D. Borowsky, et al. (2006). "Rapamycin inhibits growth of premalignant and malignant mammary lesions in a mouse model of ductal carcinoma in situ." Clin Cancer Res **12**(8): 2613-21.

Nemeth, J. A., M. L. Cher, Z. Zhou, C. Mullins, S. Bhagat and M. Trikha (2003). "Inhibition of alpha(v)beta3 integrin reduces angiogenesis, bone turnover, and tumor cell proliferation in experimental prostate cancer bone metastases." Clin Exp Metastasis **20**(5): 413-20.

Nishiyama, Y., Y. Yamamoto, T. Monden, Y. Sasakawa, K. Tsutsui, H. Wakabayashi, et al. (2005). "Evaluation of delayed additional FDG PET imaging in patients with pancreatic tumour." Nucl Med Commun **26**(10): 895-901.

Nurcombe, V., C. E. Smart, H. Chipperfield, S. M. Cool, B. Boilly and H. Hondermarck (2000). "The proliferative and migratory activities of breast cancer cells can be differentially regulated by heparan sulfates." J Biol Chem **275**(39): 30009-18.

O'Reilly, M. S., T. Boehm, Y. Shing, N. Fukai, G. Vasios, W. S. Lane, et al. (1997). "Endostatin: an endogenous inhibitor of angiogenesis and tumor growth." Cell **88**(2): 277-85.

Oken, M. M., R. H. Creech, D. C. Tormey, J. Horton, T. E. Davis, E. T. McFadden, et al. (1982). "Toxicity and response criteria of the Eastern Cooperative Oncology Group." Am J Clin Oncol **5**(6): 649-55.

Padhani, A. R. and A. Dzik-Jurasz (2004). "Perfusion MR imaging of extracranial tumor angiogenesis." Top Magn Reson Imaging **15**(1): 41-57.

Parulekar, W. R. and E. A. Eisenhauer (2004). "Phase I trial design for solid tumor studies of targeted, non-cytotoxic agents: theory and practice." J Natl Cancer Inst **96**(13): 990-7.

Pasqualini, R., E. Koivunen and E. Ruoslahti (1997). "Alpha v integrins as receptors for tumor targeting by circulating ligands." Nat Biotechnol **15**(6): 542-6.

Patlak, C. S. and R. G. Blasberg (1985). "Graphical evaluation of blood-to-brain transfer constants from multiple-time uptake data. Generalizations." J Cereb Blood Flow Metab **5**(4): 584-90.

Pauwels, E. K., E. J. Sturm, E. Bombardieri, F. J. Cleton and M. P. Stokkel (2000). "Positron-emission tomography with [18F]fluorodeoxyglucose. Part I. Biochemical uptake mechanism and its implication for clinical studies." J Cancer Res Clin Oncol **126**(10): 549-59.

Pearson, G., F. Robinson, T. Beers Gibson, B. E. Xu, M. Karandikar, K. Berman, et al. (2001). "Mitogen-activated protein (MAP) kinase pathways: regulation and physiological functions." Endocr Rev **22**(2): 153-83.

Pecheur, I., O. Peyruchaud, C. M. Serre, J. Guglielmi, C. Voland, F. Bourre, et al. (2002). "Integrin alpha(v)beta3 expression confers on tumor cells a greater propensity to metastasize to bone." Faseb J **16**(10): 1266-8.

Perumal, M., R. G. Pillai, H. Barthel, J. Leyton, J. R. Latigo, M. Forster, et al. (2006). "Redistribution of nucleoside transporters to the cell membrane provides a novel approach for imaging thymidylate synthase inhibition by positron emission tomography." Cancer Res **66**(17): 8558-64.

Pieterman, R. M., T. H. Que, P. H. Elsinga, J. Pruim, J. W. van Putten, A. T. Willemsen, et al. (2002). "Comparison of (11)C-choline and (18)F-FDG PET in primary diagnosis and staging of patients with thoracic cancer." J Nucl Med **43**(2): 167-72.

Pietras, K. and D. Hanahan (2005). "A multitargeted, metronomic, and maximum-tolerated dose "chemo-switch" regimen is antiangiogenic, producing objective responses and survival benefit in a mouse model of cancer." J Clin Oncol **23**(5): 939-52.

Pio, B. S., C. K. Park, R. Pietras, W. A. Hsueh, N. Satyamurthy, M. D. Pegram, et al. (2006). "Usefulness of 3'-[F-18]fluoro-3'-deoxythymidine with positron emission tomography in predicting breast cancer response to therapy." Mol Imaging Biol **8**(1): 36-42.

Plas, D. R., S. Talapatra, A. L. Edinger, J. C. Rathmell and C. B. Thompson (2001). "Akt and Bcl-xL promote growth factor-independent survival through distinct effects on mitochondrial physiology." J Biol Chem **276**(15): 12041-8.

Posey, J. A., M. B. Khazaeli, A. DelGrosso, M. N. Saleh, C. Y. Lin, W. Huse, et al. (2001). "A pilot trial of Vitaxin, a humanized anti-vitronectin receptor (anti alpha v beta 3) antibody in patients with metastatic cancer." Cancer Biother Radiopharm **16**(2): 125-32.

Quinn, C. M. and N. A. Wright (1990). "The clinical assessment of proliferation and growth in human tumours: evaluation of methods and applications as prognostic variables." J Pathol **160**(2): 93-102.

Ramirez de Molina, A., R. Gutierrez, M. A. Ramos, J. M. Silva, J. Silva, F. Bonilla, et al. (2002). "Increased choline kinase activity in human breast carcinomas: clinical evidence for a potential novel antitumor strategy." Oncogene **21**(27): 4317-22.

Rasey, J. S., J. J. Casciari, P. D. Hofstrand, M. Muzi, M. M. Graham and L. K. Chin (2000). "Determining hypoxic fraction in a rat glioma by uptake of radiolabeled fluoromisonidazole." Radiat Res **153**(1): 84-92.

Rasey, J. S., J. R. Grierson, L. W. Wiens, P. D. Kolb and J. L. Schwartz (2002). "Validation of FLT uptake as a measure of thymidine kinase-1 activity in A549 carcinoma cells." J Nucl Med **43**(9): 1210-7.

Ratain, M. J. and S. G. Eckhardt (2004). "Phase II studies of modern drugs directed against new targets: if you are fazed, too, then resist RECIST." J Clin Oncol **22**(22): 4442-5.

Ratain, M. J., R. Mick, R. L. Schilsky and M. Siegler (1993). "Statistical and ethical issues in the design and conduct of phase I and II clinical trials of new anticancer agents." J Natl Cancer Inst **85**(20): 1637-43.

Rew, D. A. and G. D. Wilson (2000). "Cell production rates in human tissues and tumours and their significance. Part 1: an introduction to the techniques of measurement and their limitations." Eur J Surg Oncol **26**(3): 227-38.

Roehl, H. H. and S. E. Conrad (1990). "Identification of a G1-S-phase-regulated region in the human thymidine kinase gene promoter." Mol Cell Biol **10**(7): 3834-7.

Roivainen, A., S. Forsback, T. Gronroos, P. Lehikoinen, M. Kahkonen, E. Sutinen, et al. (2000). "Blood metabolism of [methyl-11C]choline; implications for in vivo imaging with positron emission tomography." Eur J Nucl Med **27**(1): 25-32.

Roivainen, A., R. Parkkola, T. Yli-Kerttula, P. Lehikoinen, T. Viljanen, T. Mottonen, et al. (2003). "Use of positron emission tomography with methyl-11C-choline and 2-18F-fluoro-2-deoxy-D-glucose in comparison with magnetic resonance imaging for the assessment of inflammatory proliferation of synovium." Arthritis Rheum **48**(11): 3077-84.

Romain, S., P. M. Martin, J. G. Klijn, W. L. van Putten, M. P. Look, O. Guirou, et al. (1997). "DNA-synthesis enzyme activity: a biological tool useful for predicting anti-metabolic drug sensitivity in breast cancer?" Int J Cancer **74**(2): 156-61.

Rowinsky, E. K., J. J. Windle and D. D. Von Hoff (1999). "Ras protein farnesyltransferase: A strategic target for anticancer therapeutic development." J Clin Oncol **17**(11): 3631-52.

Rowlands, D. C., H. E. Brown, P. C. Barber and E. L. Jones (1991). "The effect of tissue fixation on immunostaining for proliferating cell nuclear antigen with the monoclonal antibody PC10." J Pathol **165**(4): 356-7.

Saab, G., R. A. Dekemp, H. Ukkonen, T. D. Ruddy, G. Germano and R. S. Beanlands (2003). "Gated fluorine 18 fluorodeoxyglucose positron emission tomography: determination of global and regional left ventricular function and myocardial tissue characterization." J Nucl Cardiol **10**(3): 297-303.

Samuels, Y. and V. E. Velculescu (2004). "Oncogenic mutations of PIK3CA in human cancers." Cell Cycle **3**(10): 1221-4.

Sausville, E. A. and A. M. Burger (2006). "Contributions of human tumor xenografts to anticancer drug development." Cancer Res **66**(7): 3351-4, discussion 3354.

Schipper, D. L., M. J. Wagenmans, W. H. Peters and D. J. Wagener (1998). "Significance of cell proliferation measurement in gastric cancer." Eur J Cancer **34**(6): 781-90.

Schluter, C., M. Duchrow, C. Wohlenberg, M. Becker, G. Key, H. Flad, et al. (1993). "The cell proliferation-associated antigen of antibody Ki-67: a very large, ubiquitous nuclear protein with numerous repeated elements, representing a new kind of cell cycle-maintaining proteins." J. Cell Biol. **123**(3): 513-522.

Schott, A. F., M. A. Roubidoux, M. A. Helvie, D. F. Hayes, C. G. Kleer, L. A. Newman, et al. (2005). "Clinical and radiologic assessments to predict breast cancer pathologic complete response to neoadjuvant chemotherapy." Breast Cancer Res Treat **92**(3): 231-8.

Schrag, D., H. S. Garewal, H. J. Burstein, D. J. Samson, D. D. Von Hoff and M. R. Somerfield (2004). "American Society of Clinical Oncology Technology Assessment: chemotherapy sensitivity and resistance assays." J Clin Oncol **22**(17): 3631-8.

Schuller, J., J. Cassidy, E. Dumont, B. Roos, S. Durston, L. Banken, et al. (2000). "Preferential activation of capecitabine in tumor following oral administration to colorectal cancer patients." Cancer Chemother Pharmacol **45**(4): 291-7.

Scimeca, J. C., R. Ballotti, F. Alengrin, A. M. Honegger, A. Ullrich, J. Schlessinger, et al. (1989). "Metabolic effects induced by epidermal growth factor (EGF) in cells expressing EGF receptor mutants." J Biol Chem **264**(12): 6831-5.

Shaw, R. J., N. Bardeesy, B. D. Manning, L. Lopez, M. Kosmatka, R. A. DePinho, et al. (2004). "The LKB1 tumor suppressor negatively regulates mTOR signaling." Cancer Cell **6**(1): 91-9.

Shaw, R. J. and L. C. Cantley (2006). "Ras, PI(3)K and mTOR signalling controls tumour cell growth." Nature **441**(7092): 424-30.

Sherley, J. L. and T. J. Kelly (1988). "Human cytosolic thymidine kinase. Purification and physical characterization of the enzyme from HeLa cells." J Biol Chem **263**(1): 375-82.

Sherley, J. L. and T. J. Kelly (1988). "Regulation of human thymidine kinase during the cell cycle." J Biol Chem **263**(17): 8350-8.

Sherr, C. J. (1996). "Cancer cell cycles." Science **274**(5293): 1672-7.

Shields, A. F., D. A. Briston, S. Chandupatla, K. A. Douglas, J. Lawhorn-Crews, J. M. Collins, et al. (2005). "A simplified analysis of [18F]3'-deoxy-3'-fluorothymidine metabolism and retention." Eur J Nucl Med Mol Imaging **32**(11): 1269-75.

Shields, A. F., D. V. Coonrod, R. C. Quackenbush and J. J. Crowley (1987). "Cellular sources of thymidine nucleotides: studies for PET." J Nucl Med **28**(9): 1435-40.

Shields, A. F., M. M. Graham, S. M. Kozawa, L. B. Kozell, J. M. Link, E. R. Swenson, et al. (1992). "Contribution of labeled carbon dioxide to PET imaging of carbon-11-labeled compounds." J Nucl Med **33**(4): 581-4.

Shields, A. F., J. R. Grierson, B. M. Dohmen, H. J. Machulla, J. C. Stayanoff, J. M. Lawhorn-Crews, et al. (1998). "Imaging proliferation in vivo with [F-18]FLT and positron emission tomography." Nat Med **4**(11): 1334-6.

Shields, A. F., J. R. Grierson, O. Muzik, J. C. Stayanoff, J. M. Lawhorn-Crews, J. E. Obradovich, et al. (2002). "Kinetics of 3'-deoxy-3'-[F-18]fluorothymidine uptake and retention in dogs." Mol Imaging Biol **4**(1): 83-9.

Shields, A. F., D. A. Mankoff, J. M. Link, M. M. Graham, J. F. Eary, S. M. Kozawa, et al. (1998). "Carbon-11-thymidine and FDG to measure therapy response." J Nucl Med **39**(10): 1757-62.

Shing, Y., J. Folkman, R. Sullivan, C. Butterfield, J. Murray and M. Klagsbrun (1984). "Heparin affinity: purification of a tumor-derived capillary endothelial cell growth factor." Science **223**(4642): 1296-9.

Singletary, S. E., C. Allred, P. Ashley, L. W. Bassett, D. Berry, K. I. Bland, et al. (2002). "Revision of the American Joint Committee on Cancer staging system for breast cancer." J Clin Oncol **20**(17): 3628-36.

Slamon, D. J., G. M. Clark, S. G. Wong, W. J. Levin, A. Ullrich and W. L. McGuire (1987). "Human breast cancer: correlation of relapse and survival with amplification of the HER-2/neu oncogene." Science **235**(4785): 177-82.

Slamon, D. J., W. Godolphin, L. A. Jones, J. A. Holt, S. G. Wong, D. E. Keith, et al. (1989). "Studies of the HER-2/neu proto-oncogene in human breast and ovarian cancer." Science **244**(4905): 707-12.

Slamon, D. J., E. H. Romond and E. A. Perez (2006). "Advances in adjuvant therapy for breast cancer." Clin Adv Hematol Oncol **4**(3): suppl 1, 4-9; discussion suppl 10; quiz 2 p following suppl 10.

Smith-Jones, P. M., D. Solit, F. Afroze, N. Rosen and S. M. Larson (2006). "Early tumor response to Hsp90 therapy using HER2 PET: comparison with 18F-FDG PET." J Nucl Med **47**(5): 793-6.

Smith, T. A. (1998). "FDG uptake, tumour characteristics and response to therapy: a review." Nucl Med Commun **19**(2): 97-105.

Smyczek-Gargya, B., N. Fersis, H. Dittmann, U. Vogel, G. Reischl, H. J. Machulla, et al. (2004). "PET with [18F]fluorothymidine for imaging of primary breast cancer: a pilot study." Eur J Nucl Med Mol Imaging **31**(5): 720-4.

Soghomonyan, S. A., M. Doubrovin, J. Pike, X. Luo, M. Ittensohn, J. D. Runyan, et al. (2005). "Positron emission tomography (PET) imaging of tumor-localized Salmonella expressing HSV1-TK." Cancer Gene Ther **12**(1): 101-8.

Sokoloff L, R. M., Kennedy C. (1977). "[14C]-deoxyglucose method for the measurement of local cerebral glucose utilisation: theory, procedure and normal values in conscious and anesthesized albino rat." J Neurochem **28**: 897-916.

Soret, M., S. L. Bacharach and I. Buvat (2007). "Partial-volume effect in PET tumor imaging." J Nucl Med **48**(6): 932-45.

Spaepen, K., S. Stroobants, P. Dupont, G. Bormans, J. Balzarini, G. Verhoef, et al. (2003). "[(18)F]FDG PET monitoring of tumour response to chemotherapy: does [(18)F]FDG uptake correlate with the viable tumour cell fraction?" Eur J Nucl Med Mol Imaging **30**(5): 682-8.

Stabin, M. G., R. B. Sparks and E. Crowe (2005). "OLINDA/EXM: the second-generation personal computer software for internal dose assessment in nuclear medicine." J Nucl Med **46**(6): 1023-7.

Stessels, F., G. Van den Eynden, I. Van der Auwera, R. Salgado, E. Van den Heuvel, A. L. Harris, et al. (2004). "Breast adenocarcinoma liver metastases, in contrast to colorectal cancer liver metastases, display a non-angiogenic growth pattern that preserves the stroma and lacks hypoxia." Br J Cancer **90**(7): 1429-36.

Stupack, D. G. and D. A. Cheresh (2002). "Get a ligand, get a life: integrins, signaling and cell survival." J Cell Sci **115**(Pt 19): 3729-38.

Stupack, D. G., X. S. Puente, S. Boutsaboualoy, C. M. Storgard and D. A. Cheresh (2001). "Apoptosis of adherent cells by recruitment of caspase-8 to unligated integrins." J Cell Biol **155**(3): 459-70.

Sugawara, Y., K. R. Zasadny, A. W. Neuhoff and R. L. Wahl (1999). "Reevaluation of the standardized uptake value for FDG: variations with body weight and methods for correction." Radiology **213**(2): 521-5.

Sugiyama, M., H. Sakahara, K. Sato, N. Harada, D. Fukumoto, T. Kakiuchi, et al. (2004). "Evaluation of 3'-deoxy-3'-18F-fluorothymidine for monitoring tumor response to radiotherapy and photodynamic therapy in mice." J Nucl Med **45**(10): 1754-8.

Sun, H., J. M. Collins, T. J. Mangner, O. Muzik and A. F. Shields (2003). "Imaging [18F]FAU [1-(2'-deoxy-2'-fluoro-beta-D-arabinofuranosyl) uracil] in dogs." Nucl Med Biol **30**(1): 25-30.

Sun, H., T. J. Mangner, J. M. Collins, O. Muzik, K. Douglas and A. F. Shields (2005). "Imaging DNA synthesis in vivo with 18F-FMAU and PET." J Nucl Med **46**(2): 292-6.

Sun, H., A. Sloan, T. J. Mangner, U. Vaishampayan, O. Muzik, J. M. Collins, et al. (2005). "Imaging DNA synthesis with [18F]FMAU and positron emission tomography in patients with cancer." Eur J Nucl Med Mol Imaging **32**(1): 15-22.

Sung, V., J. T. Stubbs, 3rd, L. Fisher, A. D. Aaron and E. W. Thompson (1998). "Bone sialoprotein supports breast cancer cell adhesion proliferation and migration through differential usage of the alpha(v)beta3 and alpha(v)beta5 integrins." J Cell Physiol **176**(3): 482-94.

Tamkun, J. W., D. W. DeSimone, D. Fonda, R. S. Patel, C. Buck, A. F. Horwitz, et al. (1986). "Structure of integrin, a glycoprotein involved in the transmembrane linkage between fibronectin and actin." Cell **46**(2): 271-82.

Taylor, C. W., S. Green, W. S. Dalton, S. Martino, D. Rector, J. N. Ingle, et al. (1998). "Multicenter randomized clinical trial of goserelin versus surgical ovariectomy in

premenopausal patients with receptor-positive metastatic breast cancer: an intergroup study." J Clin Oncol **16**(3): 994-9.

Teo, N. B., B. S. Shoker, C. Jarvis, J. P. Sloane and C. Holcombe (2003). "Thymidine phosphorylase expression and stromal vascularity in ductal carcinoma in situ of the breast." J Clin Pathol **56**(12): 919-23.

Therasse, P., S. G. Arbuck, E. A. Eisenhauer, J. Wanders, R. S. Kaplan, L. Rubinstein, et al. (2000). "New guidelines to evaluate the response to treatment in solid tumors. European Organization for Research and Treatment of Cancer, National Cancer Institute of the United States, National Cancer Institute of Canada." J Natl Cancer Inst **92**(3): 205-16.

Therasse, P., E. A. Eisenhauer and J. Verweij (2006). "RECIST revisited: a review of validation studies on tumour assessment." Eur J Cancer **42**(8): 1031-9.

Thorgeirsson, U. P., T. Turpeenniemi-Hujanen, J. E. Williams, E. H. Westin, C. A. Heilman, J. E. Talmadge, et al. (1985). "NIH/3T3 cells transfected with human tumor DNA containing activated ras oncogenes express the metastatic phenotype in nude mice." Mol Cell Biol **5**(1): 259-62.

Thunnissen, F. B., A. W. Ambergen, M. Koss, W. D. Travis, T. J. O'Leary and I. O. Ellis (2001). "Mitotic counting in surgical pathology: sampling bias, heterogeneity and statistical uncertainty." Histopathology **39**(1): 1-8.

Tokunaga, E., A. Kataoka, Y. Kimura, E. Oki, K. Mashino, K. Nishida, et al. (2006). "The association between Akt activation and resistance to hormone therapy in metastatic breast cancer." Eur J Cancer **42**(5): 629-35.

Tominaga, T., M. Toi, Y. Ohashi and O. Abe (2002). "Prognostic and predictive value of thymidine phosphorylase activity in early-stage breast cancer patients." Clin Breast Cancer **3**(1): 55-64.

Townsend, D. W., M. Wensveen, L. G. Byars, A. Geissbuhler, H. J. Tochon-Danguy, A. Christin, et al. (1993). "A rotating PET scanner using BGO block detectors: design, performance and applications." J Nucl Med **34**(8): 1367-76.

Toyohara, J., A. Waki, S. Takamatsu, Y. Yonekura, Y. Magata and Y. Fujibayashi (2002). "Basis of FLT as a cell proliferation marker: comparative uptake studies with [3H]thymidine and [3H]arabinothymidine, and cell-analysis in 22 asynchronously growing tumor cell lines." Nucl Med Biol **29**(3): 281-7.

Tredan, O., C. M. Galmarini, K. Patel and I. F. Tannock (2007). "Drug resistance and the solid tumor microenvironment." J Natl Cancer Inst **99**(19): 1441-54.

Troiani, T., C. Schettino, E. Martinelli, F. Morgillo, G. Tortora and F. Ciardiello (2008). "The use of xenograft models for the selection of cancer treatments with the EGFR as an example." Crit Rev Oncol Hematol **65**(3): 200-11.

Tsang, R. W., C. S. Wong, A. W. Fyles, W. Levin, L. A. Manchul, M. Milosevic, et al. (1999). "Tumour proliferation and apoptosis in human uterine cervix carcinoma II: correlations with clinical outcome." Radiother Oncol **50**(1): 93-101.

Tyler, J. L., Y. L. Yamamoto, M. Diksic, J. Theron, J. G. Villemure, C. Worthington, et al. (1986). "Pharmacokinetics of superselective intra-arterial and intravenous [11C]BCNU evaluated by PET." J Nucl Med **27**(6): 775-80.

Valk, P. E., C. A. Mathis, M. D. Prados, J. C. Gilbert and T. F. Budinger (1992). "Hypoxia in human gliomas: demonstration by PET with fluorine-18-fluoromisonidazole." J Nucl Med **33**(12): 2133-7.

van Diest, P. J., E. van der Wall and J. P. Baak (2004). "Prognostic value of proliferation in invasive breast cancer: a review." J Clin Pathol **57**(7): 675-81.

van Eijkeren, M. E., A. De Schryver, P. Goethals, E. Poupeye, K. Schelstraete, I. Lemahieu, et al. (1992). "Measurement of short-term 11C-thymidine activity in human head and neck tumours using positron emission tomography (PET)." Acta Oncol **31**(5): 539-43.

Van Goethem, M., K. Schelfout, L. Dijckmans, J. C. Van Der Auwera, J. Weyler, I. Verslegers, et al. (2004). "MR mammography in the pre-operative staging of breast cancer in patients with dense breast tissue: comparison with mammography and ultrasound." Eur Radiol **14**(5): 809-16.

van Hagen, P. M., W. A. Breeman, H. F. Bernard, M. Schaar, C. M. Mooij, A. Srinivasan, et al. (2000). "Evaluation of a radiolabelled cyclic DTPA-RGD analogue for tumour imaging and radionuclide therapy." Int J Cancer **90**(4): 186-98.

van Waarde, A., D. C. Cobben, A. J. Suurmeijer, B. Maas, W. Vaalburg, E. F. de Vries, et al. (2004). "Selectivity of 18F-FLT and 18F-FDG for differentiating tumor from inflammation in a rodent model." J Nucl Med **45**(4): 695-700.

van Waarde, A., P. L. Jager, K. Ishiwata, R. A. Dierckx and P. H. Elsinga (2006). "Comparison of Sigma-Ligands and Metabolic PET Tracers for Differentiating Tumor from Inflammation." J Nucl Med **47**(1): 150-4.

Vander Borght, T., D. Labar, S. Pauwels and L. Lambotte (1991). "Production of [2-11C]thymidine for quantification of cellular proliferation with PET." Int J Rad Appl Instrum [A] **42**(1): 103-4.

Vander Borght, T., S. Pauwels, L. Lambotte, D. Labar, S. De Maeght, G. Stroobandt, et al. (1994). "Brain tumor imaging with PET and 2-[carbon-11]thymidine." J Nucl Med **35**(6): 974-82.

Vermeulen, P. B., G. Gasparini, S. B. Fox, C. Colpaert, L. P. Marson, M. Gion, et al. (2002). "Second international consensus on the methodology and criteria of evaluation of angiogenesis quantification in solid human tumours." Eur J Cancer **38**(12): 1564-79.

Veronesi, U., P. Boyle, A. Goldhirsch, R. Orecchia and G. Viale (2005). "Breast cancer." Lancet **365**(9472): 1727-41.

Vesselle, H., J. Grierson, M. Muzi, J. M. Pugsley, R. A. Schmidt, P. Rabinowitz, et al. (2002). "In vivo validation of 3'deoxy-3'-[(18)F]fluorothymidine ([(18)F]FLT) as a proliferation imaging tracer in humans: correlation of [(18)F]FLT uptake by positron

emission tomography with Ki-67 immunohistochemistry and flow cytometry in human lung tumors." Clin Cancer Res **8**(11): 3315-23.

Vesselle, H., J. Grierson, L. M. Peterson, M. Muzi, D. A. Mankoff and K. A. Krohn (2003). "18F-Fluorothymidine radiation dosimetry in human PET imaging studies." J Nucl Med **44**(9): 1482-8.

Vincent-Salomon, A., A. Rousseau, M. Jouve, P. Beuzeboc, B. Sigal-Zafrani, P. Freneaux, et al. (2004). "Proliferation markers predictive of the pathological response and disease outcome of patients with breast carcinomas treated by anthracycline-based preoperative chemotherapy." Eur J Cancer **40**(10): 1502-8.

Visvikis, D., D. Francis, R. Mulligan, D. C. Costa, I. Croasdale, S. K. Luthra, et al. (2003). "Comparison of methodologies for the in vivo assessment of (18)FLT utilisation in colorectal cancer." Eur J Nucl Med Mol Imaging.

Wagner, M., U. Seitz, A. Buck, B. Neumaier, S. Schultheiss, M. Bangerter, et al. (2003). "3'-[18F]fluoro-3'-deoxythymidine ([18F]-FLT) as positron emission tomography tracer for imaging proliferation in a murine B-Cell lymphoma model and in the human disease." Cancer Res **63**(10): 2681-7.

Wahl, R. L., C. A. Henry and S. P. Ethier (1992). "Serum glucose: effects on tumor and normal tissue accumulation of 2-[F-18]-fluoro-2-deoxy-D-glucose in rodents with mammary carcinoma." Radiology **183**(3): 643-7.

Wahl, R. L., K. Zasadny, M. Helvie, G. D. Hutchins, B. Weber and R. Cody (1993). "Metabolic monitoring of breast cancer chemohormonotherapy using positron emission tomography: initial evaluation." J Clin Oncol **11**(11): 2101-11.

Wang, H., P. Oliver, L. Nan, S. Wang, Z. Wang, J. K. Rhie, et al. (2002). "Radiolabeled 2'-fluorodeoxyuracil-beta-D-arabinofuranoside (FAU) and 2'-fluoro-5-methyldeoxyuracil-beta -D-arabinofuranoside (FMAU) as tumor-imaging agents in mice." Cancer Chemother Pharmacol **49**(5): 419-24.

Warburg O, P. K., Negelein E (1924). "Uber den stoffwechsel der carcinomzelle." Biochem Zeitschrift **152**: 309-35.

Weber, G. and A. Cantero (1955). "Glucose-6-phosphatase activity in normal, pre-cancerous, and neoplastic tissues." Cancer Res **15**(2): 105-8.

Weber, W. A., S. I. Ziegler, R. Thodtmann, A. R. Hanauske and M. Schwaiger (1999). "Reproducibility of metabolic measurements in malignant tumors using FDG PET." J Nucl Med **40**(11): 1771-7.

Wedam, S. B., J. A. Low, S. X. Yang, C. K. Chow, P. Choyke, D. Danforth, et al. (2006). "Antiangiogenic and antitumor effects of bevacizumab in patients with inflammatory and locally advanced breast cancer." J Clin Oncol **24**(5): 769-77.

Weinberg, I. N., S. C. Huang, E. J. Hoffman, L. Araujo, C. Nienaber, M. Grover-McKay, et al. (1988). "Validation of PET-acquired input functions for cardiac studies." J Nucl Med **29**(2): 241-7.

Wells, J. M., D. A. Mankoff, J. F. Eary, A. M. Spence, M. Muzi, F. O'Sullivan, et al. (2002). "Kinetic analysis of 2-[11C]thymidine PET imaging studies of malignant brain tumors: preliminary patient results." Mol Imaging **1**(3): 145-50.

Wells, J. M., D. A. Mankoff, M. Muzi, F. O'Sullivan, J. F. Eary, A. M. Spence, et al. (2002). "Kinetic analysis of 2-[11C]thymidine PET imaging studies of malignant brain tumors: compartmental model investigation and mathematical analysis." Mol Imaging **1**(3): 151-9.

Wells, P., E. Aboagye, R. N. Gunn, S. Osman, A. V. Boddy, G. A. Taylor, et al. (2003). "2-[11C]thymidine positron emission tomography as an indicator of thymidylate synthase inhibition in patients treated with AG337." J Natl Cancer Inst **95**(9): 675-82.

Wells, P., R. N. Gunn, M. Alison, C. Steel, M. Golding, A. S. Ranicar, et al. (2002). "Assessment of proliferation in vivo using 2-[(11)C]thymidine positron emission tomography in advanced intra-abdominal malignancies." Cancer Res **62**(20): 5698-702.

Wells, P., R. N. Gunn, C. Steel, A. S. Ranicar, F. Brady, S. Osman, et al. (2005). "2-[11C]thymidine positron emission tomography reproducibility in humans." Clin Cancer Res **11**(12): 4341-7.

Wilson, C. B., A. A. Lammertsma, C. G. McKenzie, K. Sikora and T. Jones (1992). "Measurements of blood flow and exchanging water space in breast tumors using

positron emission tomography: a rapid and noninvasive dynamic method." Cancer Res **52**(6): 1592-7.

Winer, E. P., C. Hudis, H. J. Burstein, A. C. Wolff, K. I. Pritchard, J. N. Ingle, et al. (2005). "American Society of Clinical Oncology technology assessment on the use of aromatase inhibitors as adjuvant therapy for postmenopausal women with hormone receptor-positive breast cancer: status report 2004." J Clin Oncol **23**(3): 619-29.

Wohlhueter, R. M., R. Marz and P. G. Plagemann (1979). "Thymidine transport in cultured mammalian cells. Kinetic analysis, temperature dependence and specificity of the transport system." Biochim Biophys Acta **553**(2): 262-83.

Workman, P., E. O. Aboagye, Y. L. Chung, J. R. Griffiths, R. Hart, M. O. Leach, et al. (2006). "Minimally invasive pharmacokinetic and pharmacodynamic technologies in hypothesis-testing clinical trials of innovative therapies." J Natl Cancer Inst **98**(9): 580-98.

Yamaguchi, T., J. Lee, H. Uemura, T. Sasaki, N. Takahashi, T. Oka, et al. (2005). "Prostate cancer: a comparative study of 11C-choline PET and MR imaging combined with proton MR spectroscopy." Eur J Nucl Med Mol Imaging **32**(7): 742-8.

Yao, V. J., M. G. Ozawa, A. S. Varner, I. M. Kasman, Y. H. Chanthery, R. Pasqualini, et al. (2006). "Antiangiogenic therapy decreases integrin expression in normalized tumor blood vessels." Cancer Res **66**(5): 2639-49.

Yarden, Y., J. Baselga and D. Miles (2004). "Molecular approach to breast cancer treatment." Semin Oncol **31**(5 Suppl 10): 6-13.

Yoshida, S., K. Nakagomi, S. Goto, M. Futatsubashi and T. Torizuka (2005). "11C-choline positron emission tomography in prostate cancer: primary staging and recurrent site staging." Urol Int **74**(3): 214-20.

Young, H., R. Baum, U. Cremerius, K. Herholz, O. Hoekstra, A. A. Lammertsma, et al. (1999). "Measurement of clinical and subclinical tumour response using [18F]-fluorodeoxyglucose and positron emission tomography: review and 1999 EORTC recommendations. European Organization for Research and Treatment of Cancer (EORTC) PET Study Group." Eur J Cancer **35**(13): 1773-82.

Zasadny, K. R. and R. L. Wahl (1993). "Standardized uptake values of normal tissues at PET with 2-[fluorine-18]-fluoro-2-deoxy-D-glucose: variations with body weight and a method for correction." Radiology **189**(3): 847-50.

Zheng, Q. H. and G. K. Mulholland (1996). "Improved synthesis of beta-CIT and [11C]beta-CIT labeled at nitrogen or oxygen positions." Nucl Med Biol **23**(8): 981-6.

Zhuang, H., M. Pourdehnad, E. S. Lambright, A. J. Yamamoto, M. Lanuti, P. Li, et al. (2001). "Dual time point 18F-FDG PET imaging for differentiating malignant from inflammatory processes." J Nucl Med **42**(9): 1412-7.

Zhuang, H. M., A. Cortes-Blanco, M. Pourdehnad, L. E. Adam, A. J. Yamamoto, R. Martinez-Lazaro, et al. (2001). "Do high glucose levels have differential effect on

FDG uptake in inflammatory and malignant disorders?" Nucl Med Commun **22**(10): 1123-8.

Zidan, A., J. S. Christie Brown, D. Peston and S. Shousha (1997). "Oestrogen and progesterone receptor assessment in core biopsy specimens of breast carcinoma." J Clin Pathol **50**(1): 27-9.